# DEVELOPMENT OF OPTOGENETIC TOOLS FOR PLANT SYNTHETIC BIOLOGY

Inaugural-Dissertation

zur Erlangung des Doktorgrades

der Mathematisch-Naturwissenschaftlichen Fakultät

der Heinrich-Heine-Universität Düsseldorf

vorgelegt von

**Rocio Ochoa-Fernandez**

aus Elche (Spain)

Düsseldorf, December 2019

aus dem Institut für Synthetische Biologie

der Heinrich-Heine-Universität Düsseldorf

Gedruckt mit der Genehmigung der

Mathematisch-Naturwissenschaftlichen Fakultät der

Heinrich-Heine-Universität Düsseldorf

Berichterstatter:

1. Prof. Dr. Matias Zurbriggen

2. Prof. Dr. Rüdiger Simon

Tag der mündlichen Prüfung: 07.07.2020

## Eidesstattliche erklärung

Ich versichere an Eides Statt, dass die Dissertation von mir selbständig und ohne unzulässige fremde Hilfe unter Beachtung der „Grundsätze zur Sicherung guter wissenschaftlicher Praxis an der Heinrich-Heine-Universität Düsseldorf“ erstellt worden ist.

Die Dissertation habe ich in der vorgelegten oder in ähnlicher Form noch bei keiner anderen Institution eingereicht.

Ich habe bisher keine erfolglosen Promotionsversuche unternommen.

| | |
|---|---|
| Ort, Datum | Unterschrift |

## Acknowledgments

In the first place, I would like to thank Prof. Matias Zurbriggen and Prof. Wilfried Weber to give me the opportunity to do this PhD. Thanks Matias for the science and career discussions, and the trust to follow my own ideas and scientific path. Also thank you for your positive and optimistic insights. I would like to thank also my mentor Prof. Rüdiger Simon for the fruitful discussions and feedback.

I would also like to thank the people of AG Weber that welcomed and taught me when I started in Freiburg. Especially I would like to thank Sophie, which showed me a new world of protoplast and made the quest of moving to Düsseldorf way more interesting. Also thanks to Justine, my *partner in crime*, whose creativity always inspires me and always manages to take me out of the well. When we started in the lab we had very crazy and funny times. It would not have been the same without you both.

I would also like to thank all the people in the AG Zurbriggen. It is wonderful to see the lab growing so much in such a short time. Despite being challenging sometimes, thanks to the people always trying to make the work for the others easier and to create a nice environment. Thanks also to the people that always find some time to discuss science and offer some homemade engineering skills.

Thanks to all the students that have been under my supervision: Simon, Tim, Johanna, Daphne, Jay, and Giovanni. Thanks for putting so much enthusiasm in the work and to allow me to practice my teaching skills. Thanks to all the people that provided technical assistance in the everyday work, in particular, thanks to Reinhi, Michaela and Mara. Thanks to all the collaborators and people that helped in any way to this work including Leonie, Jenia, Nikolaj, Claire, Regina, Tzvetina, Sofia, and Uriel.

Me gustaría agradecer a ese *club latino* que se ha formado en los últimos meses en el lab, gracias por aportar diversión (y drama) a esta casa de locos que es el lab. También doy las gracias a mis amigas de *el pisico* porque por muy lejos que estemos siempre nos quedarán las conversaciones locas de

media noche y los skypes de los martes. También me gustaría agradecer a mi familia por su apoyo incondicional, incluso desde la distancia.

Y por último, me gustaría agradecer a Dani por el soporte emocional, por siempre estar ahí cuando necesitaba hablar. No se si hubiese podido sobrevivir a este doctorado sin ti. Qué los caminos de la ciencia no nos vuelvan a separar!

Thank you all!

# Table of contents

# List of Figures

## List of tables

# Abbreviations

| | |
|---|---|
| 2A | F2A self-cleaving peptide derived from the foot-and-mouth disease virus |
| ABA | Abscisic acid |
| AD | Activation domain |
| APA | Active PhyA-binding region |
| APB | Active PhyB-binding region |
| *As*LOV2 | LOV2 domain of *Avena sativa* Phototropin 1 |
| *At*LOV2 | LOV2 domain of *Arabidopsis thaliana* Phototropin 1 |
| ATP | Adenosine triphosphate |
| bHLH | Basic helix-loop-helix |
| BLINK1 | Blue-light-induced K(+) channel 1 |
| BLUF | Blue light receptor using FAD |
| $B_{Off}$ | Blue light gene repression switch |
| $B_{On}$ | Blue light gene activation switch |
| Bph | Bacterial phytochrome |
| BRD | B3 repression domain from *A. thaliana* |
| BV | Biliverdin |
| bZIP | Basic leucine zipper domain |
| c-di-GMP | Cyclic diguanylate |
| C120 | DNA cognate sequence of EL222 |
| cAMP | Cyclic adenosine monophosphate |
| CarH | HTH-type transcriptional repressor |
| CarO | CarH-specific operator sequence |
| Cas9 | CRISPR associated protein 9 |
| CBD | Cobalamin-binding domain |
| Cbl | Cobalamin |

| | |
|---|---|
| CcaR | Chromatic acclimation regulator |
| CcaS | Chromatic acclimation sensor |
| ChR2 | Channelrhodopsin 2 |
| CIB1 | Cryptochrome-interacting basic helix-loop-helix 1 |
| cNMP | Cyclic nucleotide monophosphate |
| COP1 | CONSTITUTIVELY PHOTOMORPHOGENIC 1 |
| CRE | Recombinase from bacteriophage P1 |
| CRISPR | Clustered regularly interspaced short palindromic repeats |
| CRY2 | CRYPTOCHROME 2 |
| DBD | DNA-binding domain |
| dCas9 | CRISPR associated protein 9 nuclease deficient |
| E | Macrolide-responsive repressor protein |
| EFR | LRR receptor-like serine/threonine-protein kinase from *A. thaliana* |
| EL222 | Transcription factor 222 from *Erythrobacter litoralis* |
| etr | DNA cognate sequence of E |
| FAD | Flavin adenine dinucleotide |
| FHL | FAR-RED-ELONGATED HYPOCOTYL 1-LIKE |
| FHY1 | FAR-RED ELONGATED HYPOCOTYL 1 |
| FKF1 | FLAVIN BINDING, KELCH REPEAT, F-BOX1 |
| Flp | Site-specific recombinase from *Saccharomyces cerevisiae* |
| FLuc | Firefly luciferase |
| FMN | Flavin mononucleotide |
| FokI | Restriction endonuclease |
| FT | FLOWERING LOCUS T from *A. thaliana* |
| GAF | cGMP phosphodiesterase/adenylyl cyclase/FhlA domain |

| | |
|---|---|
| Gal4BD | Binding domain of Gal4 regulatory protein from *Saccharomyces cerevisiae* |
| GBP | GFP binding protein |
| GFP | Green fluorescent protein |
| GI | GIGANTEA |
| goi | Gene of interest |
| gRNA | guide RNA part containing the 20 bp target sequence |
| GUS | β-glucuronidase from *E. coli* |
| H2B | Histone B2 from *A. thaliana* |
| HA-tag | Human influenza hemagglutinin-derived epitope tag |
| HK | Histidin kinase |
| HTH | Helix-turn-helix |
| IRES | Internal ribosome entry site |
| KanR | Kanamycin resistance |
| KRAB | Transcriptional repressor domain from human Krüppel Associated 8 Box |
| LED | Light-emitting diode |
| LFY | LEAFY transcription factor from *A. thaliana* |
| LOV | Light-Oxigen-Voltage domain |
| MAMP | Microbe-associated molecular pattern |
| MMC | MES, Mannitol, Calcium medium |
| MMM | MES, Mannitol, Magnesium medium |
| MS | Murashige and Skoog medium |
| MSC | MES, Sucrose, Calcium medium |
| NLS | Nuclear localization sequence |
| NMP | Nucleotide monophosphate |
| nptII | Neomycin phosphotransferase |

| | |
|---|---|
| NTD | N-terminal domain |
| $P_{35Senhancer}$ | Enhancer region of the cauliflower mosaic virus 35S promoter |
| pA | Polyadenylation signal |
| PAC | Photoactivated adenylyl cyclases |
| PAS | Period/Arnt/SIM domain |
| $P_{AtAP1}$ | *A. thaliana* APETALA1 promoter |
| $P_{AtU6\text{-}26}$ | *A. thaliana* U6-26 RNA polymerase III promoter |
| $P_{AtUbi10}$ | *A. thaliana* Ubiquitin-10 promoter |
| $P_{CaMV35S}$ | Cauliflower mosaic virus 35S promoter |
| PCA | Protoplast Culture Arabidopsis medium |
| PCB | Phycocyanobilin |
| PCR | Polymerase chain reaction |
| PEG | Polyethylene glycol |
| $P_{hCMVmin}$ | Minimal human cytomegalovirus immediate early promoter |
| PHY | Phytochrome-specific domain |
| PhyB | Phytochrome B |
| $PhyB_{fr}$ | Far-red light-absorbing conformation of PhyB |
| $PhyB_{r}$ | Red light-absorbing conformation of PhyB |
| PIF | Phytochrome interacting factor |
| $P_{nos}$ | Nopaline synthase promoter *from A. thumefaciens* |
| POI | Protein of interest |
| $P_{SlDFR}$ | Solanum lycopersicum dihydroflavonol 4-reductase promoter |
| $P_{SV40}$ | Simian virus 40 early promoter |
| PULSE | Plant Usable Light Switch-Elements |
| РΦВ | Phytochromobilin |

| | |
|---|---|
| RT-qPCR | Reverse transcription–quantitative PCR |
| RD | Repression domain |
| RLU | Relative Luminescence Units |
| RLuc | Renilla luciferase |
| $R_{Off}$ | Red light gene repression switch |
| $R_{On}$ | Red light gene activation switch |
| ROS | Reactive oxygen species |
| RR | Response regulator |
| RTK | Receptor tyrosine kinase |
| SCA | Seedling Culture Arabidopsis medium |
| SEM | Standard error of the mean |
| sgRNA | Single guide RNA from combined bacterial crRNA and tracrRNA without the target sequence |
| SRDX | EAR repression domain from *A. thaliana* |
| SynBio | Synthetic Biology |
| TALE | Transcription activator-like effector |
| TALEN | Transcription activator-like effector nucleases |
| $T_{CaMV35S}$ | Cauliflower mosaic virus 35S terminator |
| TCP | TEOSINTE BRANCHED 1, CYCLOIDEA, PCF transcription factors family |
| TF | Transcription factor |
| TMN | Transmembrane domain |
| $T_{nos}$ | Nopaline synthase terminator from *A. thumefaciens* |
| TNT | Trinitrotoluene |
| $T_{OCS}$ | Octopine synthase terminator from *A. thumefaciens* |
| TSS | Transcription start site |
| $T_{SV40}$ | Simian virus 40 early terminator |
| TULIP | Tunable, light-controlled interacting protein tag |

| | |
|---|---|
| TV | Activation domain composed by 6x TAL and 2x VP64 and NLS sequence |
| UAS | Upstream Activation Sequence, DNA cognate sequence of Gal4 |
| UirS | UV intensity response sensor |
| UirS | UV intensity response regulator |
| UTR | Untranslated region |
| UV | Ultraviolet |
| UVR8 | UV RESISTANCE LOCUS 8 |
| VEGF | Vascular endothelial growth factor |
| VP16 | Herpes simplex virus-derived transactivation domain |
| VP64 | 4x VP16 |
| VP128 | 8x VP16 |
| VVD | Vivid |
| wt | Wild type |
| YFP | Yellow fluorescent protein |
| ZF | Zinc finger |
| ZFN | Zinc-finger nucleases |
| $\lambda_{max}$ | maximum wavelength |

## Summary

Plant synthetic biology is a nascent research area and, therefore, the development and implementation of engineering methods and synthetic tools still lags behind. In particular, optogenetic switches allow a precise quantitative regulation of cellular processes, such as gene expression, at high spatiotemporal resolution, overcoming limitations of classical chemically-inducible systems. While being widely applied in animal systems, their implementation in plants imposes a challenge.

In this thesis, some of the challenges of implementing optogenetic tools in plants are addressed. Firstly, Arabidopsis protoplasts are proposed as a platform to implement and characterize optogenetic tools. The development of tools to control gene expression in this cellular system, inducible by green, red and blue light, are then described, as well as some concepts for future switches. These optogenetic tools are designed as modular components that can be used to devise complex multi-chromatic tools to control gene expression. Finally, the development of a synthetic light-inducible system for the targeted control of gene expression in plants is presented. This system is based on red and blue light-controlled photoreceptors, which in combination turn gene expression OFF under white light and ON under red light. The characterization of this tool, termed Plant Usable Light Switch-Elements (PULSE), in plant cells is shown as well as its implementation in leaf tissue, enabling the first steps towards its application in stable transformed plant lines.

This work reflects on the development of these first optogenetic systems for plants and stress on the novel perspectives they present for the study of plant signalling processes, such as the analysis of complex regulatory systems and metabolic pathways, with minimized invasiveness and high spatiotemporal resolution.

## Publications and contributions

The work in this thesis is the subject of the following publications and manuscripts. The full manuscripts can be found in Appendix A - B.

Ochoa-Fernandez, R.*, Samodelov, S.L.*, Brandl, S.M., Wehinger, E., Müller, K., Weber, W., and Zurbriggen, M.D. (2016). Optogenetics: Methods and Protocols. A. Kianianmomeni, ed. (New York, NY: Springer New York), pp. 125–139.

Contribution: Planning and analysis of the protoplasts experiments. Execution of experiments was performed together with S.M. Brandl (in the course of his B. Sc. thesis under my supervision). Writing of the manuscript and preparation of figures.

Chatelle, C., Ochoa-Fernandez, R., Engesser, R., Schneider, N., Beyer, H.M., Jones, A.R., Timmer, J., Zurbriggen, M.D., and Weber, W. (2018). A Green-Light-Responsive System for the Control of Transgene Expression in Mammalian and Plant Cells. ACS Synth. Biol. *7*, 1349–1358.

Contribution: Cloning plasmids for expression in plants. Planning, execution, and analysis of the protoplasts experiments.

Gratz, R., Brumbarova, T., Ivanov, R., Trofimov, K., Tünnermann, L., Ochoa-Fernandez, R., Blomeier, T., Meiser, J., Weidtkamp-Peters, S., Zurbriggen, M., *et al*. (2019). Phospho-mutant activity assays provide evidence for alternative phospho-regulation pathways of the transcription factor FIT. New Phytol. *225*, 250-267.

Contribution: Design of cloning for expression in mammalian cells, planning, execution and analysis of the experiments in mammalian cells together with R. Gratz and T. Blomeier.

Ochoa-Fernandez, R., Abel, N.B., Wieland, F.G., Schlegel, J., Koch, L.A., Miller, J.B., Engesser, R., Giuriani, G., Brandl, S.M., Plum J., Timmer, J., Weber ,W., Ott, T., Simon, R., and Zurbriggen, M.D. PULSE – Optogenetic control of gene expression in plants in the presence of ambient white light. *Manuscript under revision.* Nov 2019.

Contribution: Design of the system. Cloning plasmids, planning, execution and analysis of all the experiments in protoplasts. Execution of preliminary experiments was performed together with S.M. Brandl (in the course of his B. Sc. thesis under my supervision). Design of experiments in Nicotiana and execution together with N.B. Abel, J. Schlegel, and L.A. Koch. Generation of Arabidopsis transgenic lines together with J. Plum and G. Giuriani (in the course of their M.Sc. Theses, under my supervision). Preliminary screening of Arabidopsis lines was performed by G. Giurani. Execution of the experiments in Arabidopsis transgenic lines. Writing of the manuscript and preparation of all figures.

Ochoa-Fernandez, R., Schuler, M., Zurbriggen, M.D. Expanding the toolbox of optogenetic switches for red and blue light control of gene expression in plant cells. *Manuscript in preparation*. Nov 2019.

Contribution: Design of the systems. Cloning plasmids, planning, and analysis of the experiments together with M. Schuler. Writing of the manuscript and preparation of the figures.

# I. Introduction

# 1. Synthetic biology

## *1.1. Introduction to synthetic biology*

Synthetic biology (Synbio) is a field that integrates biology and engineering concepts like standardization, modularity, abstraction, predictability and decoupling design from fabrication (Decoene et al., 2018; Endy, 2005). It aims to create biological systems through a systematic design, using a "Design-Build-Test" cycle (Kelwick et al., 2014). It manages the components of the cell as "biological parts" that can be assembled to accomplish a desired function, acting as "gene devices or circuits" to perform desired operations.

The origin of this field can be found in the early 2000s with the programming of a toggle switch (Gardner et al., 2000) and a 'repressilator' (Elowitz and Leibler, 2000) in bacteria. Since the outset of the field, it has expanded to more complex systems, compared to early genetic engineering approaches. These systems have different functions and are applied to different model organisms. Some of these circuits are biosensors (Bayer and Smolke, 2005; Danino et al., 2015; Win and Smolke, 2007), Boolean logic gates (Bonnet et al., 2013; Guet et al., 2002; Kramer et al., 2004), band-pass filters (Muranaka and Yokobayashi, 2010; Sohka et al., 2009) and memory devices (Ajo-Franklin et al., 2007; Bonnet et al., 2012; Siuti et al., 2013). Among the achievements of synthetic biology can be found the production of high-value compounds like the antimalaria drug artemisinin in yeast (Paddon et al., 2013; Ro et al., 2006) or the development of a cancer-invading bacteria (Anderson et al., 2006).

**Toggle switch**: genetic circuit that can be switched between two stable states of expression with a transient stimulus.

**Repressilator**: circuit that implements an oscillatory function through three genes repressing the next one in a feedback loop.

**Logic gate**: implements a Boolean logic function (AND, OR, NOT…) on one or more inputs to produce a binary output.

**Band-pass filter**: device that eliminates or attenuates frequencies outside a certain range.

The design of these circuits could be arduous and time-consuming. To aid in the design, an increasing amount of computer-aided design (CAD) tools have been developed (Chandran et al., 2009; Czar et al., 2009; Nielsen et al., 2016). For design automation, the principles of standardization and modulation must be applied (Matsuoka et al., 2009).

## *1.2. Synthetic biology in plants (Plant SynBio)*

In the past years, synthetic biology has expanded from microbial hosts to more complex organisms, including plants. Plants are interesting from a biotechnological point of view as they are primary sources of biomass, they produce secondary metabolites and they can be used as recombinant protein factories. Plant SynBio is still an emergent field due, in part, to the plant's inherent complexity (large and redundant genomes, complex signalling pathways, many organs), longer generation times than other organisms and the difficulty of transformation for some species (Cook et al., 2014; Liu and Stewart, 2015). These last issues have been partly alleviated by exploring transient expression systems like agroinfiltration (Bartlett et al., 2008), AGROBEST (Wu et al., 2014), cell protoplast assays (Davey et al., 2005), as well as gene engineering using biolistics (Agrawal et al., 2005) and transformation of organelles (Clarke and Daniell, 2011; Maliga and Bock, 2011) or pollen (Zhao et al., 2017). Moreover, the extensive regulatory processes required as well as the public concern, in particular for plant crops, have been a limitation in the technological development of the field (Smita Rastogi, 2013). For that reason, the strategies for transgene removal and biological confinement have been thoroughly explored (Daniell, 2002; Sang et al., 2013).

However, over the past years, there has been an interest in the development of approaches and tools. They are becoming accessible to the plant community, pointing towards the revolution of the Plant SynBio field and the opportunities they can offer (Andres et al., 2019; Braguy and Zurbriggen, 2016).

While one part of Plant SynBio has a goal-oriented focus, the foundational part of SynBio aims on providing tools and resources for the plant community so it can be used for basic research and a better understanding of genes and pathways (Samodelov and Zurbriggen, 2017).

Examples of Plant Synbio to serve in biotechnology applications include the attempts of plant crop redesign in order to have a self-fertilizing crop by

engineering nitrogen symbiosis in barley and wheat (Charpentier et al., 2016; Feike et al., 2019), as well as the use of plants as “sentinels” to detect molecules like TNT (Antunes et al., 2009, 2011) or bacterial pathogens (Liu et al., 2011, 2013b). There are also some examples where Synbio approaches have been used for metabolic engineering, like the engineering of C4 metabolism in crop plants with C3 metabolism (Schuler et al., 2016), biofuel production in crops (DePaoli et al., 2014), and for the production of high value compounds like dhurrin (Kristensen et al., 2005) and carotenoids (Diretto et al., 2007). Long term applications include “smart plants”, which have molecular circuity, that enable them to sense and adapt to environmental changes (Brophy and Voigt, 2014).

In the foundational technologies part of Plant Synbio, there has been a big interest in developing DNA assembly methods that allow the construction of large amounts of DNA while using principles of modularity and standardization (Liu et al., 2013a; Patron et al., 2015). Other tools were developed for monitoring, such as hormone sensors for abscisic acid (Jones et al., 2014), auxins (Wend et al., 2013), strigolactones (Samodelov et al., 2016), and cytokinins (Zürcher et al., 2013). There has also been interest in tools for gene expression control. For instance, ZFs, TALEs, and CRISPR/Cas technologies were shown to be precise tools for genome editing (Bortesi and Fischer, 2015; Mahfouz et al., 2014). In addition, synthetic promoters and chimeric transcriptional repressors/activators to control gene expression have been developed (Dey et al., 2015; Liu and Stewart, 2016).

**Zinc-finger (ZF):** DNA binding domains that consist of arrays of zinc-fingers, each of which recognizes a triplet of nucleotides. They are termed zinc-finger nucleases (ZFNs) when they are fused to the *Fok*I endonuclease.

**Transcription activation like-effectors (TALE)**: virulence factors secreted by Xanthomonas when infecting plants. It is composed by a DNA-binding domain and an activation domain. Their DNA-binding domain can be custom-designed, each residue binds one nucleotide. They are termed transcription activation like-effectors nucleases (TALENs) when they are fused to the *Fok*I endonuclease.

**CRISPR/Cas technology:**

The nuclease Cas, typically Cas9, is directed to the DNA by a guide RNA. It triggers DNA repair mechanisms resulting in insertion, mutation or deletion of the targeted gene. Nuclease defective Cas9 (dCas9) can be used to modulate gene expression.

## *1.3. The need for controlling gene expression in plants*

In plant basic research, the classical approach to study gene function is: i) the over-expression of a given gene of interest (goi) by rendering it under the control of a constitutive promoter, or, ii) the down-regulation by the removal of the gene or its transcript known as knock-out or knock-down strategy. These approaches are used in order to address its function(s) and its phenotypic effect(s) and have been proven efficient. However, they are not always applicable depending on the gene, for instance, they could lead to a lethal

phenotype. The genes to be studied are frequently part of a key function in the cell and permanently varying their amount can have detrimental effects on the plant. Moreover, when studying the dynamics of gene regulatory networks, for example to understand the dynamics of the circadian clock having transient expression is desirable (Knowles et al., 2008).

Likewise, for biotechnological purposes, sometimes it is desirable that certain genes are expressed on command; for example, to control plant development, or in order to produce in a plant a compound of therapeutic interest which is otherwise harmful or to use the plant resources at the most optimal time and place.

## *1.4. Inducing gene expression in plants*

Several approaches have been implemented to control gene expression in plants, including using biotic and abiotic stress-inducible, light-responsive, hormone-inducible, tissue-specific, and chemical-inducible synthetic promoters (Dey et al., 2015).

Of major relevance are the tissue-specific promoters and chemical inducible switches. While tissue-specific promoters offer spatial and developmental stage control, they are unable to be switched ON and OFF on command. Chemical-inducible systems, on the other hand, provide greater control over time and space of the expression of the desired gene of interest.

Several chemical-inducible systems have been developed and applied in plants and have been extensively reviewed (Corrado and Karali, 2009; Padidam, 2003; Tang et al., 2004; Zuo and Chua, 2000). There are examples of regulatable systems inducible by antibiotics like tetracycline and pristinamycin (Frey et al., 2001), by ethanol (Caddick et al., 1998), copper (Mett et al., 1993), and systems based on steroids like the estradiol receptor (Bruce et al., 2000) and the glucocorticoid receptor (Aoyama and Chua, 1997), among others.

The use of these inducible systems has increased considerably since their first implementation, and they are now used in many labs as common tools to

regulate the gene expression in a more precise manner. However, the quantitative, spatial and temporal control that they offer is limited. While better than the use of constitutive or tissue-specific promoters, once activated, they cannot be turned off actively since the retrieval of the signal is not possible and repeated addition of the compound will be needed for sustained effect. Moreover, the spatial resolution is relative, since due to transport processes entire areas are normally activated, for example, single leaves or roots but not single cells. Another aspect to consider is the unpredictability of the compound diffusion upon administration, depending on the complexity of the tissue and the substance used. Other limitations, like undesired pleiotropic effects, toxicity, or unspecific phenotype linked with the compound concentration as well as the economic and environmental costs of using chemicals, cannot be disregarded (Moore et al., 2006).

In summary, these inducible strategies could be very useful for particular applications, however, they come with a cost in either quantitative, temporal or spatial resolution.

# 2. Light-inducible systems

## *2.1. Introduction to optogenetics*

Optogenetics is a field that builds upon using light as a stimulus to control cellular processes. It was originally developed in the neuroscience field in 2005 (Boyden et al., 2005; Li et al., 2005; Nagel et al., 2005) from the idea of using microbial ion channels regulated by light, termed opsins, first upon introduction into animal cells and then into free moving mammals, in order to control the neuronal potential. As a result, a very precise new tool to investigate behaviour in animals was developed (Deisseroth, 2011; Deisseroth and Hegemann, 2017). After that, the tool and its principles were transferred to other areas of research, like the application of the opsin ChR2 to control beating frequency in cardiac cells (Nussinovitch et al., 2014) or to control insulin secretion in beta cells (Reinbothe et al., 2014). A slew of additional tools has since been developed to control a myriad of cellular processes other than membrane

potential, including but not limited to intracellular protein trafficking, protein binding and cleavage (Mansouri et al., 2019; Mühlhäuser et al., 2017).

Light is an optimal inducer, overcoming some of the limitations of the chemicals as a trigger. First, it can be delivered with a much higher spatiotemporal resolution, to single cells and even at a subcellular level. Secondly, it can be applied in a repeatable, fast, and reversible manner (without washing steps and without leaving any trace). Normally, the optogenetic tools are very sensitive regarding their activation/deactivation state, minimizing toxic or other side effects and allowing to be used in a quantitative manner, typically reaching high activation rates. Profiting from these advantages, optogenetic tools have become increasingly available in the last years and prominently applied to mammalian cells, followed by yeast and bacteria (Figure 1).

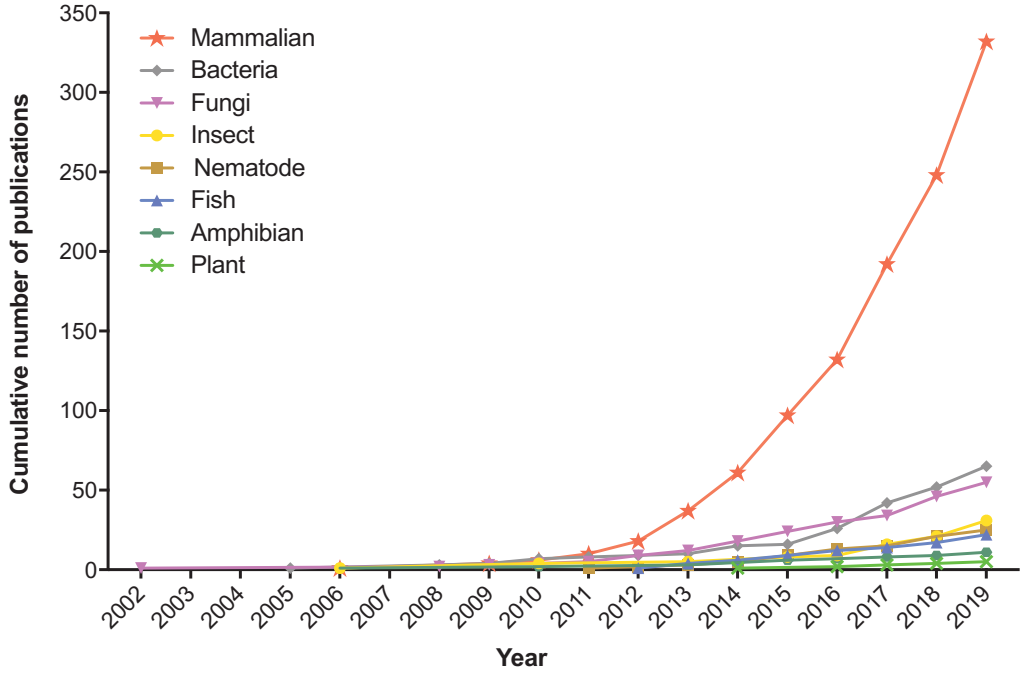


**Figure 1**. Cumulative number of the original research publications of optogenetic systems implemented in individual types of host cell lines or organisms. Data obtained from www.optobase.org/statistics on December 2019.

## 2.2. *Families of photoreceptors: classification and general mode of function*

Optogenetic tools are based on the use of proteins that are able to sense and respond to light. These proteins, the photoreceptors, contain a chromophore

that is responsible for the perception of different light wavelengths. Photoreceptors exist in multiple organisms spread among all kingdoms but are especially numerous in plants, bacteria, and fungi. The optogenetic switches based on these natural or engineered photoreceptors have a different mode of function, ultimately depending on the properties of the photoreceptor. They are classified according to their responsiveness to different wavelength ranges: i) ultraviolet light (Kianianmomeni, 2014), *e.g.* UVR8; ii) blue light (Fujisawa and Masuda, 2018; Herrou and Crosson, 2011), *e.g.* LOV (Light-Oxigen-Voltage) and BLUF (Blue Light Using FAD) domains, and cryptochromes, (using flavin mononucleotide FMN or flavin adenine dinucleotide FAD as chromophore); iii) green light, *e.g.* cobalamin-binding domains like CarH (cobalamin Cbl as cofactor); iv) red and far-red light (Burgie and Vierstra, 2014), such as plant phytochromes (Phycocyanobilin PCB or Phytochromobilin PΦB as chromophore) and bacteriophytochromes (biliverdin BV as chromophore); as well as, v) a range of cyanobacterial photoreceptors that absorb in violet, green and red light (using PCB as chromophore) (Anders and Essen, 2015). Some of the existing optogenetic switches, based on several different photoreceptors and their respective chromophores, are depicted in Figure 2, categorized by their light wavelength of activation or deactivation.

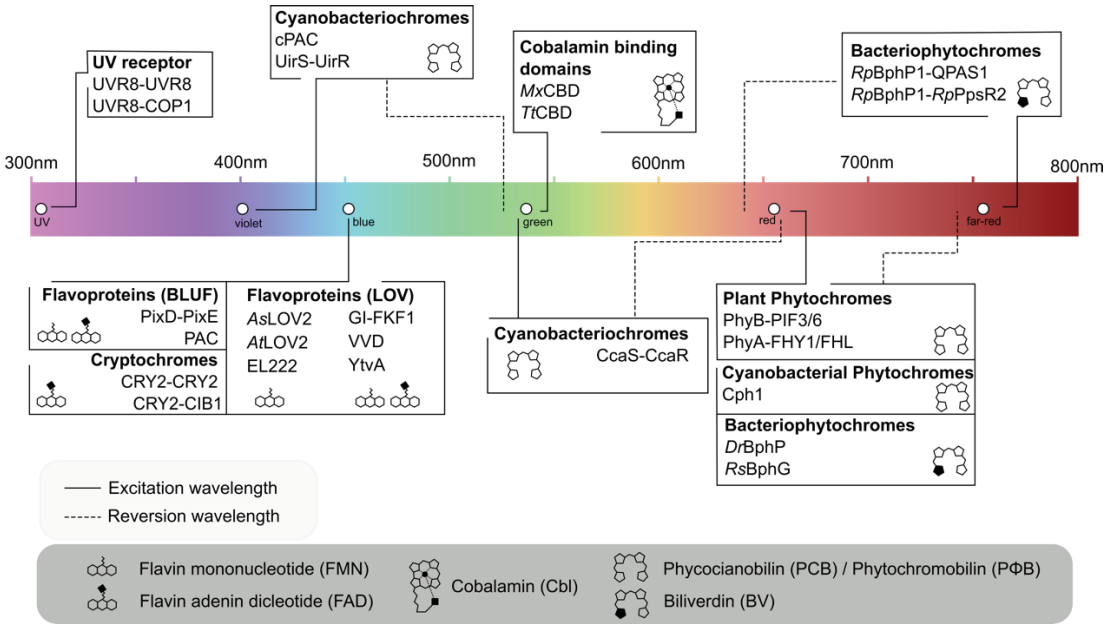


**Figure 2**. Overview of some of the available optogenetic switches (opsins and fluorescent proteins are excluded). The photoreceptors and their respective chromophores, are indicated, as well as the light

wavelength of activation or deactivation. *As*LOV2, LOV2 domain of *Avena sativa* phototropin 1; *At*LOV2, LOV2 domain of *Arabidopsis thaliana* phototropin 1; BLUF, blue light using FAD; PAC, photoactivated adenylyl cyclases; CcaS-CcaR; *Synechocystis sp.* cyanobacteriochrome two component system; CIB1, *A. thaliana* CRYPTOCHROME-INTERACTING BASIC HELIX-LOOP-HELIX 1; COP1, *A. thaliana* CONSTITUTIVELY PHOTOMORPHOGENIC 1; cPAC, cyanobacteriochrome-based photoswitchable adenylyl cyclases; Cph1, *Synechocystis sp.* cyanobacterial phytochrome 1; CRY2, *A. thaliana* CRYPTOCHROME 2; *Dr*BphP, *Deinococcus radiodurans* bacteriophytochrome; EL222; *Erythrobacter litoralis* transcription factor 222; FHL, *A. THALIANA* FAR-RED ELONGATED HYPOCOTIL 1-LIKE; FHY1, *A. thaliana* FAR-RED ELONGATED HYPOCOTIL 1; FKF1, *A. thaliana* FLAVIN BINDING, KELCH REPEAT, F-BOX1; GI, *A. thaliana* GIGANTEA; LOV, light-oxygen-voltage domain; *Mx*CBD, *Myxococcus xanthus* cobalamin binding domain; PhyA, *A. thaliana* Phytochrome A; PhyB, *A. thaliana* Phytochrome B; PIF3, *A. thaliana* PHYTOCHROME-INTERACTING FACTOR 3; PIF6, *A. thaliana* PHYTOCHROME-INTERACTING FACTOR 6; QPAS1, engineered interaction partner of *Rp*BphP1 containing PAS1 domain from *Rs*PpsR; *Rp*BphP1, *Rhodopseudomonas palustris* bacteriophytochrome P1; *Rp*PpsR2, *Rhodopseudomonas palustris* transcriptional repressor; RsBphG, *Rhodobacter sphaeroides* bacteriophytochrome G; *Tt*CBD, *Thermus thermophilus* cobalamin binding domain; UirR-UirS, *Synechocystis sp.* cyanobacteriochrome two component system; VVD, Vivid; UVR8, *A. thaliana* UV resistance locus 8; YtvA, *Bacillus subtilis* blue light photoreceptor; PixD-PixE, cyanobacteriochrome two component system.

With the exception of the opsins, the general gating mechanism of these photoreceptors can be divided as follows. After light absorption by its chromophore they undergo a conformational change that leads to: a) changes in the enzymatic activity, like nucleotide cyclases (PAC and *Rs*BphG), or kinase activity (CcaS-CcaR, UirS-UirR, Cph8(Cph1)-OmpR, YF1(YtvA)-FixJ) (Figure 3a); b) uncaging, like in the case of *As*LOV2 and *At*LOV2 (Figure 3b); c) protein-protein interaction by heterodimerization like PhyB-PIF3/6, GI-FKF1, PhyA-FHY1/FHL, or by homodimerization as for Cph1, YtvA, VVD, EL222, *Dr*BphP; or several configurations like tetramerization and dissociation (MxCBD, TtCBD), oligo- and heterodimerization (CRY), hetero- and homodimerization (UVR8, *Rp*BphP1) (Figure 3c) (Liu et al., 2018; Losi et al., 2018; Mathes, 2016; Tischer and Weiner, 2014; Toettcher et al., 2011a; Zhang and Cui, 2014).

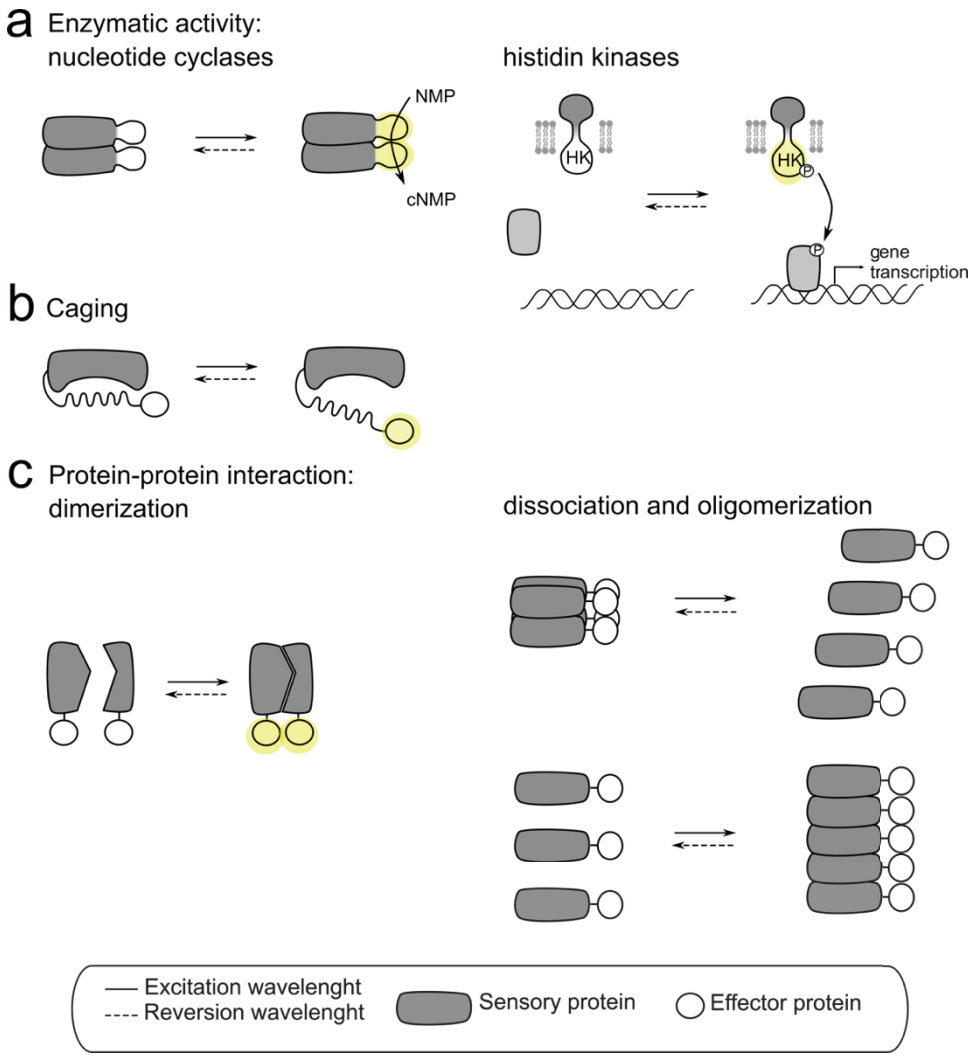


**Figure 3**. General mode of function of optogenetic switches. Photoinduced conformational change by the photoreceptor or sensory protein leads to: **(a)** enzyme activation of nucleotide cyclases (left), or histidine kinases (HK) that in turn phosphorylates a protein (response regulator, RR) which activates transcription (right), **(b)** uncaging of a fused protein releasing its activity**, (c)** protein association by homodimerization, heterodimerization (left) or oligomerization and dissociation (right). The effector protein could be any protein of interest, including often DNA binding domains or transcription activation domains and also enzymes or localization/trafficking signal peptides. Yellow shading depicts active effector protein. NMP, nucleotide monophosphate; cNMP, Cyclic nucleotide monophosphate.

Other optogenetic switches comprise fluorescent proteins such as PYP (Morgan and Woolley, 2010) and Dronpa (Zhou et al., 2012). A set of opsins to control ion channels in different wavelengths have also been developed (Deisseroth and Hegemann, 2017; Fenno et al., 2011).

Drawbacks of using light switches are the limitations in their natural availability or the delivery of the necessary chromophore. The blue light switches based

on LOV, CRY and BLUF photoreceptors do not require supplementation with the chromophore, as FMN and FAD are endogenously present in all organisms. Contrarily, when applying cobalamin-using photoreceptors, the Cbl must be added to both animals and plants, as the chromophore is not present in these hosts. For the switches using PCB or PΦB as cofactors, like plant or cyanobacterial phytochromes, supplementation when using these switches in yeast or animal cells is required, although not necessary in plants, algae, and cyanobacteria, where the chromophore is already present (Porra and Grimme, 1978; Tanaka and Tanaka, 2007). In the case of other chromophores like biliverdin used by the bacteriophytochromes, it does not need to be supplemented when applied to eukaryotes as it is already present in plants and animals.

The addition of the chromophore is a limitation for the application of optoswitches *in vivo* in animal models as well. However, some strategies have been applied to tackle this limitation such as the engineering of the PCB biosynthesis pathway in bacteria and mammalian cells in order to use PhyB-PIF systems without exogenous chromophore addition (Müller et al., 2013a; Uda et al., 2017).

Chromophore supplementation is something to consider when selecting an optoswitch, especially when applied to multicellular organisms, as it could lead to the same limitations as chemical-inducible systems in terms of control of induction. Additionally, the physical properties of light have to be taken into account. Shorter wavelengths, like UV light, have higher energy leading to potential phototoxicity, depending on the light-sensitivity of the model being used. Longer wavelengths on the other hand, like near-infrared light, have better tissue penetration than shorter wavelengths, being particularly relevant for *in vivo* applications.

## *2.3. Applications of optogenetic tools*

Optogenetic tools have been used for a broad set of applications. Some examples at the protein manipulation level include the control of protein degradation and stability (Mills and Truong, 2013; Renicke et al., 2013;

Usherenko et al., 2014), modulation of signalling cascades (Moser and Esser-Kahn, 2017; O'Banion et al., 2018; Toettcher et al., 2011b; Wend et al., 2014), and the regulation of intracellular protein localization, including but not limited to nuclear import and export (Beyer et al., 2015; Niopek et al., 2014, 2016), and protein recruitment to control cytoskeleton reorganization, cell motility and shape, and organelle positioning (Adrian et al., 2017; van Bergeijk et al., 2015; Shi et al., 2018).

At the gene expression level, a wide set of light-responsive tools allow gene expression control (endogenous gene or transgene expression), epigenetic modifications, and genome editing (Hughes, 2018; de Mena et al., 2018; Müller et al., 2015). Some examples applied to different hosts and using different activation wavelengths are listed in Table 1. These tools comprise chimeric transcription factors in which one light-dependent interactor is fused to a protein that binds DNA and the other interactor is fused to an effector protein that can be a transactivation domain (AD), a repressor domain (RD), or epigenetic modifiers. For the DNA-binding specificity, a DNA-binding domain (DBD) and an engineered synthetic promoter with the cognate sequence of the DBD can be used (Figure 4a). Alternatively, by using ZF or TALE domains, it becomes possible the control transcription of endogenous genes as it can be customized to bind a DNA sequence of interest (Figure 4a). This strategy can also be achieved by using nuclease-deficient Cas9 (dCas9). The two interactor modules react upon illumination, which triggers protein-protein association or dissociation, allowing repression/activation of the gene of interest (Figure 4a).

Additionally, light-inducible gene editing can be achieved by using split Cas9, where the protein is divided into two non-functional parts fused to light-dependent interactors. Illumination reconstitutes the nuclease activity, allowing targeted DNA cleavage and resulting in deletion, insertion or mutation of the gene of interest (Figure 4b). Similarly, some strategies use split recombinases fused to light-dependent interactors, that are only active when the recombinase is reconstituted upon illumination, then being able to recognize the specific target sites and cut out a part of the synthetic DNA (Figure 4c).

**Table 1**. Examples of optogenetic approaches for controlling gene expression using different approaches, photoreceptors and applied to different hosts.

| Approach | Light | Optogenetic switch | Applied to host |
|---|---|---|---|
| **DNA-binding domain and synthetic promoter** | UV | UVR8 (Crefcoeur et al., 2013; Müller et al., 2013b) | E.coli (Levskaya et al., 2005; Ohlendorf et al., 2012; Tabor et al., 2011) and B.subtilis (Castillo-Hair et al., 2019), *S. cerevisiae* (Crefcoeur et al., 2013; Kennedy et al., 2010; Shimizu-Sato et al., 2002), Zebrafish *in vivo* (Motta-Mena et al., 2014), mammalian cells (Crefcoeur et al., 2013; Kennedy et al., 2010; Konermann et al., 2013; Motta-Mena et al., 2014; Müller et al., 2013c, 2013b, 2014a; Quejada et al., 2017; Redchuk et al., 2017, 2018a, 2018b; Wang et al., 2012), mouse *in vivo* (Konermann et al., 2013; Redchuk et al., 2018b; Wang et al., 2012), *C. reinhardtii (Wang et al., 2017)*, *P. patens* and *N. tabacum* protoplasts (Müller et al., 2014b), Arabidopsis protoplasts (Chatelle et al., 2018; Ochoa-Fernandez et al., 2016) |
| | Blue | EL222 (Motta-Mena et al., 2014)<br>AsLOV2 (Müller et al., 2014a)<br>YtvA (Ohlendorf et al., 2012)<br>VVD (Wang et al., 2012)<br>CRY2-CIB1 (Kennedy et al., 2010; Quejada et al., 2017)<br>FKF1-GI (Quejada et al., 2017) | |
| | Green | CcaS-CcaR (Castillo-Hair et al., 2019; Tabor et al., 2011)<br>TtCBD (Chatelle et al., 2018) | |
| | Red | PhyB-PIF6 (Müller et al., 2013c, 2014b)<br>PhyB-PIF3 (Shimizu-Sato et al., 2002)<br>Cph1 (Levskaya et al., 2005) | |
| | Far-red | BphP1 (Redchuk et al., 2017, 2018a, 2018b) | |

| | | | |
|---|---|---|---|
| **Cas9** | Blue | RsLOV (Richter et al., 2016)<br>AsLOV2 (Bubeck et al., 2018; Nguyen et al., 2018)<br>EL222 (Reade et al., 2017)<br>CRY2-CIB1 (Nihongaki et al., 2015a, 2015b, 2017; Polstein and Gersbach, 2015; Putri and Chen, 2018; Takayama and Mizuguchi, 2018; Zhou et al., 2018) | *E. coli* (Richter et al., 2016), Zebrafish *in vivo* (Reade et al., 2017) or cells (Putri and Chen, 2018), mammalian cells (Bubeck et al., 2018; Nguyen et al., 2018; Nihongaki et al., 2015a, 2015b, 2017; Polstein and Gersbach, 2015; Takayama and Mizuguchi, 2018; Zhou et al., 2018), mouse *in vivo* (Shao et al., 2018; Takayama and Mizuguchi, 2018) |
| | Far-red | BphS (Shao et al., 2018) | |
| **TALE and ZF** | Blue | CRY2-CIB1 (An-adirekkun et al., 2019; Konermann et al., 2013; Lo et al., 2017)<br>FKF1-GI (Polstein and Gersbach, 2012) | *S. cerevisiae* (An-adirekkun et al., 2019), mammalian cells (Konermann et al., 2013; Lo et al., 2017; Polstein and Gersbach, 2012), mouse *in vivo* (Konermann et al., 2013) |
| **Recombinases** | Blue | CRY2-CIB1 (Jung et al., 2019; Kawano et al., 2016; Kennedy et al., 2010; Meador et al., 2019; Schindler et al., 2015; Taslimi et al., 2016) | *S. cerevisiae* (Hochrein et al., 2018; Kennedy et al., 2010; Taslimi et al., 2016), mammalian cells (Jung et al., 2019; Kawano et al., 2016; Kennedy et al., 2010; Meador et al., 2019; Taslimi et al., 2016), mouse *in vivo* (Jung et al., 2019; Kawano et al., 2016; Meador et al., 2019; Schindler et al., 2015) |
| | Red | PhyB-PIF3 (Hochrein et al., 2018) | |

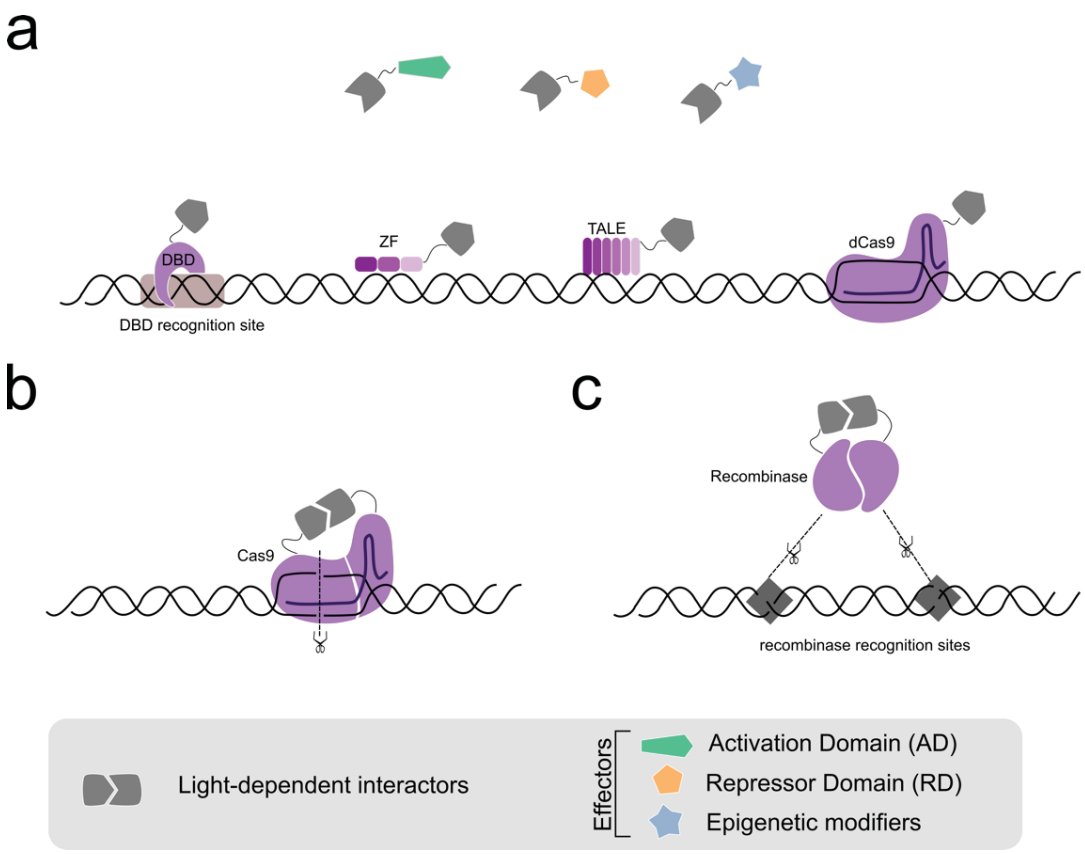


**Figure 4**. Strategies to control gene expression with light. **(a)** Chimeric transcription factors, where one of the light-dependent interactors is fused to an effector domain that can be an activator (AD), repressor (RD) or epigenetic modifier. The other light-dependent interactor is fused to either a DNA-binding domain (DBD) that targets a specific motif, or Zinc-fingers (ZF), Transcription activation like-effectors (TALE), and nuclease-deficient Cas9 and gRNA complex (dCas9-gRNA) that can be designed to target and bind a DNA sequence of interest. **(b)** Split Cas9 that is reconstituted upon association of the light-dependent interactors, restoring the nuclease activity. **(c)** Split recombinase that is reconstituted upon association of the light-dependent interactors, restoring the recombinase activity.

# 3. Applying optogenetic tools in plants

## *3.1. Plant chassis for optogenetics*

Several plant experimental platforms are currently in use for plant synthetic biology (Boehm et al., 2017) and can be considered for the implementation and characterization of optogenetic tools.

### *3.1.1. Plant protoplasts*

Plant protoplasts can be obtained from different tissues, keeping their tissue identity while offering a cell-based experimental setup. There are protocols

established for different species (Davey et al., 2005), including *Nicotiana tabacum* and *Arabidopsis thaliana*. They offer a set of advantages: the isolation and transient transformation is well-established, robust and fast, they have a high capacity of DNA co-transformation (co-transformation of several plasmids with varying DNA ratios is possible), testing of many different conditions is possible, the lack of cell wall facilitates the uptake of chemicals, and reporter genes such as luciferases can be measured directly and simply by applying the appropriate substrate. Although the expression of proteins can be monitored for hours, allowing kinetics experiments, this is limited to transient expression and the cells cannot be kept for long periods. They can be kept up to one week but it can be challenging to maintain their quality (Hansen and van Ooijen, 2016).

Protoplasts have been used to investigate signalling pathways (Sheen, 2001; Wang et al., 2005) as well as to test genetic parts and devices aided by mathematical modelling to normalize the variability observed in the data and predict their behaviour (Müller et al., 2014b; Schaumberg et al., 2016).

### *3.1.2. Leaf transient expression in Nicotiana*

*Nicotiana benthamiana* is becoming a platform of interest for the community, especially in the context of the transient transformation of their leaves. The transformation is mediated by Agrobacterium infiltration and is a well-established method, which allows the delivery of several genes, and therefore for a high capacity of screening DNA parts/devices, in a time-saving manner (Sainsbury and Lomonossoff, 2014). There are several efforts towards the refinement of the experimental conditions to make it more robust (Vazquez-Vilar et al., 2017). Additionally, a library of vectors for the Agrobacterium-mediated delivery of characterized DNA parts and devices has been generated (www.gbcloning.upv.es), including tools for the use of CRISPR/Cas technologies (Selma et al., 2019; Vilar et al., 2016).

Nicotiana is also a chassis with growing relevance in the recombinant protein production field. It has been used for the production of artemisinin precursors (van Herpen et al., 2010; Ikram and Simonsen, 2017), triterpenes (Thimmappa

et al., 2014) and vaccines (Boes et al., 2016; D'Aoust et al., 2008; Mardanova et al., 2017), among others.

### *3.1.3. Bryophytes*

Other plant chassis that is becoming more popular within plant synthetic biology are the liverwort *Merchantia polymorpha* (Delmans et al., 2017; Ishizaki et al., 2008) and the moss *Physcomitrella patens* (Reski et al., 2018). Their culture is easy to handle and versatile, as they can be cultivated in suspension, on plates or in soil. They possess less genome redundancy in comparison to higher plants while preserving conserved pathways/regulatory mechanisms which could be interesting for basic research. They have short life cycles (typically 2-3 months to complete the whole life cycle), which is relevant for stable transformants generation. Moreover, there are well-established gene transformation methods for both models and they are easy to engineer, not to mention the recently developed tools based on the CRISPR/Cas9 technology (Mallett et al., 2019; Sugano et al., 2018). Additionally, the moss *P. patens* raises biotechnological interest as it is used in recombinant protein production (Liénard and Nogué, 2009; Reski et al., 2015).

### *3.1.4. Arabidopsis*

*A. thaliana* has been widely used for plant biology research to study. There is an extensive array of developed methods, genetic resources, and libraries of gene knock-outs and transgenic lines. Also, this plant model has profited from the synthetic approaches to create novel functionalities by engineering novel genetic, signalling and metabolic pathways (Provart et al., 2016). Representative examples are a re-engineered ABA receptor that responds to an agrochemical in order to improve the stress tolerance of the plant (Park et al., 2015) or Arabidopsis used as a plant "sentinel" for TNT detection (Antunes et al., 2011).

## *3.2. Limitations, challenges, and perspectives*

To date, only a few optogenetic switches have been applied in plant systems (see Figure 1 and Table 1). The first one implemented is a red light-inducible switch to control gene expression in plant mesophyll protoplasts, relying on a split transcription factor composed by phytochrome B (PhyB) and one of the phytochrome interacting factors (PIF6) (Müller et al., 2014b). However, the application of such a tool, based on the red/far-red light-responsive PhyB-PIF6 optoswitch, is currently limited to transiently transformed plant cells, where the illumination conditions can be controlled and accidental activation by white light can be avoided. Another example is the control of the stomata opening using a blue light-inducible $K^+$ channel (BLINK1) in Arabidopsis that allows having a faster opening and closing of the stomata, improving the water usage of the plant (Papanatsiou et al., 2019). This is an example of the application of an optogenetic tool *in planta*, where daylight- or photosynthesis-dependent activation is desired. However, it also illustrates the limitations in applicability, where the normal light cycle my interfere with the optogenetic tool, depending on the cellular process of interest. Nonetheless, these pioneering approaches illustrate the potential that optogenetics applications in plants could offer, opening up novel and varied possibilities for this research area.

There are limitations when applying these tools to phototrophic organisms that rely on light and are able to perceive it with their intrinsic photoreceptors. The application of general optogenetic switches *in planta* is limited by the fact that there will be activation of the switch under standard plant growth light conditions. Additionally, accomplishing orthogonality in plant systems will be hard to achieve as, highlighted in the above examples, several of these optoswitches are based on plant photoreceptors.

A partial solution would be the use of photoreceptors from other organisms that are orthogonal to the chassis plant and/or photoreceptors that respond to light in a region of the spectrum that minimizes pleiotropic effects in the plant, avoiding unwanted effects. Other approaches to solve these limitations could include the combination with chemical systems. The latter can be used to

control the expression of the optogenetic tools, similarly to the work performed by Chen and colleagues in mammalian systems (Chen et al., 2015). An alternative approach could be the combination of different photoreceptors to accomplish a system that will be only active upon illumination with a certain wavelength of interest, but not under white or ambient light.

These tools, once optimized for use in whole plants, will be the next breakthrough for plant research. They will constitute an enabling technology to control and, therefore, investigate different cellular and developmental processes, becoming an essential aspect for basic plant research. Furthermore, it will provide a unique opportunity to control traits for generating “smart plants”. This thesis will present some of the efforts towards the development of mono- and multichromatic control of gene expression tools in plants and show the first steps towards their application *in planta*.

# II. Aims

This work addresses the challenge of applying optogenetic tools in plant biology research. The specific aims of this thesis are defined as:

- Plant protoplasts as a standard platform for the characterization of optogenetic tools: To establish, optimize, and standardize a method that allows a fast and easy screening and characterization of optogenetic tools.
- Optogenetics toolbox for plant cells: Expanding the current optogenetic switches toolbox available to mainly regulate gene expression in plant cell systems.
- Optogenetics to regulate gene expression *in planta*: Developing an optogenetic system for *in planta* use that is inactive in white ambient light and only active upon illumination with a single wavelength for on command regulation.

# III. Results and discussion

# 4. Chapter 1: Protoplasts as a platform to screen optogenetic tools

Ochoa-Fernandez, R., Samodelov, S.L., Brandl, S.M., Wehinger, E., Müller, K., Weber, W., and Zurbriggen, M.D. (2016). Optogenetics: Methods and Protocols. A. Kianianmomeni, ed. (New York, NY: Springer New York), pp. 125–139. (Appendix A)

In order to prototype optogenetic tools in plants, a platform based on transiently transformed plant cells from *Arabidopsis thaliana* was established. This is a suitable platform because the protoplast isolation and transformation are well established, yielding fast and reproducible results. Additionally, the high transformation efficiency allows for combinatorial DNA transformations. The setup allows having multiple transformations that can be subjected to different illumination treatments and kinetics set-up (dose-time response experiments). It also allows easy quantification of reporter genes, like luciferases, without cell disruption techniques being needed.

Figure 5 depicts a summarized workflow for the isolation and transformation of protoplasts of *A. thaliana* and the setup for a standard light-inducible gene expression experiment.

To validate this method in a typical optogenetic setup, the red light-inducible/far-red light-reversible system, already established in mammalian and tobacco cells (Müller et al., 2014b), was transformed in leaf protoplasts of *A. thaliana* (Figure 6). This switch functions as a chimeric transcription factor, based on a truncated version of phytochrome B – $PhyB_{(1-650)}$ – fused to the herpes simplex virus VP16 transactivation domain, and a truncated version of a phytochrome-interacting factor – $PIF6_{(1-100)}$ – fused to the macrolide repressor DNA-binding protein (E). A nuclear localization sequence (NLS) was included in both components in order to ensure localization in the nucleus. Both components are under the control of the cauliflower mosaic virus ($P_{CaMV35S}$). The E protein binds a sequence (etr) that is placed upstream of the minimal human cytomegalovirus promoter ($P_{hCMVmin}$), driving the expression of a gene of interest, here Firefly Luciferase (FLuc) which allows fast and easy quantification (Figure 6a). Upon exposure to red light, PhyB changes its conformation by photoisomerization of the covalently bound chromophore, phytochromobilin (PΦB). The activated form of PhyB ($PhyB_{fr}$) binds to PIF6 and the VP16 domain is then recruited to the etr motif in close proximity to the minimal promoter, activating transcription of the reporter gene. The PhyB-PIF6 association is readily reversed upon exposure to far-red light or darkness,

when PhyB changes its conformation to the inactive form ($PhyB_r$), resulting in the termination of reporter gene expression (Figure 6a).

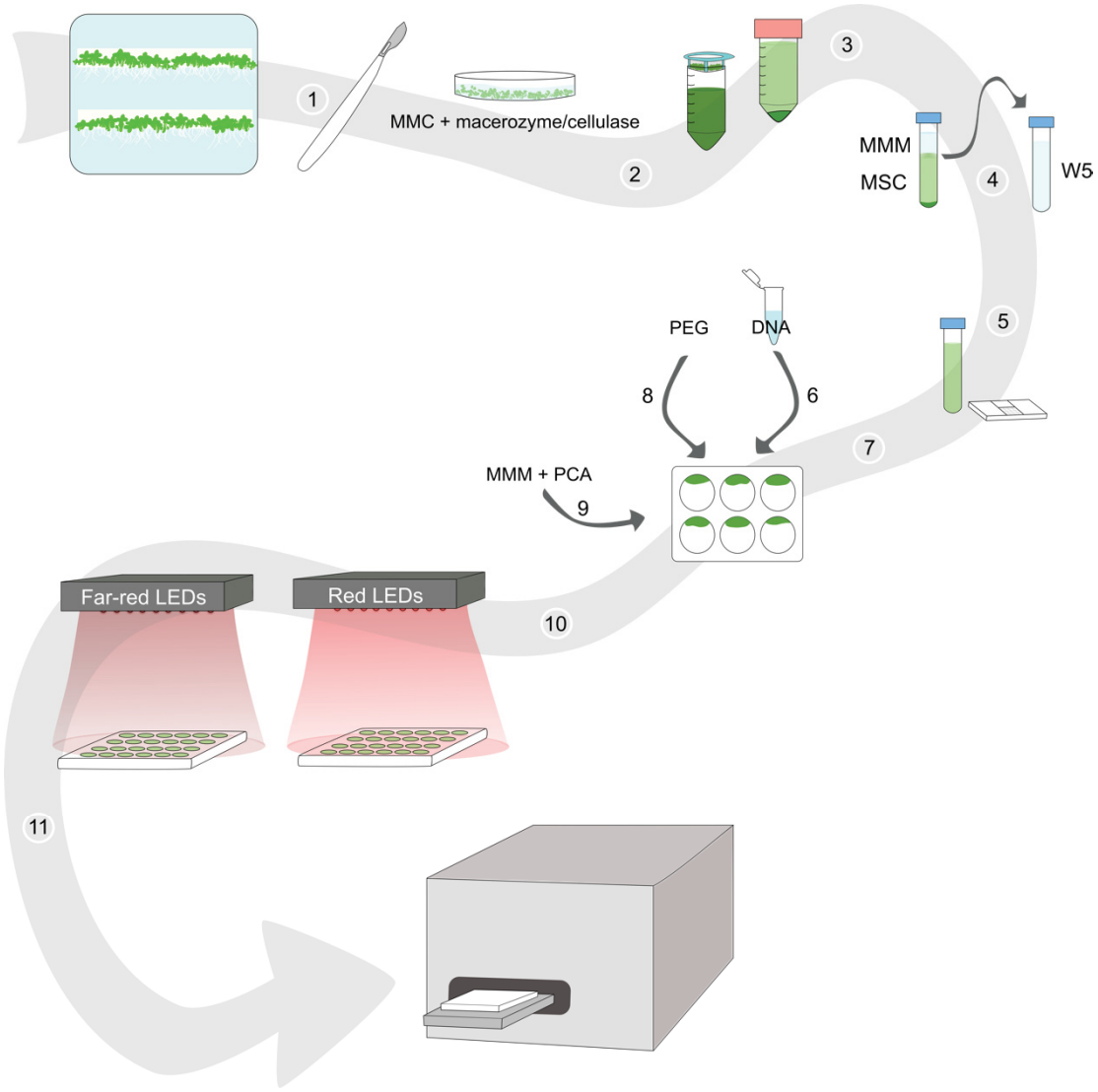


**Figure 5**. Workflow of Arabidopsis protoplasts isolation, transformation, and experimental setup. (1) The leaves of ~2 week old plantlets are cut and incubated overnight with macerozyme and cellulase in MMC medium. (2) The protoplasts are released by pipetting and filtered by a 70 µm strainer to remove the debris. The suspension is then centrifuged. (3) Resuspension of the pellet in MSC medium and careful addition of MMM medium generates an interphase after centrifugation. (4) The interphase is collected after each of three consecutive rounds of centrifugation and placed in W5 medium. (5) The concentration of the protoplast suspension is determined using a counting chamber. (6) The preparations of DNA to a final amount of 30 µg are pipetted in each well of a 6-well plate, in a final volume of 20 µl. If several plasmids are co-transformed the final DNA amount is kept constant, adjusting the amount of each plasmid and a stuffer plasmid when necessary. (7) The protoplast suspension is centrifuged and resuspended in MMM medium to a total of 5000 protoplasts/µl. Then, 100 µl of protoplast suspension is added into the DNA and incubated for 5 min. (8) 120 µl of PEG solution is added in a dropwise manner.

(9) 120 µl of MMM medium followed by 1240 µl of PCA medium is added. (10) The protoplasts are divided in 24-well plates that will be placed under the different LED arrays for each treatment. (11) Samples are taken at the desired time point(s). 80 µl/replicate are transferred into a white flat bottom 96 well-plate and 20 µl of luciferase substrate are added prior to quantification of luminescence in a plate reader.

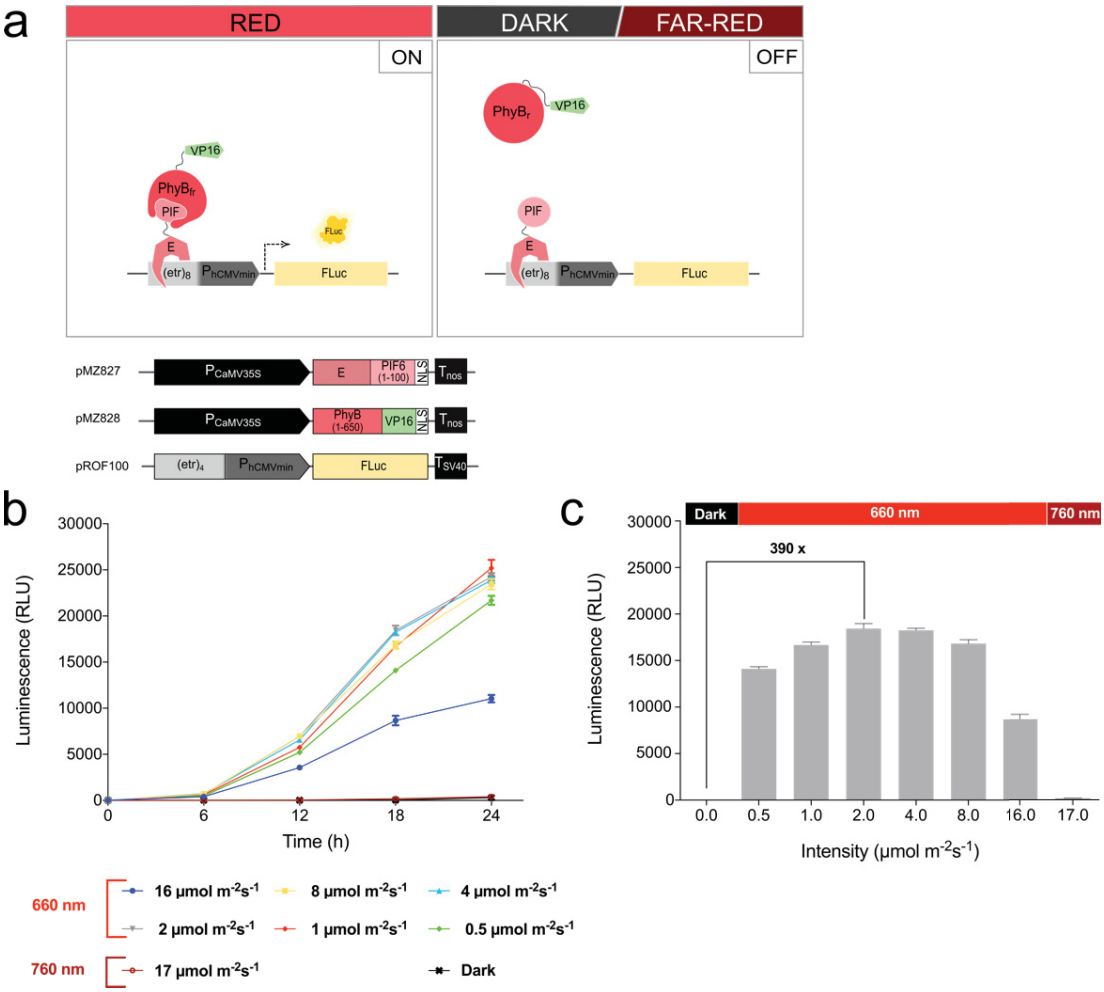


**Figure 6**. Design, time- and dose-response curves of the red light-inducible gene expression system in protoplasts of *A. thaliana*. **(a)** Configuration of the vectors and mode of function. The components of the system are: i) the first 100 amino acids of phytochrome-interacting factor - $PIF6_{(1\text{-}100)}$ - fused to the macrolide repressor DNA-binding protein E and a nuclear localization sequence (NLS), ii) the first 650 amino acids of the phytochrome B - $PhyB_{(1\text{-}650)}$ - fused to the herpes simplex VP16 transactivation domain and an NLS, iii) multiple repetitions of an etr motif, cognate binding site of the E protein, placed upstream of a CMV minimal promoter followed by the reporter gene firefly luciferase (FLuc). Upon exposure to red light, PhyB changes its conformation to its active form ($PhyB_{fr}$) that promotes the interaction with PIF6 and therefore recruitment of the transactivator VP16 domain to the minimal promoter. FLuc is expressed as a consequence. Upon far-red light ($\lambda_{max}$ 760 nm) exposure or darkness incubation, PhyB is converted back to its inactive form ($PhyB_r$), PhyB-PIF6 dissociates, thus ceasing the transcription of the reporter gene. **(b,c)** Protoplasts from *A. thaliana* were transformed for red light-inducible FLuc expression (pMZ827, pMZ828, and pROF100). After transformation, 3.5 ml aliquots of protoplast suspensions

containing approximately 1.09 × $10^6$ protoplasts, were illuminated either at different intensities of red light ( $\lambda_{max}$ 660 nm; 0.5, 1, 2, 4, 8, and 16 µmol $m^{-2}$ $s^{-1}$), far-red light ( $\lambda_{max}$ 760 nm; 17 µmol $m^{-2}$ $s^{-1}$), or were kept in the dark as a control. **(b)** Samples were taken at the indicated points in time (0, 6, 12, 18, and 24 h after transformation) and FLuc expression was determined. The graph shows the reporter luminescence values at different time points and light intensities. **(c)** Reporter luminescence values after 18 h expression at the indicated light intensities. **(b,c)** Data are means ± SEM of technical replicates (*n* = 6). RLU = Relative Luminescence Units. Adapted from Ochoa-Fernandez *et al.* (Ochoa-Fernandez et al., 2016).

Time-course and dose-response curves for the red light-inducible gene expression system in *A. thaliana* leaf protoplasts are exemplified in Figure 6b,c. Protoplasts were isolated from *A. thaliana* plantlets and 10 µg of each plasmid (pMZ827, pMZ828 and pROF100) were used for the transformation. Several transformations were made in parallel (22 transformations) and pooled together afterwards. Aliquots of 3.5 ml of the protoplasts suspension were transferred into one well of seven different 6-well plates (one plate for each illumination condition). The luminescence determinations were made for each condition at different points in time (0, 6, 12, 18, and 24 h). As a dark control, 1 ml of protoplast suspension was transferred into one well of four different 24-well plates. In this way, a single plate per time point was used and accidental exposure of the plate to ambient light avoided. The results of the kinetics and expression levels of the red light-inducible system in *A. thaliana* protoplasts (depicted in Figure 6b) indicate the optimal illumination conditions for maximum expression rates are between 1 and 4 µmol $m^{-2}$ $s^{-1}$. The highest expression levels are achieved at 24 h but a better dynamic range (399- and 395-fold induction) is obtained at 18 h of gene expression for 2-4 µmol $m^{-2}$ $s^{-1}$ red light intensities (Figure 6c).

These results are also highlighting the fact that protoplasts are sensitive to small light intensity changes, which is useful for dose-response experiments. It provides an easy set-up for time-course experiments, quantitative results, and a robust system for multiple plasmids transformations and test conditions. For all these reasons, this platform can be useful to re-design, build and test the switches, therefore fueling the “Design-Build-Test” of synthetic biology. The method here described is fundamental to the rest of the work presented in this thesis.

# 5. Chapter 2: Expanding the toolbox of optogenetics in Plant Synbio

Chatelle, C., Ochoa-Fernandez, R., Engesser, R., Schneider, N., Beyer, H.M., Jones, A.R., Timmer, J., Zurbriggen, M.D., and Weber, W. (2018). A Green-Light-Responsive System for the Control of Transgene Expression in Mammalian and Plant Cells. ACS Synth. Biol. *7*, 1349–1358. (Appendix A)

Ochoa-Fernandez, R., Schuler-Bermann, M., Zurbriggen, M.D. Expanding the toolbox of optogenetic switches for red and blue light control of gene expression in plant cells. *Manuscript in preparation.* (Appendix A)

Ochoa-Fernandez, R., Abel, N.B., Wieland, F.G., Schlegel, J., Koch, L.A., Miller, J.B., Engesser, Giuriani, G., R., Brandl, S.M., Plum, J. Timmer, J., Weber ,W., Ott, T., Simon, R., and Zurbriggen, M.D. PULSE – Optogenetic control of gene expression in plants in the presence of ambient white light. *Manuscript submitted.* (Appendix A)

## *5.1. Green light-inducible system to control gene expression*

Green light-inducible systems are of interest for application in plants due to the lesser effect of green light on endogenous plant photoreceptors and to the fact that green light available photoreceptors are orthogonal to Arabidopsis. A green light-inducible system that is ON in the dark and is turned off when illuminated with green light was intended for implementation in plant cells. After its implementation and characterization in mammalian cells, the suitability for controlling gene expression in plant cells was evaluated. A new set of plasmids for its application in plant cells was re-engineered and co-transformed in the *A. thaliana* plant protoplasts.

The plasmids comprised the transcription factor CarH from *Thermus thermophilus* fused to a VP16 domain and a synthetic promoter containing, the operator region where CarH binds - CarO - followed by a minimal promoter controlling the expression of the reporter gene FLuc. In darkness, CarH linked to the coenzyme cobalamin forms tetramers that bind the DNA operator CarO, therefore activating expression of FLuc. Upon illumination with UV, green, or blue light, these tetramers dissociate and release from the DNA, due to photolysis of the Cobalamin-C bond (Jost et al., 2015), therefore halting FLuc expression (Figure 7a).

Isolated protoplasts from *A. thaliana* were co-transformed with the reporter module carrying either two, four or eight repeats of the operator CarO – $(CarO)_2$, $(CarO)_4$, $(CarO)_8$ – with either CarH-VP16 or with a stuffer plasmid. After transformation, AdoCbl was added to a final concentration of 20 µM and cells were incubated for 24 h either in darkness or illuminated with green light ($\lambda_{max}$ 525 nm light, 5 µmol $m^{-2}$ $s^{-1}$). The overall expression of the switch was low to moderate in terms of total FLuc expression in darkness, but increasing amounts of CarO repeats in the reporter plasmid yielded increasing amounts of FLuc expression and a higher dynamic range. A maximum of 15.7-fold induction, comparing illuminated protoplasts to those kept in the dark, was achieved when co-transforming CarH-VP16 with the reporter module containing $(CarO)_8$ (Figure 7b).

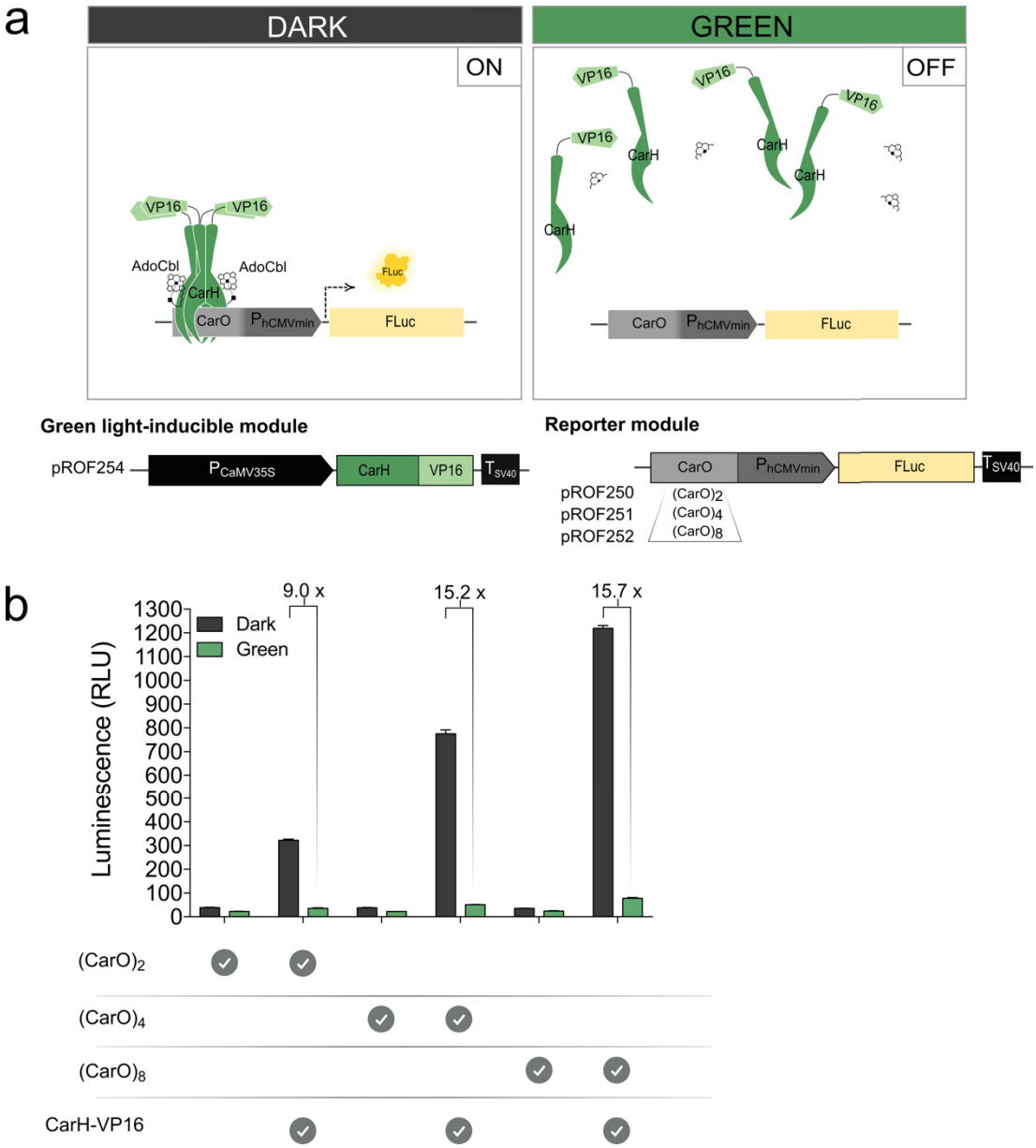


**Figure 7**. Design of the green-light-responsive gene expression system and characterization in *A. thaliana* protoplasts. **(a)** Molecular components and mode of function of the expression system. The components engineered and characterized in plant cells are: i) the green light-responsive photoreceptor CarH fused to an activation domain VP16 and placed under the control of the constitutive promoter $P_{CaMV35S}$, and ii) a promoter composed of multimeric CarO sequences upstream of a minimal promoter $P_{hCMV}$, driving the expression of the reporter gene Firefly Luciferase (FLuc). The light sensitivity of the system is conferred by the chromophore adenosylcobalamin (AdoCbl). In the dark, CarH-VP16 bound to AdoCbl forms tetramers that bind CarO starting the transcription of FLuc. Exposure to green light leads to photolysis of AdoCbl, triggering destabilization of CarH tetramers and the release of CarO, therefore halting FLuc expression. **(b)** Reporter plasmids with increasing numbers of CarO repeats - $(CarO)_2$, pROF250; $(CarO)_4$, pROF251; $(CarO)_8$, pROF252 - were transformed in a 3:1 molar ratio to the CarH-VP16 expression plasmid (pROF254) in protoplasts of *A. thaliana*. After transformation, protoplasts were supplemented with AdoCbl to a final concentration of 20 µM. After incubation for 24 h in the dark or under

green light ($\lambda_{max}$ = 525 nm, 5 µmol $m^{-2}$ $s^{-1}$), luciferase activity was determined. Data are means and error bars indicate standard error of the mean (SEM), *n* = 4 - 6. RLU = relative luminescence units. Figure adapted from Chatelle *et al.* (Chatelle et al., 2018).

Green light has been considered for long to have a minimal effect in endogenous Arabidopsis photoreceptors and plant development. However, recently it has been shown that green light has indeed some effects in the circadian rhythm as well (Battle and Jones, 2019). Additionally, the use of the cofactor cobalamin is a limitation that must be considered, especially for its application in plant tissue, due to the fact that little is known about its uptake and processing/metabolism in plants. It could also be of particular interest to compare different forms of cobalamin; the active forms adenosylcobalamin (AdoCbl) and methylcobalamin (MetCbl), and the inactive form cyanocobalamin (CnCbl). Moreover, the apoprotein, namely CarH without the cofactor, still binds to DNA but does not respond to light (data not shown), presenting a possible major limitation as well. However, this system could be re-engineered for use as a Green ON system by fusing a repressor domain to CarH and engineering an operable otherwise constitutive promoter. In this scenario, the addition of cofactor to turn ON the system would prime the system shortly before use, providing an additional level of control (AND gate), where both application of the chromophore and illumination with green light would be needed to obtain gene expression.

## *5.2. Blue light-inducible switches*

### *5.2.1. Blue light-controlled system to activate and repress gene transcription*

To date, there are no blue light-regulated switches developed for plant synthetic biology. Therefore, blue light switches to either induce ($B_{On}$) or repress ($B_{Off}$) expression of a gene of interest were egineered and tested.

An initial pre-screening of different blue light-regulated switches to activate transcription using TULIP, based on LOV2 domain of *Avena sativa* phototropin 1, *As*LOV2, fused to a peptide sequence which interacts with the protein ePDZ (Müller et al., 2014a; Strickland et al., 2012), and VVD, based on LOV domain

from *Neurospora crassa*, (Wang et al., 2012) yielded very low expression levels and dynamic ranges (data not shown). In both cases, the photoreceptors were fused to the Gal4 DNA binding domain (Gal4BD) and its cognate sequence UAS was used in a synthetic promoter. Replacing the Gal4BD-UAS by E-etr or other pair of DBD and cognate sequence could yield higher induction fold. However, for TULIP, the E protein and a synthetic promoter containing etr did not yield a higher induction rate (data not shown). It could be worth trying to optimize further these systems or test other switches that employ the LOV2 domain from *Arabidopsis thaliana* phototropin 1, *At*LOV2 (Renicke et al., 2013), or the iLID system composed by *As*LOV2-ssrA which interacts with ssrB (Guntas et al., 2015).

Nevertheless, the EL222 optogenetic switch yielded a very high dynamic range in protoplasts of *Arabidopsis thaliana*, therefore, this photoreceptor was selected for further characterization. EL222 is a transcription factor from *Erythrobacter litoralis* that is composed of a LOV domain and a helix-turn-helix (HTH) domain connected by a J-alpha (Jα) helix. The LOV domain uses FMN as a cofactor, which is ubiquitous in eukaryotes. Upon blue light application (with maximum absorption around 450 nm), the LOV domain undergoes a conformational change, thereby releasing the HTH and allowing the homodimerization of EL222. This allows for the HTH domain to bind a target DNA sequence (termed C120) (Zoltowski et al., 2013).

Following the strategy of Motta-Mena *et al.* (Motta-Mena et al., 2014), a fusion of the DNA transactivation domain VP16 to the N-term of EL222 was used for the characterization of the $B_{On}$ switch in Arabidopsis protoplasts. As a reporter module, FLuc was placed under the control of a minimal promoter ($P_{hCMVmin}$) and five repeats of the DNA target of EL222 – $(C120)_5$. The number of repeats was chosen due to the previously reported good performance in mammalian cells (Motta-Mena et al., 2014). In the dark, basal levels of FLuc expression are expected, while only upon illumination with blue light, EL222 dimerizes and binds to the cognate $(C120)_5$ sequence, thus bringing the VP16 activation domain into close proximity of the minimal promoter and activating FLuc transcription (Figure 8a).

Arabidopsis protoplasts were co-transformed with the reporter module with or without the blue-responsive module. Then they were incubated in different blue light intensities (0.25, 0.5, 1, 5, 10 µmol $m^{-2}$ $s^{-1}$) and the luminescence was determined after 18 h. A constitutive Renilla luciferase (RLuc) was included as a normalization element. Profiting from the fact that the reporter module has a recognition site for the E protein – $(etr)_8$ – (not relevant for the $B_{On}$ switch) a constitutively expressed E-VP16 was included as a positive control for light-independent activation of the reporter module. The ratios FLuc/RLuc for four technical replicates are shown in Figure 8b. The optogenetic switch showed a good dynamic range, with the maximum fold induction (8.1-fold) being achieved after incubation in 5 µmol $m^{-2}$ $s^{-1}$ blue light. It was also observed that these blue light intensities had no negative effects on the expression of FLuc or RLuc, as shown for the constitutive/positive control E-VP16 (Figure 8b), inferring that they had no toxic effects on the cells.

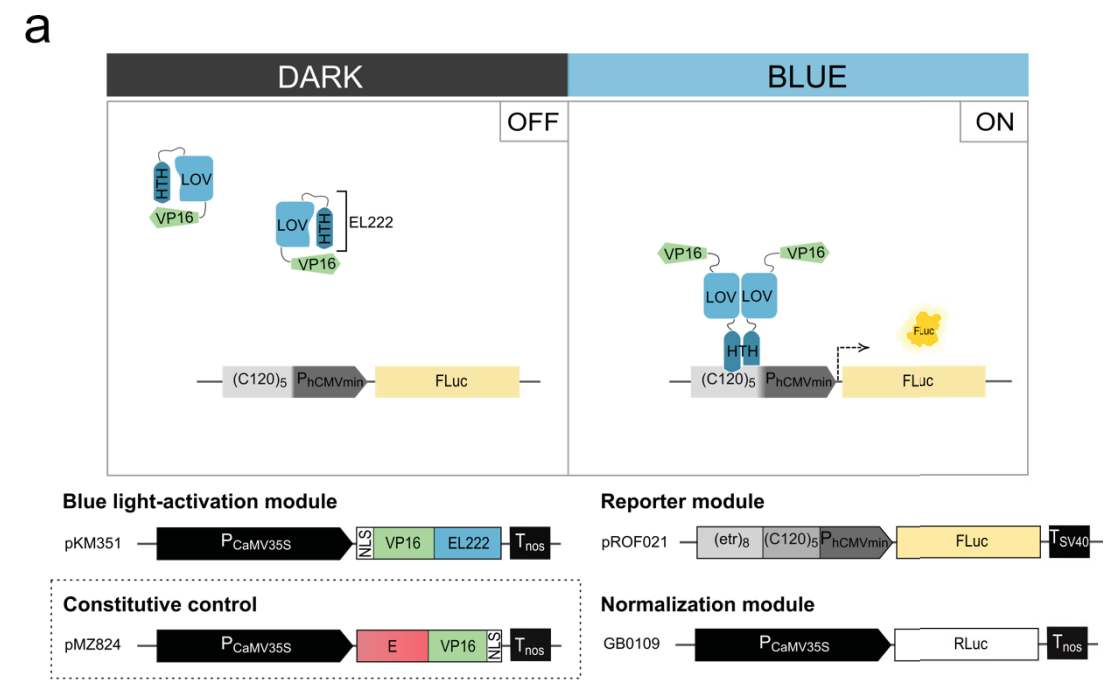


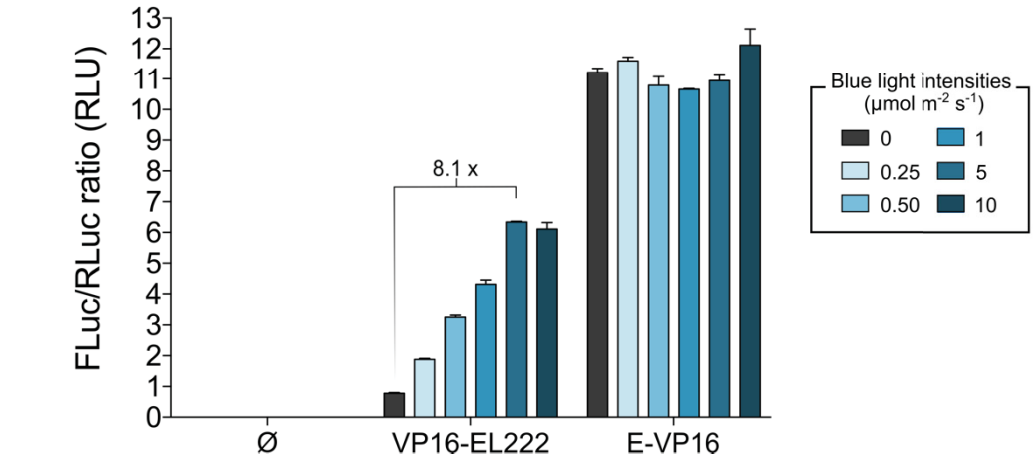


**Figure 8**. Design and characterization of the blue light-regulated gene activation switch ($B_{On}$) in Arabidopsis protoplasts. **(a)** Constructs and mode of function. The components engineered and characterized in plant cells are: i) the blue light-responsive photoreceptor EL222 fused to an activation domain VP16 and placed under the control of the constitutive promoter $P_{CaMV35S}$, ii) a synthetic promoter composed of five repeats of C120 - $(C120)_5$ - and a minimal promoter $P_{hCMV}$, driving the expression of the reporter gene FLuc, and iii) $P_{CaMV35S}$ driving the constitutive expression of the normalization element RLuc. A constitutively expressed E protein fused to VP16 is included as a positive control, where E binding to its cognate sequence $(etr)_8$ in the reporter module activates FLuc expression in a light-independent manner. The transcription factor EL222 has a Light-Oxygen-Voltage (LOV) dependent and a Helix-Turn-Helix (HTH) domain. The photoreceptor is folded in the dark due to a flavin-protein adduct and incapable of binding to DNA. As a result, there is no expression of FLuc in the dark. Upon blue light irradiation, EL222 unfolds and dimerizes, binding to the $(C120)_5$ element, bringing the transactivator domain VP16 close to the minimal promoter and initiating the transcription of FLuc. **(b)** Characterization

of the system. Arabidopsis protoplasts were transformed with the reporter module (pROF021) and the blue light-inducible element VP16-EL222 (pKM531) or without the optoswitch (ø, stuffer plasmid). Constitutively expressed RLuc (GB0109) was included for normalization. After transformation, protoplasts were kept in darkness or illuminated with different intensities of blue light (0.25, 0.5, 1, 5, 10 µmol $m^{-2}$ $s^{-1}$), and FLuc and RLuc were determined after 18 h. Shown data are the mean FLuc/RLuc ratios. Error bars indicate standard error of the mean (SEM), *n* = 4. RLU = Relative Luminescence Units. NLS = Nuclear Localization Sequence.

Subsequently, a blue light-regulated gene repression switch ($B_{Off}$) was engineered. This switch comprises: i) the constitutively expressed EL222 fused to a transcriptional repressor domain (RD), and ii) a reporter module driving the expression of a reporter gene, *e.g.* FLuc, under the control of a synthetic tripartite promoter. The promoter comprises a quintuple-repeat target sequence for EL222, $(C120)_5$, flanked by the enhancer sequence of the CaMV35S promoter and the minimal promoter $P_{hCMVmin}$. (Figure 9a).

Three versions of the blue light-repressor module were evaluated by fusing either of three different known transrepressor domains to the N-terminus of EL222; one from the human Krüppel Associated Box (KRAB) protein (Baaske et al., 2018; Moosmann et al., 1997), and two from Arabidopsis, namely the B3 repression domain (BRD) and the EAR repression domain (SRDX) (Ikeda and Ohme-Takagi, 2009). The functionality of the $B_{Off}$ optoswitches was assayed by transient co-transformation with the reporter construct in Arabidopsis protoplasts. Constitutively expressed Renilla luciferase, RLuc, was included for normalization. The cells were illuminated for 18 h at different light intensities of blue light (0, 0.25, 0.5, 1, 5 and 10 µmol $m^{-2}$ $s^{-1}$), and FLuc/RLuc activity was quantified (Figure 9b). All three versions of the repressor modules were functional although with different efficiencies, yielding a range of repression levels (SRDX, 92%; BRD, 84%; and KRAB, 53%; at 10 µmol $m^{-2}$ $s^{-1}$ blue light). The highest repression level and dynamic range was achieved with SRDX-EL222 as a trans-repressor module.

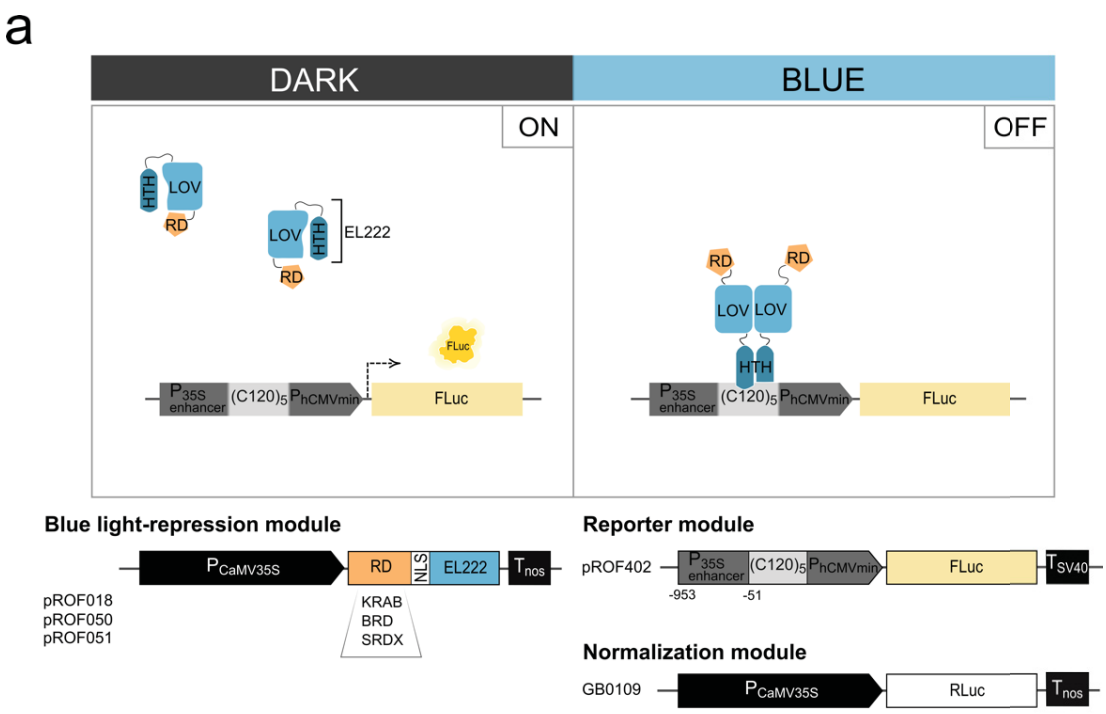


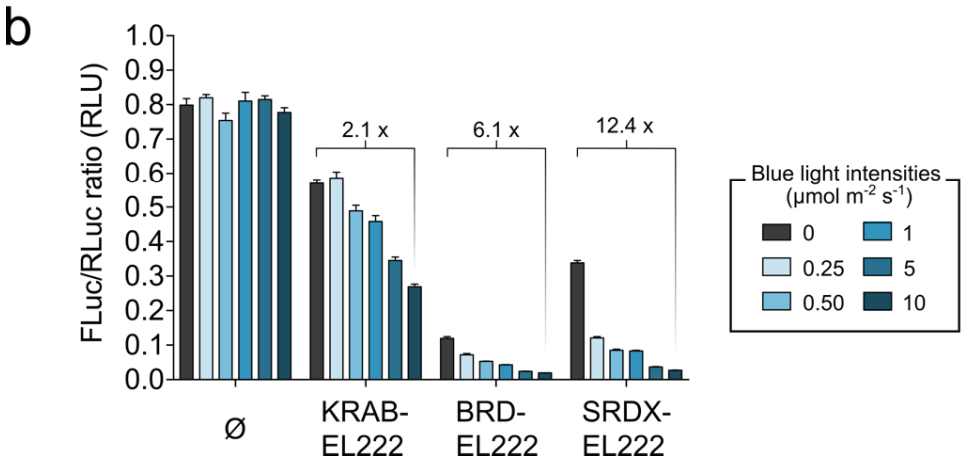


**Figure 9**. Design and characterization of the blue light-regulated gene repression switch ($B_{Off}$) in Arabidopsis protoplasts. **(a)** Constructs and mode of function. The components engineered and characterized in plant cells are: i) the blue light-responsive *E. litoralis* photoreceptor EL222 fused to either of three different repressor (RD-EL222) domains: KRAB, BRD, SRDX and placed under the control of the constitutive promoter $P_{CaMV35S}$, ii) a synthetic promoter composed of the enhancer region of $P_{CaMV35S}$, five repeats of C120 - $(C120)_5$ - and a minimal promoter $P_{hCMVmin}$, driving the expression of the reporter gene FLuc, and iii) $P_{CaMV35S}$ driving the constitutive expression of the normalization element RLuc. The transcription factor EL222 has a Light-Oxygen-Voltage (LOV) dependent domain and a Helix-Turn-Helix (HTH) domain. The photoreceptor is folded in the dark due to a flavin-protein adduct and incapable of binding to the $(C120)_5$ element. As a result, expression of FLuc is constitutively active. Upon blue light illumination RD-EL222 unfolds allowing the formation of dimers binding to the $(C120)_5$ element via the HTH. As a result, the initiation of FLuc transcription is repressed**. (b)** Characterization of the system. Arabidopsis protoplasts were transformed with the reporter module (pROF402) and the blue light-responsive element (photoreceptor, EL222) fused to either repressor: KRAB (pROF018), BRD

(pROF050), and SRDX (pROF051) or without the optoswitch (Ø, stuffer plasmid). Constitutively expressed RLuc (GB0109) was included for normalization. After transformation, protoplasts were kept in darkness or illuminated with different intensities of blue light (0.25, 0.5, 1, 5, 10 µmol $m^{-2}$ $s^{-1}$), and FLuc and RLuc were determined after 18 h. Shown data are the mean FLuc/RLuc ratios. Error bars indicate standard error of the mean (SEM), *n* = 6. RLU = Relative Luminescence Units. NLS = Nuclear Localization Sequence.

These switches are, to date, the first blue light-inducible switches to control gene expression in plant cells. The fact that the cofactor supplementation is not required and that this optoswitch is orthogonal to plants are advantages for its implementation in Arabidopsis. It comprises only one component, simplifying the construction and transformation of the required plasmids. It has, however, some remaining activity in the dark state, as it can be observed in the results. Overall, this tool presents many advantages that make it suitable for combination with other switches for multi-chromatic control of gene expression.

### *5.2.2. Blue light-gated transporter*

The implementation of light-gated ion channels based on microbial opsins to manipulate neuronal excitability has revolutionized the neurosciences. Besides the channelrhodopsins, there are some reports of regulation of ion channels by a using LOV domains (Cosentino et al., 2015; Papanatsiou et al., 2019; Schmidt et al., 2014). We attempted to develop the first light-controlled transmembrane metabolite transporter, in a collaboration project with the group of Prof. Weber at the University of Düsseldorf. The aim is to achieve an ATP transporter that is controlled by blue light. For that purpose, the $Ca^{2+}$-controlled mitochondrial ATP-phosphate carrier, APC1/2/3, was chosen to convert it from a $Ca^{2+}$-gated into a light-gated transporter. This will allow in the future the targeted functional analysis of the metabolite transport decoupled from the endogenous regulation under normal conditions and in response to stress.

Due to the fact that there is little information about the structure of *At*APC1, the human homolog hAPC1 which structure information is available (Harborne et al., 2015; Yang et al., 2014) was used as a first approach to develop such an opto-APC. The hAPC1 is composed by: an N-terminal domain (NTD)

containing the EF-hand motifs responsible for $Ca^{2+}$-binding; a peptide segment, the H9 helix also called alpha helix, which has a regulatory function (Harborne et al., 2015); and a C-terminal transmembrane domain (TMD). Under high $Ca^{2+}$ levels, the H9 is “self-sequestered” in the NTD and therefore the channel is open, while at low $Ca^{2+}$ levels, there is a rearrangement of the NTD and the H9 is excluded from the NTD, blocking the channel. It is not clear yet whether the H9 is responsible for the channel blocking or the NTD-H9 (Harborne et al., 2015). The H9 helix is annotated in different positions according to the literature, either starting at the residue 159 (Yang et al., 2014) or 164 (Monné et al., 2015) of hAPC1.

Based on the structural and functional aspects, several designs of the opto-hAPC were made. The constructs were developed for its expression in mammalian cells as a first approach to elucidate the mechanism of function. The strategies involve the removal of the NTD responsible for $Ca^{2+}$ sensing, upstream of the H9, and replacement by different versions of the LOV2 domain from *Avena sativa* Phototropin 1 corresponding to residues 404–546 (*As*LOV2). The design comprises different sites of fusion (Table 2, Figure 10a): i) fusion of the wildtype *As*LOV2 to different truncated versions of hAPC1 lacking the NTD, the Jα helix of the LOV domain was fused to the H9 helix directly (pROF300), or either keeping 6 (pROF301) or 9 amino acids (pROF307) upstream of the H9 helix; ii) fusion of the iLID version of *As*LOV2$_{(L493V,Q502Y,H519R,V520L,R521H,D522G,G528A,M530C,E537F,N538Q,D540A)}$-SsrA (Guntas et al., 2015), to the H9-TMD of hAPC1 and separated by a linker (pROF302). In this case, the Jα helix of the *As*LOV2 is fused to a bacterial SsrA peptide, which is proven to be well docked and released upon blue light irradiation, followed by a linker. Additionally, the *As*LOV2 domain has several mutations introduced to improve the docking and undocking. The SsrA and the linker that provides a spacer between the Jα helix and the H9 helix, probably giving more flexibility to the whole structure and freedom for the N-term of the protein to move out of the channel; iii) fusion of the TULIP version of *As*LOV2$_{(T406A,\ T407A,G528A,I532A,N538E)}$-pep (Strickland et al., 2012), to the H9-TMD of hAPC1 (pROF303). Similarly to iLID, the Jα helix is also fused to a peptide

(pep) which is optimally docked into the LOV domain. The *As*LOV2 domain additionally contains a different set of mutations in comparison with the wildtype.

Additionally, a set of controls were also designed and cloned: i) the full-length hAPC1 (pROF304); ii) a truncated version of hAPC1 containing the H9-TMD according to Yang (Yang et al., 2014) (pROF305) or Monné, (Monné et al., 2015) (pROF309); iii) a truncated version of hAPC1 only containing the TMD (pROF308); and, iv) a localization control of eGFP fused to truncated hAPC1 containing H9-TMD (pROF306) to test if the deletion of the N-terminal leads to mislocalization of the protein. All the versions were cloned additionally with an HAtag in the C-term to allow the subsequent detection of the protein (Table 2). Based on the first results, the constructs can be customized in the future for the Arabidopsis homolog *At*APC1.

**Table 2**. Overview of the plasmids generated for the opto-APC1 system and the controls.

| Plasmid name | Description | Plasmid name | Description |
|---|---|---|---|
| pROF300 | $P_{SV40}$-*As*LOV2-hAPC1$_{(159-477)}$-$T_{SV40}$ | pROF355 | $P_{SV40}$-HAtag-*As*LOV2-hAPC1$_{(159-477)}$-$T_{SV40}$ |
| pROF301 | $P_{SV40}$-*As*LOV2-hAPC1$_{(156-477)}$-$T_{SV40}$ | pROF356 | $P_{SV40}$-HAtag-*As*LOV2-hAPC1$_{(156-477)}$-$T_{SV40}$ |
| pROF302 | $P_{SV40}$-*As*LOV2-SsrA-linker-hAPC1$_{(159-477)}$-$T_{SV40}$ | pROF357 | $P_{SV40}$-HAtag-*As*LOV2-SsrA-linker-hAPC1$_{(159-477)}$-$T_{SV40}$ |
| pROF303 | $P_{SV40}$-*As*LOV2-pep-hAPC1$_{(159-477)}$-$T_{SV40}$ | pROF358 | $P_{SV40}$-HAtag-*As*LOV2-pep-hAPC1$_{(159-477)}$-$T_{SV40}$ |
| pROF304 | $P_{SV40}$-hAPC1$_{(1-477)}$-$T_{SV40}$ | pROF359 | $P_{SV40}$-HAtag-hAPC1$_{(1-477)}$-$T_{SV40}$ |
| pROF305 | $P_{SV40}$-hAPC1$_{(159-477)}$-$T_{SV40}$ | pROF360 | $P_{SV40}$-HAtag-hAPC1$_{(159-477)}$-$T_{SV40}$ |
| pROF306 | $P_{SV40}$-eGFP-hAPC1$_{(159-477)}$-$T_{SV40}$ | pROF361 | $P_{SV40}$-HAtag-eGFP-hAPC1$_{(159-477)}$-$T_{SV40}$ |
| pROF307 | $P_{SV40}$-*As*LOV2-hAPC1$_{(153-477)}$-$T_{SV40}$ | pROF362 | $P_{SV40}$-HAtag-*As*LOV2-hAPC1$_{(153-477)}$-$T_{SV40}$ |
| pROF308 | $P_{SV40}$-hAPC1$_{(207-477)}$-$T_{SV40}$ | pROF363 | $P_{SV40}$-HAtag-hAPC1$_{(207-477)}$-$T_{SV40}$ |
| pROF309 | $P_{SV40}$-hAPC1$_{(179-477)}$-$T_{SV40}$ | pROF364 | $P_{SV40}$-HAtag-hAPC1$_{(179-477)}$-$T_{SV40}$ |

The assumption is that in the dark, the H9 peptide will be caged into the core of the LOV2, while under blue light-irradiation it will be released from the core. One of the hypotheses is that in the docked state, the peptide will be separated from the TMD thus being the channel open, while under blue light, the released H9 will block the channel (Figure 10b). However, it could also be that the

LOV2-H9 will be blocking the channel, and in the blue light-induced open state the channel will be cleared (Figure 10c). This will depend on the size and flexibility of the linker sequence between the LOV2 and the H9-TMD. Another factor that will determine the behaviour of the switch is if the H9 alone is able to block the channel or if it is needed the LOV2-H9, as it is not yet fully clear the blocking mechanism of the native APC. In any event, these hypotheses have yet to be tested experimentally. So far only preliminary tests have been performed and further optimization needs to be done due to the fact that the different versions are expressed irregularly in the mammalian cells. Anyhow, besides getting a useful tool for studying and manipulating ATP transport, the testing of the different versions will provide useful insights into structural and functional issues of the transporter itself.

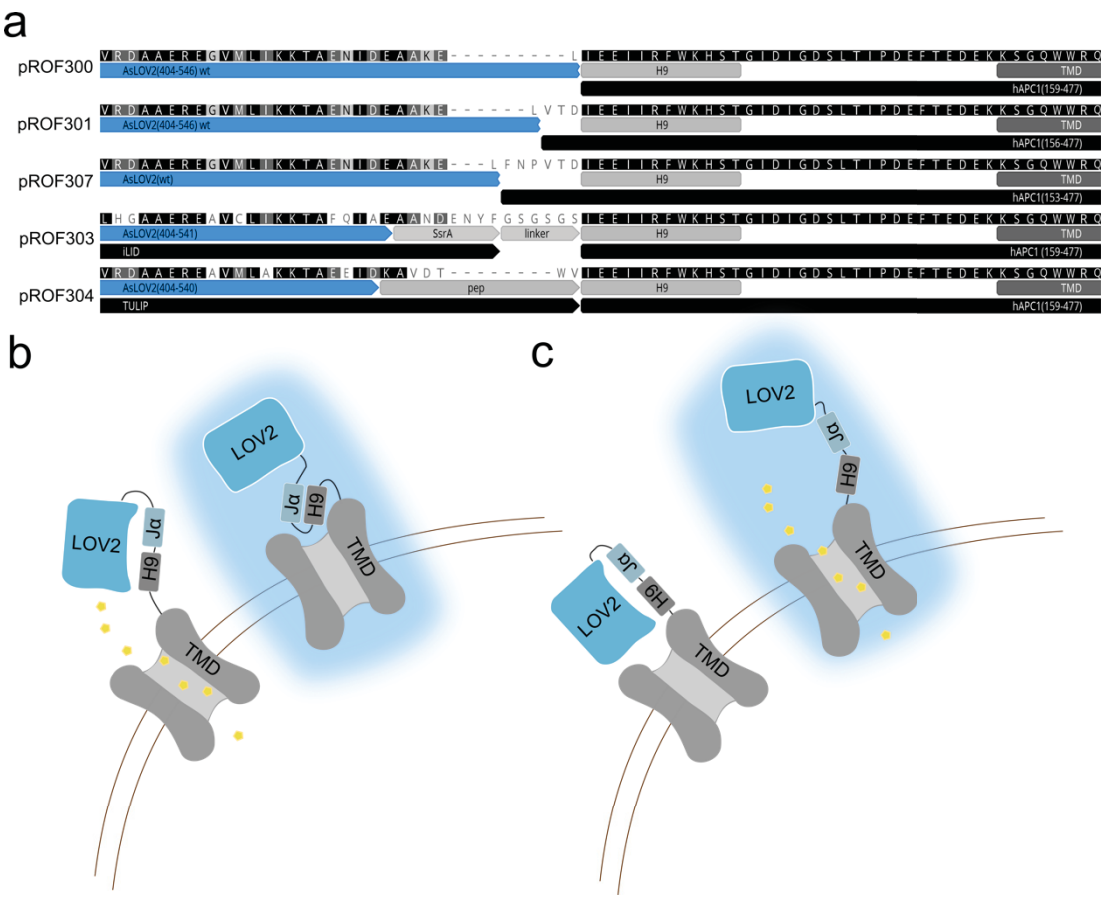


**Figure 10**. Design of the opto-hAPC1. **(a)** Alignment of the fusion region between the different versions of *As*LOV2 domain and the H9-TMD of hAPC1. **(b,c)** Proposed mode of function fo the switch. The carrier is either blocked and avoiding the ATP transport when irradiated with blue light (b) or when is kept in the dark (c), depending on linker size and flexibility separating the LOV2 and H9 as well as the affinity

of the H9 to bind the TMD and therefore block the channel. ATP is depicted as yellow pentagons. LOV2, Light-Oxygen-Voltage domain 2 from *Avena Sativa* Phototropin1; TMD, transmembrane domain.

## *5.3. Red light-inducible system to control gene expression*

The red light-inducible system has been successfully implemented in *Nicotiana tabacum* (Müller et al., 2014b) and in *Arabidopsis thaliana* mesophyll protoplasts (Ochoa-Fernandez et al., 2016). It has also been used in a proof-of-principle application to regulate hormone signalling and to express a human vascular endothelial growth factor (VEGF) in *Physcomitrella patens* (Müller et al., 2014b). It functions as a chimeric transcription factor, based on a truncated version of PhyB, fused to a VP16 transactivation domain, and a truncated version of PIF6, fused to a DNA binding domain. There is a synthetic promoter in which the cognate sequence of the DNA binding domain is placed upstream of the minimal promoter $P_{hCMVmin}$. Therefore, only under red light, when PhyB and PIF6 interact, transcription of the gene of interest is initiated (Chapter 1). The truncated $PhyB_{(1-650)}$ contains the PAS-GAF-PHY domains from the photosensory module (PSM), lacking the C-terminal module (CTM). The truncated $PIF6_{(1-100)}$ contains the active PhyB-binding (APB) region, excluding the C-terminal portion which comprises the basic helix-look-helix (bHLH) responsible for the DNA binding.

### *5.3.1. Testing of different new variants of the red light-inducible gene expression system*

To determine if the system could be improved in terms of performance and/or dynamic range, two strategies were followed.

Firstly, the exchange of the activation domain VP16 by a stronger activation domain designed and tested by Li *et al*. in Arabidopsis and rice protoplasts (Li et al., 2017) and composed by 6 TAL effectors and VP128 (termed TV).

Secondly, the exchange of the $PIF6_{(1-100)}$ by other versions such as $PIF6_{(10-52)}$ and $PIF3_{AAfus}$ (Figure 11a). The APB motif is composed of two segments, termed APB.A and APB.B, the prior being the most conserved. Therefore, $PIF6_{(10-52)}$ is a version that only includes the APB.A motif of PIF6, and $PIF3_{AAfus}$

is a version that includes two APB.A motifs of PIF3 fused. These two variants of PIFs were chosen based on their high dynamic range in mammalian cells (Golonka et al., 2019).

In protoplasts co-transformed with the different combinations of PhyB-VP16 and E-PIF with the reporter module, it was observed that the shorter version of $PIF6_{(10-52)}$ does not significantly improve the dynamic range in comparison with $PIF6_{(1-100)}$. On the other hand, the $PIF3_{AAfus}$ has a lower leakiness in the dark, resulting in a higher fold induction (Figure 11b). However, in the configurations that included PhyB-TV, the highest induction fold is achieved with the shorter version of $PIF6_{(10-52)}$, followed by the $PIF3_{AAfus}$ (Figure 11b). The positive controls show that E-VP16 has higher overall expression than E-TV probably due to the difference in size between both activation domains. This difference in the size of the E-PIF-PhyB-AD complex could also explain the diversity of induction/dynamic ranges obtained. It could be of particular interest to test in the future various linker sizes separating E-PIF and PhyB-AD, as well as different synthetic promoters with spacer sequences between the etr and the minimal promoter.

Applying similar principles to the $B_{Off}$ system (Figure 9), a red light-regulated switch to repress gene expression was designed by fusing the strong plant repressor SRDX to either the C-term or N-term of the $PhyB_{(1-650)}$. Additionally, a constitutive and operable synthetic promoter comprising the enhancer region of $P_{CaMV35S(-951\ to\ -51)}$, eight repeats of the target sequence of the protein E - $(etr)_8$ - and a minimal promoter $P_{hCMV}$, driving FLuc gene expression was designed. Figure 12 depicts the theoretical mode of function of this switch, as well as the plasmid design. The design of this system has yet to be extensively tested in protoplasts, although it is expected to be in the OFF state upon red light treatment and the ON state upon darkness or far-red light treatment. Based on the previous performance of the PhyB-PIF switch there are reasons to believe that this approach could work in plant cells, however, the perturbance of the synthetic promoter by the constitutive binding of E-PIF to it must be assessed. A lower number of etr repeats could probably be desirable,

as they would increase the activity of the operable promoter. On the other hand, this could lead also to lower repression levels upon red light-irradiation.

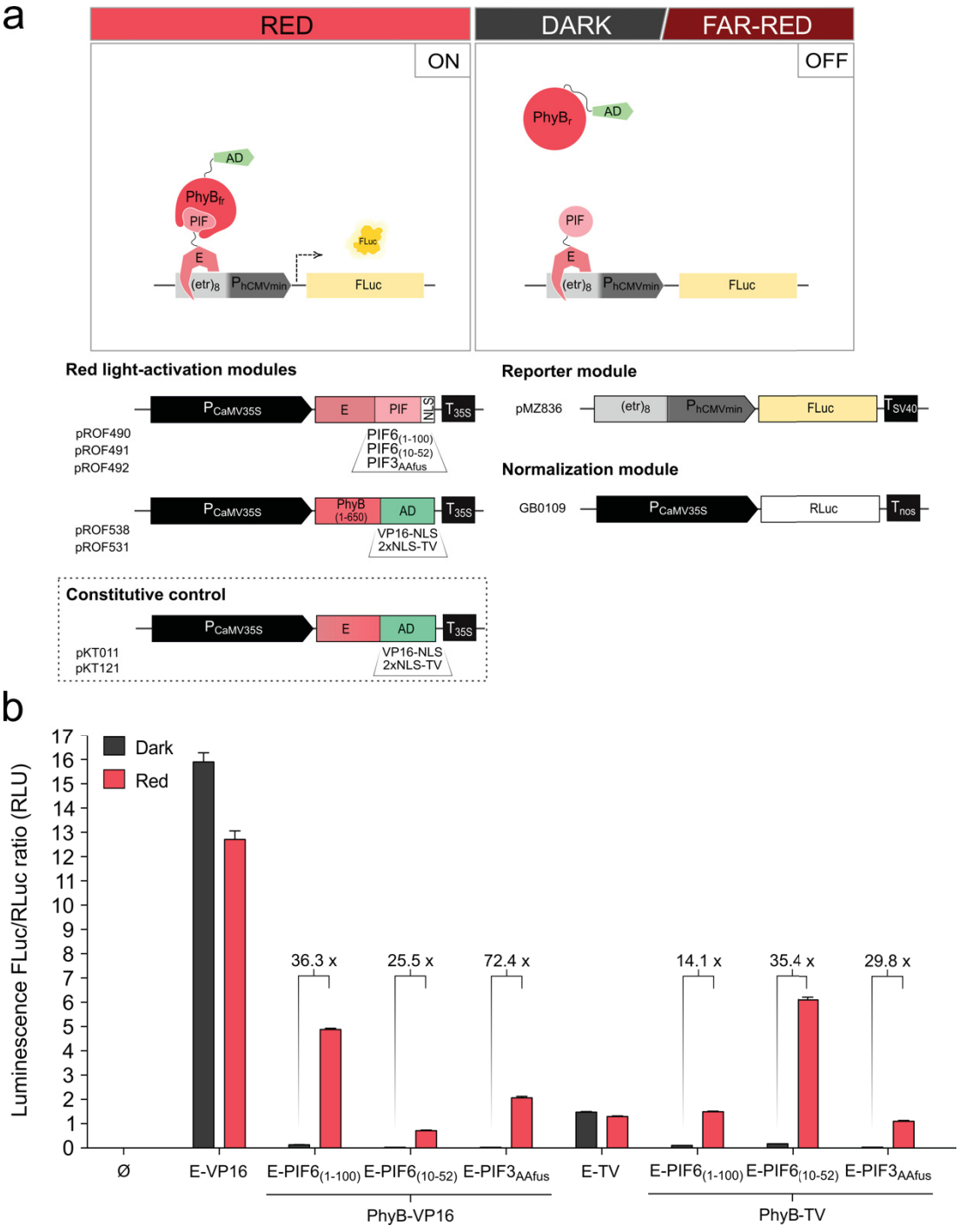


**Figure 11**. Red light-regulated gene activation switch ($R_{On}$), variants and functional test in Arabidopsis protoplasts. **(a)** Constructs and mode of function. The components engineered and characterized in plant cells are: i) the red light-activated, far-red light-inactivated switch comprising the first 650 amino acids of the PhyB photoreceptor - $PhyB_{(1-650)}$ - fused to an activation domain (AD), VP16 or TV, and the macrolide

repressor DNA-binding protein E fused to either PIF6$_{(1-100)}$, PIF6$_{(10-52)}$, or PIF3$_{AAfus}$. The two modules of the switch are constitutively expressed under the control of the promoter P$_{CaMV35S}$, ii) eight repeats of the target sequence of the protein E, etr - (etr)$_8$ - and the minimal promoter P$_{hCMVmin,}$ driving the expression of the reporter gene FLuc, and iii) P$_{CaMV35S}$ driving the constitutive expression of the normalization element RLuc. A constitutive E fused to VP16 and TV is included as a control to asses the maximum light-independent repression of the expression achievable. Under red light, PhyB is in the active form (PhyB$_{fr}$), and therefore able to interact with PIF, which is bound to (etr)$_8$ through the E protein. In consequence, there is recruitment of the activator domain to the minimal promoter, resulting in expression of FLuc (left). In darkness or far-red light, PhyB is in the inactive form (PhyB$_r$), therefore unable to bind to the synthetic promoter, resulting in no FLuc transcription (right). **(b)** Characterization of the system. Arabidopsis protoplasts were transformed with the reporter module (pMZ836) and the red light-responsive elements PhyB, fused to either activation domain VP16 (pROF538), or TV (pROF531), and E fused to either PIF6$_{1-100}$ (pROF490), PIF6$_{10-52}$ (pROF491), or PIF3$_{AAfus}$ (pROF492), or without the optoswitch (stuffer plasmid). Reporter module co-transformed with either E fused to VP16 (pKT011), or TV (pKT121), were included as positive controls. Constitutively expressed RLuc (GB0109) was included in all cases for normalization. After transformation, protoplasts were kept in darkness or illuminated with different intensities of red light (10 µmol m$^{-2}$ s$^{-1}$), and FLuc and RLuc were determined after 19 h. Shown data are the mean FLuc/RLuc ratios. Error bars indicate standard error of the mean (SEM), *n* = 6. RLU = Relative Luminescence Units. NLS = Nuclear Localization Sequence.

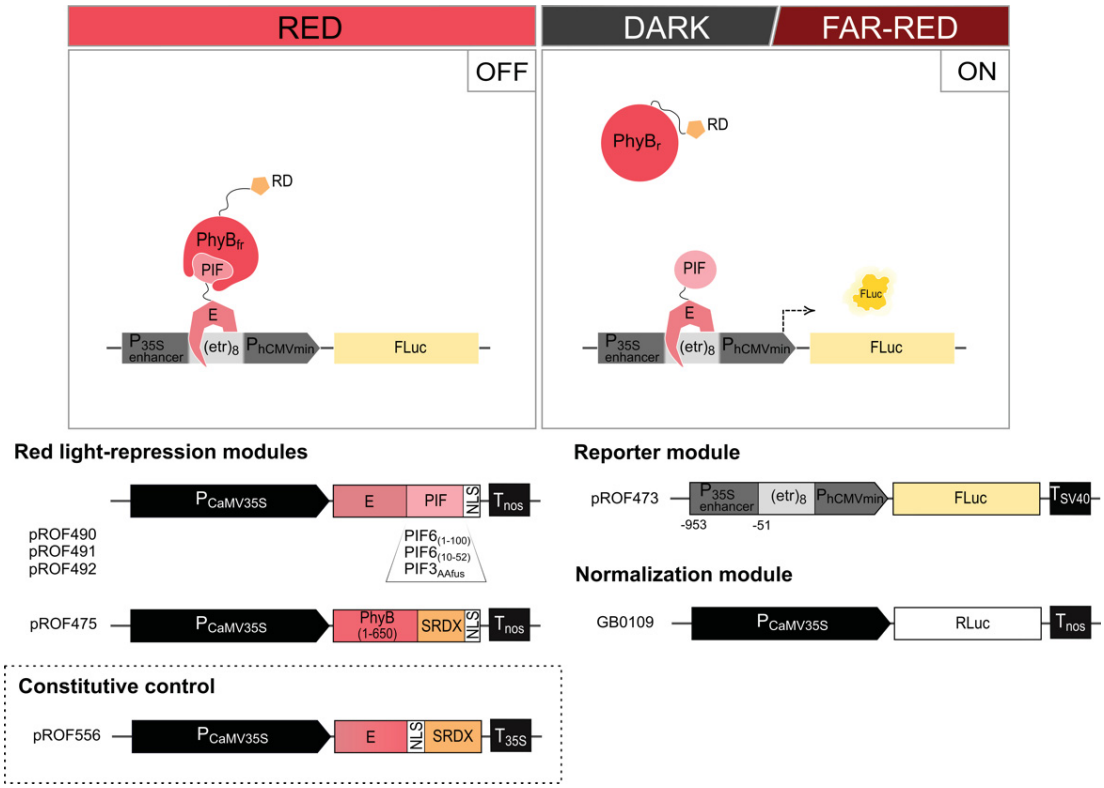


**Figure 12**. Mode of action of a theoretical red light-regulated gene repression switch (R$_{Off}$).The components are: i) the red light-inactivated switch comprising the first 650 amino acids of the PhyB photoreceptor - PhyB$_{(1-650)}$ - fused to a repressor domain (SRDX), and the macrolide repressor DNA-binding protein E fused to either PIF6$_{(1-100)}$, PIF6$_{(10-52)}$, or PIF3$_{AAfus}$. The two modules of the switch are

constitutively expressed from the promoter $P_{CaMV35S}$, ii) composed of the enhancer region of $P_{CaMV35S}$, eight repeats of the target sequence of the protein E, etr - $(etr)_8$ - and a minimal promoter $P_{hCMV}$, driving the expression of the reporter gene FLuc, and iii) $P_{CaMV35S}$ driving the constitutive expression of the normalization element RLuc. A constitutive E protein fused to SRDX is included as control to asses the maximum light-independent repression of the expression achievable. Under red light, PhyB is in active form ($PhyB_{fr}$), and therefore able to interact with PIF which is bound to $(etr)_8$ through the E protein. In consequence, there is recruitment of the repressor domain to the minimal promoter, resulting in termination of FLuc expression (left). In darkness or far-red light PhyB is in the inactive form ($PhyB_r$), therefore unable to bind to the synthetic promoter resulting in FLuc transcription (right). NLS = Nuclear Localization Sequence.

### 5.3.2. *Design and implementation of a novel red-light controlled dCas9 to up- or down-regulate gene expression*

A new concept of a red-light inducible system that could be customized to up- or down-regulate any gene of interest was engineered. For that purpose, the DNA-binding protein of the $R_{On}$ switch was exchanged by the nuclease-deficient *Streptococcus pyogenes* Cas9 (D10A, H840A) protein, dCas9 (Perez-Pinera et al., 2013). In this manner, any gene of interest can be targeted by an *ad-hoc* designed guide RNA (Figure 13a). Several constructs of dCas9 fused to different versions of PIF were generated, and PhyB was fused to the strong TV activation domain. The TV was selected due to the fact that fusions of PhyB-VP16 were found to be insufficient in activating gene expression in preliminary experiments (data not shown). This also aligns with the reported low to moderate activation by using a constitutive dCas9-VP64 in Arabidopsis and rice protoplasts and Nicotiana leaves (Li et al., 2017; Vilar et al., 2016).

For the up-regulation, two promoters and gRNAs targeting those promoters were selected. Firstly, the orthogonal promoter from *Solanum lycopersicum* dihydroflavonol 4-reductase ($P_{SlDFR}$) and a gRNA against the -150 bp region of $P_{SlDFR}$ relative to the transcription start site (TSS) was used based on results obtained by Selma *et al*. in Nicotiana leaves (Selma et al., 2019). Secondly, the promoter of the Arabidopsis gene APETALA1 ($P_{AtAP1}$), which includes the 5'UTR and - 2781 bp upstream of the TSS, was selected. Several gRNA specific for various regions in proximity of the target promoter were designed and screened for functionality (data not shown), with that against the -100 bp

region of $P_{AtAP1}$ relative to the TSS showing functionality within the system. To monitor the activation of the promoter, FLuc was used as a quantitative readout.

In both cases, the highest fold induction was achieved with the dCas9-$PIF6_{(1-100)}$ version. Red light induction of the system yielded 12.8-fold induction rates from the $P_{SlDFR}$-FLuc construct compared to dark incubation (Figure 13b), and 4.7-fold induction rates when targeting the $P_{AtAP1}$-FLuc (Figure 13c).

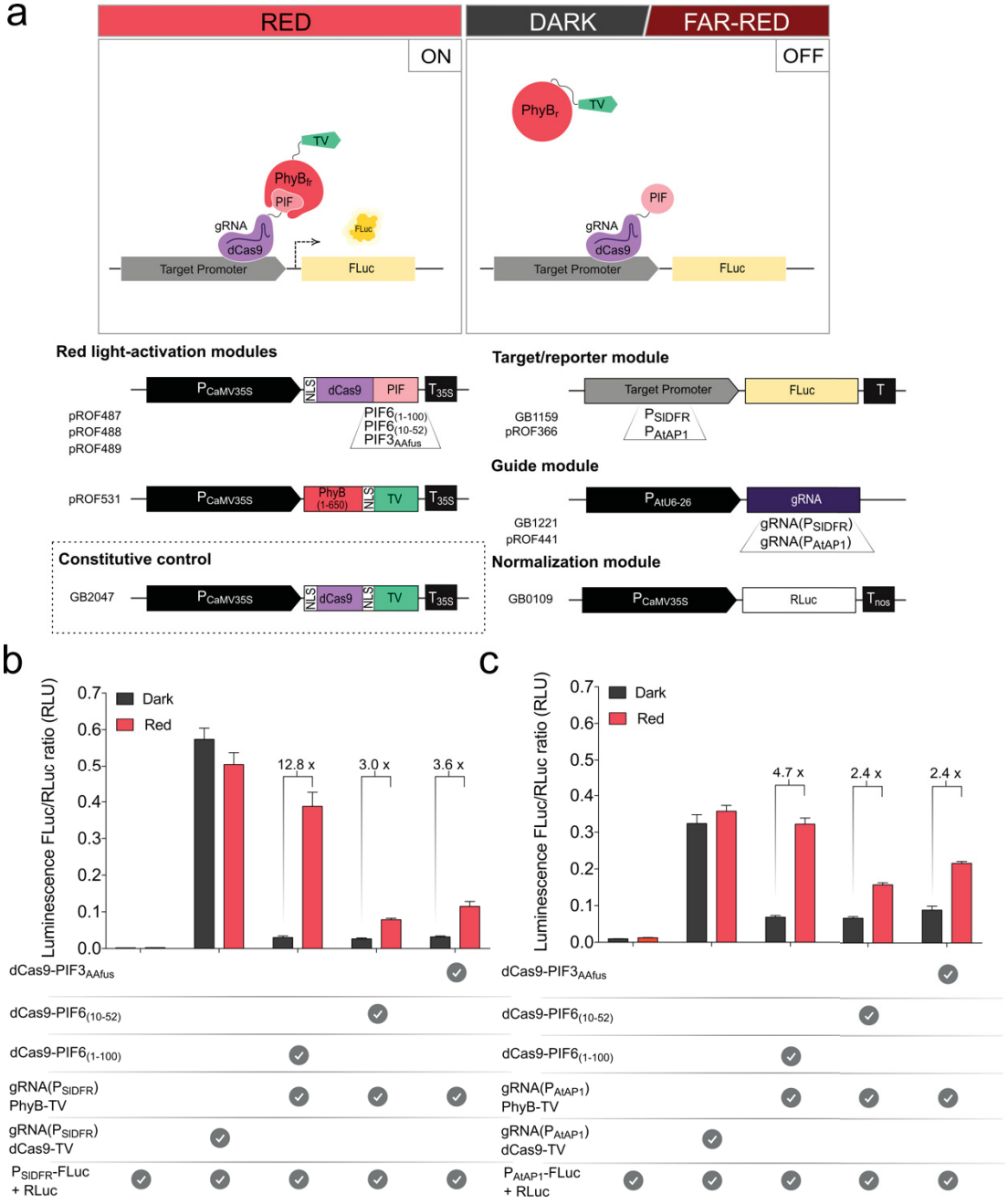


**Figure 13**. Mode of function of the red light-activated dCas9-based switch to upregulate gene expression in Arabidopsis protoplasts. **(a)** Constructs and mode of function. The components engineered and characterized in plant cells are: i) the red light-activated modules comprising the nuclease-deficient *Streptococcus pyogenes* Cas9 - dCas9 - fused to either $PIF6_{(1-100)}$, $PIF6_{(10-52)}$, or $PIF3_{AAfus}$, and the first 650 amino acids of the PhyB photoreceptor - $PhyB_{(1-650)}$ - fused to the activation domain termed TV. The two modules of the switch are constitutively expressed from the promoter $P_{CaMV35S}$, ii) the target module composed by the orthogonal promoter from *Solanum lycopersicum* dihydroflavonol 4-reductase promoter - $P_{SlDFR}$ - and the promoter from the Arabidopsis gene APETALA1 - $P_{AtAP1}$ -, driving the expression of the reporter gene FLuc, iii) the guide RNA to target either of the two promoters gRNA($P_{SlDFR}$) and gRNA($P_{AtAP1}$), and iv) $P_{CaMV35S}$ driving the constitutive expression of the normalization element RLuc. A constitutive dCas9 fused to TV is included as a control to asses the maximum light-

independent upregulation of the expression achievable. Under red light, PhyB is in the active form ($PhyB_{fr}$), and therefore able to interact with PIF which is bound to the promoter of interest. The guide RNA confers the specificity to the promoter. In consequence, there is recruitment of the strong activator domain in the proximity of the promoter which leads to transcription activation of FLuc (left). In darkness or far-red light PhyB is in the inactive form ($PhyB_r$), therefore unable to bind to PIF resulting in only basal activity of the promoter and FLuc transcription (right). **(b)** Characterization of the system using an orthogonal promoter. Arabidopsis protoplasts were co-transformed with the target/reporter module, $P_{SlDFR}$-FLuc (GB1159), either without activation and guide module (stuffer plasmid) for the negative control, or with the constitutive dCas9-TV (GB2047) and appropriate gRNA to target $P_{SlDFR}$ (GB1221) as positive control, or with the red-light activation modules together with the guide module. For the red light-responsive elements, PhyB-TV (pROF531) was co-transformed with the modules containing dCas9 fused to either $PIF6_{(1-100)}$, (pROF487), $PIF6_{(10-52)}$ (pROF488), $PIF3_{AAfus}$ (pROF489). Constitutively expressed RLuc (GB0109) was included in all cases for normalization. **(c)** Characterization of the system using an Arabidopsis promoter. Arabidopsis protoplasts were co-transformed with the target/reporter module, $P_{AtAP1}$-FLuc (pROF366) either without activation and guide module (stuffer plasmid) for the negative control, or with the constitutive dCas9-TV (GB2047) and appropriate gRNA to target $P_{AtAP1}$ (pROF441) as positive control, or with the red-light activation modules together with the guide module. For the red light-responsive elements PhyB-TV (pROF531) was co-transformed with the modules containing dCas9 fused to either $PIF6_{(1-100)}$, (pROF487), $PIF6_{(10-52)}$ (pROF488), $PIF3_{AAfus}$ (pROF489). Constitutively expressed RLuc (GB0109) was included in all cases for normalization. (b,c) After transformation, protoplasts were kept in darkness or illuminated with different intensities of red light (10 µmol $m^{-2}$ $s^{-1}$), and FLuc and RLuc were determined after 18 h. Shown data are the mean FLuc/RLuc ratios. Error bars indicate standard error of the mean (SEM), *n* = 4. RLU = Relative Luminescence Units. NLS = Nuclear Localization Sequence.

Theoretically, the dCas9 controlled with red light can be used to down-regulate the expression of a promoter. Additional plasmids were designed, as exemplified in Figure 14, to attempt the establishment of such a system to target promoters as a proof of concept. The design of this system has yet to be extensively tested in protoplasts, although it is expected to be able to down-regulate a gene of interest upon illumination with red light. For this, the PhyB is fused to a repressor, namely SRDX, and the guide RNA must be designed to target a promoter of interest that has constitutive activity. This promoter could be orthogonal like, for instance, the nopaline synthase promoter from *Agrobacterium tumefaciens* ($P_{nos}$), that was previously regulated by targeting a -161 bp upstream site relative to the TSS of said promoter (Vilar et al., 2016). Alternatively, it can also be customized to repress an endogenous promoter of interest. Whether the dCas9-PIF and gRNA complex binding the promoter

constitutively interferes with the normal activity of the promoter will have to be assessed for such a system.

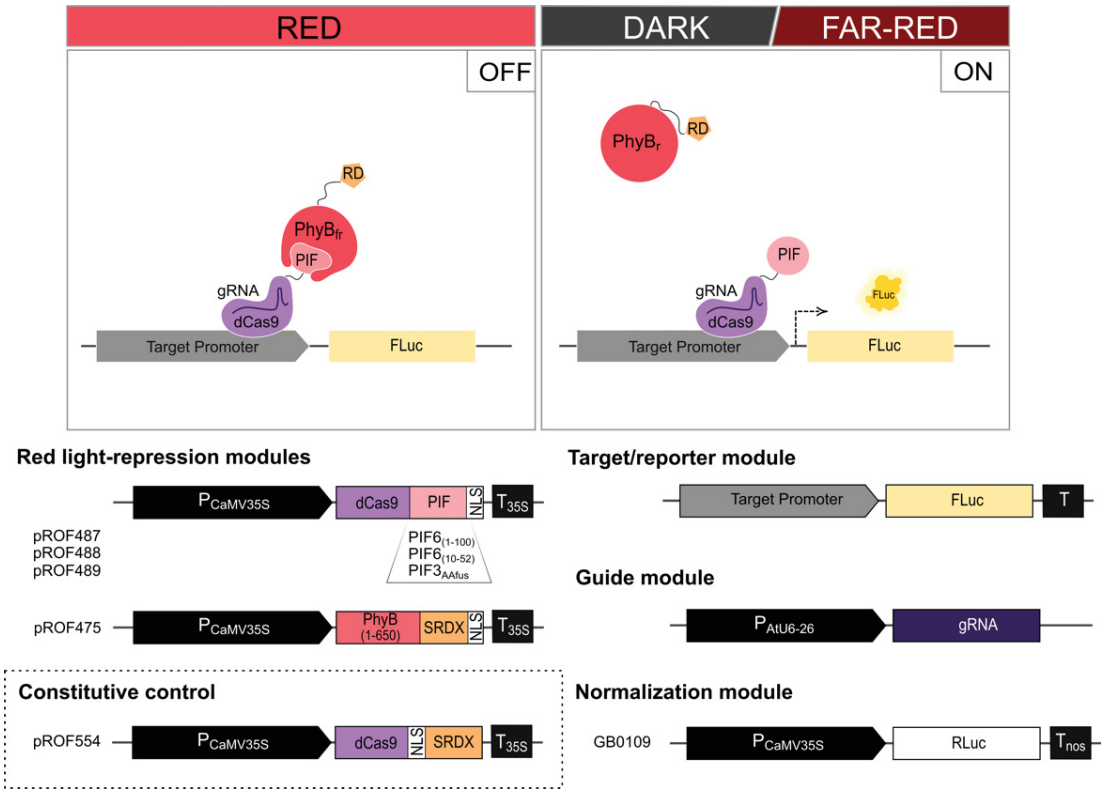


**Figure 14**. Mode of function of a theoretically red-light controlled tool to down-regulate gene expression. Constructs and mode of function. The components are: i) the red light-repression modules comprising the nuclease-deficient *Streptococcus pyogenes* Cas9 - dCas9 - fused to either $PIF6_{(1\text{-}100)}$, $PIF6_{(10\text{-}52)}$, $PIF3_{AAfus}$, and the first 650 amino acids of the PhyB photoreceptor - $PhyB_{(1\text{-}650)}$ - fused to a repressor domain (SRDX). The two modules of the switch are constitutively expressed from the promoter $P_{CaMV35S}$ promoter, ii) the target module comprises the promoter of interest driving the expression of the reporter gene FLuc, iii) the guide RNA to target the promoter of interest, and iv) $P_{CaMV35S}$ driving the constitutive expression of the normalization element RLuc. A constitutive dCas9 fused to SRDX is included as a control to asses the maximum light-independent downregulation achievable. Under red light, PhyB is in active form ($PhyB_{fr}$), and therefore able to interact with PIF which is bound to Promoter of interest trough the dCas9-gRNA complex. In consequence, there is recruitment of the repressor domain near the promoter, resulting in termination of FLuc expression (left). In darkness or far-red light PhyB is in the inactive form ($PhyB_r$), therefore, it is unable to bind to the promoter resulting in FLuc transcription (right). NLS = Nuclear Localization Sequence.

In summary, these red light-controlled switches based on PhyB and PIF have the advantage of not needing the addition of a cofactor, as it is already present in plants. Also, they are reversible in far-red light additionally to dark reversion. However, they are based on Arabidopsis genes so their stable implementation

in this platform in the future could lead to cross-talk effects. The usage of small truncated versions of PhyB and PIF could partially alleviate this issue, as the truncated PIFs lack the bHLH and, therefore, the DNA binding ability, and PhyB lacks some of the regulatory domains located in the CTM. Additionally to the PSM, the CTM has been reported to be involved in PIF binding and degradation as well as thermal reversion (Legris et al., 2019), therefore, the $PhyB_{(1-650)}$-VP16 can have different affinity for the PIF and different reversion kinetics compared to the endogenous PhyB. Another way of overcoming this issue could be to combine it with chemical inducible systems following the example of earlier works in mammalian systems (Chen et al., 2015).

The red light-inducible switch based on chimeric transcription factors yielded an array of dynamic ranges. It seems that the $PIF3_{AAfus}$ provided a good dynamic range when combined with PhyB-VP16 while showing a lower basal activity in the dark. The configurations comprising PhyB-TV, and $PIF6_{10-52}$ yielded a higher overall expression while keeping a high fold induction. Both $PIF3_{AAfus}$ and $PIF6_{(10-52)}$ are smaller, containing 57 amino acids and 43 amino acids respectively, than $PIF6_{(1-100)}$, so it could be beneficial in the future for their combination with other switches and for minimizing crosstalk with other plant components.

The dCas9 strategy stands out as very promising thanks to the possibility of, in principle, controlling endogenous gene expression on command. Additionally, it can be used to control synthetic and orthogonal promoters as exemplified here. To date, this is the first tool controlling dCas9 activation by red-light to be developed and successfully be applied in plant cells. This tool could also be implemented in animal cells or other hosts, resulting in novel applicability considering that most of the optogenetic tools to control dCas9 are developed to be activated by blue or far-red light (Table 1).

## 5.4. *Discussion*

Different tools to control gene expression with green, blue, and red light in plant cells were developed. These tools could be the basic components to generate

complex genetic circuits in the future, either combining them between themselves or with other yet to be developed switches, namely the UVR8-COP1 UV light inducible-system (Crefcoeur et al., 2013) or chemical switches.

Some of these tools have the advantage of being orthogonal such as the switches based on EL222 and CarH, while others have the advantage of not needing the addition of a cofactor like the EL222 and PhyB-PIF optoswitches. These characteristics, as well as the dynamic range, have to be taken into account if they are to be combined to generate complex and/or multi-chromatic circuits. The crosstalk between wavelength absorption is something to consider as well, as often the photoreceptors absorb in more than one range of the spectrum (see Table 3). In order to combine, for instance, the red (PhyB-PIF) light gene activation-switch with the UV (UVR8-COP1) or blue (EL222) light gene activation-switches, it would be necessary to illuminate with UV and blue light and simultaneously with far-red light, in the same manner that it was made in the past for mammalian cells (Müller et al., 2013b). This would not be necessary if the PhyB-PIF switch is combined with the CarH system, for instance.

**Table 3**. Response matrix for gene expression switches to different illumination setups.

| | | Illumination | | | |
|---|---|---|---|---|---|
| | | UV | Blue | Green | Red |
| Optoswitch | UVR8-COP1 | ✓ | | | |
| | EL222 | ✓ | ✓ | | |
| | CarH | ✓ | ✓ | ✓ | |
| | PhyB-PIF | ✓ | ✓ | | ✓ |

However, there are other options for the combination of the switches yet to be explored. It would be of particular interest for future applications *in planta* to have the dCas9 red light-inducible combined in a multi-chromatic approach with the blue light repression system as exemplified in Figure 15. In this approach, there would be activation of gene transcription only when

illuminated with red light and not during daylight – night cycles. Also, the fact that the PhyB and PIF modules are under the control of the blue switch will reduce the amount of said proteins in the plant (as they would only be produced in the night and at a lesser amounts than with a constitutive promoter), therefore potentially reducing the possible interference in endogenous PhyB/PIF signalling. This would also decrease the basal activity in the dark and the possible effect of the dCas9-PIF and gRNA complex interference of the endogenous promoter.

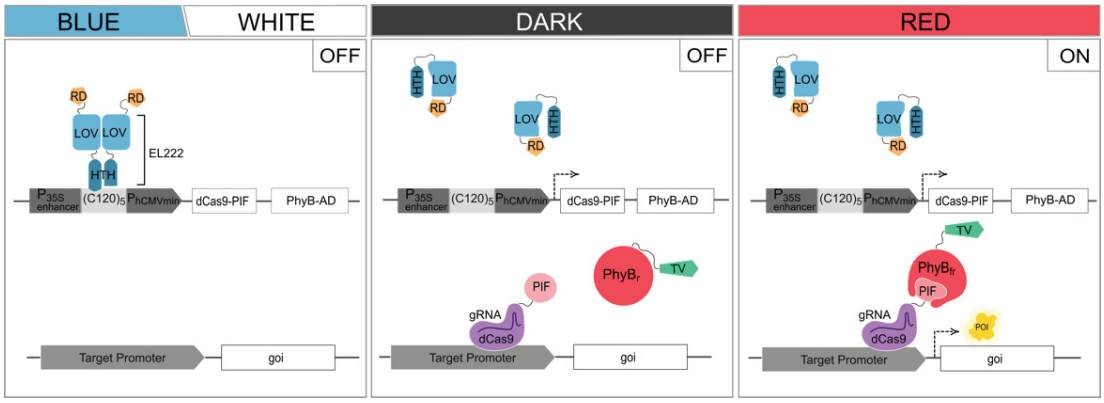


**Figure 15**. Theoretical approach for a red light endogenous gene expression control mediated by dCas9 not affected by white light. The components of the red-light activated dCas9 are under the control of the $B_{Off}$ system and therefore only expressed in the absence of blue light, *e.g.* in the night. However, only when there is red light, and in the absence of blue light, the components are expressed and interact with each other, resulting in the activation of the endogenous gene of interest. AD, activation domain; $(C120)_5$, five repeats of the DNA cognate sequence of EL222; dCas9, nuclease-deficient *Streptococcus pyogenes* Cas9; EL222, transcription factor 222 from *Erythrobacter litoralis*; gRNA, guide RNA part containing the 20 bp target sequence; goi, gene of interest; HTH, helix-turn-helix domain; LOV, light-oxygen-voltage domain; $P_{35Senhancer}$, enhancer region of the cauliflower mosaic virus 35S promoter, $P_{hCMVmin}$, minimal human cytomegalovirus immediate early promoter; PhyB, Phytochrome B; PIF, PHYTOCHROME INTERACTING FACTOR; RD, repression domain; TV, activation domain composed by 6x TAL and 2x VP64 and NLS sequence.

# 6. Chapter 3: Developing a system that is white light non-responsive

Ochoa-Fernandez, R., Abel, N.B., Wieland, F.G., Schlegel, J., Koch, L.A., Miller, J.B., Engesser, Giuriani, G., R., Brandl, S.M., Plum, J. Timmer, J., Weber ,W., Ott, T., Simon, R., and Zurbriggen, M.D. PULSE – Optogenetic control of gene expression in plants in the presence of ambient white light. *Manuscript submitted.* (Appendix A)

## *6.1. Design, implementation, and test of the Plant Usable Light Switch-Elements (PULSE) in plant cells*

PULSE is an integrated optogenetic molecular device, consisting of two components: a module providing activation of gene expression under red light ($R_{On}$) and a second one ensuring effective transcriptional repression under blue light ($B_{Off}$). The rationale behind this new conceptual and experimental approach is that the combination of both switches will yield a system that is inactive in ambient growth conditions (light and darkness) and only active upon irradiation with red light for its application in plants growing under standard light conditions (Figure 16).

To allow gene induction with PULSE, the novel blue light-repressible ($B_{Off}$) module based on the strongest repression version (Figure 9, Section 5.2.) was combined with the previously developed PhyB-PIF6 red light-inducible split transcription factor switch ($R_{On}$) (Figure 11, Chapter 2) (Müller et al., 2014b; Ochoa-Fernandez et al., 2016) (Figure 17a). PULSE thus integrates: i) a constitutively expressed red light-activation module composed of PhyB-VP16 and E-PIF6, ii) a constitutively expressed blue light-repressor module SRDX-EL222, and iii) a synthetic target promoter, $P_{Opto}$, integrating the binding domains for both switches, namely $(C120)_5$ and $(etr)_8$, upstream of a hCMV minimal promoter sequence driving the expression of a gene of interest, *e.g.* FLuc. In the presence of blue or white light (a combination of blue, green, red and far-red wavelengths as present in ambient light) both photoreceptors PhyB and EL222 bind to $P_{Opto}$. The net result of the recruitment of the transcriptional activator and repressor to the minimal promoter sets the system to the OFF state. This also applies to darkness and far red-light conditions, as the red light-switch is rendered inactive under these wavelengths. Under any other illumination condition lacking the blue light component, SRDX-EL222 is unable to bind $P_{Opto}$ and thus to repress transcription. The system is exclusively in the ON state upon monochromatic red light-illumination when the interaction between PhyB and PIF6 leads to the recruitment of the activation domain to the minimal promoter, inducing gene expression (Figure 17a).

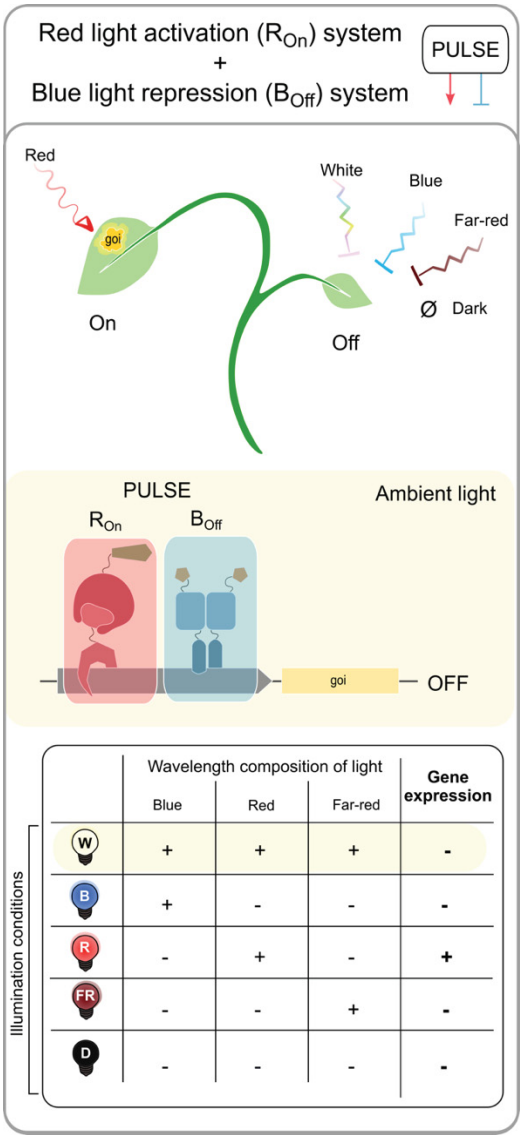


**Figure 16**. Design of PULSE, a functional optogenetic system for the control of gene expression in plants grown under light/dark cycles.PULSE (Plant Usable Light Switch-Element) is an optogenetic tool that combines a blue light-regulated repressor ($B_{Off}$) with a red light-inducible gene-expression switch ($R_{On}$). In this way gene expression is active only upon illumination with monochromatic red light, while remaining inactive in darkness and under blue, far-red, and white light, hence being applicable to plants grown under day/night cycles. (+), presence; (-), absence.

The PULSE system controlling FLuc expression was first introduced and tested in isolated Arabidopsis protoplasts (Figure 17b). The plasmids coding for the $R_{on}$ switch were co-transformed either with or without $B_{Off}$, and the protoplasts were incubated for 18 h under either red, blue, white or far-red light. In the absence of the repressor module (equivalent to $R_{On}$), efficient

activation of PhyB was observed by red light but also under blue and white, as UV and blue light (300 - 460 nm) also activate PhyB (Kelly and Lagarias, 1985; Müller et al., 2013b). Upon addition of the $B_{Off}$ repressor module (PULSE system), it was observed induction under red light treatment only, showing a high dynamic range, with up to 396.5-fold-induction rates relative to darkness, and a very low basal level of expression in blue and white light (1.7- and 1.6-fold, respectively).

## *6.2. Development of a quantitative model to describe and predict the PULSE activity*

In order to quantitatively understand the dynamics and functional characteristics of PULSE and to guide the experimental design of future applications concerning optimal light quality, intensity, and duration, an ordinary differential equations (ODE)-based quantitative mathematical model was developed in collaboration with the group of Prof. Timmer at the University of Freiburg. To parameterize the quantitative model, time-series mRNA and protein FLuc measurements (Figure 17c,d and **Supplementary Fig. S1a** - Appendix A), as well as light dose-response FLuc measurements (**Supplementary Fig. S1b,c** - Appendix A) were used as described by Müller *et al.* (Müller et al., 2013b).

The ON-OFF kinetic studies of the PULSE system were performed in protoplasts of *A. thaliana* by monitoring FLuc protein and mRNA levels (Figure 17c,d). Protoplasts transformed for PULSE-controlled FLuc expression were kept in darkness for 12 h. Illumination was started and after 3 h of red light-treatment, the samples were divided and incubated for the next 13 h: either i) in red light to quantify sustained activation, ii) transferred to darkness to assess the passive reversion of the system, or iii) transferred to blue light to determine active shut down of the system (ON-OFF) (Figure 17c). An increase of FLuc was observed under red light treatment while transfer to the dark or blue light led to termination of gene expression (faster and stronger under blue light). In addition, the latter samples (ON-OFF) were further split after 6 h of blue light

treatment further into blue and red light-incubation conditions (ON-OFF-ON). Re-activation of gene expression was observed, demonstrating the reversibility of the system. Samples illuminated for the whole period (15 h) with blue light showed only background levels of expression. To determine mRNA kinetics (Figure 17d), after transformation followed by 16 h of dark incubation, the protoplasts were illuminated for 4 h with red light and then transferred to blue light for additional 3 h. Samples were collected at the indicated time points and analyzed by quantitative reverse transcription-quantitative PCR (RT-qPCR).

In order to further characterize thresholds of time and intensity of red light illumination for protein production, endpoint measurements and dose-response experiments were performed (**Supplementary Fig. S1a,b** - Appendix A). As little as 15 min of 10 µmol $m^{-2}$ $s^{-1}$ red light treatment or very low intensities of red light (0.25 µmol $m^{-2}$ $s^{-1}$ for 18 h) was observed to be sufficient to strongly activate expression. Similarly, a blue light dose-response study, while keeping the red illumination constant, indicated that blue light-mediated repression overrides red light-mediated activation effects (**Supplementary Fig. S1c** - Appendix A).

In order to validate the model, the dynamic behaviour of PULSE was simulated at different red light-doses and illumination times and in the absence of blue light (Figure 17e), or upon simultaneous irradiation with different red and blue light intensities for 12 h (**Fig. Supplementary Fig. S2** - Appendix A). The resulting heatmaps will aid in the experimental design by guiding the targeted selection of conditions to obtain a given expression level of interest (Figure 17e,f**, Supplementary Fig. S2** - Appendix A). To illustrate this, PULSE was transformed into protoplasts and kept 12 h in the dark prior to incubation under six different combinations of red light intensities and illumination durations selected from the heatmap (Figure 17e). Figure 17f shows the experimental validation of the model predictions, namely the FLuc/RLuc ratio for the indicated experimental conditions. The two experimental conditions varied are the red light intensity and the time of continuous red light illumination. There is a strong correspondence between predicted and experimental FLuc/RLuc

determined values (Figure 17f), which indicates the applicability of the model to determine the experimental conditions (light intensity and time ranges) needed to achieve a tight control over the levels of gene expression with PULSE.

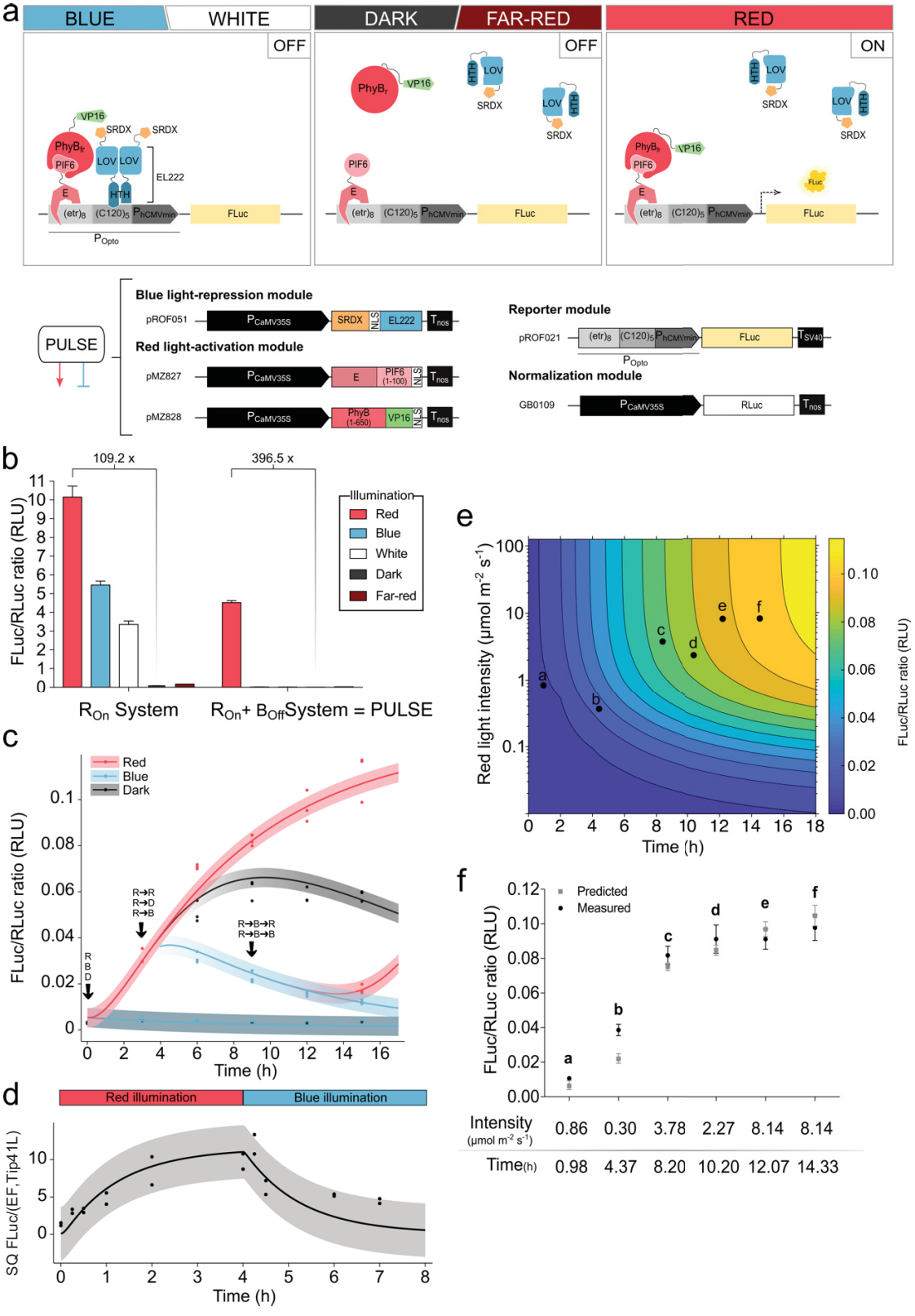


**Figure 17**. Molecular design, functional and model-based characterization of PULSE.**(a)** Mode of function of PULSE and constructs. The PULSE constructs are: i) the blue light-responsive element EL222 fused to the SRDX repressor domain, placed under the control of the constitutive promoter $P_{CaMV35S}$ ($B_{Off}$), ii) the red light-activated, far-red light-inactivated (reversible) split switch comprising the first 650

amino acids of the PhyB photoreceptor ($PhyB_{1-650}$) fused to the VP16 transactivation domain, and the macrolide repressor DNA-binding protein E 8mphR(A) fused to the first 100 amino acids of PIF6 ($PIF_{1-100}$) (Müller et al., 2014b) ($R_{On}$). The two modules of the switch are constitutively expressed from the promoter $P_{CaMV35S}$, iii) a synthetic promoter $P_{Opto}$ comprising eight repeats of the target sequence of the protein E, etr - $(etr)_8$ -, five repeats of C120 - $(C120)_5$ -, and the minimal promoter $P_{hCMVmin}$, driving the expression of the reporter gene FLuc, iv) the normalization element RLuc expressed constitutively from $P_{CaMV35S}$. Under white/ambient light or blue light, SRDX-EL222 dimerizes and binds the $(C120)_5$ element through the HTH domain. Under these conditions, PhyB is also active ($PhyB_{fr}$), due to the blue and red light components of white light (Kelly and Lagarias, 1985; Müller et al., 2013b), and, therefore, able to interact with PIF6, which is bound to $(etr)_8$ through the E protein. In consequence, there is recruitment of both the transactivator VP16 and the transcriptional repressor SRDX to the minimal promoter, resulting in no expression of FLuc as the repressor has a dominant effect on gene expression (left). In darkness or in far-red light, EL222 and PhyB are in the inactive form ($PhyB_r$), therefore, both are unable to bind to $P_{Opto}$, resulting in no FLuc transcription (middle). There is induction of FLuc expression only under monochromatic red light, in which EL222 is inactive and PhyB is in its active conformation, binding PIF6 (right). **(b)** Functional characterization of PULSE in Arabidopsis protoplasts. Protoplasts were transformed with the $R_{On}$ module (pMZ827, pMZ828), the reporter $P_{Opto}$-FLuc (pROF021) and either with the $B_{Off}$ module (pROF051, PULSE system complete) or without $B_{Off}$ (stuffer plasmid, equivalent to the $R_{On}$ system alone). The normalization element (GB0109) is additionally included. Protoplasts were kept in the dark or illuminated with white LEDs adjusted to simulate ambient light (see **Supplementary Fig. S7** and **Methods** - Appendix A), or 10 µmol $m^{-2}$ $s^{-1}$ of $red_{\lambda max\ 655\ nm}$, $blue_{\lambda max\ 461\ nm}$, or $far\text{-}red_{\lambda max\ 740\ nm}$ light. Data shows mean FLuc/RLuc ratios determined 18 h after illumination, SEM (*n* = 6). **(c,d)** Quantitative characterization of ON-OFF FLuc expression kinetics. Protoplasts of Arabidopsis were transformed with PULSE and first kept in the dark, 12 h for protein (c) and 16 h for mRNA (d) determination assays. Samples were afterwards illuminated with either 10 µmol $m^{-2}$ $s^{-1}$ of red or blue light, or kept in darkness for the indicated time periods. Arrows indicate the time point where the samples were split into different illumination conditions for response and reversibility analyses, *e.g.* red to dark, red to blue (ON-OFF), red to blue to red (ON-OFF-ON). Samples were collected every 3 h for 15 h for FLuc and RLuc determinations in a plate reader; and at 15 min, 30 min, 1 h, 2 h, 4 h, 4 h 15 min, 4 h 30 min, 6 h, 7 h for RT-qPCR determinations of mRNA production. The curves are the fits to the ODE-based model. The shaded areas represent the error bands as calculated in 95% confidence intervals with a constant Gaussian error model using the profile likelihood method. Depicted are the FLuc/RLuc ratios for protein expression kinetics, (*n* = 6) (c), and the starting quantity (SQ) of FLuc transcript normalized with internal controls EF and Tip41L, of two technical replicates (d). **(e)** Model aided prediction of PULSE-controlled protein expression levels as a function of red light intensities and illumination times. The calibrated model yields estimated FLuc/RLuc expression ranges (heatmap). **(f)** Experimental validation of the model predictions of the operating range of PULSE. Selected model simulated expression levels at different red light intensities and illumination times as indicated in (e) were experimentally tested and the resulting FLuc/RLuc ratios (2xSEM, *n* = 6) were compared to the predicted values (error bars calculated as in (c,d)). RLU = Relative Luminescence Units. NLS = Nuclear Localization Sequence.

## 6.3. *PULSE-controlled expression of CRISPR/Cas9-derived gene activator and plant transcription factors to regulate promoters in Arabidopsis protoplasts*

PULSE was customized to achieve quantitative and temporally resolved control over the expression of genes from any given promoter of interest, be it orthogonal, synthetic or endogenous (downstream activation). For this, two approaches were followed, applying PULSE: i) to induce the synthesis of a CRISPR/Cas9-derived gene activator, or ii) to induce expression of an Arabidopsis TF. These expressed transcriptional activators, in turn, activate expression from a target orthogonal promoter (Figure 18a,b) or a target Arabidopsis promoter (Figure 18c-f). The Cas9-derived gene activator is targeted to its cognate promoter by an *ad-hoc* designed guide RNA, whereas the TF binds its natural target promoter.

### *6.3.1. Optogenetic controlled expression of a Cas9-derived gene activator*

To achieve optogenetic and customizable control of potentially any target promoter, PULSE was set to control expression of a nuclease-deficient *Streptococcus pyogenes* Cas9 protein fused to a strong activation domain (named dCas9-TV) (Li et al., 2017; Selma et al., 2019). In a first proof of principle application, PULSE-induced dCas9-TV was used to drive expression from the orthogonal *S. lycopersicum* dihydroflavonol 4-reductase promoter ($P_{SlDFR}$) using FLuc as a quantitative readout in Arabidopsis protoplasts (Figure 18a). To target the promoter, a gRNA against the -150 bp relative to the TSS region of $P_{SlDFR}$ was used (Selma et al., 2019). PULSE-controlled dCas9-TV led to activation of the promoter only upon red illumination, achieving 24.5- and 40.0-fold induction rate compared to blue light and dark treatments, respectively (Figure 18b). Constitutive expression of dCas9-TV served as a positive control yielding the maximum activation capacity of $P_{SlDFR}$, 105.1-fold induction relative to the configuration without dCas9-TV (**Supplementary Fig. S3a** - Appendix A). In a second setup, optogenetically-induced dCas9-TV targeted the promoter of the Arabidopsis gene APETALA1 ($P_{AtAP1}$) fused to the reporter FLuc ($P_{AtAP1}$-FLuc) in a plasmid. A gRNA was designed to target the

-100 bp region relative to the TSS of $P_{AtAP1}$ (Figure 18c). Red light induction of dCas9-TV yielded 17.9- and 14.1-fold FLuc induction rates from the $P_{AtAP1}$-FLuc construct compared to blue and dark illumination (Figure 18e). Constitutive expression of dCas9-TV yielded a 28.6-fold induction relative to the configuration without dCas9-TV (**Supplementary Fig. S3b** - Appendix A).

### *6.3.2. Optogenetically-induced expression of the Arabidopsis transcription factor LEAFY*

For the second approach, a transcription factor was chosen to be under the control of PULSE. On one hand, the Arabidopsis transcription factor LEAFY (LFY) that is known to bind $P_{AtAP1}$ and promote the expression of AP1 (Parcy et al., 1998; Simon et al., 1996; Wagner et al., 1999) was considered. LFY and AP1 are involved in Arabidopsis flowering and are both expressed in the floral primordia. On another hand, the FLOWERING LOCUS T (FT) protein was considered as it is reported to travel from the leaf to the shoot apical meristem and promote, in conjunction with the bZIP transcription factor FD, AP1 expression and flowering (Abe et al., 2005; Wigge, 2005).

An initial pre-screening in Arabidopsis mesophyll protoplasts expressing LFY and LFY fused to the transactivator VP16, showed that LFY did not suffice to activate the expression of FLuc placed downstream of the AP1 promoter while LFY-VP16 provided activation (data not shown). This suggests that LFY has binding DNA activity but not transactivation activity and probably needs other protein(s) for the activation of AP1 which are tissue- and/or stage-specific like previously pointed out (Goslin et al., 2017; Parcy et al., 1998). Likewise, the expression of FT or FT-VP16 co-expressed with FD, did not provide expression of FLuc (data not shown), also suggesting the need of additional protein(s) for the activation of AP1, like the proposed 14-3-3 protein (Kawamoto et al., 2015; Taoka et al., 2011) or the recently proposed TEOSINTE BRANCHED1, CYCLOIDEA, PCF (TCP) family of transcription factors. (Ho and Weigel, 2014; Li et al., 2019).

Based on this pre-screening, LFY-VP16 was focused on to be placed under PULSE control. LFY-VP16 was fused to RLuc using a self-cleaving 2A

sequence, which yields equimolar amounts of both proteins from a single transcript (de Felipe et al., 2006) ($P_{Opto}$-LFY-VP16-2A-RLuc). The luminescence determination of RLuc allows the indirect quantification of the amount of LFY-VP16 protein synthesized (Figure 18d). The plasmids coding for PULSE were co-transformed in Arabidopsis protoplasts either with or without the optogenetically inducible LFY-VP16, and a $P_{AtAP1}$-FLuc target plasmid. RLuc luminescence values indicate expression of LFY-VP16 upon red light treatment, while only basal levels were obtained upon blue light or dark treatment (17.5- and 26.6-fold induction, respectively). The red light-induced expression of LFY-VP16 led to activation of $P_{AtAP1}$ and, therefore, FLuc expression achieving 31.4- and 7.4-fold induction rates compared to blue and darkness conditions, respectively (Figure 18f, controls in **Supplementary Fig. S3c** - Appendix A; FLuc determinations of the configuration without LFY-VP16-2A-RLuc were used to quantify the background promoter levels and subtracted from the samples with LFY).

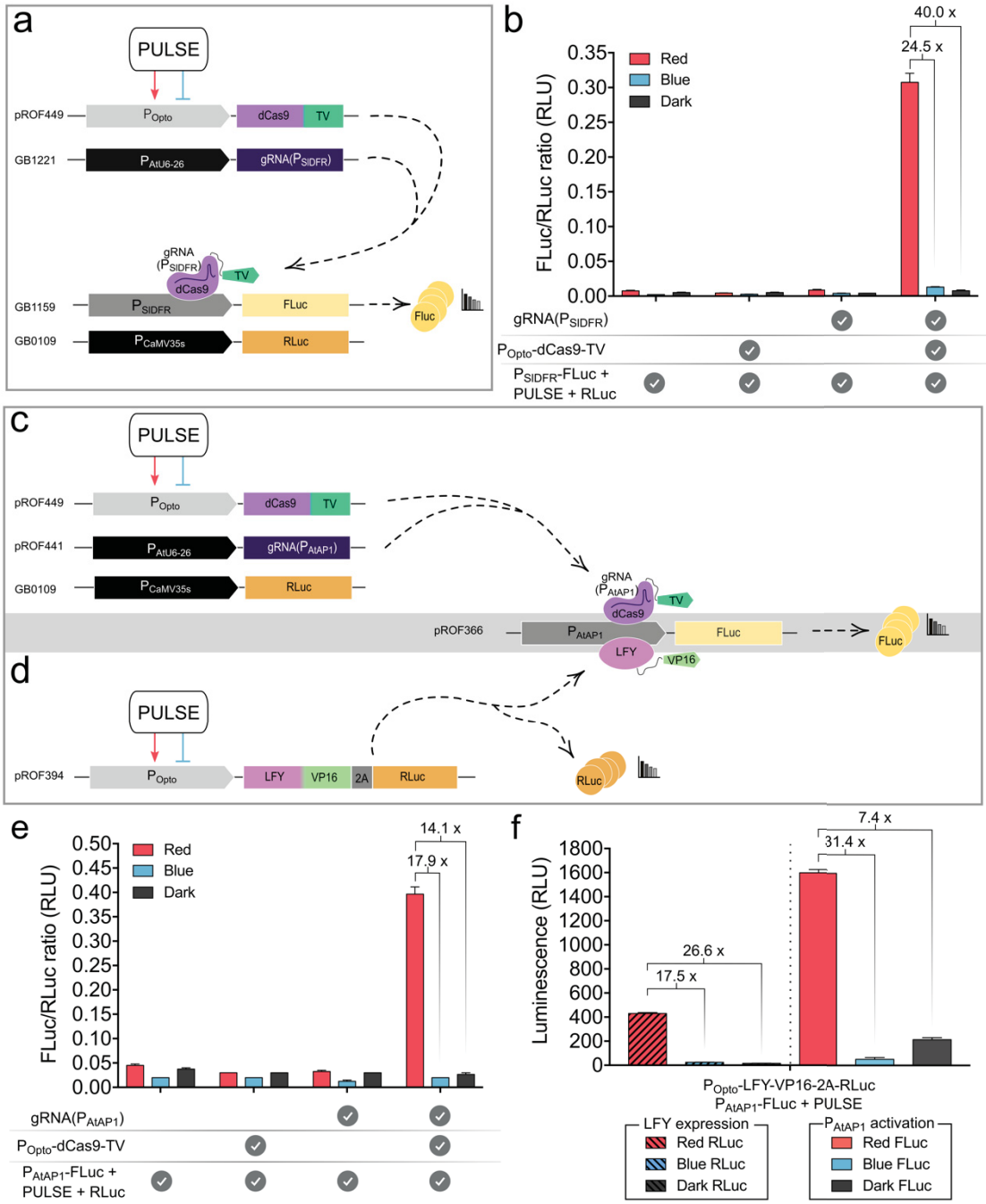


**Figure 18**. PULSE-controlled expression of a Cas9-derived gene activator (dCas9-TV) and an Aarabidopsis transcription factor for the targeted activation of promoters in Arabidopsis protoplasts. **(a,b)** Optogenetically controlled dCas9-TV expression to activate a target orthogonal promoter. In the presence of PULSE, dCas9-TV is expressed from $P_{Opto}$-dCas9-TV only under red light. dCas9-TV targets the orthogonal $P_{SIDFR}$ promoter via a gRNA (a). Activation of $P_{SIDFR}$-FLuc is quantified through the reporter FLuc, and RLuc is used for normalization (b). Data shown are means of FLuc/RLuc ratio, SEM ($n$ = 4) (b). **(c-f)** Optogenetic control of an Arabidopsis plant promoter from a plasmid construct ($P_{AtAP1}$-FLuc). In a first approach, PULSE is co-transformed with $P_{Opto}$-dCas9-TV, a gRNA directed specifically to the AtAP1 promoter sequence and the $P_{AtAP1}$-FLuc construct (c). Activation of $P_{AtAP1}$-FLuc is quantified

through the reporter FLuc, and RLuc is used for normalization (e). Data shown are means of FLuc/RLuc ratio, SEM ($n$ = 4) (e). In a second approach, PULSE controlled the expression of the transcription factor LFY-VP16, from the $P_{Opto}$-LFY-VP16-2A-RLuc construct. RLuc is co-expressed (via a 2A self-cleaving peptide) and used as a proxy of LFY-VP16 expression. LFY binds the $P_{AtAP1}$ promoter hence activating FLuc expression from the $P_{AtAP1}$-FLuc construct (d). FLuc and RLuc determinations in protoplasts co-expressing PULSE, $P_{Opto}$-LFY-VP16-2A-RLuc (striped bars) and $P_{AtAP1}$-FLuc (solid bars) under different light conditions, SEM ($n$ = 6) (f). Data shown are means of RLuc, and means of FLuc after subtraction of background values (configuration without $P_{Opto}$-LFY-VP16-2A-RLuc). **(b,e,f)** The protoplasts were incubated in darkness, red or blue light, and luminescence determinations performed after 18 h. RLU = Relative Luminescence Units.

## *6.4. In planta optogenetic control of gene expression with PULSE*

In order to evaluate the functionality of PULSE in plants, a new set of vectors was first designed and constructed for transformation via *Agrobacterium tumefaciens* with all necessary components in one binary plasmid. The vectors comprise a reporter gene under the control of PULSE ($P_{Opto}$), PULSE expressed under a constitutive promoter (either $P_{CaMV35S}$ or $P_{AtUbi10}$), and optionally, a constitutively expressed reporter gene as a normalization element and a plant selection cassette nptII which confers kanamycin resistance (for a full description of all vectors used see **Supplementary Table S1** - Appendix A).

*N. benthamiana* leaves were transformed with a construct having a fluorescent protein gene as a reporter (Venus fused to histone H2B for nuclear localization, $P_{Opto}$-Venus-H2B) placed under the control of PULSE. The performance of the system was analyzed using fluorescence microscopy. Constitutively expressed Cerulean-NLS was included as a marker for transformation. Infiltrated plants were placed in darkness for 2.5 days prior to illumination with red, blue, white light, or dark treatment. Samples were collected at different time points for analysis using confocal microscopy (Figure 19a and **Supplementary Fig. S4** - Appendix A)**.** Plots were generated after determining the Venus and Cerulean mean fluorescence intensities in nuclei (Figure 19b). An increase over time in the Venus/Cerulean ratio was observed only in samples illuminated with red light (28.7-fold induction after 9 h), demonstrating expected activation characteristics of the system *in planta*. Additionally,

PULSE control over a β-glucuronidase gene ($P_{opto}$-GUS) is shown in **Supplementary Fig. S5** - Appendix A.

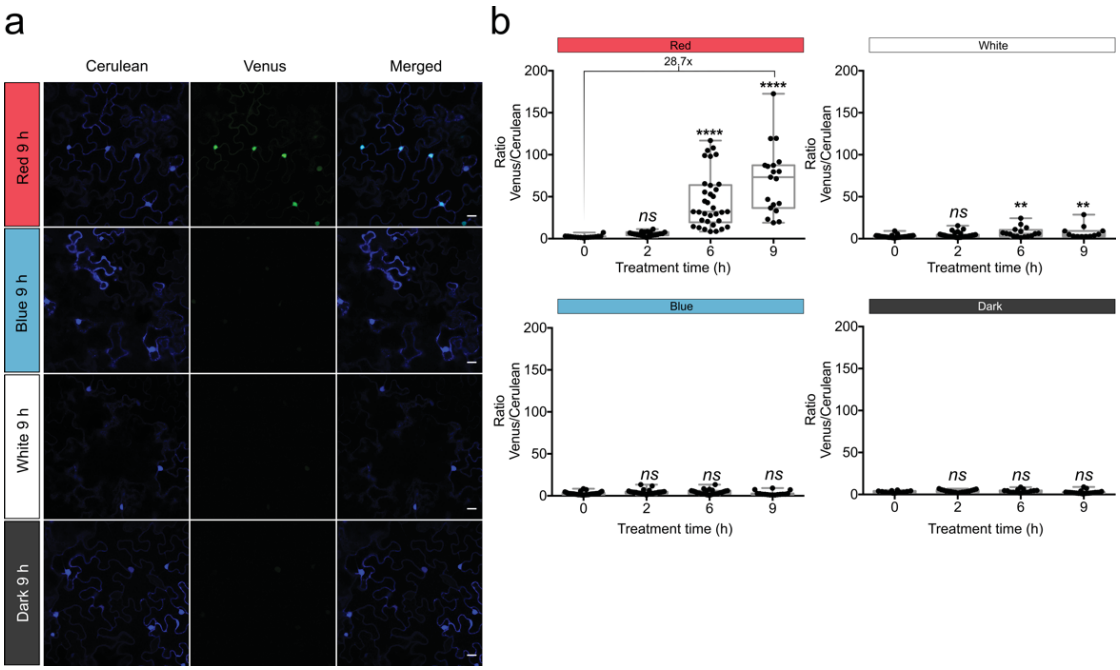


**Figure 19**. Implementation and characterization of PULSE in *Nicotiana benthamiana* leaves. Plants infiltrated with PULSE, $P_{Opto}$-Venus and a constitutively expressed Cerulean cassette (pROF346) were kept in dark for 2.5 days prior to light treatment for 2 h, 6 h, 9 h (10 µmol $m^{-2}$ $s^{-1}$ of red light, 10 µmol $m^{-2}$ $s^{-1}$ of blue light, simulated white light, or darkness (as described in **Supplementary Fig. S7 and Methods** - Appendix A). **(a)** Samples were taken at indicated time points for fluorescence confocal microscopy observation. **(b)** Data shown are the ratio of nuclear Venus and Cerulean fluorescence intensities, $12 \leq n \leq 34$. The horizontal line in the box represents the median and the statistical significance is determined by a one way-ANOVA and Dunnett's multiple comparison test (**$p < 0.01$, ***$p < 0.001$, ****$p \leq 0.0001$, *ns* not significant).

In order to show some of the potential applications of PULSE *in planta*, the system was used to induce plant immunity and to conditionally target receptors.

In plants, signal integration of extracellular stimuli is predominantly mediated by membrane-resident receptor and transport complexes. To mechanistically understand their function, is required non-invasive inducible systems that allow transcriptional induction or complex formation with high temporal precision in order to reconstitute these functional entities in homologous as well as heterologous systems. To test whether PULSE allows the generation of

immune-competent leaf epidermal cells, a heterologous pattern recognition receptor was introduced.

In *Arabidopsis*, the recognition of the bacterial microbe-associated molecular pattern (MAMP) elf18 by the plant innate immune EF-Tu Receptor (EFR) results in a fast and transient increase in cellular reactive oxygen species (ROS) (Zipfel et al., 2006). By contrast, Solanaceae species such as *N. benthamiana* are devoid of EFR and, therefore, unable to perceive the elf18 peptide. However, genetic transformation of *N. bethamiana* and tomato (*Solanum lycopersicum*) with *At*EFR allows these plants to recognize elf18 and confers increased resistance against phytopathogens such as *Ralstonia solanacearum* (Lacombe et al., 2010; Zipfel et al., 2006).

### *6.4.1. Optogenetic control of plant immunity*

To achieve optogenetically controlled induction of immunity a EFR-GFP fusion protein was expressed under the control of PULSE ($P_{Opto}$-EFR-GFP) in *N. benthamiana* leaf epidermal cells (Figure 20a). Illumination of leaves for 16 h with red light resulted in a clear GFP signal at the cell periphery indicating that EFR-GFP was successfully localized into the plasma membrane (**Supplementary Fig. S6** - Appendix A). To test whether optogenetically-controlled EFR provides susceptibility of these cells towards elf18, 1 μM of the elf18 ligand was applied. Indeed, a strong and transient production of ROS was observed approximately 10 min after elf18 application in leaves that have been red light-treated (red filled circles; Figure 20b). Quantitative assays showed 10-fold lower ROS burst triggered in white light-grown plants (black filled circles; Figure 20b), demonstrating light-repression by PULSE under ambient light conditions. No responses were found in untransformed tissue and leaves expressing EFR but incubated in the absence of elf18. These data show that PULSE can be used for inducing physiological responses *in planta* in a time-controlled manner.

### *6.4.2. Conditional targeting of receptors using nanobodies*

In mammalian cells, receptor complexes have been reconstituted and modulated using genetically encoded nanobodies (Gulati et al., 2018;

Kirchhofer et al., 2009). Given their small size and their high-affinity binding characteristics, nanobodies can be used to selectively target effector proteins to receptor complexes, to subcellularly relocalize proteins in a stimulus-dependent manner or to visualize endogenous proteins using fluorophore-tagged nanobodies. To test the applicability of PULSE for such experiments, the immune receptor EFR was constitutively expressed in *N. benthamiana* leaf epidermal cells and co-transformed a genetically encoded GFP nanobody (GFP binding protein, GBP) that binds GFP in plant cells (Schornack et al., 2009). To monitor receptor targeting, additionally GBP was fused to a mCherry fluorophore (GBP-mCherry). As the inducibility of effector delivery to receptor complexes will provide the basis for modulating their activity, PULSE provides a temporal control over GBP-mCherry expression ($P_{Opto}$-GBP-mCherry) and, therefore, conditionally controls nanobody targeting (Figure 20c). While EFR-deficient cells illuminated with white light did not yield any detectable fluorescence, red light-induction of GBP-mCherry resulted in a cytosolic localization of the soluble protein. By contrast, red light-induced cells constitutively expressing EFR-GFP and co-transformed with $P_{Opto}$-GBP-mCherry showed an almost exclusive targeting of the fluorescently-tagged nanobody to the plasma membrane, indicating efficient binding of the GFP-tag by GBP (Figure 20d). This demonstrates the ability to conduct time-resolved conditional targeting experiments by using a PULSE/nanobody combination allowing precision targeting of receptors and consequently modulating receptor complex composition and/or activity in future experiments.

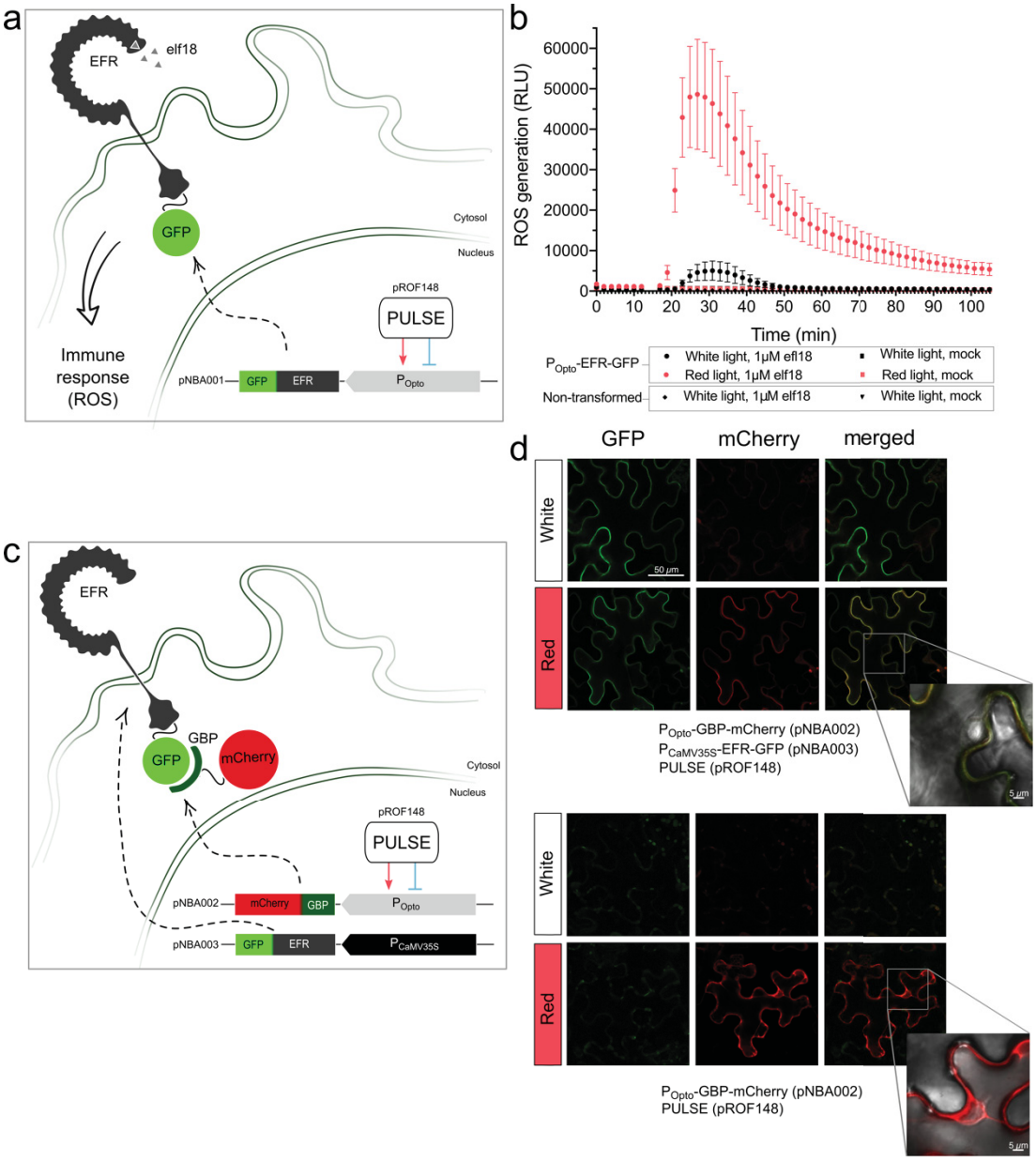


**Figure 20**. *In planta* optogenetic heterologous induction of immunity and conditional subcellular targeting of receptors. **(a,b)** PULSE-controlled conditional gain of immunity *in planta*. *N. benthamiana* leaves were infiltrated with PULSE and $P_{Opto}$-EFR-GFP. Two plants were used for each illumination condition. Four disks from one leaf of each plant were collected and treated with 1 µM elf18 or mock previous to ROS quantification. Data shown are luminescence mean values, SEM (*n* = 8). **(c,d)** Conditional targeting of receptors by optogenetically controlled expression of a nanobody (GBP-mCherry). The figure shows representative results of *N. benthamiana* leaves infiltrated with PULSE, $P_{Opto}$-GBP-mCherry, and $P_{CaMV35S}$-EFR-GFP and with different illumination treatments prior to observation in the fluorescence confocal microscope. As a control, plants were infiltrated with PULSE and $P_{Opto}$-GBP-mCherry. **(b,d)** Plants were kept in standard growth conditions (16 h simulated white light – 8 h dark) for 2 d prior to induction with 10 µmol $m^{-2}$ $s^{-1}$ red light for additional 16 h (white light illumination was used as control). RLU = Relative Luminescence Units.

## *6.5. PULSE characterization in stable transgenic lines*

To test the functionality of PULSE in whole plants, transgenic Arabidopsis lines were generated using the plasmids coding for PULSE and $P_{Opto}$-FLuc as a reporter. Additionally, a plant selection cassette (KanR) and a constitutive RLuc was incorporated into the plasmid. Different versions were engineered with either of two constitutive promoters controlling the expression of the three light switchable elements of PULSE, either $P_{CaMV35S}$ (BM00654) or $P_{AtUbi10}$ (BM00655). A pre-screening to assess expression levels was performed on several lines and the ones showing better performance were selected (results not shown). Seedlings of homozygous T3 plants were grown in media in a multi-well plate for 7 days, were incubated with luciferin and the luminescence was quantified while the plate was subjected to different light treatments as indicated in Figure 21. Results for three independent PULSE lines (two with the $P_{CaMV35S}$ and one with the $P_{AtUbi10}$ promoters) show different levels of expression with activation levels ranging from 10- to 372-fold, depending on the choice of promoters driving PULSE expression and the integration event of the transgene (Figure 21). For all lines, transfer from simulated white light to red light led to activation of expression, and subsequent reversion was achieved when the plants were moved back to white light, demonstrating reversibility of the system. It was observed that the system remained active when transferred from white light to dark probably due to the accumulated amount of PhyB at the end of the day and sudden removal of the repressor. However, this could be reduced when applying a short far-red pulse before the dark cycle, returning to almost FLuc basal levels in the line with $P_{AtUbi10}$, probably due to the lesser amount of photoreceptor accumulated. It is worth noting that, contrarily to the lines with $P_{CaMV35S}$, the line with $P_{AtUbi10}$ shows a decrease of FLuc expression after *ca.* 10 hours of sustained red light treatment. Nonetheless, other independent lines will have to be tested in order to exclude integration-dependent behaviour.

These different dynamic ranges show that the system is functional in Arabidopsis whole plants to control the expression of a transgene. It is

probably more desirable to have the photoreceptors under the control of a weaker promoter, such as $P_{AtUbi10}$, in order to have a lower amount of the photoreceptors and minimum interference with the endogenous PhyB and PIF signalling. However, further photobiological experiments need to be carried out in follow up work, like hypocotyl elongation, seed germination to evaluate the interference. In any case, the performance of the switch and expression levels will have to be assessed for each particular gene of interest and application.

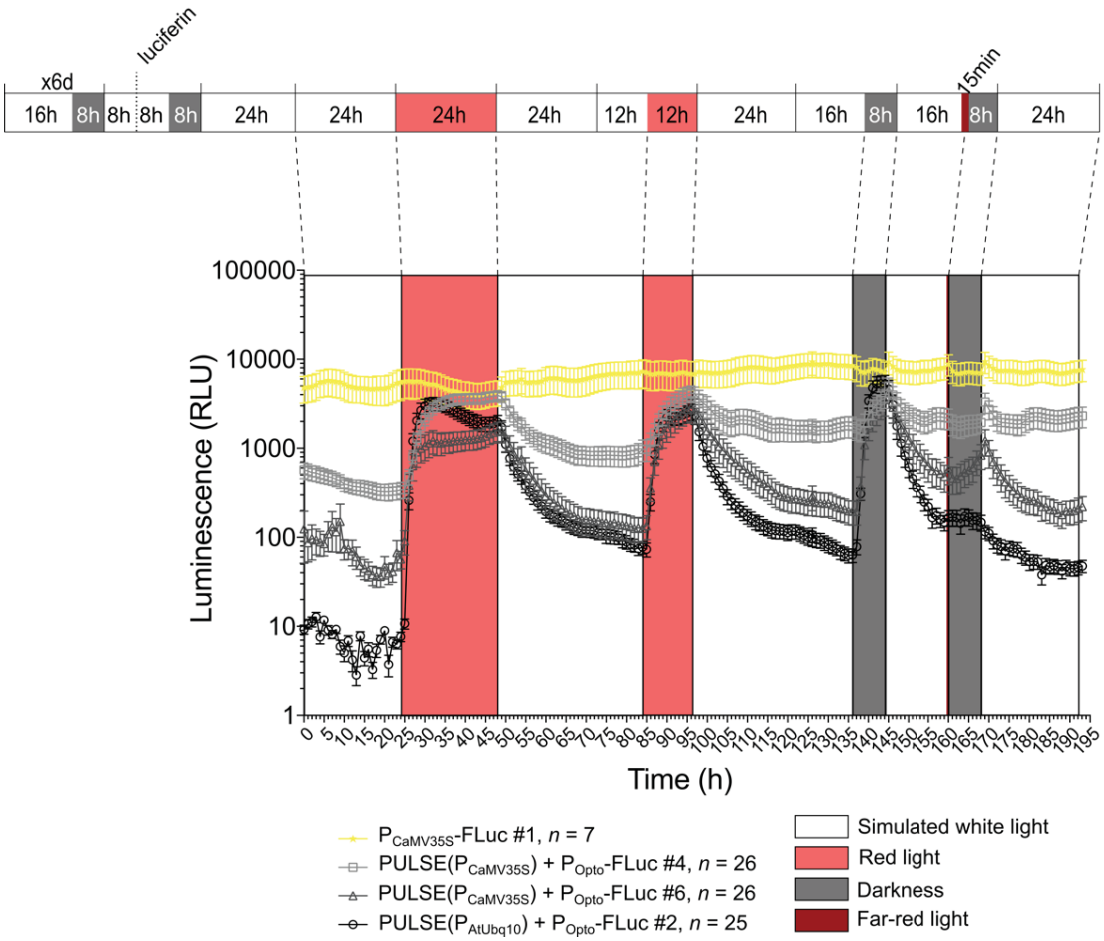


**Figure 21**. PULSE functionality in Arabidopsis plants. Stable Arabidopsis transgenic lines transformed with PULSE controlling $P_{Opto}$-FLuc, were seeded in a white 96-well plate with plant growth media. Transgenic plants constitutively expressing FLuc and wild type plants were used as positive and negative controls, respectively. After 8 d, luminescence determinations in a plate reader started with data points taken every hour for over 8 days while the plate was under illumination as indicated. Simulated white light (as described in **Supplementary Fig. S7 and Methods** - Appendix A), red light (10 µmol $m^{-2}$ $s^{-1}$), and far-red light (8 µmol $m^{-2}$ $s^{-1}$). Three different independent homozygous PULSE lines were tested with the components under the control of the CaMV35S – PULSE($P_{CaMV35S}$) + $P_{Opto}$-FLuc #4 and #6 – and AtUbi10 – PULSE($P_{AtUbi10}$) + $P_{Opto}$- FLuc #2 – constitutive promoters. *n* = 25 – 26 for PULSE lines and *n* = 6 – 7 for the controls. The determinations of six wild type seedlings at each time point were averaged

and subtracted from the measurements of the lines. Plotted data are averages and SEM. RLU = Relative Luminescence Units.

Other plasmids and transgenic lines were generated but are still under characterization (see overview in Table 4). Some lines are aimed at the characterization of the system, like those controlling reporter genes FLuc and Venus, but others could be used to control processes of the plant such as the control of flowering by inducing the expression of FT. Additionally, a driver line with PULSE without any gene of interest is being generated for the facilitation of the generation of future applications to control the desired gene of interest.

**Table 4**. Generated transgenic Arabidopsis lines overview.

| Plasmid | $P_{Opto}$-goi | Promoters PULSE | Normalization cassette | Status |
|---|---|---|---|---|
| BM00654 | FLuc | $P_{CaMV35S}$ | RLuc | 2x homozygous T3 lines |
| BM00655 | FLuc | $P_{AtUbi10}$ | RLuc | 1x homozygous T3 line |
| pROF346 | Venus-H2B | $P_{AtUbi10}$ | Cerulean-NLS | 1x homozygous T3 line |
| pROF405 | FT-VP16-HAtag | $P_{AtUbi10}$ | Venus-H2B | 1x homozygous T3 line |
| pROF415 | FT | $P_{AtUbi10}$ | Venus-H2B | 1x homozygous T3 line |
| pROF450 | - | $P_{AtUbi10}$ | - | 1x T2 line |

## *6.6. Discussion*

In conclusion, an optogenetic device for the control of gene expression in plants that is non-responsive to ambient illumination conditions and can be activated by illuminating with a narrow wavelength spectrum was enineered. The novel conceptual approach implements the design of a dual-wavelength optogenetic switch combining a blue light-regulated repressor with a red light-inducible gene expression switch. In this way, PULSE shuts expression off under ambient light, and induces transcription under red light.

The system showed a high dynamic range in Arabidopsis protoplasts with approximately a 400-fold activation (red light vs. darkness), reversibility and no toxicity. PULSE is applicable for the targeted study of signalling and metabolic networks by, in principle, allowing the control of any endogenous or synthetic promoter of interest. This was exemplified with the light-driven expression of an Arabidopsis TF, which in turn activates expression of its target promoter, or upon the use of the CRISPR/Cas9-derived transcriptional activator. *In planta*, implementation of PULSE demonstrated tight temporal control over subcellular conditional protein targeting, and the capability to induce immunity in *N. benthamiana* leaves.

However, the temporal control depends on the stability of the protein of interest (POI). FLuc has a short half-life of 4-5 h (Feeney et al., 2016; Urquiza-García and Millar, 2019), so fast dynamics can be observed. If studying, for instance, a transcription factor with longer half-life, slower ON-OFF dynamics will be observed. Re-engineering the goi to make it more unstable might be desirable, for instance by using destabilizing sequences. Likewise, with an unstable POI a long light treatment might be needed in order to see an effect. In that case, a re-engineering of the gene or a positive transcriptional feedback loop might be desirable.

As a proof-of-principle, it was showed that the system could be implemented stably in Arabidopsis to control the expression of a reporter gene, showing different expression levels depending on the choice of PULSE promoters and the integration of the transgene. The lines showed activation when shifted from white to red light and reversibility when switched back to white light. There is FLuc expression in the dark that is significantly reduced when a pulse of far-red is applied prior to the dark cycle, which points that the $PhyB_{(1-650)}$-VP16 that has been accumulated and still bound to the E-PIF during the day leads to a sudden activation of the system when the repressor is rapidly removed in the dark. It could also be that $PhyB_{(1-650)}$-VP16 has a slower reversion kinetics than previously observed in protoplasts. This issue could be solved in the future by adding a second step of control over the PhyB module, either placing it under the control of a chemical inducible system or another optogenetic

switch (similar to the strategy conceptualized in Figure 15). Another possibility is to use a mutated PhyB with enhanced dark reversion such as PhyB S86D or Y276I (Medzihradszky et al., 2013; Su and Lagarias, 2007). It could also be interesting to test different fusions between PhyA and PhyB that confer different responses to red light, far-red light, and dark (Oka et al., 2012).

Despite the future improvement needed, up to date, this is the first example of an optogenetic tool controlling gene expression applied *in planta*, opening up many opportunities in the field of plant sciences.

# IV. Conclusion

In this work, different optogenetic switches that contribute to the expansion of the toolbox to control gene expression in plant cells and plant tissue was shown. The first steps towards the application of optoswitches in stable transformed plants have also been made.

The use of plant protoplasts from the leaves of *Arabidopsis thaliana* has proven useful in the screening and quickly assessment of the performance of optogenetic switches. It is fast and robust and provides quantitative data that can be used for mathematical modelling that can aid in future experimental design or even in the development of new switches. It is a good method to use for testing in iterations, following the “Design-Build-Test” doctrine of synthetic biology.

Three different switches controlled by green, blue and red light were implemented and characterized in protoplasts, expanding the available tools to control gene expression in plant systems. Notwithstanding, the application is, at the moment, only in plant cells. However, these could be optimized in the future for their application *in planta*. Additionally, the red light-controlled dCas9 is, to date, the first inducible Cas9-based tool inducible by red light and could be applied in the future to manipulate synthetic and endogenous signalling pathways. These tools could be fundamental components in the design of novel multi-chromatic gene control systems.

Finally, a tool that is suitable for application *in planta* by designing a dual chromatic switch was developed. This tool, termed PULSE, was characterized in Arabidopsis protoplasts and applied to control transcription factors and to activate promoters by controlling dCas9. The system was also applied to Nicotiana leaves for controlling plant immunity and conditional subcellular targeting of receptors. The first steps towards their implementation in Arabidopsis stable lines have shown promising results as well.

This work reflects the ground-breaking opportunities for plant fundamental and biotechnological fields provided by optogenetics. Due to the quantitative modulation, spatiotemporal resolution and the reversible control capabilities provided, the generalized application of PULSE could facilitate in the future the

targeted manipulation and study of biological processes including plant development, metabolic engineering, hormone perception and signalling, and stress responses. Such tools will play a part in developing “smart plants” that could have desired functionalities, for instance towards controlling flowering, the development of sensor plants or the bioproduction of compounds with therapeutical interest.

# V. References


Abe, M., Kobayashi, Y., Yamamoto, S., Daimon, Y., Yamaguchi, A., Ikeda, Y., Ichinoki, H., Notaguchi, M., Goto, K., and Araki, T. (2005). FD, a bZIP Protein Mediating Signals from the Floral Pathway Integrator FT at the Shoot Apex. Science *309*, 1052–1056.

Adrian, M., Nijenhuis, W., Hoogstraaten, R.I., Willems, J., and Kapitein, L.C. (2017). A Phytochrome-Derived Photoswitch for Intracellular Transport. ACS Synth. Biol. *6*, 1248–1256.

Agrawal, P.K., Kohli, A., Twyman, R.M., and Christou, P. (2005). Transformation of Plants with Multiple Cassettes Generates Simple Transgene Integration Patterns and High Expression Levels. Mol. Breed. *16*, 247–260.

Ajo-Franklin, C.M., Drubin, D.A., Eskin, J.A., Gee, E.P.S., Landgraf, D., Phillips, I., and Silver, P.A. (2007). Rational design of memory in eukaryotic cells. Genes Dev. *21*, 2271–2276.

An-adirekkun, J. (My), Stewart, C.J., Geller, S.H., Patel, M.T., Melendez, J., Oakes, B.L., Noyes, M.B., and McClean, M.N. (2019). A yeast optogenetic toolkit (yOTK) for gene expression control in *Saccharomyces cerevisiae*. BioRxiv 663393.

Anders, K., and Essen, L.-O. (2015). The family of phytochrome-like photoreceptors: diverse, complex and multi-colored, but very useful. Curr. Opin. Struct. Biol. *35*, 7–16.

Anderson, J.C., Clarke, E.J., Arkin, A.P., and Voigt, C.A. (2006). Environmentally Controlled Invasion of Cancer Cells by Engineered Bacteria. J. Mol. Biol. *355*, 619–627.

Andres, J., Blomeier, T., and Zurbriggen, M.D. (2019). Synthetic Switches and Regulatory Circuits in Plants. Plant Physiol. *179*, 862–884.

Antunes, M.S., Morey, K.J., Tewari-Singh, N., Bowen, T.A., Smith, J.J., Webb, C.T., Hellinga, H.W., and Medford, J.I. (2009). Engineering key components in a synthetic eukaryotic signal transduction pathway. Mol. Syst. Biol. *5*, 270.

Antunes, M.S., Morey, K.J., Smith, J.J., Albrecht, K.D., Bowen, T.A., Jeffrey, K., Troupe, J.F., Cuneo, M.J., Webb, C.T., Hellinga, H.W., et al. (2011). Programmable Ligand Detection System in Plants through a Synthetic Signal Transduction Pathway. PLoS ONE *6*, e16292.

Aoyama, T., and Chua, N.-H. (1997). A glucocorticoid-mediated transcriptional induction system in transgenic plants. Plant J. *11*, 605–612.

Baaske, J., Gonschorek, P., Engesser, R., Dominguez-Monedero, A., Raute, K., Fischbach, P., Müller, K., Cachat, E., Schamel, W.W.A., Minguet, S., et al. (2018). Dual-controlled optogenetic system for the rapid down-regulation of protein levels in mammalian cells. Sci. Rep. *8*, 15024.

Bartlett, J.G., Alves, S.C., Smedley, M., Snape, J.W., and Harwood, W.A. (2008). High-throughput *Agrobacterium*-mediated barley transformation. Plant Methods *4*, 22.

Battle, M.W., and Jones, M.A. (2019). Cryptochromes integrate green light signals into the circadian system. Plant Cell Environ. *n/a*.

Bayer, T.S., and Smolke, C.D. (2005). Programmable ligand-controlled riboregulators of eukaryotic gene expression. Nat. Biotechnol. *23*, 337–343.

van Bergeijk, P., Adrian, M., Hoogenraad, C.C., and Kapitein, L.C. (2015). Optogenetic control of organelle transport and positioning. Nature *518*, 111–114.

Beyer, H.M., Juillot, S., Herbst, K., Samodelov, S.L., Müller, K., Schamel, W.W., Römer, W., Schäfer, E., Nagy, F., Strähle, U., et al. (2015). Red Light-Regulated Reversible Nuclear Localization of Proteins in Mammalian Cells and Zebrafish. ACS Synth. Biol. *4*, 951–958.

Boehm, C.R., Pollak, B., Purswani, N., Patron, N., and Haseloff, J. (2017). Synthetic Botany. Cold Spring Harb. Perspect. Biol. *9*, a023887.

Boes, A., Reimann, A., Twyman, R.M., Fischer, R., Schillberg, S., and Spiegel, H. (2016). A Plant-Based Transient Expression System for the Rapid Production of Malaria Vaccine Candidates. In Vaccine Design: Methods and Protocols, Volume 2: Vaccines for Veterinary Diseases, S. Thomas, ed. (New York, NY: Springer New York), pp. 597–619.

Bonnet, J., Subsoontorn, P., and Endy, D. (2012). Rewritable digital data storage in live cells via engineered control of recombination directionality. Proc. Natl. Acad. Sci. U. S. A. *109*, 8884–8889.

Bonnet, J., Yin, P., Ortiz, M.E., Subsoontorn, P., and Endy, D. (2013). Amplifying genetic logic gates. Science *340*, 599–603.

Bortesi, L., and Fischer, R. (2015). The CRISPR/Cas9 system for plant genome editing and beyond. Biotechnol. Adv. *33*, 41–52.

Boyden, E.S., Zhang, F., Bamberg, E., Nagel, G., and Deisseroth, K. (2005). Millisecond-timescale, genetically targeted optical control of neural activity. Nat. Neurosci. *8*, 1263–1268.

Braguy, J., and Zurbriggen, M.D. (2016). Synthetic strategies for plant signalling studies: molecular toolbox and orthogonal platforms. Plant J. *87*, 118–138.

Brophy, J.A.N., and Voigt, C.A. (2014). Principles of genetic circuit design. Nat. Methods *11*, 508–520.

Bruce, W., Folkerts, O., Garnaat, C., Crasta, O., Roth, B., and Bowen, B. (2000). Expression Profiling of the Maize Flavonoid Pathway Genes Controlled by Estradiol-Inducible Transcription Factors CRC and P. Plant Cell *12*, 65–80.

Bubeck, F., Hoffmann, M.D., Harteveld, Z., Aschenbrenner, S., Bietz, A., Waldhauer, M.C., Börner, K., Fakhiri, J., Schmelas, C., Dietz, L., et al. (2018). Engineered anti-CRISPR proteins for optogenetic control of CRISPR–Cas9. Nat. Methods *15*, 924–927.

Burgie, E.S., and Vierstra, R.D. (2014). Phytochromes: An Atomic Perspective on Photoactivation and Signaling. Plant Cell *26*, 4568–4583.

Caddick, M.X., Greenland, A.J., Jepson, Ian, Krause, K.-P., Qu, N., Riddell, K.V., Salter, M.G., Schuch, W., Sonnewald, U., and Tomsett, A.B. (1998). An ethanol inducible gene switch for plants used to manipulate carbon metabolism. Nat. Biotechnol. *16*, 177–180.

Castillo-Hair, S.M., Baerman, E.A., Fujita, M., Igoshin, O.A., and Tabor, J.J. (2019). Optogenetic control of *Bacillus subtilis* gene expression. Nat. Commun. *10*, 3099.

Chandran, D., Bergmann, F.T., and Sauro, H.M. (2009). TinkerCell: modular CAD tool for synthetic biology. J. Biol. Eng. *3*, 19.

Charpentier, M., Sun, J., Martins, T.V., Radhakrishnan, G.V., Findlay, K., Soumpourou, E., Thouin, J., Véry, A.-A., Sanders, D., Morris, R.J., et al. (2016). Nuclear-localized cyclic nucleotide–gated channels mediate symbiotic calcium oscillations. Science *352*, 1102–1105.

Chatelle, C., Ochoa-Fernandez, R., Engesser, R., Schneider, N., Beyer, H.M., Jones, A.R., Timmer, J., Zurbriggen, M.D., and Weber, W. (2018). A Green-Light-Responsive System for the Control of Transgene Expression in Mammalian and Plant Cells. ACS Synth. Biol. *7*, 1349–1358.

Chen, X., Li, T., Wang, X., Du, Z., Liu, R., and Yang, Y. (2015). Synthetic dual-input mammalian genetic circuits enable tunable and stringent transcription control by chemical and light. Nucleic Acids Res. *44*, 2677–2690.

Clarke, J.L., and Daniell, H. (2011). Plastid biotechnology for crop production: present status and future perspectives. Plant Mol. Biol. *76*, 211–220.

Cook, C., Martin, L., and Bastow, R. (2014). Opportunities in plant synthetic biology. J. Exp. Bot. *65*, 1921–1926.

Corrado, G., and Karali, M. (2009). Inducible gene expression systems and plant biotechnology. Biotechnol Adv *27*, 733–743.

Cosentino, C., Alberio, L., Gazzarrini, S., Aquila, M., Romano, E., Cermenati, S., Zuccolini, P., Petersen, J., Beltrame, M., Van Etten, J.L., et al. (2015). Engineering of a light-gated potassium channel. Science *348*, 707–710.

Crefcoeur, R.P., Yin, R., Ulm, R., and Halazonetis, T.D. (2013). Ultraviolet-B-mediated induction of protein-protein interactions in mammalian cells. Nat. Commun. *4*, 1779.

Czar, M.J., Cai, Y., and Peccoud, J. (2009). Writing DNA with GenoCAD. Nucleic Acids Res. *37*, W40–W47.

Daniell, H. (2002). Molecular strategies for gene containment in transgenic crops. Nat. Biotechnol. *20*, 581–586.

Danino, T., Prindle, A., Kwong, G.A., Skalak, M., Li, H., Allen, K., Hasty, J., and Bhatia, S.N. (2015). Programmable probiotics for detection of cancer in urine. Sci. Transl. Med. *7*, 289ra84.

D'Aoust, M.-A., Lavoie, P.-O., Couture, M.M.-J., Trépanier, S., Guay, J.-M., Dargis, M., Mongrand, S., Landry, N., Ward, B.J., and Vézina, L.-P. (2008). Influenza virus-like particles produced by transient expression in Nicotiana benthamiana induce a protective immune response against a lethal viral challenge in mice. Plant Biotechnol. J. *6*, 930–940.

Davey, M., Anthony, P., Power, J., and Lowe, K. (2005). Plant protoplasts: Status and biotechnological perspectives. Biotechnol. Adv. *23*, 131–171.

Decoene, T., De Paepe, B., Maertens, J., Coussement, P., Peters, G., De Maeseneire, S.L., and De Mey, M. (2018). Standardization in synthetic biology: an engineering discipline coming of age. Crit. Rev. Biotechnol. *38*, 647–656.

Deisseroth, K. (2011). Optogenetics. Nat. Methods *8*, 26–29.

Deisseroth, K., and Hegemann, P. (2017). The form and function of channelrhodopsin. Science *357*, eaan5544.

Delmans, M., Pollak, B., and Haseloff, J. (2017). MarpoDB: An Open Registry for *Marchantia Polymorpha* Genetic Parts. Plant Cell Physiol. *58*, e5.

DePaoli, H.C., Borland, A.M., Tuskan, G.A., Cushman, J.C., and Yang, X. (2014). Synthetic biology as it relates to CAM photosynthesis: challenges and opportunities. J. Exp. Bot. *65*, 3381–3393.

Dey, N., Sarkar, S., Acharya, S., and Maiti, I.B. (2015). Synthetic promoters in planta. Planta *242*, 1077–1094.

Diretto, G., Al-Babili, S., Tavazza, R., Papacchioli, V., Beyer, P., and Giuliano, G. (2007). Metabolic Engineering of Potato Carotenoid Content through Tuber-Specific Overexpression of a Bacterial Mini-Pathway. PLoS ONE *2*, e350.

Elowitz, M.B., and Leibler, S. (2000). A synthetic oscillatory network of transcriptional regulators. Nature *403*, 335–338.

Endy, D. (2005). Foundations for engineering biology. Nature *438*, 449–453.

Feeney, K.A., Putker, M., Brancaccio, M., and O'Neill, J.S. (2016). In-depth Characterization of Firefly Luciferase as a Reporter of Circadian Gene Expression in Mammalian Cells. J. Biol. Rhythms *31*, 540–550.

Feike, D., Korolev, A.V., Soumpourou, E., Murakami, E., Reid, D., Breakspear, A., Rogers, C., Radutoiu, S., Stougaard, J., Harwood, W.A., et al. (2019). Characterizing standard genetic parts and establishing common principles for engineering legume and cereal roots. Plant Biotechnol. J. *17*, 2234–2245.

de Felipe, P., Luke, G.A., Hughes, L.E., Gani, D., Halpin, C., and Ryan, M.D. (2006). *E unum pluribus*: multiple proteins from a self-processing polyprotein. Trends Biotechnol. *24*, 68–75.

Fenno, L., Yizhar, O., and Deisseroth, K. (2011). The Development and Application of Optogenetics. Annu. Rev. Neurosci. *34*, 389–412.

Frey, A.D., Rimann, M., Bailey, J.E., Kallio, P.T., Thompson, C.J., and Fussenegger, M. (2001). Novel pristinamycin-responsive expression systems for plant cells. Biotechnol. Bioeng. *74*, 154–163.

Fujisawa, T., and Masuda, S. (2018). Light-induced chromophore and protein responses and mechanical signal transduction of BLUF proteins. Biophys. Rev. *10*, 327–337.

Gardner, T.S., Cantor, C.R., and Collins, J.J. (2000). Construction of a genetic toggle switch in Escherichia coli. Nature *403*, 339–342.

Golonka, D., Fischbach, P., Jena, S.G., Kleeberg, J.R.W., Essen, L.-O., Toettcher, J.E., Zurbriggen, M.D., and Möglich, A. (2019). Deconstructing and repurposing the light-regulated interplay between Arabidopsis phytochromes and interacting factors. Commun. Biol. *2*, 448.

Goslin, K., Zheng, B., Serrano-Mislata, A., Rae, L., Ryan, P.T., Kwaśniewska, K., Thomson, B., Ó'Maoiléidigh, D.S., Madueño, F., Wellmer, F., et al. (2017). Transcription Factor Interplay between LEAFY and APETALA1/CAULIFLOWER during Floral Initiation. Plant Physiol. *174*, 1097–1109.

Guet, C.C., Elowitz, M.B., Hsing, W., and Leibler, S. (2002). Combinatorial Synthesis of Genetic Networks. Science *296*, 1466–1470.

Gulati, S., Jin, H., Masuho, I., Orban, T., Cai, Y., Pardon, E., Martemyanov, K.A., Kiser, P.D., Stewart, P.L., Ford, C.P., et al. (2018). Targeting G protein-coupled receptor signaling at the G protein level with a selective nanobody inhibitor. Nat. Commun. *9*, 1996.

Guntas, G., Hallett, R. a., Zimmerman, S.P., Williams, T., Yumerefendi, H., Bear, J.E., and Kuhlman, B. (2015). Engineering an improved light-induced dimer (iLID) for controlling the localization and activity of signaling proteins. Proc. Natl. Acad. Sci. U. S. A. *112*, 112–117.

Hansen, L.L., and van Ooijen, G. (2016). Rapid Analysis of Circadian Phenotypes in Arabidopsis Protoplasts Transfected with a Luminescent Clock Reporter. J. Vis. Exp. JoVE 54586.

Harborne, S.P.D., Ruprecht, J.J., and Kunji, E.R.S. (2015). Calcium-induced conformational changes in the regulatory domain of the human mitochondrial ATP-Mg/Pi carrier. Biochim. Biophys. Acta BBA - Bioenerg. *1847*, 1245–1253.

van Herpen, T.W.J.M., Cankar, K., Nogueira, M., Bosch, D., Bouwmeester, H.J., and Beekwilder, J. (2010). Nicotiana benthamiana as a Production Platform for Artemisinin Precursors. PLoS ONE *5*, e14222.

Herrou, J., and Crosson, S. (2011). Function, structure and mechanism of bacterial photosensory LOV proteins. Nat. Rev. Microbiol. *9*, 713–723.

Ho, W.W.H., and Weigel, D. (2014). Structural Features Determining Flower-Promoting Activity of *Arabidopsis* FLOWERING LOCUS T. Plant Cell *26*, 552–564.

Hochrein, L., Mitchell, L.A., Schulz, K., Messerschmidt, K., and Mueller-Roeber, B. (2018). L-SCRaMbLE as a tool for light-controlled Cre-mediated recombination in yeast. Nat. Commun. *9*, 1931.

Hughes, R.M. (2018). A compendium of chemical and genetic approaches to light-regulated gene transcription. Crit. Rev. Biochem. Mol. Biol. *53*, 453–474.

Ikeda, M., and Ohme-Takagi, M. (2009). A novel group of transcriptional repressors in Arabidopsis. Plant Cell Physiol. *50*, 970–975.

Ikram, N.K.B.K., and Simonsen, H.T. (2017). A Review of Biotechnological Artemisinin Production in Plants. Front. Plant Sci. *8*, 1966–1966.

Ishizaki, K., Chiyoda, S., Yamato, K.T., and Kohchi, T. (2008). *Agrobacterium*-Mediated Transformation of the Haploid Liverwort *Marchantia polymorpha* L., an Emerging Model for Plant Biology. Plant Cell Physiol. *49*, 1084–1091.

Jones, A.M., Danielson, J.Å., ManojKumar, S.N., Lanquar, V., Grossmann, G., and Frommer, W.B. (2014). Abscisic acid dynamics in roots detected with genetically encoded FRET sensors. ELife *3*, e01741.

Jost, M., Fernández-Zapata, J., Polanco, M.C., Ortiz-Guerrero, J.M., Chen, P.Y.-T., Kang, G., Padmanabhan, S., Elías-Arnanz, M., and Drennan, C.L. (2015). Structural basis for gene regulation by a B12-dependent photoreceptor. Nature *526*, 536–541.

Jung, H., Kim, S.-W., Kim, M., Hong, J., Yu, D., Kim, J.H., Lee, Y., Kim, S., Woo, D., Shin, H.-S., et al. (2019). Noninvasive optical activation of Flp recombinase for genetic manipulation in deep mouse brain regions. Nat. Commun. *10*, 314.

Kawamoto, N., Sasabe, M., Endo, M., Machida, Y., and Araki, T. (2015). Calcium-dependent protein kinases responsible for the phosphorylation of a bZIP transcription factor FD crucial for the florigen complex formation. Sci. Rep. *5*, 8341.

Kawano, F., Okazaki, R., Yazawa, M., and Sato, M. (2016). A photoactivatable Cre–loxP recombination system for optogenetic genome engineering. Nat. Chem. Biol. *12*, 1059–1064.

Kelly, J.M., and Lagarias, J.C. (1985). Photochemistry of 124-kilodalton Avena phytochrome under constant illumination in vitro. Biochemistry *24*, 6003–6010.

Kelwick, R., MacDonald, J.T., Webb, A.J., and Freemont, P. (2014). Developments in the Tools and Methodologies of Synthetic Biology. Front. Bioeng. Biotechnol. *2*, 60.

Kennedy, M.J., Hughes, R.M., Peteya, L.A., Schwartz, J.W., Ehlers, M.D., and Tucker, C.L. (2010). Rapid blue-light-mediated induction of protein interactions in living cells. Nat. Methods *7*, 973–975.

Kianianmomeni, A. (2014). UVB-based optogenetic tools. Trends Biotechnol. *33*, 59–61.

Kirchhofer, A., Helma, J., Schmidthals, K., Frauer, C., Cui, S., Karcher, A., Pellis, M., Muyldermans, S., Casas-Delucchi, C.S., Cardoso, M.C., et al. (2009). Modulation of protein properties in living cells using nanobodies. Nat. Struct. Mol. Biol. *17*, 133–138.

Knowles, S.M., Lu, S.X., and Tobin, E.M. (2008). Testing time: can ethanol-induced pulses of proposed oscillator components phase shift rhythms in Arabidopsis? J. Biol. Rhythms *23*, 463–471.

Konermann, S., Brigham, M.D., Trevino, A.E., Hsu, P.D., Heidenreich, M., Cong, L., Platt, R.J., Scott, D. a, Church, G.M., and Zhang, F. (2013). Optical control of mammalian endogenous transcription and epigenetic states. Nature *500*, 472–476.

Kramer, B.P., Fischer, C., and Fussenegger, M. (2004). BioLogic gates enable logical transcription control in mammalian cells. Biotechnol. Bioeng. *87*, 478–484.

Kristensen, C., Morant, M., Olsen, C.E., Ekstrøm, C.T., Galbraith, D.W., Lindberg Møller, B., and Bak, S. (2005). Metabolic engineering of dhurrin in transgenic Arabidopsis plants with marginal inadvertent effects on the

metabolome and transcriptome. Proc. Natl. Acad. Sci. U. S. A. *102*, 1779–1784.

Lacombe, S., Rougon-Cardoso, A., Sherwood, E., Peeters, N., Dahlbeck, D., van Esse, H.P., Smoker, M., Rallapalli, G., Thomma, B.P.H.J., Staskawicz, B., et al. (2010). Interfamily transfer of a plant pattern-recognition receptor confers broad-spectrum bacterial resistance. Nat. Biotechnol. *28*, 365–369.

Legris, M., Ince, Y.Ç., and Fankhauser, C. (2019). Molecular mechanisms underlying phytochrome-controlled morphogenesis in plants. Nat. Commun. *10*, 5219.

Levskaya, A., Chevalier, A.A., Tabor, J.J., Simpson, Z.B., Lavery, L.A., Levy, M., Davidson, E.A., Scouras, A., Ellington, A.D., Marcotte, E.M., et al. (2005). Engineering Escherichia coli to see light. Nature *438*, 441–442.

Li, D., Zhang, H., Mou, M., Chen, Y., Xiang, S., Chen, L., and Yu, D. (2019). Arabidopsis Class II TCP Transcription Factors Integrate with the FT–FD Module to Control Flowering. Plant Physiol. *181*, 97–111.

Li, X., Gutierrez, D.V., Hanson, M.G., Han, J., Mark, M.D., Chiel, H., Hegemann, P., Landmesser, L.T., and Herlitze, S. (2005). Fast noninvasive activation and inhibition of neural and network activity by vertebrate rhodopsin and green algae channelrhodopsin. Proc. Natl. Acad. Sci. U. S. A. *102*, 17816–17821.

Li, Z., Zhang, D., Xiong, X., Yan, B., Xie, W., Sheen, J., and Li, J.-F. (2017). A potent Cas9-derived gene activator for plant and mammalian cells. Nat. Plants *3*, 930–936.

Liénard, D., and Nogué, F. (2009). Physcomitrella patens : A Non-Vascular Plant for Recombinant Protein Production. In Recombinant Proteins From Plants: Methods and Protocols, L. Faye, and V. Gomord, eds. (Totowa, NJ: Humana Press), pp. 135–144.

Liu, W., and Stewart, C.N. (2015). Plant synthetic biology. Trends Plant Sci *20*, 309–317.

Liu, W., and Stewart, C.N. (2016). Plant synthetic promoters and transcription factors. Curr. Opin. Biotechnol. *37*, 36–44.

Liu, W., Mazarei, M., Rudis, M.R., Fethe, M.H., and Stewart, C.N. (2011). Rapid *in vivo* analysis of synthetic promoters for plant pathogen phytosensing. BMC Biotechnol. *11*, 108.

Liu, W., Yuan, J.S., and Stewart Jr, C.N. (2013a). Advanced genetic tools for plant biotechnology. Nat. Rev. Genet. *14*, 781–793.

Liu, W., Mazarei, M., Rudis, M.R., Fethe, M.H., Peng, Y., Millwood, R.J., Schoene, G., Burris, J.N., and Stewart Jr, C.N. (2013b). Bacterial pathogen

phytosensing in transgenic tobacco and Arabidopsis plants. Plant Biotechnol. J. *11*, 43–52.

Liu, Z., Zhang, J., Jin, J., Geng, Z., Qi, Q., and Liang, Q. (2018). Programming Bacteria With Light—Sensors and Applications in Synthetic Biology. Front. Microbiol. *9*, 2692.

Lo, C.-L., Choudhury, S.R., Irudayaraj, J., and Zhou, F.C. (2017). Epigenetic Editing of *Ascl1* Gene in Neural Stem Cells by Optogenetics. Sci. Rep. *7*, 42047.

Losi, A., Gardner, K.H., and Möglich, A. (2018). Blue-Light Receptors for Optogenetics. Chem. Rev. *118*, 10659–10709.

Mahfouz, M.M., Piatek, A., and Stewart Jr, C.N. (2014). Genome engineering via TALENs and CRISPR/Cas9 systems: challenges and perspectives. Plant Biotechnol. J. *12*, 1006–1014.

Maliga, P., and Bock, R. (2011). Plastid Biotechnology: Food, Fuel, and Medicine for the 21st Century. Plant Physiol. *155*, 1501–1510.

Mallett, D.R., Chang, M., Cheng, X., and Bezanilla, M. (2019). Efficient and modular CRISPR-Cas9 vector system for Physcomitrella patens. Plant Direct *3*, e00168.

Mansouri, M., Strittmatter, T., and Fussenegger, M. (2019). Light-Controlled Mammalian Cells and Their Therapeutic Applications in Synthetic Biology. Adv. Sci. *6*, 1800952.

Mardanova, E.S., Blokhina, E.A., Tsybalova, L.M., Peyret, H., Lomonossoff, G.P., and Ravin, N.V. (2017). Efficient Transient Expression of Recombinant Proteins in Plants by the Novel pEff Vector Based on the Genome of Potato Virus X. Front. Plant Sci. *8*, 247–247.

Mathes, T. (2016). Natural Resources for Optogenetic Tools. In Optogenetics: Methods and Protocols, A. Kianianmomeni, ed. (New York, NY: Springer New York), pp. 19–36.

Matsuoka, Y., Ghosh, S., and Kitano, H. (2009). Consistent design schematics for biological systems: standardization of representation in biological engineering. J. R. Soc. Interface *6*, S393–S404.

Meador, K., Wysoczynski, C.L., Norris, A.J., Aoto, J., Bruchas, M.R., and Tucker, C.L. (2019). Achieving tight control of a photoactivatable Cre recombinase gene switch: new design strategies and functional characterization in mammalian cells and rodent. Nucleic Acids Res.

Medzihradszky, M., Bindics, J., Ádám, É., Viczián, A., Klement, É., Lorrain, S., Gyula, P., Mérai, Z., Fankhauser, C., Medzihradszky, K.F., et al. (2013).

Phosphorylation of Phytochrome B Inhibits Light-Induced Signaling via Accelerated Dark Reversion in *Arabidopsis*. Plant Cell *25*, 535–544.

de Mena, L., Rizk, P., and Rincon-Limas, D.E. (2018). Bringing Light to Transcription: The Optogenetics Repertoire. Front. Genet. *9*, 518.

Mett, V.L., Lochhead, L.P., and Reynolds, P.H. (1993). Copper-controllable gene expression system for whole plants. Proc. Natl. Acad. Sci. U. S. A. *90*, 4567–4571.

Mills, E., and Truong, K. (2013). Photoswitchable protein degradation: A generalizable control module for cellular function? Chem Biol *20*, 458–460.

Monné, M., Miniero, D.V., Obata, T., Daddabbo, L., Palmieri, L., Vozza, A., Nicolardi, M.C., Fernie, A.R., and Palmieri, F. (2015). Functional characterization and organ distribution of three mitochondrial ATP–Mg/Pi carriers in *Arabidopsis thaliana*. Biochim. Biophys. Acta BBA - Bioenerg. *1847*, 1220–1230.

Moore, I., Samalova, M., Kurup, S., For, T., and Analysis, M. (2006). Transactivated and chemically inducible gene expression in plants. Plant J. *45*, 651–683.

Moosmann, P., Georgiev, O., Thiesen, H., Hagmann, M., and Schaffner, W. (1997). Silencing of RNA polymerases II and III-dependent transcription by the KRAB protein domain of KOX1, a Krüppel-type zinc finger factor. Biol. Chem. *378*, 669–677.

Morgan, S.-A., and Woolley, G.A. (2010). A photoswitchable DNA-binding protein based on a truncated GCN4-photoactive yellow protein chimera. Photochem. Photobiol. Sci. *9*, 1320–1326.

Moser, B.A., and Esser-Kahn, A.P. (2017). A Photoactivatable Innate Immune Receptor for Optogenetic Inflammation. ACS Chem. Biol. *12*, 347–350.

Motta-Mena, L.B., Reade, A., Mallory, M.J., Glantz, S., Weiner, O.D., Lynch, K.W., and Gardner, K.H. (2014). An optogenetic gene expression system with rapid activation and deactivation kinetics. Nat. Chem. Biol. *10*, 196–202.

Mühlhäuser, W.W.D., Fischer, A., Weber, W., and Radziwill, G. (2017). Optogenetics - Bringing light into the darkness of mammalian signal transduction. Biochim. Biophys. Acta BBA - Mol. Cell Res. *1864*, 280–292.

Müller, K., Engesser, R., Timmer, J., Nagy, F., Zurbriggen, M.D., and Weber, W. (2013a). Synthesis of phycocyanobilin in mammalian cells. Chem. Commun. *49*, 8970–8972.

Müller, K., Engesser, R., Schulz, S., Steinberg, T., Tomakidi, P., Weber, C.C., Ulm, R., Timmer, J., Zurbriggen, M.D., and Weber, W. (2013b). Multi-

chromatic control of mammalian gene expression and signaling. Nucleic Acids Res. *41*, e124.

Müller, K., Engesser, R., Metzger, S., Schulz, S., Kämpf, M.M., Busacker, M., Steinberg, T., Tomakidi, P., Ehrbar, M., Nagy, F., et al. (2013c). A red/far-red light-responsive bi-stable toggle switch to control gene expression in mammalian cells. Nucleic Acids Res. *41*, e77.

Müller, K., Engesser, R., Timmer, J., Zurbriggen, M.D., and Weber, W. (2014a). Orthogonal Optogenetic Triple-Gene Control in Mammalian Cells. ACS Synth. Biol. *3*, 796–801.

Müller, K., Siegel, D., Rodriguez Jahnke, F., Gerrer, K., Wend, S., Decker, E.L., Reski, R., Weber, W., and Zurbriggen, M.D. (2014b). A red light-controlled synthetic gene expression switch for plant systems. Mol BioSyst *10*, 1679–1688.

Müller, K., Naumann, S., Weber, W., and Zurbriggen, M.D. (2015). Optogenetics for gene expression in mammalian cells. Biol. Chem. *396*, 145–152.

Muranaka, N., and Yokobayashi, Y. (2010). A synthetic riboswitch with chemical band-pass response. Chem. Commun. *46*, 6825–6827.

Nagel, G., Brauner, M., Liewald, J.F., Adeishvili, N., Bamberg, E., and Gottschalk, A. (2005). Light Activation of Channelrhodopsin-2 in Excitable Cells of Caenorhabditis elegans Triggers Rapid Behavioral Responses. Curr. Biol. *15*, 2279–2284.

Nguyen, N.T., He, L., Martinez-Moczygemba, M., Huang, Y., and Zhou, Y. (2018). Rewiring Calcium Signaling for Precise Transcriptional Reprogramming. ACS Synth. Biol. *7*, 814–821.

Nielsen, A.A.K., Der, B.S., Shin, J., Vaidyanathan, P., Paralanov, V., Strychalski, E.A., Ross, D., Densmore, D., and Voigt, C.A. (2016). Genetic circuit design automation. Science *352*, aac7341.

Nihongaki, Y., Yamamoto, S., Kawano, F., Suzuki, H., and Sato, M. (2015a). CRISPR-Cas9-based Photoactivatable Transcription System. Chem. Biol. *22*, 169–174.

Nihongaki, Y., Kawano, F., Nakajima, T., and Sato, M. (2015b). Photoactivatable CRISPR-Cas9 for optogenetic genome editing. Nat. Biotechnol. *9*, 1–8.

Nihongaki, Y., Furuhata, Y., Otabe, T., Hasegawa, S., Yoshimoto, K., and Sato, M. (2017). CRISPR–Cas9-based photoactivatable transcription systems to induce neuronal differentiation. Nat. Methods *14*, 963–966.

Niopek, D., Benzinger, D., Roensch, J., Draebing, T., Wehler, P., Eils, R., and Di Ventura, B. (2014). Engineering light-inducible nuclear localization signals for precise spatiotemporal control of protein dynamics in living cells. Nat. Commun. *5*, 4404.

Niopek, D., Wehler, P., Roensch, J., Eils, R., and Di Ventura, B. (2016). Optogenetic control of nuclear protein export. Nat. Commun. *7*, 10624.

Nussinovitch, U., Shinnawi, R., and Gepstein, L. (2014). Modulation of cardiac tissue electrophysiological properties with light-sensitive proteins. Cardiovasc. Res. *102*, 176–187.

O'Banion, C.P., Priestman, M.A., Hughes, R.M., Herring, L.E., Capuzzi, S.J., and Lawrence, D.S. (2018). Design and Profiling of a Subcellular Targeted Optogenetic cAMP-Dependent Protein Kinase. Cell Chem. Biol. *25*, 100-109.e8.

Ochoa-Fernandez, R., Samodelov, S.L., Brandl, S.M., Wehinger, E., Müller, K., Weber, W., and Zurbriggen, M.D. (2016). Optogenetics: Methods and Protocols. A. Kianianmomeni, ed. (New York, NY: Springer New York), pp. 125–139.

Ohlendorf, R., Vidavski, R.R., Eldar, A., Moffat, K., and Möglich, A. (2012). From Dusk till Dawn: One-Plasmid Systems for Light-Regulated Gene Expression. J. Mol. Biol. *416*, 534–542.

Oka, Y., Ono, Y., Toledo-Ortiz, G., Kokaji, K., Matsui, M., Mochizuki, N., and Nagatani, A. (2012). Arabidopsis phytochrome a is modularly structured to integrate the multiple features that are required for a highly sensitized phytochrome. Plant Cell *24*, 2949–2962.

Paddon, C.J., Westfall, P.J., Pitera, D.J., Benjamin, K., Fisher, K., McPhee, D., Leavell, M.D., Tai, A., Main, A., Eng, D., et al. (2013). High-level semi-synthetic production of the potent antimalarial artemisinin. Nature *496*, 528–532.

Padidam, M. (2003). Chemically regulated gene expression in plants. Curr Opin Plant Biol *6*, 169–177.

Papanatsiou, M., Petersen, J., Henderson, L., Wang, Y., Christie, J.M., and Blatt, M.R. (2019). Optogenetic manipulation of stomatal kinetics improves carbon assimilation, water use, and growth. Science *363*, 1456–1459.

Parcy, F., Nilsson, O., Busch, M.A., Lee, I., and Weigel, D. (1998). A genetic framework for floral patterning. Nature *395*, 561–566.

Park, S.-Y., Peterson, F.C., Mosquna, A., Yao, J., Volkman, B.F., and Cutler, S.R. (2015). Agrochemical control of plant water use using engineered abscisic acid receptors. Nature *520*, 545–548.

Patron, N.J., Orzaez, D., Marillonnet, S., Warzecha, H., Matthewman, C., Youles, M., Raitskin, O., Leveau, A., Farré, G., Rogers, C., et al. (2015). Standards for plant synthetic biology: a common syntax for exchange of DNA parts. New Phytol. *208*, 13–19.

Perez-Pinera, P., Kocak, D.D., Vockley, C.M., Adler, A.F., Kabadi, A.M., Polstein, L.R., Thakore, P.I., Glass, K.A., Ousterout, D.G., Leong, K.W., et al. (2013). RNA-guided gene activation by CRISPR-Cas9–based transcription factors. Nat. Methods *10*, 973–976.

Polstein, L.R., and Gersbach, C.A. (2012). Light-inducible spatiotemporal control of gene activation by customizable zinc finger transcription factors. J Am Chem Soc *134*, 16480–16483.

Polstein, L.R., and Gersbach, C.A. (2015). A light-inducible CRISPR-Cas9 system for control of endogenous gene activation. Nat Chem Biol *11*, 198–200.

Porra, R.J., and Grimme, L.H. (1978). Tetrapyrrole biosynthesis in algae and higher plants: A discussion of the importance of the 5-aminolaevulinate synthase and the dioxovalerate transaminase pathways in the biosynthesis of chlorophyll. Int. J. Biochem. *9*, 883–886.

Provart, N.J., Alonso, J., Assmann, S.M., Bergmann, D., Brady, S.M., Brkljacic, J., Browse, J., Chapple, C., Colot, V., Cutler, S., et al. (2016). 50 years of Arabidopsis research: highlights and future directions. New Phytol. *209*, 921–944.

Putri, R.R., and Chen, L. (2018). Spatiotemporal control of zebrafish (Danio rerio) gene expression using a light-activated CRISPR activation system. Gene *677*, 273–279.

Quejada, J.R., Park, S.-H.E., Awari, D.W., Shi, F., Yamamoto, H.E., Kawano, F., Jung, J.C., and Yazawa, M. (2017). Optimized light-inducible transcription in mammalian cells using Flavin Kelch-repeat F-box1/GIGANTEA and CRY2/CIB1. Nucleic Acids Res. *45*, e172–e172.

Reade, A., Motta-Mena, L.B., Gardner, K.H., Stainier, D.Y., Weiner, O.D., and Woo, S. (2017). TAEL: a zebrafish-optimized optogenetic gene expression system with fine spatial and temporal control. Development *144*, 345–355.

Redchuk, T.A., Omelina, E.S., Chernov, K.G., and Verkhusha, V.V. (2017). Near-infrared optogenetic pair for protein regulation and spectral multiplexing. Nat. Chem. Biol. *13*, 633–639.

Redchuk, T.A., Karasev, M.M., Omelina, E.S., and Verkhusha, V.V. (2018a). Near-Infrared Light-Controlled Gene Expression and Protein Targeting in Neurons and Non-neuronal Cells. ChemBioChem *19*, 1334–1340.

Redchuk, T.A., Kaberniuk, A.A., and Verkhusha, V.V. (2018b). Near-infrared light–controlled systems for gene transcription regulation, protein targeting and spectral multiplexing. Nat. Protoc. *13*, 1121–1136.

Reinbothe, T.M., Safi, F., Axelsson, A.S., Mollet, I.G., and Rosengren, A.H. (2014). Optogenetic control of insulin secretion in intact pancreatic islets with β-cell-specific expression of Channelrhodopsin-2. Islets *6*, e28095.

Renicke, C., Schuster, D., Usherenko, S., Essen, L.O., and Taxis, C. (2013). A LOV2 domain-based optogenetic tool to control protein degradation and cellular function. Chem. Biol. *20*, 619–626.

Reski, R., Parsons, J., and Decker, E. (2015). Moss-made pharmaceuticals: From bench to bedside. Plant Biotechnol. J. *13*, 1191–1198.

Reski, R., Bae, H., and Simonsen, H.T. (2018). Physcomitrella patens, a versatile synthetic biology chassis. Plant Cell Rep. *37*, 1409–1417.

Richter, F., Fonfara, I., Bouazza, B., Schumacher, C.H., Bratovič, M., Charpentier, E., and Möglich, A. (2016). Engineering of temperature- and light-switchable Cas9 variants. Nucleic Acids Res. *44*, gkw930.

Ro, D.-K., Paradise, E.M., Ouellet, M., Fisher, K.J., Newman, K.L., Ndungu, J.M., Ho, K.A., Eachus, R.A., Ham, T.S., Kirby, J., et al. (2006). Production of the antimalarial drug precursor artemisinic acid in engineered yeast. Nature *440*, 940–943.

Sainsbury, F., and Lomonossoff, G.P. (2014). Transient expressions of synthetic biology in plants. Curr Opin Plant Biol *19*, 1–7.

Samodelov, S.L., and Zurbriggen, M.D. (2017). Quantitatively Understanding Plant Signaling: Novel Theoretical–Experimental Approaches. Trends Plant Sci. *22*, 685–704.

Samodelov, S.L., Beyer, H.M., Guo, X., Augustin, M., Jia, K.-P., Baz, L., Ebenho h, O., Beyer, P., Weber, W., Al-Babili, S., et al. (2016). StrigoQuant: A genetically encoded biosensor for quantifying strigolactone activity and specificity. Sci. Adv. *2*, e1601266.

Sang, Y., Millwood, R.J., and Neal Stewart Jr, C. (2013). Gene use restriction technologies for transgenic plant bioconfinement. Plant Biotechnol. J. *11*, 649–658.

Schaumberg, K.A., Antunes, M.S., Kassaw, T.K., Xu, W., Zalewski, C.S., Medford, J.I., and Prasad, A. (2016). Quantitative characterization of genetic parts and circuits for plant synthetic biology. Nat. Methods *13*, 94–100.

Schindler, S.E., Mccall, J.G., Yan, P., Hyrc, K.L., Li, M., Tucker, C.L., Lee, J., Bruchas, M.R., and Diamond, M.I. (2015). Photo-activatable Cre recombinase regulates gene expression in vivo. Sci. Rep. *5*, 13627.

Schmidt, D., Tillberg, P.W., Chen, F., and Boyden, E.S. (2014). A fully genetically encoded protein architecture for optical control of peptide ligand concentration. Nat. Commun. *5*, 3019.

Schornack, S., Fuchs, R., Huitema, E., Rothbauer, U., Lipka, V., and Kamoun, S. (2009). Protein mislocalization in plant cells using a GFP-binding chromobody. Plant J. *60*, 744–754.

Schuler, M.L., Mantegazza, O., and Weber, A.P.M. (2016). Engineering C4 photosynthesis into C3 chassis in the synthetic biology age. Plant J. *87*, 51–65.

Selma, S., Bernabé-Orts, J.M., Vazquez-Vilar, M., Diego-Martin, B., Ajenjo, M., Garcia-Carpintero, V., Granell, A., and Orzaez, D. (2019). Strong gene activation in plants with genome-wide specificity using a new orthogonal CRISPR/Cas9-based programmable transcriptional activator. Plant Biotechnol. J. *17*, 1703–1705.

Shao, J., Wang, M., Yu, G., Zhu, S., Yu, Y., Heng, B.C., Wu, J., and Ye, H. (2018). Synthetic far-red light-mediated CRISPR-dCas9 device for inducing functional neuronal differentiation. Proc. Natl. Acad. Sci. U. S. A. *115*, E6722–E6730.

Sheen, J. (2001). Signal Transduction in Maize and Arabidopsis Mesophyll Protoplasts. Plant Physiol. *127*, 1466–1475.

Shi, F., Kawano, F., Park, S.E., Komazaki, S., Hirabayashi, Y., Polleux, F., and Yazawa, M. (2018). Optogenetic Control of Endoplasmic Reticulum–Mitochondria Tethering. ACS Synth. Biol. *7*, 2–9.

Shimizu-Sato, S., Huq, E., Tepperman, J.M., and Quail, P.H. (2002). A light-switchable gene promoter system. Nat Biotechnol *20*, 1041–1044.

Simon, R., Igeño, M.I., and Coupland, G. (1996). Activation of floral meristem identity genes in Arabidopsis. Nature *384*, 59–62.

Siuti, P., Yazbek, J., and Lu, T.K. (2013). Synthetic circuits integrating logic and memory in living cells. Nat. Biotechnol. *31*, 448–452.

Smita Rastogi, V. (2013). Genetically Modified Plants: Public and Scientific Perceptions. ISRN Biotechnol. *2013*, 11 pages.

Sohka, T., Heins, R.A., Phelan, R.M., Greisler, J.M., Townsend, C.A., and Ostermeier, M. (2009). An externally tunable bacterial band-pass filter. Proc. Natl. Acad. Sci. U. S. A. *106*, 10135–10140.

Strickland, D., Lin, Y., Wagner, E., Hope, C.M., Zayner, J., Antoniou, C., Sosnick, T.R., Weiss, E.L., and Glotzer, M. (2012). TULIPs: tunable, light-controlled interacting protein tags for cell biology. Nat. Methods *9*, 379–384.

Su, Y., and Lagarias, J.C. (2007). Light-independent phytochrome signaling mediated by dominant GAF domain tyrosine mutants of Arabidopsis phytochromes in transgenic plants. Plant Cell *19*, 2124–2139.

Sugano, S.S., Nishihama, R., Shirakawa, M., Takagi, J., Matsuda, Y., Ishida, S., Shimada, T., Hara-Nishimura, I., Osakabe, K., and Kohchi, T. (2018). Efficient CRISPR/Cas9-based genome editing and its application to conditional genetic analysis in *Marchantia polymorpha*. PLoS ONE *13*, e0205117.

Tabor, J.J., Levskaya, A., and Voigt, C.A. (2011). Multichromatic control of gene expression in *Escherichia coli*. J. Mol. Biol. *405*, 315–324.

Takayama, K., and Mizuguchi, H. (2018). Generation of Optogenetically Modified Adenovirus Vector for Spatiotemporally Controllable Gene Therapy. ACS Chem. Biol. *13*, 449–454.

Tanaka, R., and Tanaka, A. (2007). Tetrapyrrole Biosynthesis in Higher Plants. Annu. Rev. Plant Biol. *58*, 321–346.

Tang, W., Luo, X., and Samuels, V. (2004). Regulated gene expression with promoters responding to inducers. Plant Sci *166*, 827–834.

Taoka, K., Ohki, I., Tsuji, H., Furuita, K., Hayashi, K., Yanase, T., Yamaguchi, M., Nakashima, C., Purwestri, Y.A., Tamaki, S., et al. (2011). 14-3-3 proteins act as intracellular receptors for rice Hd3a florigen. Nature *476*, 332–335.

Taslimi, A., Zoltowski, B., Miranda, J.G., Pathak, G.P., Hughes, R.M., and Tucker, C.L. (2016). Optimized second-generation CRY2–CIB dimerizers and photoactivatable Cre recombinase. Nat. Chem. Biol. *12*, 425–430.

Thimmappa, R., Geisler, K., Louveau, T., O'Maille, P., and Osbourn, A. (2014). Triterpene Biosynthesis in Plants. Annu. Rev. Plant Biol. *65*, 225–257.

Tischer, D., and Weiner, O.D. (2014). Illuminating cell signalling with optogenetic tools. Nat. Rev. Mol. Cell Biol. *15*, 551–558.

Toettcher, J.E., Voigt, C. a, Weiner, O.D., and Lim, W. a (2011a). The promise of optogenetics in cell biology: interrogating molecular circuits in space and time. Nat. Methods *8*, 35–38.

Toettcher, J.E., Gong, D., Lim, W., and Weiner, O.D. (2011b). Light-based feedback for controlling intracellular signaling dynamics. Nat. Methods *8*, 837–839.

Uda, Y., Goto, Y., Oda, S., Kohchi, T., Matsuda, M., and Aoki, K. (2017). Efficient synthesis of phycocyanobilin in mammalian cells for optogenetic control of cell signaling. Proc. Natl. Acad. Sci. U. S. A. *114*, 11962–11967.

Urquiza-García, U., and Millar, A.J. (2019). Expanding the bioluminescent reporter toolkit for plant science with NanoLUC. Plant Methods *15*, 68–68.

Usherenko, S., Stibbe, H., Muscò, M., Essen, L.-O., Kostina, E. a, and Taxis, C. (2014). Photo-sensitive degron variants for tuning protein stability by light. BMC Syst. Biol. *8*, 128.

Vazquez-Vilar, M., Quijano-Rubio, A., Fernandez-del-Carmen, A., Sarrion-Perdigones, A., Ochoa-Fernandez, R., Ziarsolo, P., Blanca, J., Granell, A., and Orzaez, D. (2017). GB3.0: a platform for plant bio-design that connects functional DNA elements with associated biological data. Nucleic Acids Res. *45*, 2196–2209.

Vilar, M.V., Miquel, J., Orts, B., Fernandez, A., Ziarsolo, P., Blanca, J., Granell, A., and Orzaez, D. (2016). A modular toolbox for gRNA – Cas9 genome engineering in plants based on the GoldenBraid standard. Plant Methods *12*, 10.

Wagner, D., Sablowski, R.W.M., and Meyerowitz, E.M. (1999). Transcriptional Activation of APETALA1 by LEAFY. Science *285*, 582–584.

Wang, S., Tiwari, S.B., Hagen, G., and Guilfoyle, T.J. (2005). AUXIN RESPONSE FACTOR7 Restores the Expression of Auxin-Responsive Genes in Mutant Arabidopsis Leaf Mesophyll Protoplasts. Plant Cell *17*, 1979–1993.

Wang, X., Chen, X., and Yang, Y. (2012). Spatiotemporal control of gene expression by a light-switchable transgene system. Nat Methods *9*, 266–269.

Wang, Y., Jiang, X., Hu, C., Sun, T., Zeng, Z., Cai, X., Li, H., and Hu, Z. (2017). Optogenetic regulation of artificial microRNA improves H2 production in green alga *Chlamydomonas reinhardtii*. Biotechnol. Biofuels *10*, 257.

Wend, S., Dal Bosco, C., Kämpf, M.M., Ren, F., Palme, K., Weber, W., Dovzhenko, A., and Zurbriggen, M.D. (2013). A quantitative ratiometric sensor for time-resolved analysis of auxin dynamics. Sci. Rep. *3*, 2052.

Wend, S., Wagner, H.J., Müller, K., Zurbriggen, M.D., Weber, W., and Radziwill, G. (2014). Optogenetic control of protein kinase activity in mammalian cells. ACS Synth. Biol. *3*, 280–285.

Wigge, P.A. (2005). Integration of Spatial and Temporal Information During Floral Induction in Arabidopsis. Science *309*, 1056–1059.

Win, M.N., and Smolke, C.D. (2007). A modular and extensible RNA-based gene-regulatory platform for engineering cellular function. Proc. Natl. Acad. Sci. U. S. A. *104*, 14283–14288.

Wu, H.-Y., Liu, K.-H., Wang, Y.-C., Wu, J.-F., Chiu, W.-L., Chen, C.-Y., Wu, S.-H., Sheen, J., and Lai, E.-M. (2014). AGROBEST: an efficient

Agrobacterium-mediated transient expression method for versatile gene function analyses in Arabidopsis seedlings. Plant Methods *10*, 19.

Yang, Q., Brüschweiler, S., and Chou, J.J. (2014). A Self-Sequestered Calmodulin-like Ca2+ Sensor of Mitochondrial SCaMC Carrier and Its Implication to Ca2+-Dependent ATP-Mg/Pi Transport. Structure *22*, 209–217.

Zhang, K., and Cui, B. (2014). Optogenetic control of intracellular signaling pathways. Trends Biotechnol. *33*, 92–100.

Zhao, X., Meng, Z., Wang, Y., Chen, W., Sun, C., Cui, B., Cui, J., Yu, M., Zeng, Z., Guo, S., et al. (2017). Pollen magnetofection for genetic modification with magnetic nanoparticles as gene carriers. Nat. Plants *3*, 956–964.

Zhou, X.X., Chung, H.K., Lam, A.J., and Lin, M.Z. (2012). Optical Control of Protein Activity by Fluorescent Protein Domains. Science *338*, 810–814.

Zhou, X.X., Zou, X., Chung, H.K., Gao, Y., Liu, Y., Qi, L.S., and Lin, M.Z. (2018). A Single-Chain Photoswitchable CRISPR-Cas9 Architecture for Light-Inducible Gene Editing and Transcription. ACS Chem. Biol. *13*, 443–448.

Zipfel, C., Kunze, G., Chinchilla, D., Caniard, A., Jones, J.D.G., Boller, T., and Felix, G. (2006). Perception of the Bacterial PAMP EF-Tu by the Receptor EFR Restricts Agrobacterium-Mediated Transformation. Cell *125*, 749–760.

Zoltowski, B.D., Motta-Mena, L.B., and Gardner, K.H. (2013). Blue light-induced dimerization of a bacterial LOV-HTH DNA-binding protein. Biochemistry *52*, 6653–6661.

Zuo, J., and Chua, N.H. (2000). Chemical-inducible systems for regulated expression of plant genes. Curr. Opin. Biotechnol. *11*, 146–151.

Zürcher, E., Tavor-Deslex, D., Lituiev, D., Enkerli, K., Tarr, P.T., and Müller, B. (2013). A Robust and Sensitive Synthetic Sensor to Monitor the Transcriptional Output of the Cytokinin Signaling Network in Planta. Plant Physiol. *161*, 1066–1075.

# Appendix

# A. Original publications and manuscripts

# Chapter 9

# Optogenetics in Plants: Red/Far-Red Light Control of Gene Expression

**Rocio Ochoa-Fernandez, Sophia L. Samodelov, Simon M. Brandl, Elke Wehinger, Konrad Müller, Wilfried Weber, and Matias D. Zurbriggen**

## Abstract

Optogenetic tools to control gene expression have many advantages over the classical chemically inducible systems, overcoming intrinsic limitations of chemical inducers such as solubility, diffusion, and cell toxicity. They offer an unmatched spatiotemporal resolution and permit quantitative and noninvasive control of the gene expression. Here we describe a protocol of a synthetic light-inducible system for the targeted control of gene expression in plants based on the plant photoreceptor phytochrome B and one of its interacting factors (PIF6). The synthetic toggle switch system is in the ON state when plant protoplasts are illuminated with red light (660 nm) and can be returned to the OFF state by subsequent illumination with far-red light (760 nm). In this protocol, the implementation of a red light-inducible expression system in plants using Light-Emitting Diode (LED) illumination boxes is described, including the isolation and transient transformation of plant protoplasts from *Arabidopsis thaliana* and *Nicotiana tabacum*.

**Key words** Plant synthetic biology, Plant optogenetics, Red light-inducible gene expression system, Plant leaf protoplasts, *Arabidopsis thaliana*, *Nicotiana tabacum*

## 1 Introduction

Inducible gene expression systems in plants are essential to study cellular processes, to control target gene expression with minimal or no interference to developmental or growth processes, and for efficient large-scale biopharmaceutical production. Spatial control of gene expression in plants has traditionally been achieved by the use of tissue-specific promoters. This leads to highly specific spatial gene expression, however, once such an expression cassette has been implemented, the promoters can no longer be exogenously controlled [1]. Likewise, classical chemically inducible systems offer temporal control over gene expression in plants (such as ethanol- or

The original version of this chapter was revised. The erratum to this chapter is available at: DOI 10.1007/978-1-4939-3512-3_28

Arash Kianianmomeni (ed.), *Optogenetics: Methods and Protocols*, Methods in Molecular Biology, vol. 1408, DOI 10.1007/978-1-4939-3512-3_9, © Springer Science+Business Media New York 2016

dexamethasone-inducible systems [2]) but do not fulfill key requirements of inducible gene expression systems. This is due to the intrinsic limitations of chemical inducers like solubility, diffusion, inability to revert induction without washing steps, inducer-removal in sample processing and pleiotropic effects, limiting their application in vitro and in vivo and their use in long-term treatments [1, 3]. Light as a *stimulus* overcomes these limitations, offering advantages such as reversibility, fast reactivity, and minimal cell toxicity, therefore allowing a precise control of gene expression in a quantitative and noninvasive manner, with both high spatial and temporal resolution.

Several light-responsive gene expression systems have been developed for gene control with UVB, blue, or red light and adapted for use in mammalian cell culture and in vivo in animals (reviewed in [4, 5]). However, the application of these optogenetic tools in plants has not yet taken root, mainly due to the fact that light is essential for plant growth and development, therefore having pleiotropic effects. Thus far, only a red/far-red light-inducible system has been applied to plants [6], in principle due to its ability to revert between ON and OFF states with two different wavelengths. In this sense, this toggle switch system is unique and differs from the rest of the optogenetic tools based on photoreceptors which can be activated by light of one wavelength but can only revert to the basal, inactive state nonphotochemically, with shut off kinetics depending on their photobiological properties (dark reversion). The red/far-red light-inducible system is based on the photoreceptor Phytochrome B (PhyB) and phytochrome-interacting factor 6 (PIF6) from *Arabidopsis* thaliana. This system is a split transcription factor in which the components interact in a light-dependent manner. It is based on three constructs: (1) PIF6 (amino acids 1–100) fused to the mphR(A) (macrolide repressor DNA-binding protein E) and a nuclear localization sequence (NLS); (2) PhyB (amino acids 1–650) fused to the *Herpes simplex* VP16 transactivation domain and an NLS; and (3) multiple repetitions of an etr motif (cognate binding site of the E protein), placed upstream of a CMV minimal promoter followed by a reporter gene, e.g. firefly luciferase (Fig. 1a, Table 1). Upon exposure to red light, PhyB changes its conformation by photoisomerization of the covalently bound chromophore, phytochromobilin (PΦB). The activated form of PhyB ($P_{fr}$) binds to PIF6 and the VP16 domain is then recruited to the etr motif in close proximity to the minimal promoter, activating transcription of the reporter gene. The PhyB-PIF6 association is readily reversed upon exposure to far-red light, when PhyB changes its conformation to the inactive form ($P_r$) resulting in the termination of reporter gene expression (Fig. 1b).

Here we describe a protocol for a light-inducible expression system that is activated by red light and deactivated by far-red light to control gene expression in leaf protoplasts of *Nicotiana tabacum* and *Arabidopsis thaliana*. The control of gene expression with high resolution in time and space overcomes intrinsic limitations of

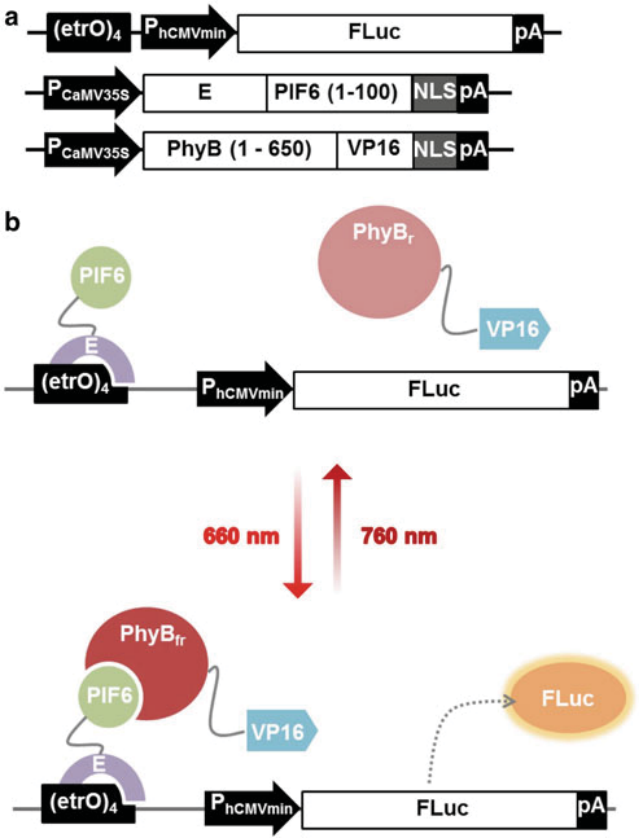


**Fig. 1** Design of the red light-controlled gene expression system in plants. (**a**) Configuration of the vectors. (**b**) Mode of function. Upon exposure to red light (660 nm), PhyB changes its conformation to its active form ($P_{fr}$) that allows the binding to PIF6 and therefore recruitment of the transactivator to the minimal promoter, firefly luciferase is expressed as a consequence. Under far-red (760 nm) light illumination, PhyB is converted to its inactive form ($P_r$), PhyB-PIF6 dissociates, thus ceasing the transcription of the reporter gene

existing systems and facilitates novel applications including the precise interrogation of complex biological signaling processes in a quantitative and noninvasive manner.

## 2 Materials

Prepare all solutions using double distilled water and p.a. purity grade chemicals. Use plant cell culture tested reagents for plant growth and protoplast isolation media. Prepare and store all reagents at 4 °C unless indicated otherwise.

### 2.1 Plant Growth

1. SCN (*S*eedling *C*ulture *N*icotiana) (modified from [7]): 0.32 % (w/v) Gamborg B5 basal salt powder with vitamins (bioWORLD, GeneLinx International, Inc., USA), 4 mM $MgSO_4 \cdot 7H_2O$, 58.4 mM sucrose and 0.15 % (w/v) gelrite. Mix and adjust to

**Table 1**
**Description of the plasmids encoding the red light-controlled gene expression system for plants used in this protocol**

| Vector | Description | References |
|---|---|---|
| pROF100 | $(etrO)_4$-$P_{hCMVmin}$-FLuc-pA<br>Vector encoding firefly luciferase (Fluc) under the control of the human cytomegalovirus minimal promoter ($P_{hCMVmin}$); placed downstream of multiple repetitions of an operator sequence for the E protein $(etrO)_4$. | This work |
| pMZ827 | $P_{CaMV35S}$-E-*AtPIF6*(1-100)-NLS-pA<br>Vector comprising the macrolide repressor DNA-binding protein (E) fused to the N-terminal 100 amino acids of *AtPIF6* under control of the cauliflower mosaic virus 35S promoter ($P_{CaMV35S}$). The fusion protein is targeted to the nucleus by C-terminal fusion of a nuclear localization sequence (NLS). | [6] |
| pMZ828 | $P_{CaMV35S}$-*AtPhyB*(1-650)-VP16-NLS-pA<br>Vector encoding a fusion protein of the N-terminal 650 amino acids fragment of *AtPhyB* fused to the Herpes simplex-derived VP16 transactivation domain under the control of the cauliflower mosaic virus 35S promoter ($P_{CaMV35S}$). The fusion protein is targeted to the nucleus by C-terminal fusion of a nuclear localization sequence (NLS). | [6] |

Abbreviations: *E* macrolide repressor DNA-binding protein, *etrO* operator sequence for E protein, *Fluc* firefly luciferase, *NLS* nuclear localization sequence, *pA* polyadenylation signal, $P_{CaMV35S}$ cauliflower mosaic virus 35S promoter, $P_{hCMVmin}$ human cytomegalovirus minimal promoter, *VP16 Herpes simplex* virus-derived transactivation domain

pH 5.8 and autoclave. After autoclaving, add 0.1 % (v/v) of Gamborg B5 Vit Mix (bioWORLD) and pour 50 ml of the medium into each Magenta Plant Culture Box (*see* **Note 1**).

2. SCA (*S*eedling *C*ulture *A*rabidopsis) (modified from [8]): 0.32 % (w/v) Gamborg B5 basal salt powder with vitamins (bioWORLD), 4 mM $MgSO_4 \cdot 7H_2O$, 43.8 mM sucrose and 0.8 % (w/v) phytoagar in $H_2O$. Mix and adjust to pH 5.8. Autoclave and add 0.1 % (v/v) Gamborg B5 Vit Mix (bioWORLD) then pour 50 ml of the medium into each Magenta Plant Culture Box; or alternatively add 1:2000 ampicillin and pour 50 ml of the medium into each 12 cm square plate (*see* **Note 1**).
3. Seed sterilization solution for *A. thaliana* (modified from [9]): 5 % (w/v) calcium hypochlorite, 0.02 % (v/v) Triton X-100 in 80 % (v/v) EtOH. Combine the chemicals in a bottle and mix for few hours at room temperature. A precipitate will form. Place the bottle to 4 °C for storage. Allow the precipitate to settle and do not agitate the bottle before use.
4. Seed sterilization solution for tobacco: 5 % active chlorine from NaOCl solution (12 % active chlorine stock solution), 0.5 % (v/v) Tween 20 in autoclaved $H_2O$. Sterilize with a 0.22 μm filter. Prepare fresh prior to each use.
5. Parafilm.
6. Syringe and 22 μm filter.
7. Ampicillin stock (100 mg/ml).

### 2.2 Protoplast Isolation and PEG Mediated Protoplast Transformation

1. MMC (*M*ES, *M*annitol, *C*alcium) [8]: 10 mM MES, 40 mM $CaCl_2 \cdot H_2O$, add mannitol until obtaining an osmolarity of 550 mOsm (ca. 85 g/l). Adjust to pH 5.8 and filter sterilize.
2. F-PIN (*F*ast *P*rotoplast *I*ncubation *N*icotiana) (modified from [7]): 10 mM MES, 0.32 % (w/v) Gamborg B5 basal salt powder with vitamins (bioWORLD), 0.38 M sucrose. Adjust to pH 5.8 and filter sterilize.
3. Enzyme solution stock 5 % (10× concentrated): cellulase Onozuka R10 and macerozyme R10 (SERVA Electrophoresis GmbH, Germany) in F-PIN or MMC. Weigh 10 g of cellulase and 10 g of macerozyme and dissolve in F-PIN solution or MMC (preheated to 37 °C) to a total volume of 200 ml $H_2O$ (*see* **Note 2**). Sterile filter the solution with a bottle-top filter into a sterile bottle and make aliquots of 2 ml. Store at −20 °C, avoid thaw–refreeze cycles.
4. MSC (*M*ES, *S*ucrose, *C*alcium) [8]: 10 mM MES, 0.4 M sucrose, 20 mM $MgCl_2 \cdot 6H_2O$, add mannitol until obtaining an osmolarity of 550 mOsm (ca. 85 g/l). Adjust to pH 5.8 and filter sterilize.
5. W5 solution (modified from [10]): 2 mM MES, 154 mM NaCl, 125 mM $CaCl_2 \cdot 2H_2O$, 5 mM KCl, 5 mM glucose. Adjust to pH 5.8 and filter sterilize.

6. MMM (*M*ES, *M*annitol, *M*agnesium) [8]: 15 mM $MgCl_2$, 5 mM MES, mannitol to 600 mOsm (ca. 85 g/l). Adjust to pH 5.8 and filter sterilize.
7. PEG solution: Mix 2.5 ml of 0.8 M mannitol, 1 ml of 1 M $CaCl_2$ and 4 g $PEG_{4000}$ and 3 ml $H_2O$. Made fresh for each experiment. Not filtered, prepare fresh and place the tube at 37 °C for PEG dissolution, then use directly.
8. PCA (*P*rotoplast *C*ulture *A*rabidopsis) (modified from [8]): 0.32 % (w/v) Gamborg B5 basal salt powder with vitamins (bioWORLD), 2 mM $MgSO_4 \cdot 7H_2O$, 3.4 mM $CaCl_2 \cdot 2H_2O$, 5 mM MES, 0.342 mM l-glutamine, 58.4 mM sucrose, glucose 550 mOsm (ca. 80 g/l), 8.4 µM Ca-panthotenate, 2 % (v/v) biotin from a biotin solution 0.02 % (w/v) in $H_2O$ (warm up the biotin solution to dissolve). Adjust to pH 5.8 and filter sterilize, add 0.1 % (v/v) Gamborg B5 Vitamin Mix and 1:2000 ampicillin to the PCA before use.
9. Scalpel.
10. Disposable 100 µm and 40–70 µm pore size sieve (Greiner bio-one international, Germany).
11. Petri dish 94 × 16 mm.
12. Parafilm.
13. 200 µl and 1 ml large orifice pipette tips.
14. Round-bottom 15 ml Falcon tubes.
15. Rosenthal cell counting chamber.
16. Nontreated 6-, and 12-, or 24-well plates.

### 2.3 Illumination Treatment

1. 660 and 760 nm light-emitting diode (LED) illumination boxes.

In brief, the LED illumination boxes are custom-made boxes of PVC that exclude external light and at the same time allow gas exchange. The light boxes contain panels of LEDs (Roithner Lasertechnik GmbH, Austria) of one or several wavelengths. In addition, the irradiation intensity and illumination schemes can be set by using a programmable control unit (for full description see [11] and [12]). As an example, such a box is shown in Fig. 2. The light box is composed of three parts: a base for placing the cell culture plate, the walls, and the lid where the LEDs of specific emission wavelengths are built-in. In this protocol, boxes equipped with either red (660 nm) or far-red (760 nm) LEDs were used.

### 2.4 Luminescence Reporter Assay

1. Costar® 96-well flat-bottom white plate.
2. Firefly luciferase substrate: 20 mM tricine, 2.67 mM $MgSO_4 \cdot 7H_2O$, 0.1 mM EDTA·$2H_2O$, 33.3 mM DTT, 0.52 mM ATP, 0.27 mM acetyl-CoA, 0.47 mM d-luciferin (Biosynth AG), 5 mM NaOH, 264 µM $MgCO_3 \cdot 5H_2O$, in $H_2O$. Prepare

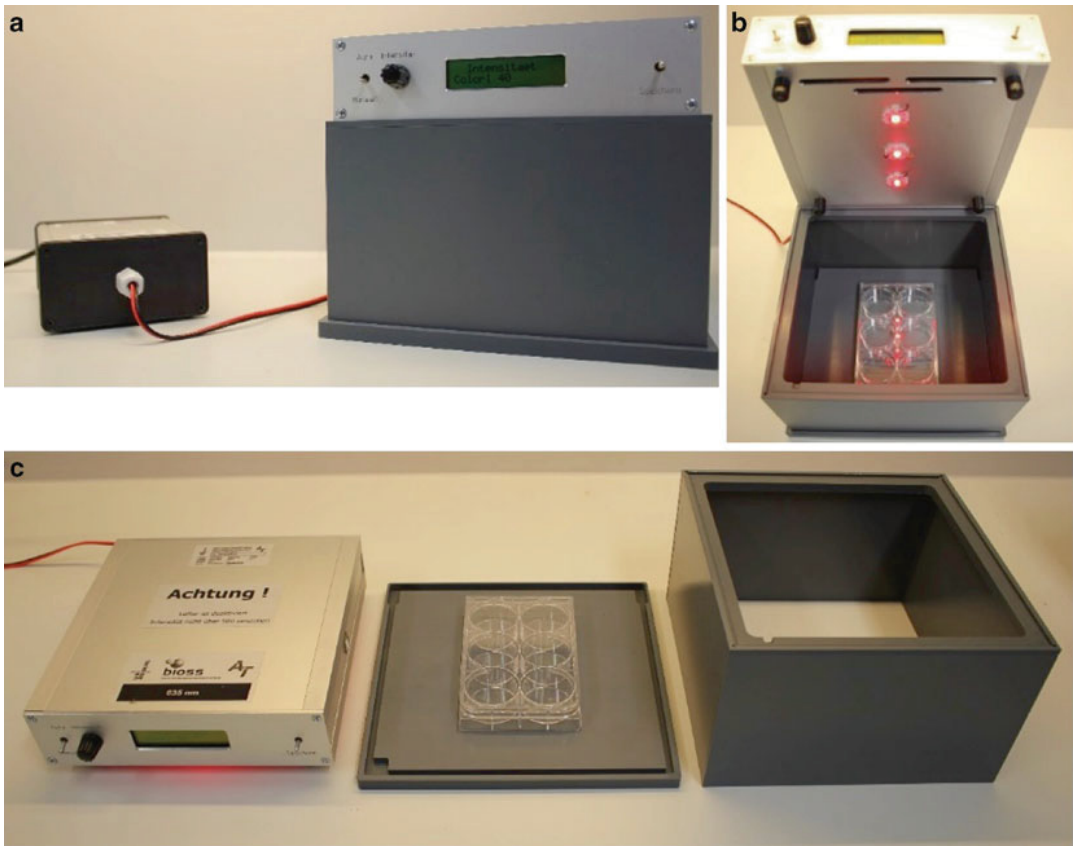


**Fig. 2** LED illumination box. (**a**) Illumination box for one cell culture plate. (**b**) Opened illumination box. The LEDs are located in the lid of the box. (**c**) Three components of the light box

a beaker with a magnetic stirrer and add the components in the order as above, then add the luciferin and $H_2O$ and mix the solution, proceed with the addition of the last two components (NaOH and $MgCO_3{\cdot}5H_2O$). Adjust to pH 8, aliquot the substrate in precooled black Falcon tubes and freeze them at −80 °C (*see* **Note 3**).

## 3 Methods

### *3.1 Seed Sterilization and Plant Material*

#### *3.1.1 Arabidopsis thaliana (Wild Type, Columbia-0)*

1. Seed sterilization should be done in 1.5 ml tubes in a sterile working hood. For large-scale seed sterilization, fill tubes to a maximum of approximately 250 µl volume. Avoid sterilizing a larger volume in a single tube, as results (efficiency) may vary.
2. Rinse seeds multiple times with 80 % (v/v) ethanol until all large dirt and other plant particles are removed.
3. Sterilize the seeds with 1 ml of the *A. thaliana* sterilization solution under agitation for 10 min.

4. Remove the solution and replace with 1 ml of 80 % (v/v) EtOH. Incubate 5 min under agitation.
5. Repeat **step 4** but incubating for 2 min.
6. Replace the solution with 1 ml absolute ethanol (≥99.5 %) and incubate for 1 min under agitation.
7. Remove all ethanol and let the seeds dry completely under the sterile hood.
8. Add autoclaved water and plate in a line on autoclaved filter paper strips (200–300 seeds/strip) placed on 12 cm square plates containing SCA medium and seal with parafilm. Multiple strips may be placed in one plate. Alternatively, place 1–16 seeds, evenly dispersed, in a Magenta Box containing 50 ml SCA medium.
9. Place the plates in a growth chamber with a 16 h light regime at 22 °C. Two- to three-week old plantlets from 12 cm square plates can be used for protoplast isolation. Three- to four-week old plants grown in Magenta boxes can be used for protoplast isolation.

#### *3.1.2 Nicotiana tabacum cv Petit Havana*

1. Incubate the desired number of seeds with 1 ml of seed sterilization solution for tobacco for 5 min at room temperature under agitation. Large-scale seed sterilization for *N. tabacum* has not been tested, due to the small amount of seeds necessary when growing plants in Magenta boxes.
2. Remove the solution (centrifuge if necessary to sediment the seeds) and rinse the seeds 3–4 times with 1 ml of $H_2O$ in the same manner.
3. Place one or two seeds in the middle of a Magenta Box containing 50 ml SCN medium. When more than one seed germinates, the seedlings must be separated to different boxes (around day 4–6 after germination) in order to have only one plant per box for optimal growth.
4. Place the Magenta boxes in a growth chamber with a 16 h light regime at 22–25 °C (plants will grow faster at higher temperatures). Leaves from 2- to 3-week old plants can be used for protoplast isolation.

### *3.2 Protoplast Isolation and Polyethylene Glycol-Mediated Transformation*

*A. thaliana* and *N. tabacum* protoplast isolation per flotation and polyethylene glycol-mediated transformation were performed as described before ([8] and [13], respectively) with a few alterations. All pipetting is done with wide orifice tips to avoid damaging the protoplasts. Preferentially use medium acceleration and lowest deceleration settings for the centrifugation steps (140 s acceleration and 300 s deceleration according to DIN58970).

1. Cut the tobacco leaves in 1 mm strips with the abaxial surface facing up starting from the middle lamella with a sterile scalpel

(*see* **Note 4**). Finely slice the plant leaves of *A. thaliana* with the scalpel in 2 ml of MMC (*see* **Note 5**).

2. Transfer the cut leaf material into a new Petri dish containing 9 ml F-PIN (tobacco) or 7 ml of MMC (*A. thaliana*).
3. Proceed with the enzymatic digestion of cut plant material by adding 1 ml of 10× enzyme stock solution (the final concentration of each enzyme should be 0.5 %).
4. Seal the dish with parafilm and cover it with aluminum foil. Incubate overnight (12–16 h) in the dark at 22 °C.
5. Carefully homogenize the digested leaf material by pipetting the leaf-enzyme mixture up and down to release the protoplasts from the plant material.
6. Pass through a disposable 100 μm (tobacco) or 40–70 μm (*A. thaliana*) pore size sieve.
7. Transfer the filtered protoplast solution to 15 ml round bottom Falcon tubes. One tube should be used for each plate of digested leaf material. The remaining steps should be completed in these tubes.
8. For *A. thaliana*, centrifuge the filtered protoplast solution in round bottom Falcon tubes at 100 × *g* for 10–20 min to sediment the protoplasts. Remove supernatant and resuspend in 10 ml of MSC. For tobacco protoplasts, centrifugation is not necessary, as the flotation of protoplasts can be done directly in the F-PIN solution.
9. Very carefully overlay 10 ml of protoplast solution with 2 ml of MMM (*see* **Note 6**).
10. For *A. thaliana* protoplasts, centrifuge for 10 min at 80 × *g* for accumulation of the protoplasts at the interphase of MSC and MMM. For tobacco protoplasts, instead of centrifugation, incubate the tubes at room temperature for 20–30 min, in which time the protoplasts will float to the interphase of F-PIN and MMM (*see* **Note 7**).
11. Collect the protoplasts at the interphase and transfer into a new Falcon tube with 7 ml of W5 solution. For each floatation tube to be used, prepare two W5-filled collection Falcon tubes. Multiple rounds of protoplast collection can be done (if necessary overlay again with MMM) until no further protoplasts float to the interphase or enough protoplasts are obtained.
12. Centrifuge the collected protoplasts for 10 min at 100 × *g* to pellet and resuspend in a defined volume of W5 for counting (*see* **Note 8**).
13. Determine the cell density using a Rosenthal cell counting chamber.

14. Sediment the protoplasts by centrifuging for 5 min at 80 × *g*. Discard supernatant and adjust with MMM solution to a density of $5 \times 10^5$ cells/ml for tobacco and $5 \times 10^6$ cells/ml for *A. thaliana*.

15. (a) For the transformation of tobacco protoplasts, prepare 50 μg of DNA in $H_2O$ (*see* **Note 9**) in a round bottom Falcon tube and add 1 ml of the protoplasts in MMM. Carefully mix by pipetting and incubate for 5 min.

    (b) For *A. thaliana* protoplasts, prepare 15–30 μg of DNA in $H_2O$ (*see* **Note 9**) adjusted to a maximum volume of 20 μl (volume adjustment with MMM). Transfer the 20 μl DNA solution to the rim of a well of a 6-well culture plate (slightly tilt the plate for easier pipetting in the following steps). Dispense 100 μl of the protoplast solution to each well with DNA and mix by gentle pipetting. Incubate for 5 min.

16. (a) For tobacco protoplast transformation, add 1 ml $PEG_{4000}$ solution to the protoplasts in a drop-wise manner with a tip-in-tip method while slowly rotating the Falcon tube (*see* **Note 10**). After 8 min (*see* **Note 11**), consecutively add 1, 2, 3, and 4 ml of W5 per minute to the tube as a stepwise dilution of the transformation, and gently tilt the tube after each step for mixing.

    (b) For *A. thaliana* protoplast transformation, gently shake the 6-well plate from side to side to distribute the protoplasts and DNA along the rim before directly adding 120 μl of $PEG_{4000}$ solution drop-wise, tip-in-tip. Do not mix after the addition of PEG. Incubate for 8 min (*see* **Notes 11** and **12**) and quickly add 120 μl of MMM and, directly afterwards, at least 1.2 ml of PCA. Gently mix by tilting the plate after the addition of PCA (final volume should be at least 1.6 ml).

17. Only for tobacco, sediment the cells at 5 min at 80 × *g*, discard the supernatant and resuspended in at least 1.6 ml PCA.

18. After transformation, if only one condition is to be tested, leave the *A. thaliana* protoplast suspension in a well of a 6-well plate. In the case of tobacco protoplasts transfer the 1.6 ml from the tube into a well of a 6-well plate.

    If more than one condition is to be tested, split the protoplasts in different plates according to the number of light conditions to be assayed. The volume pipetted to each well in the new plates will depend on the number of replicates per condition. Considering that 25,000 protoplasts (see below) will be used

for each measurement (80 µl protoplast suspension), it follows that for 6 replicates 150,000 protoplasts are needed, amounting to 480 µl protoplast suspension. Scale down to 12- or 24-well plate to avoid high evaporation rates. Seal the plate(s) with parafilm.

### 3.3 Illumination Treatment and Reporter Assay

1. After transformation of the protoplasts, illuminate the plates with the appropriate wavelength (i.e. 660, 760 nm) and intensity of light with LED arrays, or incubate in the dark prior to reporter quantification. The spectra of the LEDs and the radiation intensity can be determined with a spectroradiometer (e.g. AvaSpec-ULS2048-USB2 FC/PC and FC-UVIR200-2-ME-1FCPC, Avantes, Netherlands).

   As an example, Fig. 3a shows time-course and dose-response curves for the red light-inducible gene expression system. Protoplasts were isolated from *A. thaliana* plantlets and 10 µg of each plasmid (pMZ827, pMZ828 and pROF100) were transformed into the protoplasts. Several transformations were made in parallel (22 transformations) and after transformation all the protoplasts were pooled. Aliquots of 3.5 ml of the protoplasts suspension were transferred into one well of seven different 6-well plates (one plate for each illumination condition). The luminescence determination was made for each condition at different points in time (0, 6, 12, 18, and 24 h). As a dark control, 1 ml of protoplast suspension was transferred into one well of four different 24-well plates. In this way, a single plate per time point was used and accidental exposure of the plate to ambient light avoided. The results of the kinetics and expression levels of the red light-inducible system in *A. thaliana* protoplast depicted in Fig. 3a indicate between 1 and 4 µE/m$^2$/s as optimal illumination conditions for maximum expression rates. The highest expression levels are achieved at 24 h but a better dynamic range (399 and 395 × fold induction) is obtained at 18 h of gene expression for 2–4 µE/m$^2$/s red-light intensities (Fig. 3b). It is, however, recommended to adjust the protocol to the application of interest.
2. To determine reporter expression, first gently mix the protoplast suspension with the pipette and transfer 80 µl (25,000 protoplasts) into a Costar® 96-well flat-bottom white plate, including 4–6 replicates for each condition (*see* **Note 13**).
3. Add 20 µl of firefly luciferase substrate and monitor the luminescence in a plate reader [14]. 10 s of shaking plate for homogeneous substrate availability and directly luminescence measurement for 20 min kinetics (interval of 2 min) are advisable.

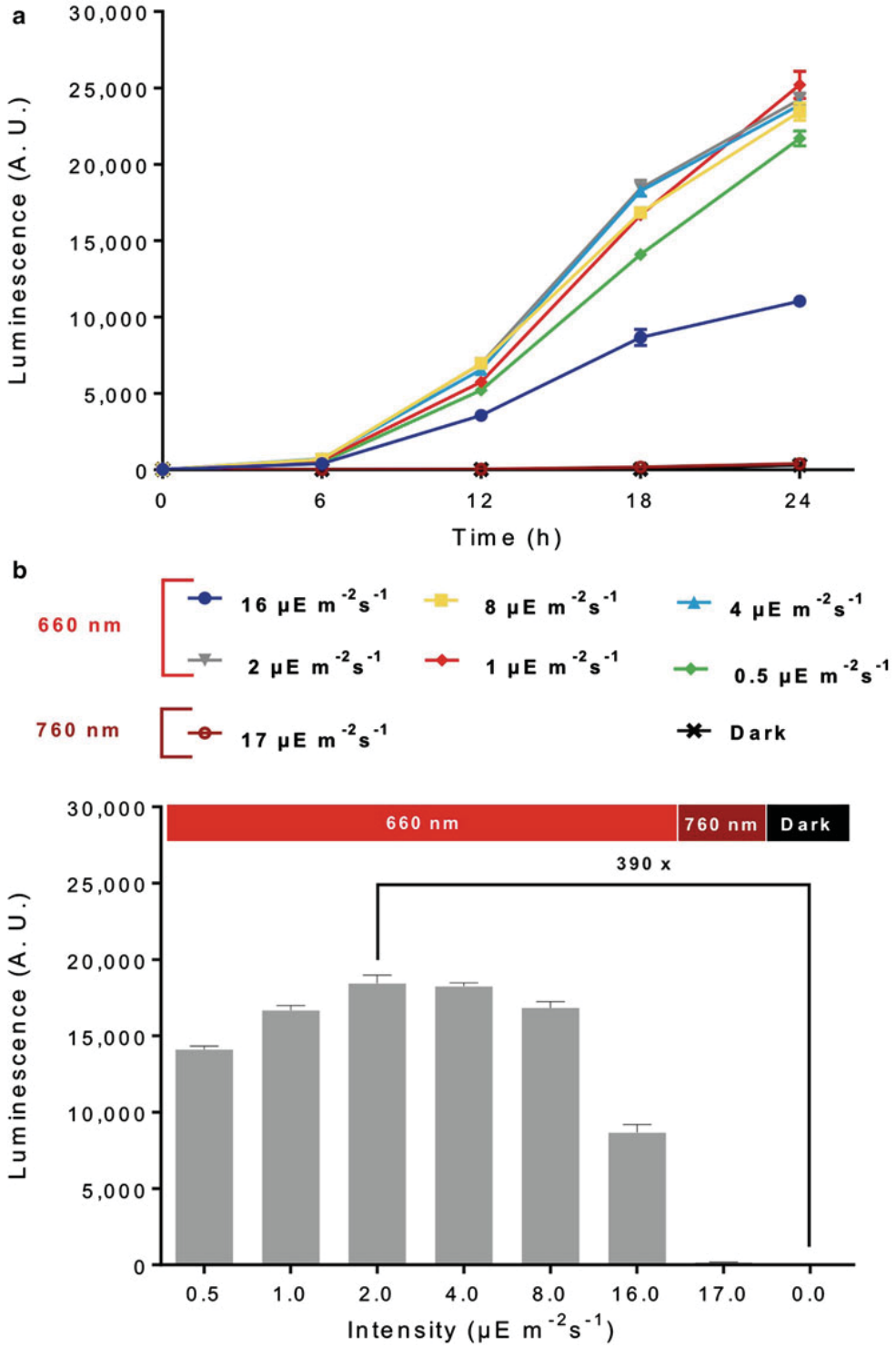


**Fig. 3** Time- and dose-response curves of the red light inducible gene expression system in protoplasts of *A. thaliana*. Protoplasts from *A. thaliana* were transformed for red light–inducible firefly luciferase expression (pMZ827, pMZ828, and pROF100). After transformation, 3.5 ml aliquots of protoplast suspensions containing approximately $1.09 \times 10^6$ protoplasts, were illuminated either at different intensities of 660 nm (0.5, 1, 2, 4, 8, and 16 µE/m$^2$/s), at 760 nm (17 µE/m$^2$/s) light, or were kept in the dark as a control. (**a**) Samples were taken at the indicated points (0, 6, 12, 18, and 24 h after transformation) and firefly luciferase expression was determined.

## 4 Notes

1. Prepare the plates or Magenta Plant Culture boxes directly after autoclaving because the gelrite and phytoagar will not dissolve upon reheating.
2. Both enzyme extracts are not to be inhaled and are poorly soluble. For these reasons: solve under a fume hood by adding 10 ml of prewarmed (37 °C) MMC/F-PIN to each bottle directly, shake, and pour into beaker and rinse bottles repeatedly. Fill beaker to 200 ml. The solution will not be clear, should, however, be a clear brown after filtration.
3. For certain solutions, a stock solution can be prepared in advance; however, tricine, DTT, ATP, and acetyl-CoA should be prepared fresh. From the addition of DTT on, all steps should be performed under a fume hood. Moreover, luciferin is sensitive to light, oxygen, and high temperature so that from its addition on, the preparation should be performed in darkness and as quickly as possible. Due to the high price of acetyl-CoA, it is also preferable to purchase this substrate in small amounts (50 mg for the preparation of 200 ml of firefly luciferase substrate) and use the entire content in a single preparation of substrate to avoid freeze–thaw cycles and waste.
4. Choose healthy leaves not showing nutritional deficiency, chlorosis, or mechanical damage.
5. *A. thaliana* plant material grown in plates should be carefully cut from the plate with a scalpel in a way that avoids including roots and seeds, and should then be cut finely into small pieces. When cutting the plant material from Magenta Plant Culture Boxes, take only the leaves and either cut them in strips as described for tobacco or slice them finely. Sterile featherweight forceps are helpful in holding *A. thaliana* leaves from Magenta boxes to be cut in strips without inflicting damage to them.
6. Gentle inversion of the tube before adding the MMM solution slowly helps for a clear separation of phases. For addition of MMM use a tip-in-tip technique i.e. placing a smaller tip into the tip of a bigger tip for a slow solution dispense.
7. Collecting the first band of protoplasts at the interphase after 10–15 min increases the speed of protoplast floatation.
8. Protoplasts will not be successfully pelleted if the collection tube contains less W5 than MMM.

**Fig. 3** (continued) The graph shows the reporter luminescence values at different time points and different illumination conditions. (**b**) Reporter luminescence values after 18 h expression at the indicated light intensities. Data are means ± SEM ($n = 6$ technical replicates)

9. DNA amounts mentioned in the protocol are total amounts of DNA. When more than one plasmid is used, the amounts of each plasmid must be adjusted proportionally, keeping the total DNA amount constant. Purify the plasmid DNA using midiprep or maxiprep kits and check the quality of the plasmid DNA by agarose gel electrophoresis (e.g. RNA content).
10. If the PEG has sedimented to the bottom of the tube, mixing by gently tilting the tube will be necessary.
11. The duration of PEG treatment is critical in the transformation; the suggested 8 min treatment leads to high transformation efficiency in our experience.
12. Gently shaking the plate side to side before PEG addition avoids the aggregation of protoplasts.
13. It is recommended to pipette the protoplasts in the following order: 660 nm (highest to low intensities)—760 nm—dark, as the system is rapidly activated by ambient light. Due to the sensitivity of the system, it is also recommended to work in a darkroom with green safelight emitted by LEDs (~520 nm). Green light illumination at moderate intensities does not lead to noticeable activation of PhyB.

## Acknowledgments

This work was supported in part by the Excellence Initiative of the German Federal and State Governments (EXC294-BIOSS, GSC-4 Spemann Graduate School (SGBM)) and the Alexander von Humbolt Foundation (research Grant no. 1141629). We thank Susanne Knall and Frauke Bartels-Burgahn for experimental assistance. We thank J. Schmidt, D. Schächtele and J. Meßmer (University of Freiburg) for designing and constructing the illumination boxes.

### References

1. Corrado G, Karali M (2009) Inducible gene expression systems and plant biotechnology. Biotechnol Adv 27(6):733–743
2. Junker A, Junker B (2012) Synthetic gene networks in plant systems. In: Weber W, Fussenegger M (eds) Synthetic gene networks, vol 813, Methods in molecular biology. Humana, New York, pp 343–358
3. Padidam M (2003) Chemically regulated gene expression in plants. Curr Opin Plant Biol 6(2):169–177
4. Zhang K, Cui B (2015) Optogenetic control of intracellular signaling pathways. Trends Biotechnol 33(2):92–100
5. Müller K, Naumann S, Weber W, Zurbriggen MD (2015) Optogenetics for gene expression in mammalian cells. Biol Chem 396(2):145–152
6. Müller K, Siegel D, Rodriguez Jahnke F, Gerrer K, Wend S, Decker EL, Reski R, Weber W, Zurbriggen MD (2014) A red light-controlled synthetic gene expression switch for plant systems. Mol BioSyst 10(7):1679–1688

7. Dovzhenko A, Bergen U, Koop HU (1998) Thin-alginate-layer technique for protoplast culture of tobacco leaf protoplasts: shoot formation in less than two weeks. Protoplasma 204(1-2):114–118
8. Dovzhenko A, Dal Bosco C, Meurer J, Koop HU (2003) Efficient regeneration from cotyledon protoplasts in Arabidopsis thaliana. Protoplasma 222(1–2):107–111
9. Luo Y, Koop H-U (1997) Somatic embryogenesis in cultured immature zygotic embryos and leaf protoplasts of Arabidopsis thaliana ecotypes. Planta 202(3):387–396
10. Menczel L, Galiba G, Nagy F, Maliga P (1982) Effect of radiation dosage on efficiency of chloroplast transfer by protoplast fusion in nicotiana. Genetics 100(3):487–495
11. Müller K, Zurbriggen MD, Weber W (2014) Control of gene expression using a red- and far-red light-responsive bi-stable toggle switch. Nat Protoc 9(3):622–632
12. Müller K, Engesser R, Metzger S, Schulz S, Kämpf MM, Busacker M, Steinberg T, Tomakidi P, Ehrbar M, Nagy F, Timmer J, Zubriggen MD, Weber W (2013) A red/far-red light-responsive bi-stable toggle switch to control gene expression in mammalian cells. Nucleic Acids Res 41(7):e77
13. Koop H-U, Steinmüller K, Wagner H, Rößler C, Eibl C, Sacher L (1996) Integration of foreign sequences into the tobacco plastome via polyethylene glycol-mediated protoplast transformation. Planta 199(2):193–201
14. Wend S, Bosco CD, Kämpf MM, Ren F, Palme K, Weber W, Dovzhenko A, Zurbriggen MD (2013) A quantitative ratiometric sensor for time-resolved analysis of auxin dynamics. Sci Rep 3:2052

ACS SyntheticBiology

Research Article

Cite This: ACS Synth. Biol. 2018, 7, 1349−1358

pubs.acs.org/synthbio

# A Green-Light-Responsive System for the Control of Transgene Expression in Mammalian and Plant Cells

Claire Chatelle,[†,‡] Rocio Ochoa-Fernandez,[§,∥,⊥] Raphael Engesser,[‡,#] Nils Schneider,[†,‡] Hannes M. Beyer,[†,‡,§,▽] Alex R. Jones,[○] Jens Timmer,[‡,#] Matias D. Zurbriggen,*[,∥,⊥] and Wilfried Weber*[,†,‡,§]

[†]Faculty of Biology, [‡]BIOSS Centre for Biological Signalling Studies, [§]SGBM Spemann Graduate School of Biology and Medicine, and [#]Institute of Physics, University of Freiburg, Freiburg, 79104, Germany

[∥]Institute of Synthetic Biology, and [⊥]iGRAD Plant Graduate School, Heinrich Heine University, Düsseldorf, 40225, Germany

[○]National Physical Laboratory, Teddington, Middlesex TW11 0LW, U.K.

Supporting Information

**ABSTRACT:** The ever-increasing complexity of synthetic gene networks and applications of synthetic biology requires precise and orthogonal gene expression systems. Of particular interest are systems responsive to light as they enable the control of gene expression dynamics with unprecedented resolution in space and time. While broadly used in mammalian backgrounds, however, optogenetic approaches in plant cells are still limited due to interference of the activating light with endogenous photoreceptors. Here, we describe the development of the first synthetic light-responsive system for the targeted control of gene expression in mammalian and plant cells that responds to the green range of the light spectrum in which plant photoreceptors have minimal activity. We first engineered a system based on the light-sensitive bacterial transcription factor CarH and its cognate DNA operator sequence CarO from *Thermus thermophilus* to control gene expression in mammalian cells. The system was functional in various mammalian cell lines, showing high induction (up to 350-fold) along with low leakiness, as well as high reversibility. We quantitatively described the systems characteristics by the development and experimental validation of a mathematical model. Finally, we transferred the system into *A. thaliana* protoplasts and demonstrated gene repression in response to green light. We expect that this system will provide new opportunities in applications based on synthetic gene networks and will open up perspectives for optogenetic studies in mammalian and plant cells.

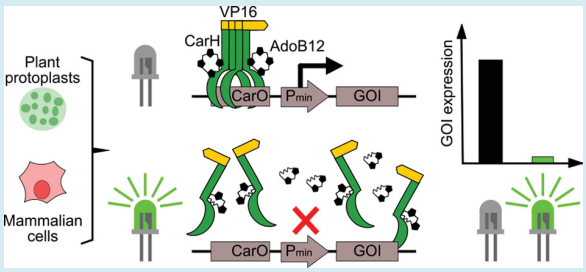


**KEYWORDS:** *optogenetics, light-responsive gene expression, green light, CarH, AdoB12, plants*

Inducible gene switches are core innovations in synthetic biology that enable the programming of cellular function.[1,2] Such programming has provided novel opportunities in functional genomics[3] as well as in drug discovery[4] but has also enabled the implementation of smart biomaterials[5] or the design of closed loop-controlled gene and cell therapeutic networks.[6,7] Inducible gene expression technology in mammalian cells was pioneered by antibiotic-responsive gene switches[8−10] and has rapidly expanded in the inducer spectrum. Gene activity can now be controlled in response to different drugs, metabolites, quorum-sensing messengers or, more recently, in response to light of a specific wavelength.[11−14] Light as inducer offers control opportunities with unmatched resolution in space and time. Such optogenetic switches are based on wiring plant- or bacteria-derived photoreceptors to genetic control elements to activate or repress transcription in animal cells in response to UVB, blue, red or far-red light (www.optobase.org).[13] While such control is now routine in mammalian cells, the application of optogenetic strategies in plant cells lags behind[15] as it is still limited by the endogenous plant photoreceptors that would be cross-activated by the inducing light and thereby might yield off-target signaling responses.[16,17] One opportunity to foster the potential of optogenetics in plants, however, would be the design of a green light-responsive gene switch, as plant photoreceptors show reduced activity in this part of the light spectrum.[18] In this work, we describe the development and characterization of the first green-light-responsive gene switch in mammalian and plant cells. This work extends the toolbox for optogenetic control in mammalian cells and opens opportunities for targeted genetic interventions in plant cell backgrounds. The system is inspired by a naturally occurring defense mechanism found in Gram-negative bacteria such as *Myxococcus xanthus* and *Thermus thermophilus* to protect themselves against photo-oxidative stress.[19−21] In those organisms, CarH, a light-responsive

**Received:** December 12, 2017
**Published:** April 10, 2018




DOI: 10.1021/acssynbio.7b00450
ACS Synth. Biol. 2018, 7, 1349−1358

transcription factor, regulates the expression of a carotenogenic gene cluster. CarH activity and light-sensitivity is dependent on the coenzyme, 5′deoxyadenosylcobalamin (AdoB12). In darkness, AdoB12-linked CarH binds to the DNA operator CarO as a tetramer leading to repression of the carotenogenic target genes. Upon illumination, the Co−C bond in AdoB12 is disrupted by photolysis,[22] which triggers disassembly and release of the tetramer from CarO thus derepressing gene expression.[22,23] Recently, a light-responsive fibroblast growth factor receptor[24] (FGFR) and a light-tunable polymer matrix[25] based on this light-inducible CarH dissociation have been constructed. As AdoB12 features an absorption peak in the green region of the light spectrum (525 nm),[26] we hypothesized that the system could be used for the implementation of a green-light-responsive gene expression system. We engineered the light-responsive CarH-CarO interaction to control gene expression in different mammalian cell lines. We quantitatively characterized the performance of the system by the development and parametrization of a mathematical model. We finally demonstrated the utility of the system for light-regulated gene expression in plant protoplasts.

The green light-responsive gene expression system in mammalian cells consists of two constructs (Figure 1a). The

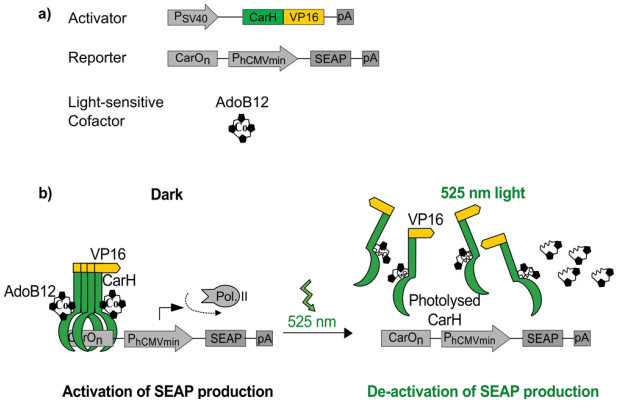


**Figure 1.** Design of the green-light-responsive gene expression system. (a) Molecular components of the expression system. The activator plasmid encodes the DNA binding protein CarH fused to the *Herpes simplex* transactivation domain VP16 under the control of the constitutive simian virus 40 promoter ($P_{SV40}$). The reporter plasmid is composed of multimeric CarO sequences upstream of a human cytomegalovirus-derived minimal promoter ($P_{hCMVmin}$) controlling expression of secreted alkaline phosphatase (SEAP). The light-sensitivity of the system is conferred by the chromophore AdoB12. (b) Mode of function. In the dark, CarH-VP16 bound to AdoB12 forms tetramers that bind CarO thereby recruiting RNA polymerase II (Pol II) and activating SEAP expression. Exposure to green light leads to photolysis of AdoB12 what triggers destabilization of CarH tetramers and the release of CarO thereby deactivating SEAP expression.

first one encodes the CarH protein fused to the *Herpes simplex* virus-derived VP16 transactivation domain[27] to be expressed under the control of the constitutive simian virus 40 promoter ($P_{SV40}$). The second one is a reporter plasmid composed of a multimeric CarO sequence upstream of the minimal human cytomegalovirus promoter sequence ($P_{hCMVmin}$) controlling the expression of a gene of interest, here the secreted alkaline phosphatase (SEAP) reporter gene. Transfection of the constructs into mammalian cells, followed by supplementation with AdoB12 in the dark, leads to the formation of CarH-VP16 tetramers binding to the CarO sequence. VP16 will recruit the transcription initiation complex to start RNA polymerase II-dependent SEAP expression (Figure 1b). However, upon green light exposure, CarH-VP16 tetramers dissociate and release CarO, which terminates SEAP expression (Figure 1b). Although only produced by microorganisms, AdoB12 is essential for many metabolic processes in mammals and hence, mammalian cells are capable of both AdoB12 import and conversion of biologically inactive forms of B12 into AdoB12.[28,29]

To analyze the functionality of the system in mammalian cells, a first proof-of-principle experiment was performed using the activator CarH-VP16 and the reporter $CarO_2$, containing two consecutive repeat sequences of the DNA operator, upstream of the minimal promoter mediating SEAP expression. The light insensitive E-OFF system,[30] consisting of the activator E-VP16 binding to the DNA operator ETR, upstream of a minimal promoter mediating SEAP expression, was used as control to analyze possible effects of AdoB12 and green light on gene expression. Human embryonic kidney 293 (HEK-293) cells were transfected with the corresponding activator and reporter plasmids. Twenty-four hours post-transfection the culture medium was supplemented (when indicated) with 10 $\mu$M AdoB12. Cells were kept in the dark or exposed to green (525 nm) light (5 $\mu$mol $m^{-2}$ $s^{-1}$) for another 24 h, before measuring SEAP production (Figure 2). Cells transfected with

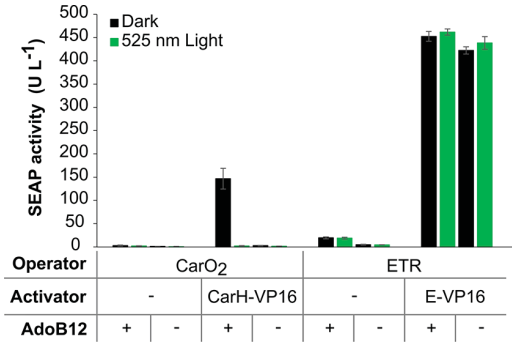


**Figure 2.** Proof of principle experiment showing the functionality of the green light-responsive gene expression system in mammalian cells. HEK-293 cells were transfected with reporter ($CarO_2$, pCVC034; ETR, pWW37) and activator (CarH-VP16, pHB144; E-VP16, pWW35) plasmids as indicated. After 24 h cells were supplemented with 10 $\mu$M AdoB12 where indicated (+) and either kept in dark (black bars) or exposed to 525 nm light (5 $\mu$mol $m^{-2}$ $s^{-1}$, green bars) for another 24 h. SEAP production was determined from cell culture supernatants. Data are means ± Stdev ($n$ = 3).

the ETR reporter plasmid only expressed SEAP in the presence of the corresponding activator E-VP16. Neither the addition of AdoB12 nor illumination resulted in significantly changed SEAP production. Cells transfected with the $CarO_2$ reporter plasmid only expressed SEAP in the presence of CarH-VP16 upon supplementation with AdoB12 and cultivation in the dark. Exposure to green light, however, reduced SEAP production 73-fold to levels observed in negative controls (without CarH-VP16).

However, maximum SEAP production levels of the CarH-based system (147 U $L^{-1}$) were still lower than the ones obtained using the well-established E-system (450 U $L^{-1}$), which prompted us to evaluate different optimization strategies.



DOI: 10.1021/acssynbio.7b00450
ACS Synth. Biol. 2018, 7, 1349−1358

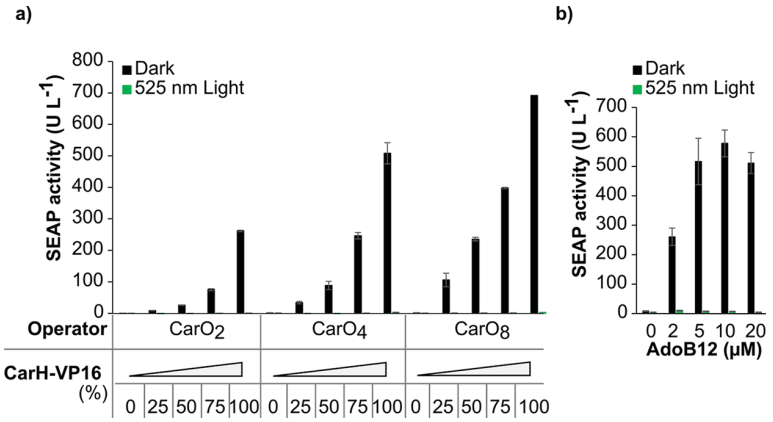


**Figure 3.** Optimization of the green-light-responsive gene expression system. (a) Impact of the number of CarO repeats and the CarH/CarH-VP16 ratio on SEAP activity. HEK-293 cells were transfected with reporter plasmids containing an increasing number of CarO repeats ($CarO_2$, pCVC034; $CarO_4$, pCVC035; $CarO_8$, pCVC036) and with different amounts of expression plasmids for CarH-VP16 (pHB144, indicated in %) completed to 100% with plasmid pCVC025 for expression of CarH. After 24 h cells were supplemented with 10 $\mu$M AdoB12 and either kept in the dark (black bars) or exposed to 525 nm light (5 $\mu$mol $m^{-2}$ $s^{-1}$, green bars) for another 24 h. SEAP activity was determined from cell culture supernatants. (b) Impact of AdoB12 concentration on SEAP activity. HEK-293 cells were transfected with plasmids pCVC036 ($CarO_8$) and pHB144 (CarH-VP16). After 24 h, the concentrations of AdoB12 indicated were added followed by 24 h cultivation in the dark or under 525 nm light prior to measurement of SEAP activity. Data are means ± Stdev ($n$ = 3).

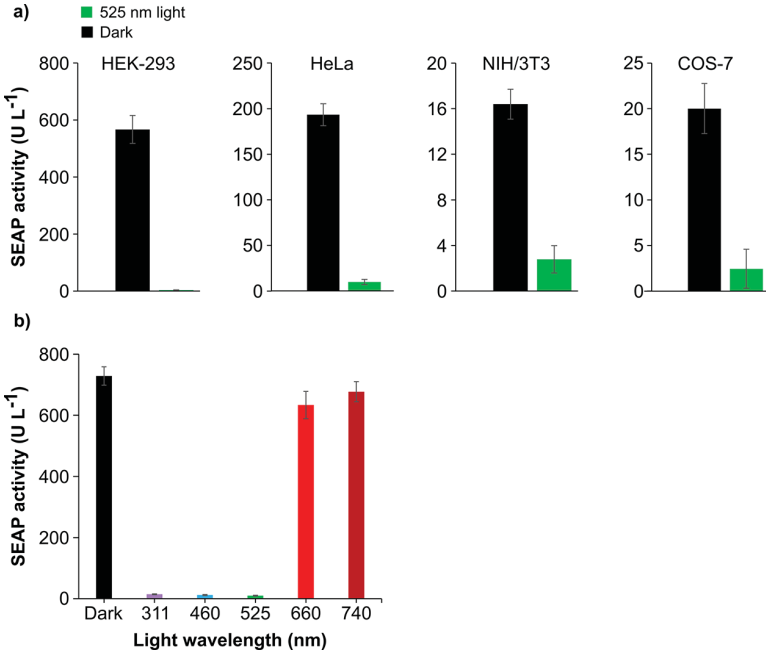


**Figure 4.** Characterization of the green light-responsive expression system in different mammalian cell lines and for different illumination wavelengths. (a) Human embryonic kidney cells (HEK-293), human cervix carcinoma cells (HeLa), mouse fibroblasts (NIH/3T3), and African green monkey kidney fibroblast-like cells (COS-7) were transfected with plasmids pCVC036 ($CarO_8$) and pHB144 (CarH-VP16). After 24 h cells were supplemented with 10 $\mu$M AdoB12 and either kept in dark (black bars) or exposed to 525 nm light (green bars). After 24 h, SEAP activity was determined. (b) Response to light of different wavelengths. The following illumination regimes were used: UVB (cycles of pulsed 311 nm light, 0.8 $\mu$mol $m^{-2}$ $s^{-1}$ for 2 min followed by 48 min dark); blue light (460 nm, 4 $\mu$mol $m^{-2}$ $s^{-1}$); green light (525 nm, 5 $\mu$mol $m^{-2}$ $s^{-1}$); red light (660 nm, 8 $\mu$mol $m^{-2}$ $s^{-1}$); far-red light (740 nm, 80 $\mu$mol $m^{-2}$ $s^{-1}$). Data are means ± Stdev ($n$ = 3).

The system involves three main components: CarH-VP16, CarO and AdoB12. Any of these components could be modified/adjusted to optimize gene induction characteristics. We hypothesized that the fusion to VP16 might impact CarH activity and that the addition of wild type CarH might overcome such issues, for example, by the formation of heterotetramers. To analyze this possibility, we supplemented CarH-VP16 with wild type CarH, in different ratios. The results, however, revealed that SEAP activity was maximal in cells transfected with 100% CarH-VP16, indicating that free CarH did not have beneficial effects on gene expression characteristics (Figure 3a). Next, in order to determine an optimized promoter configuration we varied the number of CarO sequences in the reporter plasmid. The experiments



DOI: 10.1021/acssynbio.7b00450
ACS Synth. Biol. 2018, 7, 1349−1358

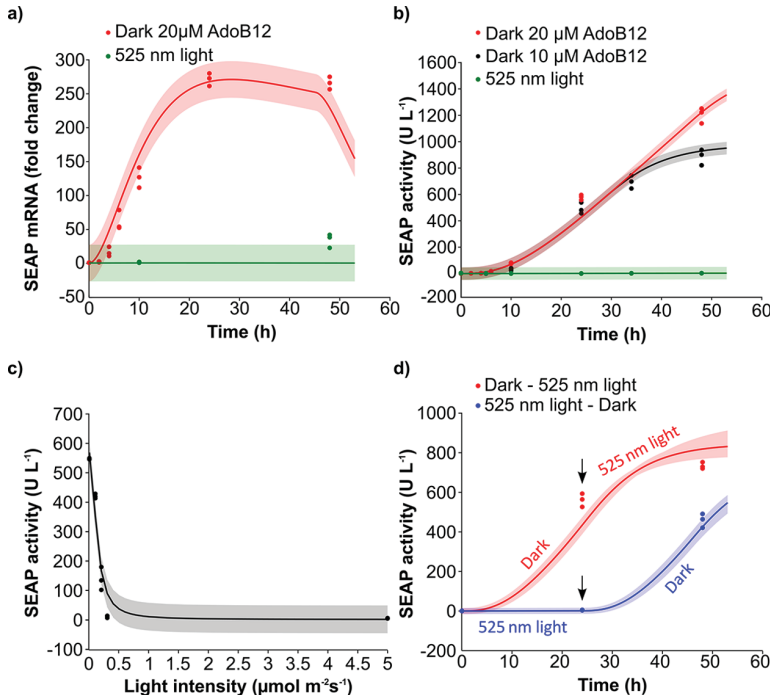


**Figure 5.** Quantitative characterization of the green-light-responsive expression system. In all experiments HEK-293 cells were transfected with plasmids pCVC036 ($CarO_8$) and pHB144 (CarH-VP16). After 24 h cells were supplemented with the indicated concentrations of AdoB12 and cultivated for another 48 h using the indicated illumination schemes prior to determining SEAP mRNA or protein production. (a) Time course of SEAP mRNA production. (b) Time course of SEAP protein production. (c) Impact of different light intensities on gene expression. 525 nm light was used at the indicated intensities and SEAP production was quantified after 24 h. In panels a–c the points represent individual data values from triplicate measurements. The curves represent the model fit to the data, and the shaded error bands are estimated by an error model with a constant Gaussian error. (d) Validation of the model predictions. Model-based prediction of SEAP production kinetics for the indicated illumination schemes (assuming 20 $\mu$M AdoB12 addition at $t = 0$). The shaded bands indicate the 95% prediction confidence interval. The black arrows indicate the change in illumination conditions. The data points represent results from triplicate validation experiments using the indicated experimental conditions.

revealed that increasing the number of operator sequences, and thus of binding sites for CarH-VP16, led to a higher activation of the system, reflected by an increased SEAP production (Figure 3a). Doubling the number of operator sites from two to four resulted in a 2-fold increase in SEAP production; adding another four CarO operators resulted in a further 1.4-fold increased SEAP production. Finally, we analyzed the impact of AdoB12 concentration. We found that 10 $\mu$M AdoB12 were sufficient for complete activation of the system (Figure 3b). To conclude, the optimized system consists of a reporter plasmid containing an octameric $CarO_8$ operator, the light-regulated activator CarH-VP16, and supplementation of the cell culture medium with 10 $\mu$M AdoB12. In HEK-293 cells, this configuration showed to be very tightly repressed under green light and could be induced by up to 350-fold in darkness. These experimental conditions were used throughout the subsequent experiments. We next evaluated the suitability of the system for green light-responsive gene expression in different human-, mouse- and monkey-derived cell lines. We observed high induction levels, suggesting cross-species applicability of this expression control strategy (Figure 4a). However, there were differences in absolute SEAP production values. Such cell line-dependent differences are commonly observed with inducible expression systems and can be attributed to several cell-dependent factors, such as transfection efficiency, cell line-specific promoter strength or interference with endogenous signaling pathways.[30−33] Next, we analyzed the responsiveness of the CarH system to illumination wavelengths and intensities commonly used in other optogenetic systems.[34] To this end, we evaluated SEAP production in response to UVB (311 nm), blue (460 nm), red (660 nm), and far-red (740 nm) light. Whereas illumination in the red spectrum did not affect CarH-dependent gene expression, blue and UVB light reduced SEAP production (Figure 4b). This cross-reactivity can be explained by the photolysis of AdoB12 also at shorter wavelengths.[22] These data further demonstrate that the CarH system could be used in combination with red light-responsive optogenetic systems[33,35,36] for the orthogonal control of cellular processes and that red light can be used as safe light when handling the system.

To enable predictable and reliable application of green light-responsive gene expression, we next performed a detailed quantitative characterization of the system's performance. To characterize the early stages of reporter expression, we quantified mRNA expression levels with RT-qPCR in the presence of 20 $\mu$M AdoB12 for 48 h (Figure 5a). In the dark and after an initial lag-phase of approximately 1 h, SEAP mRNA levels increased rapidly and reached a maximum of approximately 270-fold induction after 24 h and stagnated afterward. In parallel, we determined SEAP protein production kinetics in the dark and under green light (Figure 5b). While gene expression remained at background levels under 525 nm light, cultivation in the dark resulted in continuously increasing SEAP levels. We further hypothesized, that one limiting factor of the



DOI: 10.1021/acssynbio.7b00450
ACS Synth. Biol. 2018, 7, 1349−1358

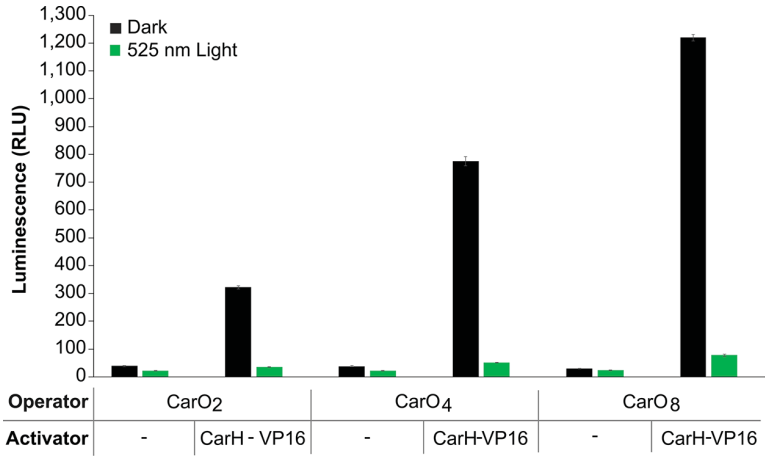


**Figure 6.** Characterization of the green light-responsive expression system in *A. thaliana* protoplasts. Reporter plasmids with increasing number of CarO repeats ($CarO_2$, pROF250; $CarO_4$, pROF251; $CarO_8$, pROF252) were transformed in a 3:1 molar ratio over the CarH-VP16 expression plasmid pROF254. After transformation, protoplasts were supplemented with AdoB12 to a final concentration of 20 $\mu$M. After cultivation in the dark or under 525 nm light (5 $\mu$mol $m^{-2}$ $s^{-1}$) luciferase activity was determined. Data are means ± SEM ($n$ = 6). RLU: relative luminescence units.

system could be the availability of AdoB12. Indeed, while SEAP protein production in the presence of 10 $\mu$M AdoB12 showed comparable early stage dynamics as for 20 $\mu$M, the SEAP production rate declined after approximately 30 h. This decline can be attributed to AdoB12 degradation as time-course experiments revealed a half-life time for AdoB12 of 22.6 ± 4.9 h in a cell culture environment (Supplementary Figure 1). This suggests that higher initial AdoB12 concentrations or a resupplementation of the cofactor would be required for longer experiments. Next, we analyzed the adjustability of the system in response to increasing light intensities (Figure 5c). Maximum expression levels were reached in the dark, whereas very low light intensities (0.1−0.3 $\mu$mol $m^{-2}$ $s^{-1}$ corresponding to 2.3−6.8 $\mu$W $cm^{-2}$) resulted in intermediate expression values. At light intensities of 5 $\mu$mol $m^{-2}$ $s^{-1}$ gene expression was in the low off state.

To obtain quantitative insight into the systems characteristics, we developed a mathematical model and inferred kinetic parameters from the experiments described above (Figure 5a,b,c and Supplementary Figure 1). We based the model on the following ordinary differential equations:

$$\frac{d[AdoB12](t)}{dt} = -Nk_{deg,B12}[AdoB12] - k_{form,CarH\_B12}[CarH][AdoB12] \quad (1)$$

$$\frac{d[CarH](t)}{dt} = GDk_{prod,CarH} - k_{deg,CarH}[CarH] - k_{form,CarH\_B12}[CarH][AdoB12] \quad (2)$$

$$\frac{d[CarH\_B12](t)}{dt} = -k_{deg,CarH}[CarH\_B12] + k_{form,CarH\_B12}[CarH][B12] - k_{off}I(t)[CarH\_B12] \quad (3)$$

$$\frac{d[CarH\_B12_{off}](t)}{dt} = k_{off}I(t)[CarH\_B12] \quad (4)$$

$$\frac{d[mRNA1](t)}{dt} = GD\left(k_{basal,mRNA} + k_{tc,mRNA}\frac{[CarH\_B12]^2}{K_{m,tc}^2 + [CarH\_B12]^2}\right) - k_{process,mRNA}[mRNA1] \quad (5)$$

$$\frac{d[mRNA2](t)}{dt} = k_{process,mRNA}[mRNA1] - k_{deg,mRNA}[mRNA2] \quad (6)$$

$$\frac{d[SEAP](t)}{dt} = k_{tl,SEAP}[mRNA2]N \quad (7)$$

$$\frac{dN(t)}{dt} = k_{growth}N\left(1 - \frac{N}{N_{max}}\right) \quad (8)$$

with

$$GD = \frac{1}{N}$$

The model describes the temporal evolution of the concentrations of the relevant molecules. The first three equations capture the dynamics of AdoB12 and CarH-VP16 (denoted as CarH). AdoB12 degrades linearly and binds with CarH-VP16 to the CarH-VP16_AdoB12 complex (denoted as CarH_B12). CarH-VP16 is produced at a constant rate by the constitutive promoter $P_{SV40}$ and degraded by first order kinetics. It is further inactivated by 525 nm light at a rate proportional to the light intensity, $I(t)$. The production of the target mRNA is induced by the active CarH-VP16_AdoB12 complex with a Hill-function. To represent transcription and mRNA transport out of the nucleus, mRNA synthesis is modeled in two steps. The resulting mRNA is degraded linearly and translated into the SEAP protein at the rate $k_{tl,SEAP}$. The growth of cell number ($N$) is described by a logistic growth curve with the specific growth rate $k_{growth}$ and the maximal cell count $N_{max}$. Plasmid dilution in transient transfections is covered by the factor gene dose (GD), which is inversely proportional to the number of cells. A detailed description and derivation of the mathematical model is presented in the Supporting Information. The unknown model parameters were estimated from experimental data by utilizing a maximum likelihood approach, which follows the strategy described by Müller *et al.*[34] For the calibration, we used the time course data shown in Figure 5a (SEAP mRNA time course) and Figure 5b (SEAP protein time course), the light dose−response data depicted in Figure 5c, AdoB12 dose−response data (Supplementary Figure 1a), as well as stability measurements of AdoB12 (Supplementary Figure 1b). The measuring error (shaded bands) was captured by an error model with a constant Gaussian error that was estimated simultaneously with the dynamical parameters. To assess the uncertainty of the estimated parameter in terms of their 95%



DOI: 10.1021/acssynbio.7b00450
ACS Synth. Biol. 2018, 7, 1349−1358

**Table 1. Vectors Used in This Study**

| Plasmid | Description | Reference |
|---|---|---|
| pHB144 | $P_{SV40}$-CarH-VP16-pA<br>DNA sequence for CarH-VP16 (CarH, italics; VP16, underlined)<br>*ATGACCTCCTCCGGGGGTGTACACCATCGCCGAGGTGGAAGCCATGACCGGC*<br>*CTTTCCGCCGAGGTGCTCCGCCAGTGGGAGCGCCGCTACGGCTTCCCCAAG*<br>*CCCCGGCGTACCCCGGGAGGGCATCGCCTCTACAGCGCGGAAGACGTGGA*<br>*GGCCCTGAAGACGATCAAGCGCTGGCTGGAGGAGGGGGCCACGCCTAAAG*<br>*CGGCCATCCGCCGCTACCTGGCCCAGGAGGTGCGCCCCGAGGACCTGGGG*<br>*ACCGGCCTCCTCGAGGCCCTCCTCCGGGGGGACCTCGCCGGGGCCGAGGC*<br>*CCTCTTCCGCCGGGGGCTCAGGTTTTGGGGCCCGGAGGGCGTCCTGGAGC*<br>*ACCTCCTCCTCCCCGTCCTCCGGGAGGTGGGGGAGGCCTGGCACCGGGGG*<br>*GAGATCGGGGTGGCGGAGGAGCACCTGGCCTCCACCTTCCTCCGGGCAAG*<br>*GCTCCAGGAACTTTTGGACCTCGCGGGCTTCCCGCCCGGGCCCCCCGTCCT*<br>*CGTCACCACCCCTCCCGGGGAGCGGCACGAGATCGGGGCCATGCTCGCCG*<br>*CCTACCACCTCCGCCGCAAAGGGGTCCCCGCCCTCTACCTCGGCCCCGACA*<br>*CACCTCTCCCCGACCTCAGGGCCTTGGCCCGGCGGCTCGGGGCGGGGGCG*<br>*GTGGTCCTCTCCGCCGTCCTTTCCGAGCCTTTAAGGGCCCTCCCCGACGGG*<br>*GCCCTTAAGGACCTCGCCCCCCGGGTCTTCCTCGGGGGGCAGGGGGCGGG*<br>*GCCGGAGGAGGCCAGGAGGCTCGGCGCCGAGTACATGGAGGACCTGAAGG*<br>*GCCTCGCCGAGGCCCTTTGGCTCCCTAGGGGGCCGGAAAAGGAGGCGATA*<br>GGCGCCGGCGCCGGCGCGCGTACGAAAAACAATTACGGGTCTACCATCGAG<br>GGCCTGCTCGATCTCCCGGACGACGACGCCCCCGAAGAGGCGGGGGCTGGC<br>GGCTCCGCGCCTGTCCTTTCTCCCCGCGGGACACACGCGCAGACTGTCGAC<br>GGCCCCCCCGACCGATGTCAGCCTGGGGGACGAGCTCCACTTAGACGGCG<br>AGGACGTGGCGATGGCGCATGCCGACGCGCTAGACGATTTCGATCTGGACA<br>TGTTGGGGGACGGGGATTCCCCGGGTCCGGGATTTACCCCCCACGACTCCG<br>CCCCCTACGGCGCTCTGGATATGGCCGACTTCGAGTTTGAGCAGATGTTTAC<br>CGATGCCCTTGGAATTGACGAGTACGGTGGGTAG | This work |
| pCVC025 | $P_{CMV}$-CarH-pA<br>DNA sequence for CarH<br>ATGACCTCCTCCGGGGGTGTACACCATCGCCGAGGTGGAAGCCATGACCGGC<br>CTTTCCGCCGAGGTGCTCCGCCAGTGGGAGCGCCGCTACGGCTTCCCCAAG<br>CCCCGGCGTACCCCGGGAGGGCATCGCCTCTACAGCGCGGAAGACGTGGA<br>GGCCCTGAAGACGATCAAGCGCTGGCTGGAGGAGGGGGCCACGCCTAAAG<br>CGGCCATCCGCCGCTACCTGGCCCAGGAGGTGCGCCCCGAGGACCTGGGG<br>ACCGGCCTCCTCGAGGCCCTCCTCCGGGGGGACCTCGCCGGGGCCGAGGC<br>CCTCTTCCGCCGGGGGCTCAGGTTTTGGGGCCCGGAGGGCGTCCTGGAGC<br>ACCTCCTCCTCCCCGTCCTCCGGGAGGTGGGGGAGGCCTGGCACCGGGGG<br>GAGATCGGGGTGGCGGAGGAGCACCTGGCCTCCACCTTCCTCCGGGCAAG<br>GCTCCAGGAACTTTTGGACCTCGCGGGCTTCCCGCCCGGGCCCCCCGTCCT<br>CGTCACCACCCCTCCCGGGGAGCGGCACGAGATCGGGGCCATGCTCGCCG<br>CCTACCACCTCCGCCGCAAAGGGGTCCCCGCCCTCTACCTCGGCCCCGACA<br>CACCTCTCCCCGACCTCAGGGCCTTGGCCCGGCGGCTCGGGGCGGGGGCG<br>GTGGTCCTCTCCGCCGTCCTTTCCGAGCCTTTAAGGGCCCTCCCCGACGGG<br>GCCCTTAAGGACCTCGCCCCCCGGGTCTTCCTCGGGGGGCAGGGGGCGGG<br>GCCGGAGGAGGCCAGGAGGCTCGGCGCCGAGTACATGGAGGACCTGAAGG<br>GCCTCGCCGAGGCCCTTTGGCTCCCTAGGGGGCCGGAAAAGGAGGCGATAT<br>AG | This work |
| pCVC034 | $CarO_2$-$P_{hCMVmin}$-SEAP-pA<br>DNA sequence (5'->3') of $CarO_2$-$P_{hCMVmin}$ (CarO, italics; $P_{hCMVmin}$, underlined)<br>*ACACTCCGCAGAGATGTACAAAAGCTTGACAAAAACCTA*GCTAGA*ACACTCC*<br>*GCAGAGATGTACAAAAGCTTGACAAAAACCTA*GCTAGCGATATCATCGCCGG<br>TACCTGATATATAGTTAGGCGTGTACGGTGGGAGGCCTATATAAGCAGAGCT<br>CGTTTAGTGAACCGTCAGATCGCCTGGAGACGCCATCCACGCTGTTTTGACC<br>TCCATAGAAGACACCGGGACCGATCCAGCCT | This work |
| pCVC035 | $CarO_4$-$P_{hCMVmin}$-SEAP-pA<br>DNA sequence (5'->3') of $CarO_4$-$P_{hCMVmin}$ (CarO, italics; $P_{hCMVmin}$, underlined)<br>*ACACTCCGCAGAGATGTACAAAAGCTTGACAAAAACCTA*GCTAGA*ACACTCC*<br>*GCAGAGATGTACAAAAGCTTGACAAAAACCTA*GCTAGA*ACACTCCGCAGAGA*<br>*TGTACAAAAGCTTGACAAAAACCTA*GCTAGA*ACACTCCGCAGAGATGTACAAA*<br>*AGCTTGACAAAAACCTA*GCTAGCGATATCATCGCCGGTACCTGATATATAGTT<br>AGGCGTGTACGGTGGGAGGCCTATATAAGCAGAGCTCGTTTAGTGAACCGTC<br>AGATCGCCTGGAGACGCCATCCACGCTGTTTTGACCTCCATAGAAGACACCG<br>GGACCGATCCAGCCT | This work |



DOI: 10.1021/acssynbio.7b00450
*ACS Synth. Biol.* 2018, 7, 1349−1358

Table 1. continued

| Plasmid | Description | Reference |
|---|---|---|
| pCVC036 | $CarO_8$-$P_{hCMVmin}$-SEAP-pA<br>DNA sequence (5'->3') of $CarO_8$-$P_{hCMVmin}$ (CarO, italics; $P_{hCMVmin}$, underlined)<br>*ACACTCCGCAGAGATGTACAAAAGCTTGACAAAAACCTA*GCTAGAACACTCC<br>*GCAGAGATGTACAAAAGCTTGACAAAAACCTA*GCTAGAACACTCCGCAGAGA<br>*TGTACAAAAGCTTGACAAAAACCTA*GCTAGAACACTCCGCAGAGATGTACAAA<br>*AGCTTGACAAAAACCTA*GCTAGAACACTCCGCAGAGATGTACAAAAGCTTGA<br>*CAAAAACCTA*GCTAGAACACTCCGCAGAGATGTACAAAAGCTTGACAAAAAC<br>*CTA*GCTAGAACACTCCGCAGAGATGTACAAAAGCTTGACAAAAACCTAGCTA<br>GAACACTCCGCAGAGATGTACAAAAGCTTGACAAAAACCTAGCTAGCGATAT<br>CATCGCCGGTACCTGATATATAGTTAGGCGTGTACGGTGGGAGGCCTATATA<br>AGCAGAGCTCGTTTAGTGAACCGTCAGATCGCCTGGAGACGCCATCCACGCT<br>GTTTTGACCTCCATAGAAGACACCGGGACCGATCCAGCCT | This work |
| pROF250 | $CarO_2$-$P_{hCMVmin}$-Luciferase-pA | This work |
| pROF251 | $CarO_4$-$P_{hCMVmin}$-Luciferase-pA | This work |
| pROF252 | $CarO_8$-$P_{hCMVmin}$-Luciferase-pA | This work |
| pROF254 | $P_{CaMV35s}$-CarH-VP16-pA | This work |
| pWW35 | $P_{SV40}$-E-VP16-pA | [30] |
| pWW37 | ETR-$P_{hCMVmin}$-SEAP-pA | [30] |

confidence intervals the parameter profile likelihood was evaluated.[37] The analysis was performed with the Data2-Dynamics framework[38] (see Supporting Information for details on the parameter estimation and uncertainty analysis).

We finally analyzed whether the model can be applied to predict gene expression profiles as a function of the illumination regime. We simulated SEAP production profiles in the dark ($I(t) = 0$) and under green light ($I(t) = 5$ $\mu$mol $m^{-2}$ $s^{-1}$), and when swapping the illumination conditions after 24 h. The model prediction revealed a high reversibility of the system: after 24 h illumination under 525 nm light no significant activation was expected, whereas transferring the system to the dark initiated SEAP production (Figure 5d, blue curve). On the other hand, turning on the green light after 24 h stopped SEAP production (Figure 5d, red curve). The prediction uncertainties in terms of their 95% confidence intervals (Figure 5d) were inferred by propagating the uncertainty of the estimated parameters.[39] We next validated these predictions by performing the corresponding experiments. This experimental validation (Figure 5d, single data points) confirmed the model simulations thus demonstrating the predictive power of the quantitative model.

Following this comprehensive characterization of the green-light-responsive gene expression system in mammalian cells, we finally evaluated its suitability for controlling gene expression in plant cells. This would open the possibility of using optically induced gene expression in plant cells with reduced interference by endogenous plant photoreceptors primarily inducing signaling responses upon light in the UV-B, blue, and red parts of the spectrum.[16,17] For this purpose, we reengineered the constructs for use in plant backgrounds by cloning CarH-VP16 under the control of a constitutive CaMV35S promoter and by replacing SEAP by the firefly luciferase reporter. We transformed protoplasts isolated from *Arabidopsis thaliana* with the plasmid coding for CarH-VP16 and with reporter constructs harboring two, four, or eight CarO operator sites. After transformation, AdoB12 was added to a final concentration of 20 $\mu$M and cells were either illuminated for 24 h with 525 nm light (5 $\mu$mol $m^{-2}$ $s^{-1}$) or kept in the dark. Assaying luciferase activity revealed increasing luminescence values with an increasing number of CarO operators (Figure 6). In alignment with the data obtained in mammalian cells, the reporter with eight CarO operator sites resulted in the highest absolute activity and fold-repression (ca. 16-fold) in response to 525 nm light illumination. These data demonstrate that the green light-responsive gene expression system is also functional in plant cells.

In this work, we describe the development and characterization of the first green-light-responsive gene expression system functional in mammalian and plant cells. The quantitative characterization of the systems performance using the mathematical model enables the *in silico*-based, rational design of expression profiles as demonstrated in the validation of the model predictions. This will strongly facilitate the application of this system for programming desired expression profiles. The green light-responsive-system requires the chromophore AdoB12. While potentially representing a limitation for future use in whole plants as they do not synthesize the cofactor, this dependence however is highly favorable in mammalian and plant cell culture as it enables the engineering of the biological system under ambient light while avoiding the inadvertent activation of CarH. The light-responsive properties can subsequently be conferred by the addition of AdoB12 that is readily taken up by mammalian and plant cells. The functionality of the system in plant protoplasts represents an important step toward the application of optogenetic systems in plant backgrounds. As plant photoreceptors are minimally responsive to green light, it is possible to achieve the orthogonal control of transgene activity with minimized cross-activation of endogenous light-responsive pathways. The synthetic switch based on CarH bridges the gap of wavelengths of use by adding green light to the existing systems in mammalian cells sensitive to UV-B, blue, red, and far-red light (see www.optobase.org)[13] and complements the red light-inducible gene expression switch in plant protoplasts previously reported[15,40] expanding the optogenetic toolbox for studies in plant cells. With these properties taken together, we believe that our expression system will foster advances in fundamental and application-oriented synthetic biology and optogenetics.



DOI: 10.1021/acssynbio.7b00450
ACS Synth. Biol. 2018, 7, 1349−1358

## METHODS

**DNA Cloning.** The expression vectors were assembled by Gibson and AQUA[41] cloning. The resulting DNA sequences are indicated in Table 1.

**Mammalian Cell Culture and Transfection.** Human embryonic kidney cells (HEK-293, ATCC CRL-1573), human cervix carcinoma cells (HeLa, ATCC CCL-2), mouse fibroblasts (NIH-3T3, ATCC CRL-1658), and African green monkey fibroblast-like cells (COS-7, ATCC CRL-1651), were cultivated in DMEM-complete medium (Dulbecco's modified Eagle's medium (PAN, cat. no. P04-03550) supplemented with 10% fetal calf serum (FCS, PAN, cat. no. P30-3602, batch no. P101003TC) and 1% penicillin/streptomycin (PAN, cat. no. P06-07100)). Cells were transfected using a polyethylenimine (PEI)-based method as described before.[34] The expression vector encoding the activator CarH-VP16 (pHB144) was used in 4-fold excess (w:w) over the respective reporter plasmids (pCVC034/035/036). Unless indicated otherwise, after 24 h, the medium was replaced with fresh medium supplemented with 10 $\mu$M AdoB12 (Sigma, cat. no. C0884-10 mg). All experimental procedures after the addition of AdoB12 were carried out under safe red LED light (660 nm). After 1 h cultivation in the dark, the cells were illuminated with green LED light (525 nm; 5 $\mu$mol $m^{-2}$ $s^{-1}$) unless indicated otherwise.

**Protoplast Preparation and Transformation.** Protoplast of *Arabidopis thaliana* were isolated from one to two-week old plantlet leaves (plants grown in a 23 °C, 16 h light−8 h dark regime) using the floatation method and the plasmids were transferred by polyethylene glycol-mediated transformation as described before.[42,40] Mixtures of the different plasmids as described in the figures to a final amount of 30 $\mu$g DNA (reporter plasmids pROF250/251/252 were added in a 3:1 molar ratio over the plasmid encoding CarH-VP16 pROF254) were used to transform 500 000 protoplasts in a final volume of 1.6 mL. After transformation, protoplasts were divided in aliquots of ca. 78 000 cells prior to the addition of AdoB12 to a final concentration of 20 $\mu$M, and subsequent illumination with green LED light (525 nm, 5 $\mu$mol $m^{-2}$ $s^{-1}$) or incubation in dark for 24 h.

**RNA Isolation and Real-Time Quantitative PCR Analysis.** Cells were harvested at the indicated points in time and lysed for 5 min in 600 $\mu$L of peqGOLD TriFast (Peqlab/VWR, cat. no. 30-2010). Total RNA was isolated according to the manufacturer's instructions (Peqlab) and RNA integrity was validated by gel electrophoresis. Phenol/guanidin-isothiocyanat-based RNA isolation does not exclude plasmid DNA from the RNA fraction.[43] Accordingly, RNA samples of 5 $\mu$g were treated with DNase I for 30 min at room temperature, followed by purification with the RNA Clean & Concentrator kit (Zymo Research, R1013). cDNA was synthesized from 500 ng of total RNA using the First Strand cDNA Synthesis Kit (Thermo Fisher, K1612). To this end, total RNA was first mixed with both random hexamer and oligo $(dT)_{18}$-primers, incubated at 65 °C for 5 min and rapidly cooled to 4 °C. Synthesis of cDNA was conducted for 5 min at 25 °C, 60 min at 37 °C and terminated at 70 °C for 5 min. Quantitative PCR was performed directly with 0.5 $\mu$L of cDNA with the Absolute qPCR SYBR Green ROX Mix (Thermo Scientific, #AB-1162/B) in a total volume of 20 $\mu$L and in a qTOWER 2.0/2.2 device (Analytik Jena). For relative quantification of gene expression of SEAP, primers oNS092 (5′-CATGGACATTGACGTGATCCT-3′) and oNS093 (5′-CACCTTGGCTGTAGTCATCTG-3′) were used at final concentrations of 70 nM. For normalization, the reference gene beta-actin (ACTB) was amplified with the primers oNS100 (5′-CCCTGGAGAAGAGCTACGAG-3′) and oNS101 (5′-TCCATGCCCAGGAAGGAAG-3′). Each time-point was measured with three biological replicates in three repeats. Accumulation of the PCR-product was measured after every cycle for 40 cycles. The specificity of the amplification products was subsequently validated with both melting profiles and by gel electrophoresis. Furthermore, negative controls were included, in which the reverse transcriptase was omitted during cDNA synthesis to validate that residual plasmid DNA did not interfere with the sensitivity of the assay. $C_q$ values were obtained with the qPCRsoft V3 software (Analytik Jena). PCR amplification efficiencies were determined as 100% with standard curves and relative expression levels were accordingly determined with the $\Delta\Delta C_q$ method.

**Analytics.** SEAP activity was determined in the cell culture medium using a colorimetric assay as described previously.[44] Firefly luciferase activity was determined in whole protoplasts as detailed elsewhere.[42,40] AdoB12 degradation was determined by seeding $0.3 \times 10^6$ HEK-293 cells $mL^{-1}$ and adding 10 $\mu$M AdoB12. The decrease in AdoB12 concentration was followed by measuring the absorption spectrum of the cell medium every hour for 40 h. The AdoB12 concentration was calculated according to the height of its absorption peak at 525 nm, normalized with the absorption of medium lacking the cofactor.

## ASSOCIATED CONTENT

### Supporting Information

The Supporting Information is available free of charge on the ACS Publications website at DOI: 10.1021/acssynbio.7b00450.

Derivation of the mathematical model; measured and modeled dose−response characteristics and stability of AdoB12; identifiability analysis utilizing the parameter profile likelihood; fitted parameter values obtained by maximum likelihood estimation (PDF)

## AUTHOR INFORMATION


### Corresponding Authors

*E-mail: matias.zurbriggen@uni-duesseldorf.de.
*E-mail: wilfried.weber@bioss.uni-freiburg.de.

### ORCID

Alex R. Jones: 0000-0001-6021-7824
Wilfried Weber: 0000-0003-4340-4446

### Present Address

[▽]H.M.B.: Institute of Biotechnology, University of Helsinki, Finland.


### Author Contributions

Conceptualization, M.Z., A.R.J., W.W.; methodology, C.V.C., R.O.F., R.E., N.S., H.B., J.T., M.Z., W.W.; investigation, C.V.C., R.O.F., R.E., N.S.; writing-original draft, C.V.C., R.O.F., R.E.; writing-review and editing, J.T., A.R.J., M.Z., W.W.; visualization, C.V.C., R.O.F., R.E.; supervision, J.T., M.Z., W.W.; funding acquisition, J.T., M.Z., W.W.

### Notes

The authors declare no competing financial interest.



DOI: 10.1021/acssynbio.7b00450
ACS Synth. Biol. 2018, 7, 1349−1358

## ■ ACKNOWLEDGMENTS

We would like to thank Susanne Knall, Elke Wehinger, and Reinhild Wurm for their excellent technical assistance and Montserrat Elias-Arnanz for fruitful discussions. This work was supported by the Excellence Initiative of the German Federal and State Governments (BIOSS EXC-294, CEPLAS EXC-1028, SGBM GSC-4, and iGRAD-Plant GRK-1525) as well as by DFG grants to WW (WE 4733/4-1) and MZ (SPP1926 Z259/2-1).

## ■ REFERENCES

(1) Ausländer, S., and Fussenegger, M. (2013) From gene switches to mammalian designer cells : present and future prospects. *Trends Biotechnol. 31*, 155−168.

(2) Ausländer, S., Ausländer, D., and Fussenegger, M. (2017) Synthetic Biology — The Synthesis of Biology. *Angew. Chem., Int. Ed. 56*, 6396−6419.

(3) Baumgärtel, K., Genoux, D., Welzl, H., Tweedie-cullen, R. Y., Koshibu, K., Livingstone-zatchej, M., Mamie, C., and Mansuy, I. M. (2008) Control of the establishment of aversive memory by calcineurin and Zif268. *Nat. Neurosci. 11*, 572−578.

(4) Weber, W., Schoenmakers, R., Keller, B., Gitzinger, M., Grau, T., Sander, P., Fussenegger, M., and Daoud-El Baba, M. (2008) A synthetic mammalian gene circuit reveals antituberculosis compounds. *Proc. Natl. Acad. Sci. U. S. A. 105*, 9994−8.

(5) Ehrbar, M., Schoenmakers, R., Christen, E. H. E. H., Fussenegger, M., and Weber, W. (2008) Drug-sensing hydrogels for the inducible release of biopharmaceuticals. *Nat. Mater. 7*, 800−4.

(6) Xie, M., Ye, H., Wang, H., Charpin-El Hamri, G., Lormeau, C., Saxena, P., Stelling, J., and Fussenegger, M. (2016) Beta-cell-mimetic designer cells provide closed-loop glycemic control. *Science (Washington, DC, U. S.) 354*, 1296−1301.

(7) Kojima, R., Aubel, D., and Fussenegger, M. (2016) Toward a world of theranostic medication : Programming biological sentinel systems for therapeutic intervention. *Adv. Drug Delivery Rev. 105*, 66−76.

(8) Gossen, M., and Bujard, H. (1992) Tight control of gene expression in mammalian cells by tetracycline-responsive promoters. *Proc. Natl. Acad. Sci. U. S. A. 89*, 5547−51.

(9) Kramer, B. P., and Fussenegger, M. (2005) Hysteresis in a Synthetic Mammalian Gene Network. *Proc. Natl. Acad. Sci. U. S. A. 102*, 9517−9522.

(10) Fussenegger, M., Morris, R. P., Fux, C., Rimann, M., von Stockar, B., Thompson, C. J., and Bailey, J. E. (2000) Streptogramin-based gene regulation systems for mammalian cells. *Nat. Biotechnol. 18*, 1203−1208.

(11) Müller, K., Naumann, S., Weber, W., and Zurbriggen, M. D. M. D. (2015) Optogenetics for gene expression in mammalian cells. *Biol. Chem. 396*, 145−152.

(12) Weber, W., and Fussenegger, M. (2010) Synthetic gene networks in mammalian cells. *Curr. Opin. Biotechnol. 21*, 690−6.

(13) Kolar, K., and Weber, W. (2017) Synthetic biological approaches to optogenetically control cell signaling. *Curr. Opin. Biotechnol. 47*, 112−9.

(14) Olson, E. J., and Tabor, J. J. (2014) Optogenetic characterization methods overcome key challenges in synthetic and systems biology. *Nat. Chem. Biol. 10*, 502−511.

(15) Müller, K., Siegel, D., Rodriguez Jahnke, F., Gerrer, K., Wend, S., Decker, E. L., Reski, R., Weber, W., and Zurbriggen, M. D. (2014) A red light-controlled synthetic gene expression switch for plant systems. *Mol. BioSyst. 10*, 1679−88.

(16) Costa Galvão, V., and Fankhauser, C. (2015) Sensing the light environment in plants : photoreceptors and early signaling steps. *Curr. Opin. Neurobiol. 34*, 46−53.

(17) Kong, S. G., and Okajima, K. (2016) Diverse photoreceptors and light responses in plants. *J. Plant Res. 129*, 111−114.

(18) Wang, Y., and Folta, K. M. (2013) Contributions of green light to plant growth and development. *Am. J. Bot. 100*, 70−78.

(19) Ortiz-Guerrero, J. M., Polanco, M. C., Murillo, F. J., Padmanabhan, S., and Elías-Arnanz, M. (2011) Light-dependent gene regulation by a coenzyme B12-based photoreceptor. *Proc. Natl. Acad. Sci. U. S. A. 108*, 7565−7570.

(20) Jones, A. R. (2017) The photochemistry and photobiology of vitamin B $_{12}$. *Photochem. Photobiol. Sci. 16*, 820−834.

(21) Padmanabhan, S., Jost, M., Drennan, C. L., and Elías-Arnanz, M. (2017) A New Facet of Vitamin B $_{12}$ : Gene Regulation by Cobalamin-Based Photoreceptors. *Annu. Rev. Biochem. 86*, 485−514.

(22) Jost, M., Fernández-Zapata, J., Polanco, M. C., Ortiz-Guerrero, J. M., Chen, P. Y., Kang, G., Padmanabhan, S., Elías-Arnanz, M., and Drennan, C. L. (2015) Structural basis for gene regulation by a B 12 -dependent photoreceptor. *Nature 526*, 536−541.

(23) Díez, A. I., Ortiz-Guerrero, J. M., Ortega, A., Elías-Arnanz, M., Padmanabhan, S., and Garcia de la Torre, J. (2013) Analytical ultracentrifugation studies of oligomerization and DNA-binding of TtCarH, a Thermus thermophilus coenzyme B12-based photosensory regulator. *Eur. Biophys. J. 42*, 463−476.

(24) Kainrath, S., Stadler, M., Reichhart, E., Distel, M., and Janovjak, H. (2017) Green-Light-Induced Inactivation of Receptor Signaling Using Cobalamin-Binding Domains. *Angew. Chem., Int. Ed. 56*, 4608−4611.

(25) Wang, R., Yang, Z., Luo, J., Hsing, I.-M., and Sun, F. (2017) B12-dependent photoresponsive protein hydrogels for controlled stem cell/protein release. *Proc. Natl. Acad. Sci. U. S. A. 114*, 5912−5917.

(26) Kutta, R. J., Hardman, S. J. O., Johannissen, L. O., Bellina, B., Messiha, H. L., Ortiz-Guerrero, J. M., Elías-Arnanz, M., Padmanabhan, S., Barran, P., Scrutton, N. S., and Jones, A. R. (2015) The photochemical mechanism of a B12-dependent photoreceptor protein. *Nat. Commun. 6*, 7907.

(27) Triezenberg, S. J., Kingsbury, R. C., and McKnight, S. L. (1988) Functional dissection of VP16, the trans-activator of herpes simplex virus immediate early gene expression. *Genes Dev. 2*, 718−729.

(28) Jacobsen, D. W., and Glushchenko, A. V. (2009) The transcobalamin receptor, redux. *Blood 113*, 3−4.

(29) Quadros, E. V., and Sequeira, J. M. (2013) Cellular uptake of cobalamin: Transcobalamin and the TCblR/CD320 receptor. *Biochimie 95*, 1008−1018.

(30) Weber, W., Fux, C., Daoud-el Baba, M., Keller, B., Weber, C. C., Kramer, B. P., Heinzen, C., Aubel, D., Bailey, J. E., and Fussenegger, M. (2002) Macrolide-based transgene control in mammalian cells and mice. *Nat. Biotechnol. 20*, 901−7.

(31) Rang, A., and Will, H. (2000) The tetracycline-responsive promoter contains functional interferon-inducible response elements. *Nucleic Acids Res. 28*, 1120−5.

(32) Verkhusha, V., Redchuk, T., Karasev, M., and Omelina, E. (2018) Near-infrared light-controlled gene expression and protein targeting in neurons and non-neuronal cells. *ChemBioChem*, DOI: 10.1002/cbic.201700642.

(33) Müller, K., Engesser, R., Metzger, S., Schulz, S., Kämpf, M. M. M., Busacker, M., Steinberg, T., Tomakidi, P., Ehrbar, M., Nagy, F., Timmer, J., Zubriggen, M. D. M. D., and Weber, W. (2013) A red/far-red light-responsive bi-stable toggle switch to control gene expression in mammalian cells. *Nucleic Acids Res. 41*, No. 377.

(34) Müller, K., Engesser, R., Schulz, S., Steinberg, T., Tomakidi, P., Weber, C. C. C., Ulm, R., Timmer, J., Zurbriggen, M. D. M. D., and Weber, W. (2013) Multi-chromatic control of mammalian gene expression and signaling. *Nucleic Acids Res. 41*, e124.

(35) Beyer, H. M. H. M., Juillot, S., Herbst, K., Samodelov, S. L. S. L., Müller, K., Schamel, W. W. W., Römer, W., Schäfer, E., Nagy, F., Strähle, U., Weber, W., and Zurbriggen, M. D. M. D. (2015) Red Light-Regulated Reversible Nuclear Localization of Proteins in Mammalian Cells and Zebrafish. *ACS Synth. Biol. 4*, 951−8.

(36) Levskaya, A., Weiner, O. D., Lim, W. A., and Voigt, C. A. (2009) sup: Spatiotemporal control of cell signalling using a light-switchable protein interaction. *Nature 461*, 997−1001.



DOI: 10.1021/acssynbio.7b00450
*ACS Synth. Biol.* 2018, 7, 1349−1358

(37) Raue, A., Kreutz, C., Maiwald, T., Bachmann, J., Schilling, M., Klingmüller, U., and Timmer, J. (2009) Structural and practical identifiability analysis of partially observed dynamical models by exploiting the profile likelihood. *Bioinformatics 25*, 1923−1929.
(38) Raue, A., Steiert, B., Schelker, M., Kreutz, C., Maiwald, T., Hass, H., Vanlier, J., Tönsing, C., Adlung, L., Engesser, R., Mader, W., Heinemann, T., Hasenauer, J., Schilling, M., Hofer, T., Klipp, E., Theis, F., Klingmüller, U., Schöberl, B., and Timmer, J. (2015) Data2-Dynamics: A modeling environment tailored to parameter estimation in dynamical systems. *Bioinformatics 31*, 3558−3560.
(39) Raue, A., Becker, V., Klingmüller, U., and Timmer, J. (2010) Identifiability and observability analysis for experimental design in nonlinear dynamical models. *Chaos 20*, 45105.
(40) Ochoa-Fernandez, R., Samodelov, S. L., Brandl, S. M., Wehinger, E., Müller, K., Weber, W., and Zurbriggen, M. D. (2016) Optogenetics in plants: Red/Far-red light control of gene expression, in *Optogenetics Methods and Protocols—Methods in Molecular Biology* (Kianianmomeni, A., Ed.) pp 125−139, Springer, New York.
(41) Beyer, H. M., Gonschorek, P., Samodelov, S. L., Meier, M., Weber, W., and Zurbriggen, M. D. (2015) AQUA cloning: A versatile and simple enzyme-free cloning approach. *PLoS One 10*, 1−20.
(42) Wend, S., Dal Bosco, C., Kämpf, M. M., Ren, F., Palme, K., Weber, W., Dovzhenko, A., and Zurbriggen, M. D. (2013) A quantitative ratiometric sensor for time-resolved analysis of auxin dynamics. *Sci. Rep. 3*, 2052.
(43) Rio, D. C., Ares, M. J., Hannon, G. J., and Nilsen, T. W. (2010) Removal of DNA from RNA. *Cold Spring Harb. Protoc. 2010*, 1−3.
(44) Schlatter, S., Rimann, M., Kelm, J., and Fussenegger, M. (2002) SAMY, a novel mammalian reporter gene derived from Bacillus stearothermophilus alpha-amylase. *Gene 282*, 19−31.



DOI: 10.1021/acssynbio.7b00450
*ACS Synth. Biol.* 2018, 7, 1349−1358

# A green light-responsive system for the control of transgene expression in mammalian and plant cells

Claire Chatelle[1,2], Rocio Ochoa-Fernandez[3,4,5], Raphael Engesser[2,6], Hannes M. Beyer[1,2,3,7], Alex R. Jones[8], Jens Timmer[2,6], Matias D. Zurbriggen[4,5] and Wilfried Weber[1,2,3]

[1]Faculty of Biology, University of Freiburg, Schänzlestrasse 18, 79104 Freiburg, Germany

[2]BIOSS Centre for Biological Signalling Studies, University of Freiburg, Schänzlestrasse 18, 79104 Freiburg, Germany.

[3]SGBM Spemann Graduate School of Biology and Medicine, University of Freiburg, Albertstrasse 19A, 79104 Freiburg, Germany

[4]Institute of Synthetic Biology, Heinrich Heine University, Universitätsstrasse 1, 40225 Düsseldorf, Germany.

[5]iGRAD Plant Graduate School, Heinrich-Heine University, Universitätsstrasse 1, 40225 Düsseldorf, Germany.

[6]Institute of Physics, University of Freiburg, Hermann-Herder-Str. 3, 79104 Freiburg, Germany.

[7]Present address: Institute of Biotechnology, University of Helsinki, Finland

[8] National Physical Laboratory, Hampton Road, Teddington, Middlesex, TW11 0LW, UK.

## Supplementary Information

| | |
|---|---|
| **Supplementary Information** | Design and parameterization of the mathematical model |
| **Supplementary Figure 1** | Dose-response characteristics and stability of AdoB12 |
| **Supplementary Figure 2** | Identifiability analysis with the parameter profile likelihood |
| **Supplementary Table S1** | Estimated model parameters |

# 1. Derivation of the mathematical model

In the following, the mathematical model of the green light-responsive gene expression system is derived. The model is based on a set of ordinary differential equations (ODE) describing the temporal evolution of the concentrations of the relevant species. The unknown model parameters are estimated from experimental data using a maximum likelihood-based approach. The model strategy chosen is similar to the modeling of the light-inducible gene switches published in[1–3].

The model equations are:

$$\frac{d[AdoB12](t)}{dt} = -N\, k_{deg,B12}[AdoB12] - k_{form,CarH\_B12}[CarH][AdoB12] \quad (1)$$

$$\frac{d[CarH](t)}{dt} = GD\, k_{prod,CarH} - k_{deg,CarH}[CarH] - k_{form,CarH\_B12}[CarH][AdoB12] \quad (2)$$

$$\frac{d[CarH\_B12](t)}{dt} = -k_{deg,CarH}[CarH\_B12] + k_{form,CarH\_B12}[CarH][B12] - k_{off} I(t)[CarH\_B12] \quad (3)$$

$$\frac{d[CarH\_B12_{off}](t)}{dt} = k_{off} I(t)[CarH\_B12] \quad (4)$$

$$\frac{d[mRNA1](t)}{dt} = GD\left(k_{basal,mRNA} + k_{tc,mRNA}\frac{[CarH\_B12]^2}{K_{m,tc}^2+[CarH\_B12]^2}\right) - k_{process,mRNA}\,[mRNA1] \quad (5)$$

$$\frac{d[mRNA2](t)}{dt} = k_{process,mRNA}[mRNA1] - k_{deg,mRNA}\,[mRNA2] \quad (6)$$

$$\frac{d[SEAP](t)}{dt} = k_{tl,SEAP}\,[mRNA2]\,N \quad (7)$$

$$\frac{dN(t)}{dt} = k_{growth}\,N\left(1-\frac{N}{N_{max}}\right) \quad (8)$$

with $GD = \frac{1}{N}$

The first three equations describe the dynamics of the concentrations of AdoB12 and CarH-VP16 (denoted as CarH). AdoB12 is supplied to the cells in the cell culture medium at the start of each experiment. It is degraded by the cells with a linear rate, which is proportional to the number of cells *N*. AdoB12, together with CarH, forms the complex CarH-AdoB12 (denoted as CarH_B12). In the mathematical model this complex formation process is described by mass action kinetics with the binding rate constant, $k_{form,CarH\_B12}$. The CarH_B12 complex is assumed as stable; therefore, no dissociation rate is included in the model. CarH is produced at a constant rate $k_{prod,CarH}$ by the constitutive promoter $P_{SV40}$. To capture the dilution of the $P_{SV40}$ promoter due to cell growth, we included a factor for the gene dose *GD*, which is just the inverse of the number of cells, *N*. CarH is degraded linearly with the rate constant, $k_{deg,CarH}$. For the sake of simplicity, the degradation of the CarH_B12 complex is modeled with the same rate constant, $k_{deg,CarH}$.

Illumination of the system with green light of intensity, *I*(*t*), leads to the deactivation of CarH_B12 with a rate proportional to *I*(*t*). The transcription of the target gene mRNA is induced by CarH_B12. This is modeled by using the Hill function:

$$k_{tc,mRNA}\frac{[CarH_{B12}]^2}{K_{m,tc}^2+[CarH_{B12}]^2}$$

The exponent of two captures cooperative binding effects, since CarH binds as tetramers to the CarO operator sites. The parameter $k_{basal,mRNA}$ in eq. (5) captures the basal promoter activity. As for CarH, the production rate of the target mRNA is proportional to the gene dose *GD*. In order to capture the duration of the synthesis of the mRNA, the transcription of the mRNA is modeled with two steps. The resulting mRNA, denoted with mRNA2, is degraded linearly with the rate constant, $k_{deg,mRNA}$. The target protein SEAP is translated with a rate proportional to the mRNA concentration. Since SEAP is secreted to the cell culture medium by the cells its production is also proportional to the number of cells, *N*. Due to the high stability of SEAP its degradation rate is neglected. The growth of cell number (*N*) was modeled with a logistic growth curve with the growth rate $k_{\mathrm{growth}} = 2.04 \times 10^{-2}$ h$^{-1}$ which corresponds to a doubling time of 34 hours. The maximum number of cells ($N_{max}$) was set to twice the initial cell number.

# 2. Parameterization of the model by fitting to experimental data

## 2.1 Maximum likelihood estimation

To introduce the maximum likelihood estimation, we briefly repeat the approach as described in Müller *et al.*[2]. The mathematical model and the observation function can be written in the following scheme:

$$\frac{d\boldsymbol{x}(t)}{dt} = \boldsymbol{f}(\boldsymbol{x}(t), \boldsymbol{u}(t), \boldsymbol{p})$$
$$\boldsymbol{y}(t) = \boldsymbol{g}(\boldsymbol{x}(t), \boldsymbol{s}) + \epsilon(t).$$

The first equation is the system of ordinary differential equations written in vectorized form. The vector $\boldsymbol{x}(t)$ contains the dynamical states, which describe the temporal evolution of the concentrations of the involved substances. $\boldsymbol{p}$ is the vector of the dynamical parameters and the function $\boldsymbol{u}(t)$ describes time dependent external inputs; i.e., the intensity *I*(*t*) of the applied green light. The second equation contains the observation function $\boldsymbol{g}(\boldsymbol{x}(t), \boldsymbol{s})$, which links the internal states $\boldsymbol{x}(t)$ to the experimental observations $\boldsymbol{y}(t)$. $\boldsymbol{s}$ are scaling parameters and $\epsilon(t)$ is the measurement noise. For solving the system the initial concentrations $\boldsymbol{x}(0)$ of the internal states are required. The vector of initial concentrations can also depend on the dynamical parameters $\boldsymbol{p}$; e.g., when the system is assumed to be in a steady state at the start of the experiment.

The measurement errors are captured with an error model with a constant Gaussian error $\epsilon_0 \sim N(0, \sigma_0^2)$ with the variance $\sigma_0^2$.

With this error model, we can calculate the likelihood function for a single experiment j:

$$L_j(\boldsymbol{y_j}|\boldsymbol{\theta_j}) = \frac{1}{\sqrt{2\pi}\,\sigma_0} \prod_{i=1}^{N_{data}} e^{-\frac{\left(y_{t_i} - g(\boldsymbol{x}(t_i,\boldsymbol{\theta_j}),\boldsymbol{s})\right)^2}{2\,\sigma_0^2}}$$

The vector $\boldsymbol{\theta_j} = (\boldsymbol{p}, \boldsymbol{x_j}(0), \boldsymbol{s_j}, \sigma_j)$ of all parameters depends on the conditions of the experiment j. $\boldsymbol{y_j} = \left(y_{t_1}, y_{t_2}, \dots, y_{t_{N_{data}}}\right)_j$ is the vector of the measured data in the experiment j at the time points $t_i$.

The overall likelihood for multiple experiments is the product of the single likelihoods $L_j$ over all experiments

$$L(\boldsymbol{y}|\boldsymbol{\theta}) = \prod_{j=1}^{N_{ex}} L_j(\boldsymbol{y}_j|\boldsymbol{\theta_j}).$$

$L(\boldsymbol{y}|\boldsymbol{\theta})$ is the probability of the measured data $\boldsymbol{y}$ given the parameters $\boldsymbol{\theta}$. The aim of a maximum likelihood estimation is to find the parameter set $\boldsymbol{\theta}$ that maximizes the likelihood function $L(\boldsymbol{y}|\boldsymbol{\theta})$

$$\boldsymbol{\theta_{opt}} = \underset{\boldsymbol{\theta}}{\operatorname{argmax}}(L(\boldsymbol{y}, \boldsymbol{\theta})).$$

Instead of maximizing the likelihood function $L(y|\theta)$ it is equivalent to minimize $\chi^2 = -2\log(L)$. For Gaussian distributed errors $\chi^2 = -2\ \log(L)$ is the sum of squared residuals with a second sum due to the error model:

$$\chi^2(\boldsymbol{\theta}, \mathbf{y}) = \sum_{\mathrm{i}} \mathrm{res}^2_{\mathrm{data,i}} + \sum_{\mathrm{i}} \mathrm{res}^2_{\mathrm{error,i}}$$

Minimizing $\chi^2(\boldsymbol{\theta}, \mathbf{y})$

$$\boldsymbol{\theta_{opt}} = \arg\min_{\theta}\ \chi^2(\boldsymbol{\theta}, \mathbf{y})$$

is equivalent to a least squares problem.

To determine the parameter uncertainties in terms of confidence intervals we used the approach introduced by Raue *et al.*[4] and calculated the profile likelihood for each parameter $\theta_j$

$$\chi^2_{PL}(\theta_j) = \min_{\theta_{i\neq j}} \chi^2(\boldsymbol{\theta}, \mathbf{y}).$$

The numerical integration of the ODE was performed with CVODES[5]. For optimization we used a trust region algorithm implemented in MATLAB (lsqnonlin)[6] with user-supplied sensitivities, which were calculated together with the ODE system. To improve convergence and scan the parameters over orders of magnitude the optimization was performed in logarithmic parameter space. To find the global optimum we performed multiple optimization runs with initial parameter guesses chosen from a latin hypercube sampling of the parameter space. The mathematical modeling was performed with the Data2Dynamics modeling environment.[7]

## 2.2 Implementation of the single experiments

In this section, we describe the single experiments utilized to calibrate the mathematical model. To this end, we define the experimental conditions, observation functions and initial concentrations for the

single experiments. The model was fitted to five independent experiments. If not stated otherwise, we used the following initial concentrations for the state variables:

$$[AdoB12](0) = input\_AdoB12$$
$$[CarH](0) = \frac{k_{prod,CarH}}{k_{deg,CarH}}$$
$$[CarH\_B12](0) = 0$$
$$\left[CarH\_B12_{off}\right](0) = 0$$
$$[mRNA1](0) = \frac{k_{basal,mRNA}}{k_{process,mRNA}}$$
$$[mRNA2](0) = [mRNA1](0)\frac{k_{process,mRNA}}{k_{deg,mRNA}} = \frac{k_{basal,mRNA}}{k_{deg,mRNA}}$$
$$[SEAP](0) = 0$$
$$N(0) = 1$$

The initial concentration of AdoB12 was set to the concentration that was supplied to the medium at the beginning of the corresponding experiment. At the time point zero CarH is assumed to be in its steady state without any AdoB12. For the same reason CarH_B12 is set to 0 at the time point zero. For the calculation of these steady states we assume that the cell growth is on a much slower time scale than the dynamics of the production and degradation of CarH. The concentrations of the two mRNA states are also set to their steady state values without CarH_B12. The initial amount of the target protein SEAP in the medium is assumed to be zero at time point zero. The cell growth is only considered on a relative scale. Therefore, we set the number of cells at time point zero to 1.

**Experiment 1: Kinetics on mRNA level**

In this experiment, the activation kinetics was determined by measuring the mRNA of the target protein SEAP in the dark with an AdoB12 input concentration of 20 µM. Additionally, the system was examined under illumination with green light ($I(t)$ = 5 µmol $m^{-1}$ $s^{-1}$) with an AdoB12 concentration of 20 µM.

As observation function we used:

$$[mRNA_{t,measured}] = [mRNA2](t).$$

This means, this experiment determines the unit of the simulated mRNA concentrations. Since the mRNA was measured in multiples of its initial value, the unit of the mRNA in the model corresponds to a fold change.

The measurement error was modeled with a constant Gaussian error with the standard deviation $sd_{mRNA,SEAP}$, which was estimated simultaneously with the dynamical parameters. The experimental data and the model fit are shown in Figure 5a.

**Experiment 2: Kinetics on protein level**

In this experiment, the activation kinetics was determined by measuring the target protein SEAP in the dark with AdoB12 input concentrations of 10 and 20 µM. Additionally, the system was examined under illumination with green light ($I(t)$ = 5 µmol $m^{-1}$ $s^{-1}$) with an AdoB12 concentration of 10 µM. As observation function we used:

$$[SEAP_{t,measured}] = [SEAP](t).$$

This means, this experiment determines the unit of the simulated SEAP concentrations.

The measurement error was modeled with a constant Gaussian error with the standard deviation $sd_{SEAP}$, which was estimated simultaneously with the dynamical parameters. The experimental data and the model fit are shown in Figure 5b.

**Experiment 3: Light intensity dose response**

In this experiment, we measured the response of the system to different intensities of green light. For this purpose, the system was set up with an AdoB12 input concentration of 10 µM and cultivated under illumination with green light with different intensities. After 24 h, the amount of SEAP in the medium was determined. As observation function we used:

$$[SEAP_{measured}] = scale_{light,DR} \cdot [SEAP](t = 24\ h).$$

The measurement error was modeled with the same constant Gaussian error with the standard deviation $sd_{SEAP}$, as used in experiment 1. The experimental data and the model fit are shown in Figure 5c.

**Experiment 4: AdoB12 dose response**

In this experiment, the response of the system to different AdoB12 input concentrations was measured. For this purpose, the system was supplied with AdoB12 and cultivated in the dark. After 24 h the resulting amount of SEAP in the medium was determined. As observation function we used

$$[SEAP_{measured}] = scale_{B12,DR} \cdot [SEAP](t = 24\ h).$$

The measurement error was modeled with the same constant Gaussian error with the standard deviation $sd_{SEAP}$, as used in experiment 2.

Additionally, the system was set up without the pHB144 plasmid, which is required for the production of the protein CarH-VP16. Therefore, the parameter $k_{prod,CarH}$ is set to zero for this experimental

condition. Additionally, the measurement error was modeled with a constant Gaussian error with the standard deviation $sd_{SEAP,no,CarH}$. The experimental data and the model fit are shown in Supplementary Figure 1a.

**Experiment 5: AdoB12 stability**

The purpose of this experiment is to determine the stability of AdoB12. To this end, the system was set up without the plasmid pHB144, which is required for the production of the protein CarH-VP16. In the beginning of the experiment, 10 µM AdoB12 was added to the cell culture medium and the system was cultivated in the dark, to measure the concentration of AdoB12 in the medium at different time points. As observation function we used:

$$[AdoB12_{t,measured}] = [AdoB12](t).$$

The measurement error was modeled with a constant Gaussian error with the standard deviation $sd_{B12}$, which was estimated simultaneously with the dynamical parameters. The experimental data and the model fit are shown in Supplementary Figure 1b.

## 2.3 Results of the parameter estimation

The green light model has in total 17 free parameters, which were inferred from 159 data points. We performed 1,000 optimization runs with randomly sampled initial parameter guesses. Each parameter was sampled from $10^{-5}$ to $10^{+3}$, which are eight orders of magnitude. The best parameter set $\boldsymbol{\theta_{opt}}$ was found 315 times, which is a strong indication that we identified the global optimum.

The analysis of the profile likelihood suggests that 14 parameters are identifiable by the experimental data, whereas three parameters are experimentally non-identifiable (Supplementary Figure 2a).

The profile for the parameter $k_{form,CarH\_B12}$ shows that the formation of CarH_B12 happens on a very fast time scale, which cannot be resolved by the measured data. This practical non-identifiability can be resolved by a model reduction which models CarH_B12 in quasi steady state[8]. However, this reduction is not performed here, since the calculation of the corresponding quasi steady state requires the solution of quadratic equations, which would complicate the comprehensible model formulation.

The likelihood profiles of the practical non-identifiable parameters $K_{m,tc}$ and $k_{off}$ are coupled. Simulating the model trajectories for the parameter sets along the likelihood profile of $K_{m,tc}$, shows that the concentration scale of the CarH_B12 complex is not identifiable (Supplementary Figure 2b). This non-identifiability can be resolved by fixing $K_{m,tc}$, since this parameter has the same unit as the CarH_B12 complex.

## 3. Model validation

For the calibration of the model, we used only experiments with light conditions did not change over time. To test the predictive power of the model, we performed experiments with swapping light conditions. To this end, the green light-responsive system was supplied with 20 µM AdoB12. Subsequently, the system was cultivated in the dark and under green light ($I(t)$ = 5 µmol $m^{-1}$ $s^{-1}$). After 24 h the light conditions were switched. The calibrated mathematical model was used to simulate the SEAP time course over 50 h for these light conditions. To translate the uncertainties of the estimated parameters to prediction uncertainties, we used the approach proposed by Raue *et al.*[9], which simulates the predicted SEAP time courses for all parameter sets along the profile likelihood of each parameter. The predicted time course of SEAP is shown in Figure 5d, the shaded bands indicate the prediction uncertainty, by propagating the 95 % parameter confidence interval.

The model prediction was validated experimentally. To link the validation data with the predicted time courses, we used the observation function

$$[SEAP_{t,measured}] = scale_{SEAP,validation} \cdot [SEAP](t).$$

The scaling parameter was estimated from the validation data to $scale_{SEAP,validation} = 1.016$. The validation data are in agreement with the model simulations, which demonstrates the predictive power of the mathematical model.

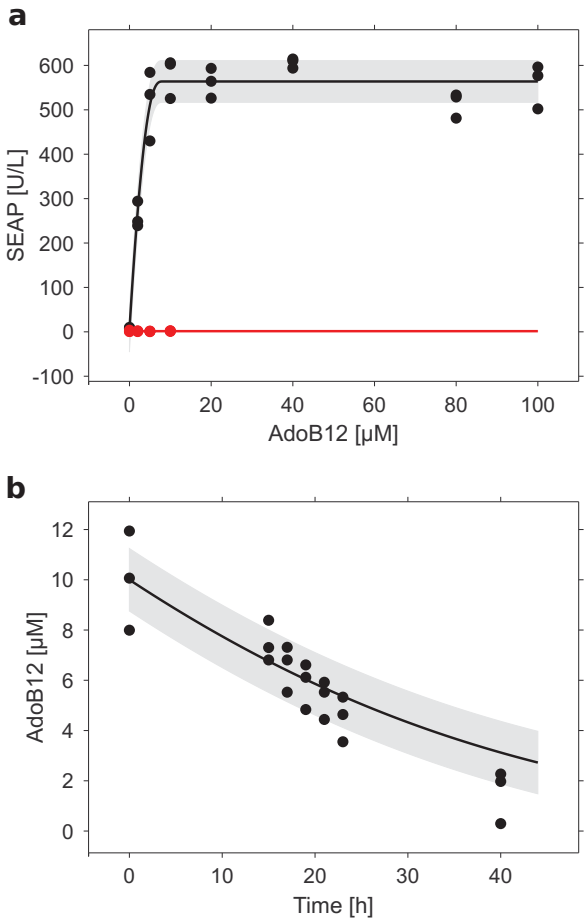


**Supplementary Figure 1.** Dose-response characteristics and stability of AdoB12. **(a)** Dose-response characteristic of the green light-responsive system to different concentrations of AdoB12. The dose response of the full system is shown black and the dose response of the system without the plasmid pHB144 is shown in red. **(b)** Stability of AdoB12 in the absence of pHB144. **(a,b)** The points denote the measured data points. The curves represent the model fit to the data. The shaded error bands are estimated by an error model with constant Gaussian error and denote one standard deviation.

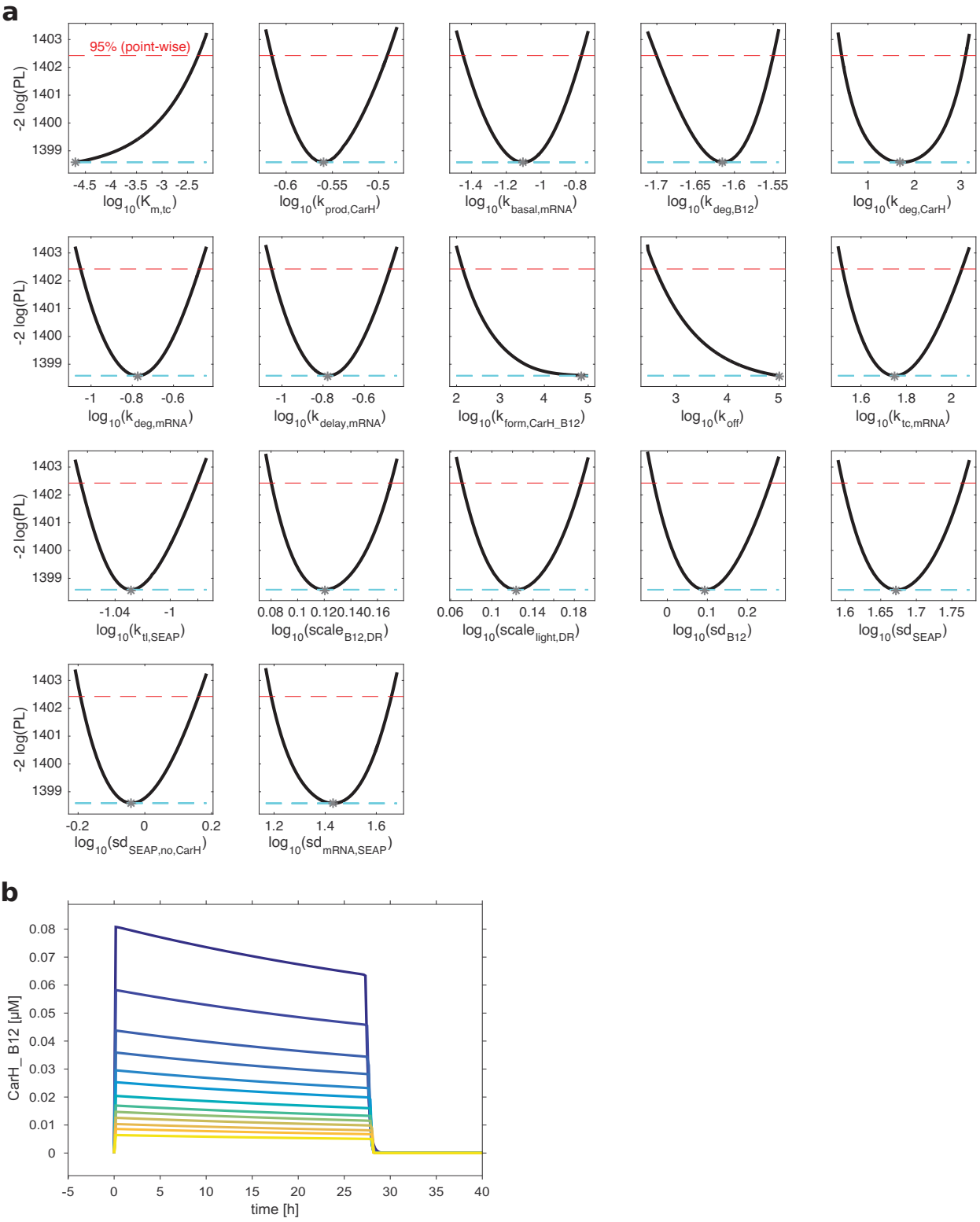


**Supplementary Figure 2.** Identifiability analysis utilizing the parameter profile likelihood. **(a)** Profile likelihood of the estimated parameters. The solid lines indicate the profile likelihood; the optimal parameter set is marked with a grey star. The red dashed line marks the 95 % confidence level. The light blue dashed line indicates the –2log(PL) value of the optimal parameter set. The parameter axis is on a logarithmic scale. **(b)** Model trajectories of CarH_B12, simulated for ten parameter sets along the parameter profile of $K_{m,tc}$.

**Table S1.** Fitted parameter values obtained by maximum likelihood estimation. $\sigma^-$ and $\sigma^+$ indicate the 95 % point-wise confidence intervals calculated by exploiting the profile likelihood.

| **Parameter** | $\hat{\theta}$ | $\sigma^-$ | $\sigma^+$ | **Unit** |
|---|---|---|---|---|
| $k_{deg,B12}$ | $2.43 \cdot 10^{-02}$ | $1.99 \cdot 10^{-02}$ | $2.82 \cdot 10^{-02}$ | $h^{-1}$ |
| $k_{form,CarH\_B12}$ | $6.89 \cdot 10^{+04}$ | $1.38 \cdot 10^{+02}$ | + inf | $\mu M^{-1} \cdot h^{-1}$ |
| $k_{prod,CarH}$ | $2.75 \cdot 10^{-01}$ | $2.42 \cdot 10^{-01}$ | $3.23 \cdot 10^{-01}$ | $\mu M \cdot h^{-1}$ |
| $k_{deg,CarH}$ | $5.02 \cdot 10^{+01}$ | $2.72 \cdot 10^{+00}$ | $1.24 \cdot 10^{+03}$ | $h^{-1}$ |
| $k_{off}$ | $1.00 \cdot 10^{+05}$ | $3.86 \cdot 10^{+02}$ | + inf | $h^{-1}$ |
| $k_{tc,mRNA}$ | $5.61 \cdot 10^{+01}$ | $3.30 \cdot 10^{+01}$ | $1.11 \cdot 10^{+02}$ | $h^{-1} \cdot mRNA(0)$ |
| $k_{process,mRNA}$ | $1.68 \cdot 10^{-01}$ | $8.90 \cdot 10^{-02}$ | $3.35 \cdot 10^{-01}$ | $h^{-1}$ |
| $k_{basal.mRNA}$ | $7.89 \cdot 10^{-02}$ | $3.57 \cdot 10^{-02}$ | $1.71 \cdot 10^{-01}$ | $h^{-1} \cdot mRNA(0)$ |
| $K_{m,tc}$ | $1.99 \cdot 10^{-05}$ | 0 | $5.13 \cdot 10^{-03}$ | $\mu M$ |
| $k_{deg,mRNA}$ | $1.68 \cdot 10^{-01}$ | $8.90 \cdot 10^{-02}$ | $3.35 \cdot 10^{-01}$ | $h^{-1}$ |
| $k_{tl,SEAP}$ | $9.36 \cdot 10^{-02}$ | $8.61 \cdot 10^{-02}$ | $1.05 \cdot 10^{-01}$ | $h^{-1} \cdot mRNA(0)^{-1} \cdot U \cdot L^{-1}$ |
| $k_{growth}$ | $2.04 \cdot 10^{-02*}$ | – | – | $h^{-1}$ |
| $N_{max}$ | $2.00 \cdot 10^{+00*}$ | – | – | $h^{-1}$ |
| $scale_{B12,DR}$ | $1.32 \cdot 10^{+00}$ | $1.20 \cdot 10^{+00}$ | $1.48 \cdot 10^{+00}$ | 1 |
| $scale_{light,DR}$ | $1.33 \cdot 10^{+00}$ | $1.18 \cdot 10^{+00}$ | $1.54 \cdot 10^{+00}$ | 1 |
| $sd_{mRNA,SEAP}$ | $2.70 \cdot 10^{+01}$ | $1.54 \cdot 10^{+01}$ | $4.56 \cdot 10^{+01}$ | mRNA(0) |
| $sd_{SEAP}$ | $4.70 \cdot 10^{+01}$ | $3.95 \cdot 10^{+01}$ | $5.83 \cdot 10^{+01}$ | $U \cdot L^{-1}$ |
| $sd_{SEAP,no,CarH}$ | $9.13 \cdot 10^{-01}$ | $6.41 \cdot 10^{-01}$ | $1.45 \cdot 10^{+00}$ | $U \cdot L^{-1}$ |
| $sd_{B12}$ | $1.24 \cdot 10^{+00}$ | $9.24 \cdot 10^{-01}$ | $1.81 \cdot 10^{+00}$ | $\mu M$ |

* Value fixed.

## Supplementary References

1. Müller, K., Engesser, R., Timmer, J., Zurbriggen, M. D. & Weber, W. Orthogonal optogenetic triple-gene control in Mammalian cells. *ACS Synth. Biol.* **3,** 796–801 (2014).
2. Müller, K. *et al.* Multi-chromatic control of mammalian gene expression and signaling. *Nucleic Acids Res.* **41,** e124 (2013).
3. Müller, K. *et al.* A red/far-red light-responsive bi-stable toggle switch to control gene expression in mammalian cells. *Nucleic Acids Res.* **41,** e77 (2013).
4. Raue, A. *et al.* Structural and practical identifiability analysis of partially observed dynamical models by exploiting the profile likelihood. *Bioinformatics* **25,** 1923–1929 (2009).
5. Hindmarsh, A. C. *et al.* SUNDIALS: Suite of Nonlinear and Differential/Algebraic Equation Solvers. *ACM Trans. Math. Softw.* **31,** 363–396 (2005).
6. Coleman, T. & Li, Y. An Interior Trust Region Approach for Nonlinear Minimization Subject to Bounds. *SIAM J. Optim.* **6,** 418–445 (1996).
7. Raue, A. *et al.* Data2Dynamics: a modeling environment tailored to parameter estimation in dynamical systems. *Bioinformatics* **31,** 3558–3560 (2015).
8. Maiwald, T. *et al.* Driving the model to its limit: Profile likelihood based model reduction. *PLOS One* **11,** e0162366 (2016).
9. Raue, A., Becker, V., Klingmüller, U. & Timmer, J. Identifiability and observability analysis for experimental design in nonlinear dynamical models. *Chaos* **20,** 45105 (2010).

# Expanding the toolbox of optogenetic switches for red and blue light control of gene expression in plant cells

Rocio Ochoa-Fernandez[1,2], Mara Schuler-Bermann[1], Matias D. Zurbriggen[1,2,3,#]

[1]Institute of Synthetic Biology, University of Düsseldorf, Germany
[2]iGRAD Plant Graduate School, University of Düsseldorf, Germany.
[3]CEPLAS - Cluster of Excellence on Plant Sciences, Düsseldorf, Germany

[#]Corresponding author: MDZ matias.zurbriggen@uni-duesseldorf.de

## INTRODUCTION

Optogenetic tools provide high spatio-temporal resolution, minimized toxicity, and they act in a quantitative manner for the control of cellular processes. These aspects make them desirable tools for basic and applied plant research. There are to date few optoswitches developed to regulate gene expression with light in plants.

The tools that have been developed to control gene expression in plant platforms include: a red light activation/far-red deactivation switch based on Phytochrome B (PhyB) and one of its interacting factors PHYTOCHROME INTERACTING FACTOR 6 (PIF6)[1,2]; a green light-controlled switch based on CarH[3]; a blue light repressible switch based on EL222[4]; and a dual chromatic-controlled switch, termed PULSE[4].

In this work we aim for the expansion of the currently available tools, focusing in red and blue light-regulated tools. We developed a blue light-inducible ($B_{On}$) switch and assessed the performance of different versions of the red light PhyB-PIF switch. Furthermore, we developed a tool to control gene expression with the nuclease deactivated Cas9 that is only active in red light and that can be used to upregulate orthologous or endogenous plant promoters.

We believe these tools can be combined with other optogenetic or chemical switches in order to develop and control complex gene circuits. Once these tools are optimized they could be applied *in planta*, opening up many opportunities in the field of plant sciences.

## RESULTS

### Blue light switch to induce gene transcription

Based on the performance of blue light-repressible ($B_{Off}$) switch developed for *Arabidopsis thaliana* protoplasts[4], we engineer a blue light switch to induce ($B_{On}$) expression of a gene of interest. This switch is based on the EL222 transcription factor from *Erythrobacter litoralis,* that is composed of a LOV domain and a helix-turn-helix (HTH) domain connected by a J-alpha helix. The LOV domain uses Flavin mononucleotide (FMN) as a cofactor, which is ubiquitous in eukaryotes. Upon blue light application (with maximum absorption around 450 nm), the LOV domain undergoes a conformational change, thereby releasing the HTH and allowing the homodimerization of EL222. This allows for the HTH domain to bind a target DNA sequence (termed C120)[5].

Following the strategy of Motta-Mena and colleages[6], a fusion of the DNA transactivation domain VP16 to the N-term of EL222 was used for the characterization of the $B_{On}$ switch in Arabidopsis protoplasts. As a reporter module, Firefly Luciferase (FLuc) was placed under the control of the minimal human cytomegalovirus promoter ($P_{hCMVmin}$) and five repeats of the DNA target of EL222 $(C120)_5$. In the dark, basal levels of Fluc expression are expected, while only upon illumination with blue light, EL222 dimerises and binds to the cognate $(C120)_5$ sequence, thus bringing the VP16 activation domain into close proximity of the minimal promoter, thereby activating FLuc transcription (**Fig. 1a**).

Arabidopsis protoplasts were co-transformed with the reporter module with or without the blue-responsive module. Then, they were incubated in different blue light intensities (0.25, 0.5, 1, 5, 10 µmol $m^{-2}$ $s^{-1}$) and the luminescence was determined after 18 h. A constitutive Renilla luciferase (RLuc) was included as normalization element. Profiting from the fact that the reporter module has a recognition site for E protein – $(etr)_8$ – (not relevant for the $B_{On}$ switch) a constitutively expressed E-VP16 was included as positive control for light-independent activation of the reporter module. The ratios FLuc/RLuc for four technical replicates are shown in **Fig. 1b**. The optogenetic switch showed a good dynamic range, with the maximum fold induction (8.1-fold) being achieved after incubation in 5 µmol $m^{-2}$ $s^{-1}$ blue light. It was also observed that these blue light intensities had no negative effects on the expression of FLuc or RLuc, as for the constitutive/positive control E-VP16 (**Fig. 1b**), inferring that they had no toxic effects on the cells.

**New variants of the red light-inducible gene expression system**

The red light-inducible system was implemented successfully in the past in *Nicotiana tabacum*[1] and in *Arabidopsis thaliana* plant protoplasts[2]. It was also used as a proof-of-principle application to regulate hormone signalling and to express a human vascular endothelial growth factor (VEGF) in *Physcomitrella patens*[1]. It functions as a chimeric transcription factor, based on the truncated version of PhyB fused to a VP16 transactivation domain, and the truncated version PIF6 fused to the macrolide repressor DNA-binding protein (E). There is a synthetic promoter in which eight repeats of the cognate sequence of the E protein – $(etr)_8$ – are placed upstream of the minimal promoter ($P_{hCMVmin}$), driving the expression of the gene of interest, *e.g.* FLuc. Therefore, only under red light, when PhyB and PIF6 interact, transcription of the gene of interest is initiated. The truncated $PhyB_{(1-650)}$ contains the PAS-GAF-PHY domains

from the photosensory module (PSM), lacking the C-terminal module (CTM). The truncated $PIF6_{(1-100)}$ contains the active PhyB-binding (APB) region, excluding the C-terminal portion which comprises the basic helix-look-helix (bHLH) responsible of the DNA binding.

To determine if the system could be improved in terms of performance and/or dynamic range, two strategies were followed. Firstly, the exchange of the activation domain (AD) by a stronger activation domain designed and tested by Li *et al.* in Arabidopsis and rice protoplasts[7] and composed by 6 TAL effectors and VP128 (termed TV). Secondly, the exchange of the $PIF6_{(1-100)}$ by other versions such as $PIF6_{(10-52)}$ and $PIF3_{AAfus}$ (**Fig. 2a**). The APB motif is composed of two segments, termed APB.A and APB.B, the prior being the most conserved. Therefore, $PIF6_{(10-52)}$ is a version that only includes the APB.A motif of PIF6, and $PIF3_{AAfus}$ is a version that includes two APB.A motifs of PIF3 fused together. These two variants of PIFs were chosen based on their high dynamic range in mammalian cells[8].

We observed in protoplasts co-transformed with the different combinations of PhyB and PIF that the sorter version $PIF6_{(10-52)}$ does not significantly improve the dynamic range when compared to $PIF6_{(1-100)}$. On the other hand, the $PIF3_{AAfus}$ has a lower leakiness in the dark, resulting in a higher fold induction (**Fig. 2b**). However, in the configurations that included PhyB-TV, the highest induction fold is achieved with the shorter version of $PIF6_{(10-52)}$, followed by the $PIF3_{AAfus}$ (**Fig. 2b**). The positive controls, show that E-VP16 has higher overall expression than E-TV probably due to the difference in size between both activation domains. This difference in size of the E-PIF-PhyB-AD complex could also explain diversity of induction/dynamic ranges obtained. It could be of particular interest to test in the future various linker sizes separating E-PIF and PhyB-AD, as well as different synthetic promoters with spacer sequences between the etr and the minimal promoter.

**Design and implementation of a novel red-light controlled dCas9 to up-regulate gene expression**

We additionally engineered a new concept of red-light inducible system that could be customized to upregulate expression of endogenous genes of interest. For that purpose, the DNA-binding protein of the $R_{On}$ switch was exchanged by the nuclease-deficient Streptococcus pyogenes Cas9 (D10A, H840A) protein, dCas9[9]. In this manner, we could target any gene of interest by an *ad-hoc* designed guide RNA (**Fig. 3a**). Several constructs of dCas9 fused to different versions of PIF were generated,

and PhyB was fused to the TV strong activation domain. The TV was selected due to the fact that fusions of PhyB-VP16 were found to be insufficient in activating gene expression in preliminary experiments (data not shown). This also aligns with the reported low to moderate activation by using a constitutive dCas9-VP64 in Arabidopsis protoplast and Nicotiana leaves[7,10].

We chose two promoters to upregulate: the orthologous promoter from *Solanum lycopersicum* dihydroflavonol 4-reductase promoter ($P_{SlDFR}$), and the endogenous promoter of the Arabidopsis gene APETALA1 ($P_{AtAP1}$), using FLuc as a quantitative readout. We used a gRNA against the -150 bp region of $P_{SlDFR}$[11] and a gRNA that was designed to target the -100 bp region of $P_{AtAP1}$[4].

In both cases the highest induction fold was achieved with the dCas9-PIF6$_{(1-100)}$ version. Red light induction of the system yielded 12.8-fold induction rates from the $P_{SlDFR}$-FLuc construct compared to dark incubation (**Fig. 3b**), and 4.7-fold induction rates when targeting the $P_{AtAP1}$-FLuc (**Fig. 3c**). To date, this is the first tool to control dCas9 activation by red-light to be developed and to successfully be applied in plant cells.

## DISCUSSION

We implemented a blue light switch to induce gene expression. This tool is as of yet the first blue light switch to activate gene expression in plant cells. The fact that the cofactor supplementation is not required and that this optoswitch is orthologous to plants are advantages for its implementation in Arabidopsis. It comprises only one component, simplifying the construction and transformation of the required plasmids. It provided a good dynamic range having, however, some remaining activity in the dark state, as it can be observed in the results. Overall, this tool presents many advantages that makes it suitable for combination with other switches for multi-chromatic control of gene expression.

Additionally, we developed and characterized red light-inducible switches based on PhyB-PIF, and functioning as a chimeric transcription factor or mediating activation by dCas9 promoter targeting. These red light switches based on PhyB and PIF have the advantage of not needing the addition of a cofactor, as it is already present in plants. Also, they are reversible in far-red light additionally to dark reversion. However, they are based on Arabidopsis genes so their stable implementation in this platform in the future could lead to cross-talk effects. The usage of small truncated versions of PhyB

and PIF could partially alleviate this issue, as the truncated PIFs lack the bHLH and, therefore, the DNA binding ability, and PhyB lacks some of the regulatory domains located in the CTM. Additionally to the PSM, the CTM has been reported to be involved in PIF binding and degradation as well as thermal reversion[12], therefore, the $PhyB_{(1-650)}$-VP16 can have different affinity for the PIF and different reversion kinetics compared to the endogenous PhyB. Another way of overcoming this issue could be to combine it with chemical inducible systems following the example of earlier works in mammalian systems[13].

The red light-inducible switch based on chimeric transcription factors yielded an array of dynamic ranges. It seems that the $PIF3_{AAfus}$ provided a good dynamic range when combined with PhyB-VP16 while showing a lower basal activity in the dark. The configurations comprising PhyB-TV and $PIF6_{(10-52)}$ yielded a higher overall expression while keeping a high fold induction. Both $PIF3_{AAfus}$ and $PIF6_{(10-52)}$ are smaller, containing 57 amino acids and 43 aminoacids, respectively, than $PIF6_{(1-100)}$, so it could be beneficial in the future for their combination with other switches and for minimizing crosstalk with other plant components.

The dCas9 strategy stands out as very promising, thanks to the possibility of controlling endogenous gene expression on command. Additionally, it can be used to control synthetic and orthologous promoters as exemplified here. Despite similar control has been achieved by using it in a combined strategy with PULSE[4], this is a simpler approach with lesser components that does not rely in downstream delayed activation. Theoretically, the dCas9 controlled with red light could be used to downregulate expression of a gene of interest by fusing PhyB to a repressor domain and designing the guide RNA to target the promoter of said gene.

We think that these tools could be the basic components to generate complex genetic circuits in the future. Despite the fact that they can only be used at the moment in transient expression in cells or leaves, once optimized for its implementation *in* planta, they will be the next breakthrough for plant applied and basic research.

## METHODS

### Plasmid construction

A description about the plasmid construction can be found in **Supplementary Table S1.** DNA fragments were released by restriction from existing plasmids or amplified by PCR using primers synthesized by Sigma Aldrich (listed in **Supplementary Table S2**).

The PCR reactions were performed using Q5 High-Fidelity DNA Polymerase (New England Biolabs). Gel extractions were performed using NucleoSpin® Gel and PCR Clean-up kit (Macherey-Nagel). Assemblies were performed using either Gibson[14], AQUA[15], GoldenBraid[16] or restriction-ligation cloning methods prior to transformation into chemically competent *Escherichia coli* strain 10-beta (NEB). The plasmid purifications were performed using Wizard® Plus SV Minipreps DNA Purification Systems (Promega), NucleoBond® Xtra Midi kit (Macherey-Nagel). All preparations were tested by restriction enzyme digests and sequencing (GATC-biotech/SeqLab). All restriction enzymes were purchased from New England Biolabs.

**Arabidopsis protoplast isolation and transformation**

Protoplasts were isolated from two- to three-week old *Arabidopsis thaliana* plantlet leaves by the floatation method and PEG-mediated transformed, as described before[2]. Mixtures of the different plasmids, as described in the figures, with a total amount of 30 µg DNA were used to transform 500,000 protoplasts into a final volume of 1.6 mL of protoplast suspension. After transformation, protoplasts were then divided in different 24-well plates in 640 µL aliquots (200,000 protoplasts-necessary to measure four technical replicates for both FLuc and RLuc). Transformed protoplasts were then either kept in dark or either illuminated with LED arrays of appropriate wavelength and intensity (as indicated in the figures), for 18 - 20 h at 19 - 23 °C unless indicated otherwise.

**Illumination conditions**

Custom made LED light boxes were used as described before[2,17]. The panels contain LEDs from Roithner: blue (461 nm) and red (655 nm). The intensity was adjusted to 10 µmol $m^{-2}$ $s^{-1}$ for blue and red light treatment, unless indicated otherwise. Cell- and plant- handling as well as sampling was performed under safe light conditions (*e.g.* green LED 510 nm light) which does not affect the systems. Spectra and intensities were obtained with a spectroradiometer (AvaSpec-ULS2048 with fiber-optic FC-UVIR200-2, AVANTES).

**Luciferase protoplast assay**

Firefly (FLuc) and Renilla luciferase (RLuc) activities were quantified in intact protoplasts as detailed elsewhere[2]. Four technical replicates of 80 µL protoplast suspensions (approximately 25,000 protoplasts) were pipetted into two separate 96-well white flat bottom plates (Costar) for simultaneous parallel quantification of both luciferases. Addition of 20 µL of either FLuc substrate (0.47 mM D-luciferin (Biosynth

l

AG), 20 mM tricine, 2.67 mM $MgSO_4 \cdot 7H_2O$, 0.1 mM $EDTA \cdot 2H_2O$, 33.3 mM dithiothreitol, 0.52 mM adenosine 5′-triphosphate, 0.27 mM acetyl–coenzyme A, 5 mM NaOH, 264 µM $MgCO_3 \cdot 5H_2O$, in $H_2O$, pH 8), or RLuc substrate (0.472 mM coelenterazine stock solution in methanol, diluted directly before use, 1:15 in phosphate buffered saline, PBS) was performed prior luminescence determination in a plate reader (determination of 20 min kinetics, integration time 0.1 s). RLuc luminescence was measured with a BertholdTriStar2 S LB 942 multimode plate reader and FLuc luminescence was determined with a Berthold Centro XS3 LB 960 microplate luminometer. When applicable, FLuc/RLuc was determined and the average of the replicates and SEM was plotted.

## REFERENCES

1. Müller, K. *et al.* A red light-controlled synthetic gene expression switch for plant systems. *Mol BioSyst* **10**, 1679–1688 (2014).
2. Ochoa-Fernandez, R. *et al.* Optogenetics: Methods and Protocols. in (ed. Kianianmomeni, A.) 125–139 (Springer New York, 2016). doi:10.1007/978-1-4939-3512-3_9.
3. Chatelle, C. *et al.* A Green-Light-Responsive System for the Control of Transgene Expression in Mammalian and Plant Cells. *ACS Synth. Biol.* **7**, 1349–1358 (2018).
4. Ochoa-Fernandez, R. *et al.* PULSE – Optogenetic control of gene expression in plants in the presence of ambient white light. (Manuscript submitted).
5. Zoltowski, B. D., Motta-Mena, L. B. & Gardner, K. H. Blue light-induced dimerization of a bacterial LOV-HTH DNA-binding protein. *Biochemistry* **52**, 6653–6661 (2013).
6. Motta-Mena, L. B. *et al.* An optogenetic gene expression system with rapid activation and deactivation kinetics. *Nat. Chem. Biol.* **10**, 196–202 (2014).
7. Li, Z. *et al.* A potent Cas9-derived gene activator for plant and mammalian cells. *Nat. Plants* **3**, 930–936 (2017).
8. Golonka, D. *et al.* Deconstructing and repurposing the light-regulated interplay between Arabidopsis phytochromes and interacting factors. *Commun. Biol.* **2**, 448 (2019).
9. Perez-Pinera, P. *et al.* RNA-guided gene activation by CRISPR-Cas9–based transcription factors. *Nat. Methods* **10**, 973 (2013).
10. Vilar, M. V. *et al.* A modular toolbox for gRNA – Cas9 genome engineering in plants based on the GoldenBraid standard. *Plant Methods* 1–12 (2016) doi:10.1186/s13007-016-0101-2.
11. Selma, S. *et al.* Strong gene activation in plants with genome-wide specificity using a new orthogonal CRISPR/Cas9-based programmable transcriptional activator. *Plant Biotechnol. J.* **17**, 1703–1705 (2019).
12. Legris, M., Ince, Y. Ç. & Fankhauser, C. Molecular mechanisms underlying phytochrome-controlled morphogenesis in plants. *Nat. Commun.* **10**, 5219 (2019).
13. Chen, X. *et al.* Synthetic dual-input mammalian genetic circuits enable tunable and stringent transcription control by chemical and light. *Nucleic Acids Res.* **44**, 2677–2690 (2015).
14. Gibson, D. G. *et al.* Enzymatic assembly of DNA molecules up to several hundred kilobases. *Nat. Methods* **6**, 343 (2009).

15. Beyer, H. M. *et al.* AQUA Cloning: A Versatile and Simple Enzyme-Free Cloning Approach. *PLoS ONE* **10**, e0137652 (2015).
16. Sarrion-Perdigones, A. *et al.* GoldenBraid 2.0: A Comprehensive DNA Assembly Framework for Plant Synthetic Biology. *Plant Physiol.* **162**, 1618 (2013).
17. Müller, K., Zurbriggen, M. D. & Weber, W. Control of gene expression using a red- and far-red light–responsive bi-stable toggle switch. *Nat. Protoc.* **9**, 622 (2014).

## FIGURE LEGENDS

**Fig. 1.** Design and characterization of the blue light-regulated gene activation switch ($B_{On}$) in Arabidopsis protoplasts. **(a)** Constructs and mode of function. The components engineered and characterized in plant cells are: i) the blue light-responsive photoreceptor EL222 fused to an activation domain VP16 and placed under the control of the constitutive promoter $P_{CaMV35S}$, ii) a synthetic promoter composed of five repeats of C120 - $(C120)_5$ - and a minimal promoter $P_{hCMV}$, driving the expression of the reporter gene FLuc, and iii) $P_{CaMV35S}$ driving the constitutive expression of the normalization element RLuc. A constitutively expressed E protein fused to VP16 is included as positive control, where E binding to its cognate sequence $(etr)_8$ in the reporter module activates FLuc expresssion in a light-independent manner. The transcription factor EL222 has a Light-Oxygen-Voltage (LOV) dependent and a Helix-Turn-Helix (HTH) domain. The photoreceptor is folded in the dark due to a flavin-protein adduct and incapable of binding to DNA. As a result, there is no expression of FLuc in the dark. Upon blue light irradiation, EL222 unfolds and dimerizes, binding to the $(C120)_5$ element, bringing the transcativator domain VP16 close to the minimal promoter and initiating the transcription of FLuc. **(b)** Characterization of the system. Arabidopsis protoplasts were transformed with the reporter module (pROF021) and the blue light-inducible element VP16-EL222 (pKM531) or without the optoswitch (Ø, stuffer plasmid). Constitutively expressed RLuc (GB0109) was included for normalization. After transformation, protoplasts were kept in darkness or illuminated with different intensities of blue light (0.25, 0.5, 1, 5, 10 µmol $m^{-2}$ $s^{-1}$), and FLuc and RLuc were determined after 18 h. Shown data are the mean FLuc/RLuc ratios. Error bars indicate standard error of the mean (SEM), $n$ = 4. RLU = Relative Luminescence Units. NLS = Nuclear Localization Sequence.

**Fig. 2.** Red light-regulated gene activation switch ($R_{On}$), variants and functional test in Arabidopsis protoplasts. **(a)** Constructs and mode of function. The components engineered and characterized in plant cells are: i) the red light-activated, far-red light-inactivated switch comprising the first 650 amino acids of the PhyB photoreceptor - $PhyB_{(1-650)}$ - fused to an activation domain (AD), VP16 or TV, and the macrolide repressor DNA-binding protein E fused to either $PIF6_{(1-100)}$, $PIF6_{(10-52)}$, or $PIF3_{AAfus}$. The two modules of the switch are constitutively expressed under the control of the promoter $P_{CaMV35S}$, ii) eight repeats of the target sequence of the protein E, etr - $(etr)_8$

- and the minimal promoter $P_{hCMVmin,}$ driving the expression of the reporter gene FLuc, and iii) $P_{CaMV35S}$ driving the constitutive expression of the normalization element RLuc. A constitutive E fused to VP16 and TV is included as control to asses the maximum light-independent repression of the expression achievable. Under red light, PhyB is in active form ($PhyB_{fr}$), and therefore able to interact with PIF, which is bound to $(etr)_8$ through the E protein. In consequence, there is recruitment of the activator domain to the minimal promoter, resulting in expression of FLuc (left). In darkness or in far-red light, PhyB is in the inactive form ($PhyB_r$), therefore unable to bind to the synthetic promoter, resulting in no FLuc transcription (right). **(b)** Characterization of the system. Arabidopsis protoplasts were transformed with the reporter module (pMZ836) and the red light-responsive elements PhyB, fused to either activation domain VP16 (pROF538), or TV (pROF531), and E fused to either $PIF6_{1-100}$ (pROF490), $PIF6_{10-52}$ (pROF491), or $PIF3_{AAfus}$ (pROF492), or without the optoswitch (stuffer plasmid). Reporter module co-transformed with either E fused to VP16 (pKT011), or TV (pKT121), were included as positive controls. Constitutively expressed RLuc (GB0109) was included in all cases for normalization. After transformation, protoplasts were kept in darkness or illuminated with different intensities of red light (10 µmol $m^{-2}$ $s^{-1}$), and FLuc and RLuc were determined after 19 h. Shown data are the mean FLuc/RLuc ratios. Error bars indicate standard error of the mean (SEM), *n* = 6. RLU = Relative Luminescence Units. NLS = Nuclear Localization Sequence.

**Fig. 3**. Mode of function of the red light-activated dCas9-based switch to upregulate gene expression in Arabidopsis protoplasts. **(a)** Constructs and mode of function. The components engineered and characterized in plant cells are: i) the red light-activated modules comprising the nuclease-deficient *Streptococcus pyogenes* Cas9 - dCas9 - fused to either $PIF6_{(1-100)}$, $PIF6_{(10-52)}$, or $PIF3_{AAfus}$, and the first 650 amino acids of the PhyB photoreceptor - $PhyB_{(1-650)}$ - fused to the activation domain termed TV. The two modules of the switch are constitutively expressed from the promoter $P_{CaMV35S}$, ii) the target module composed by the orthologous promoter from *Solanum lycopersicum* dihydroflavonol 4-reductase promoter - $P_{SlDFR}$ - and the endogenous promoter from the Arabidopsis gene APETALA1 - $P_{AtAP1}$ -, driving the expression of the reporter gene FLuc, iii) the guide RNA to target either of the two promoters gRNA($P_{SlDFR}$) and gRNA($P_{AtAP1}$) , and iv) $P_{CaMV35S}$ driving the constitutive expression of the normalization element RLuc. A constitutive dCas9 fused to TV is included as control to asses the

maximum light-independent upregulation of the expression achievable. Under red light, PhyB is in the active form ($PhyB_{fr}$), and therefore able to interact with PIF which is bound to the promoter of interest. The guide RNA confers the specificity towards the promoter. In consequence there is recruitment of the strong activator domain in the proximity of the promoter which leads to transcription activation of FLuc (left). In darkness or in far-red light PhyB is in the inactive form ($PhyB_r$), therefore unable to bind to PIF resulting in only basal activity of the promoter and FLuc transcription (right). **(b)** Characterization of the system using an orthologous promoter. Arabidopsis protoplasts were co-transformed with the target/reporter module, $P_{SlDFR}$-FLuc (GB1159), either without activation and guide module (stuffer plasmid) for the negative control, or with the constitutive dCas9-TV (GB2047) and appropriate gRNA to target $P_{SlDFR}$ (GB1221) as positive control, or with the red-light activation modules together with the guide module. For the red light-responsive elements, PhyB-TV (pROF531) was co-transformed with the modules containing dCas9 fused to either $PIF6_{(1-100)}$, (pROF487), $PIF6_{(10-52)}$ (pROF488), $PIF3_{AAfus}$ (pROF489). Constitutively expressed RLuc (GB0109) was included in all cases for normalization. **(c)** Characterization of the system using an endogenous promoter. Arabidopsis protoplasts were co-transformed with the target/reporter module, $P_{AtAP1}$-FLuc (pROF366) either without activation and guide module (stuffer plasmid) for the negative control, or with the constitutive dCas9-TV (GB2047) and appropriate gRNA to target $P_{AtAP1}$ (pROF441) as positive control, or with the red-light activation modules together with the guide module. For the red light-responsive elements PhyB-TV (pROF531) was co-transformed with the modules containing dCas9 fused to either $PIF6_{(1-100)}$, (pROF487), $PIF6_{(10-52)}$ (pROF488), $PIF3_{AAfus}$ (pROF489). Constitutively expressed RLuc (GB0109) was included in all cases for normalization. (b,c) After transformation, protoplasts were kept in darkness or illuminated with different intensities of red light (10 µmol $m^{-2}$ $s^{-1}$), and FLuc and RLuc were determined after 18 h. Shown data are the mean FLuc/RLuc ratios. Error bars indicate standard error of the mean (SEM), $n = 4$. RLU = Relative Luminescence Units. NLS = Nuclear Localization Sequence.

a

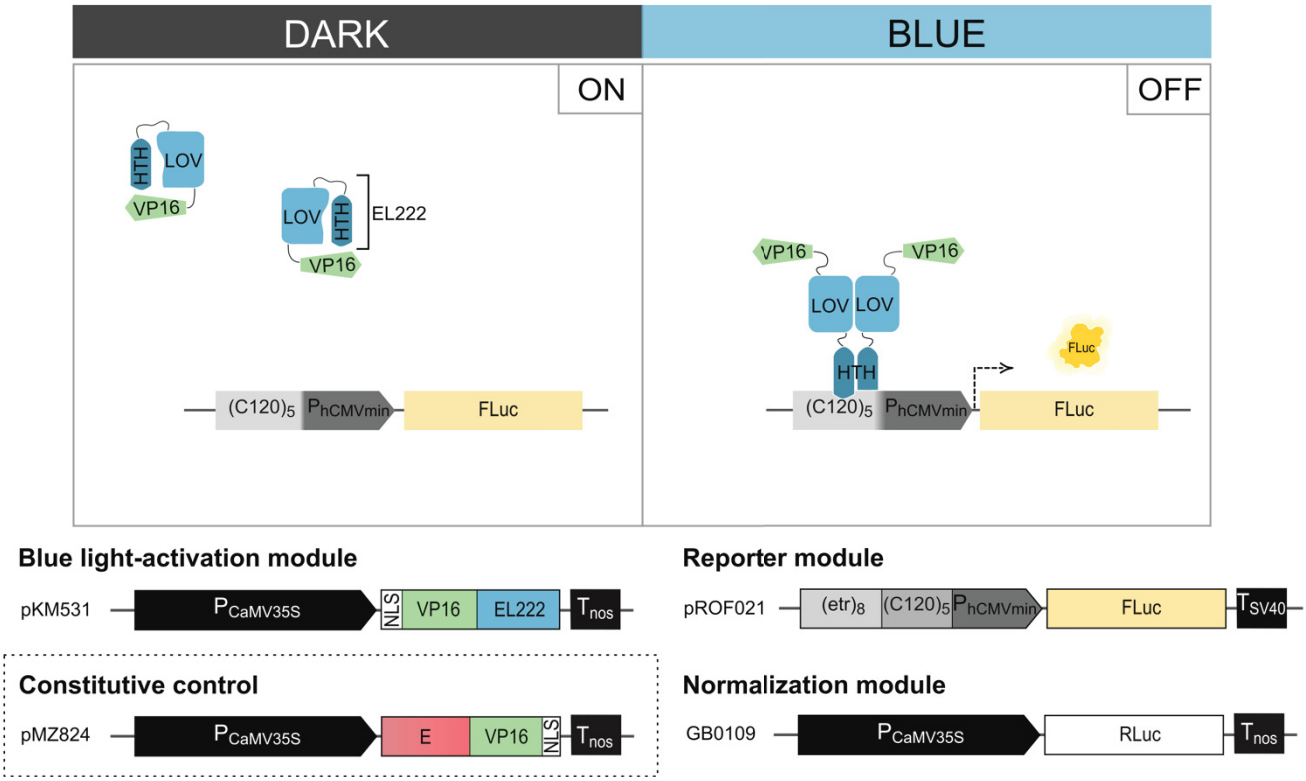
DARK
BLUE
ON
OFF
HTH
LOV
VP16
EL222
FLuc
(C120)5
PhCMVmin
Blue light-activation module
pKM531
PCaMV35S
NLS
VP16
EL222
Tnos
Reporter module
pROF021
(etr)8
(C120)5
PhCMVmin
FLuc
TSV40
Constitutive control
pMZ824
E
Normalization module
GB0109
RLuc

b

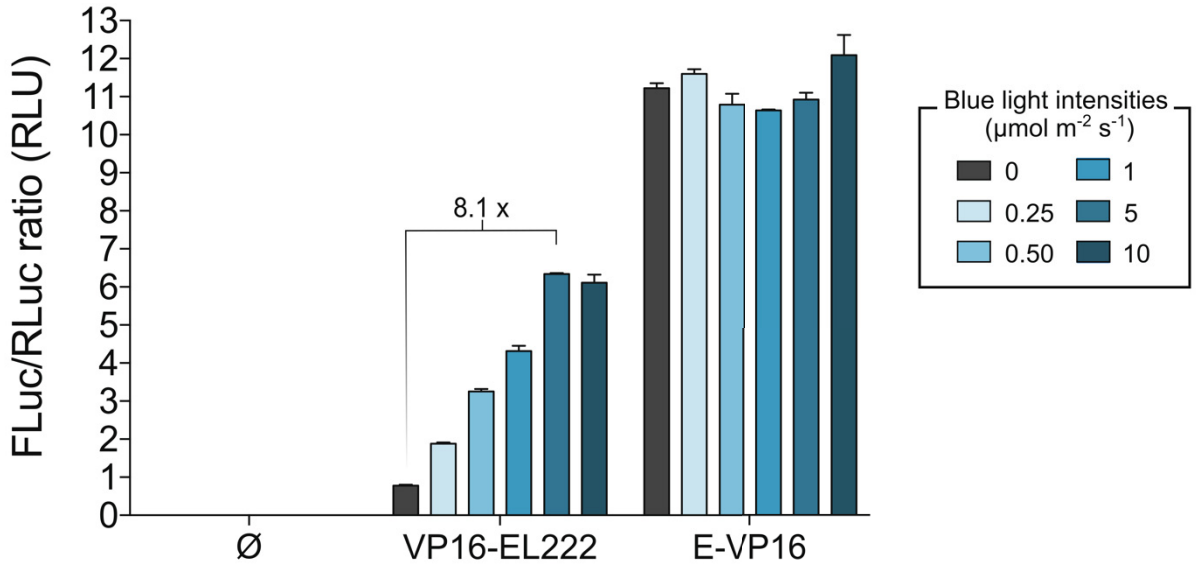
FLuc/RLuc ratio (RLU)
8.1 x
Ø
VP16-EL222
E-VP16
Blue light intensities
(µmol m-2 s-1)
0
0.25
0.50
1
5
10

a

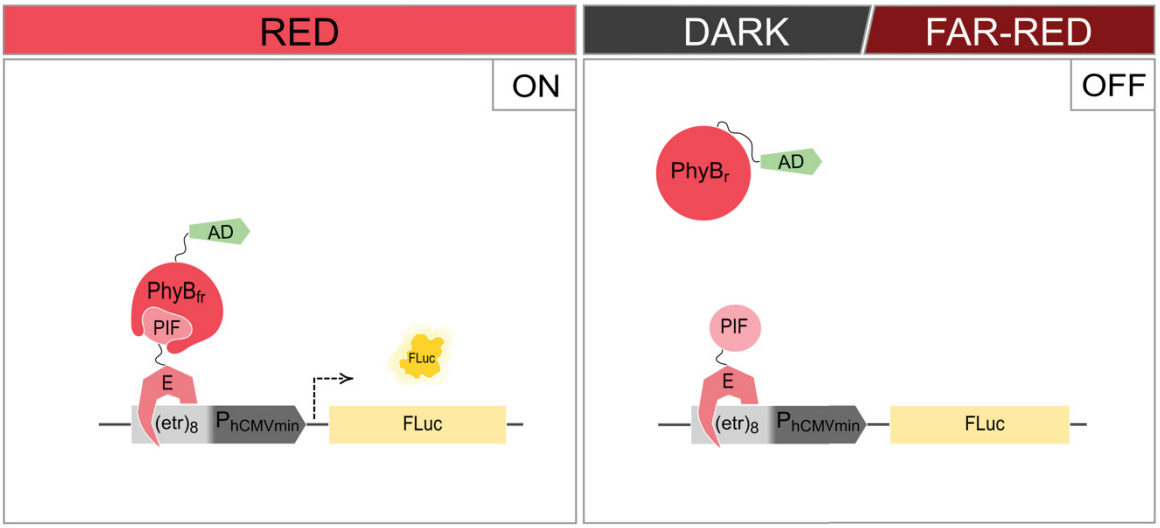


**Red light-activation modules**

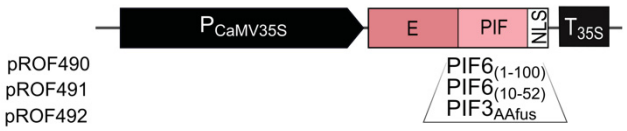



**Constitutive control**


**Reporter module**


**Normalization module**


b

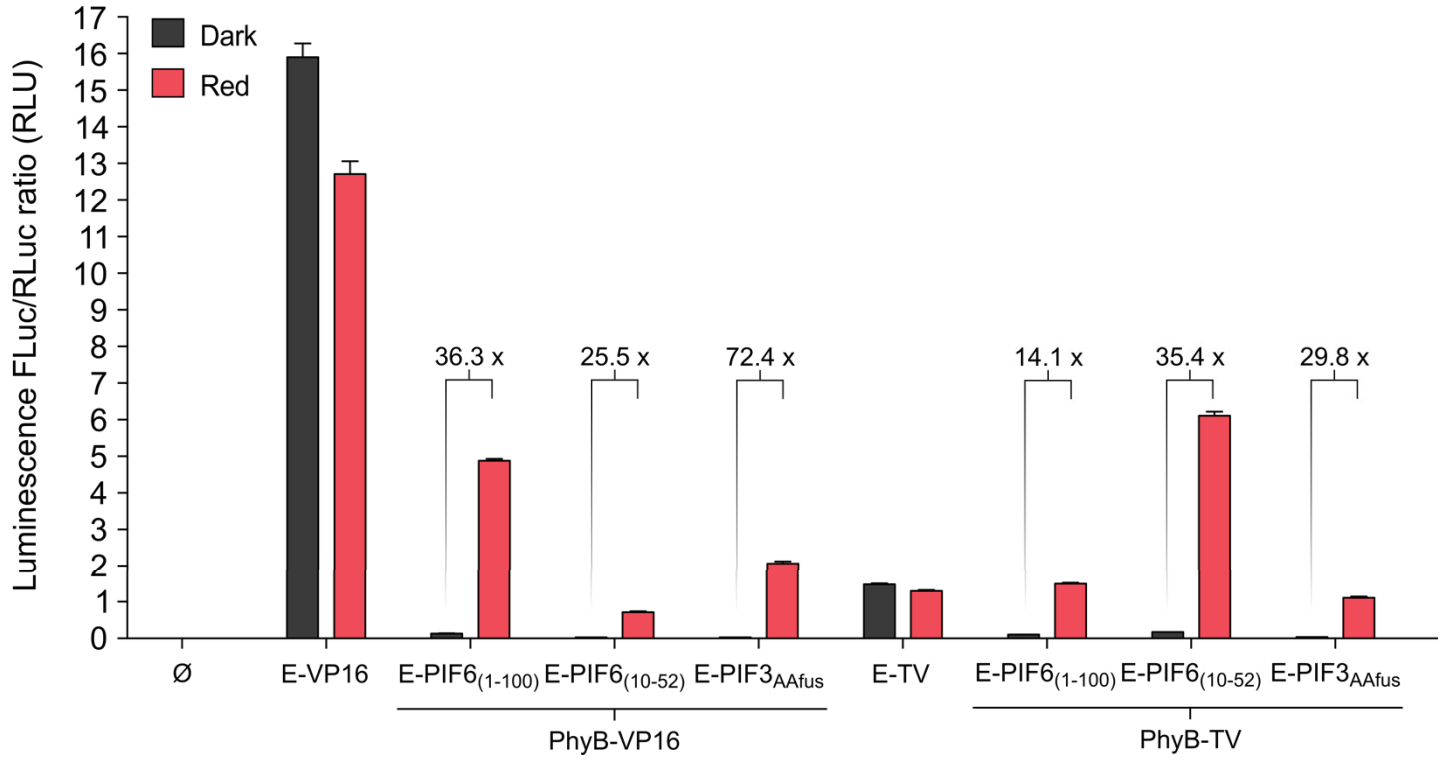

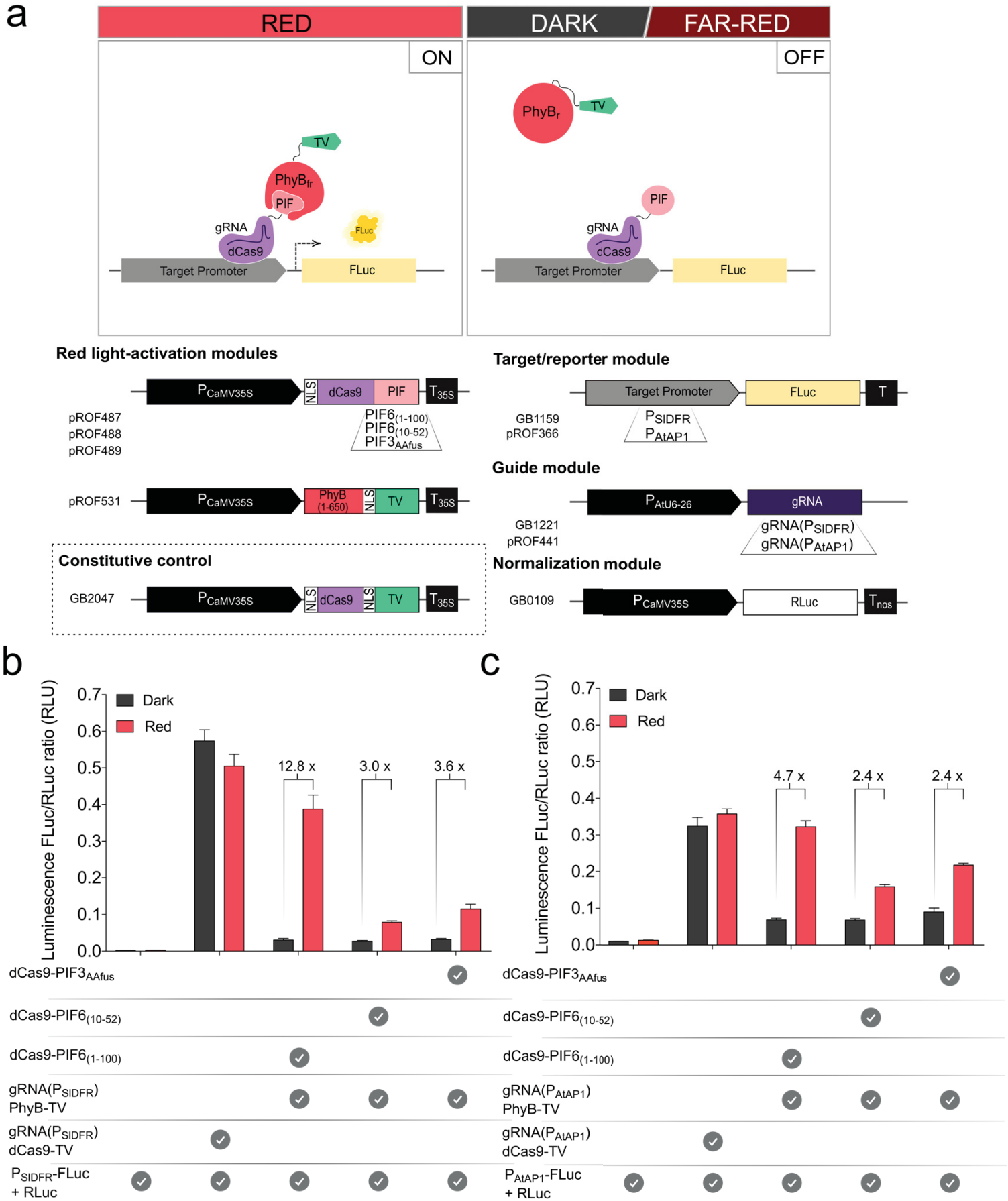
a
RED
DARK
FAR-RED
ON
OFF
TV
PhyBfr
PIF
gRNA
dCas9
FLuc
Target Promoter
PhyBr
Red light-activation modules
Target/reporter module
Guide module
Constitutive control
Normalization module
pROF487
pROF488
pROF489
PIF6(1-100)
PIF6(10-52)
PIF3AAfus
pROF531
GB1159
pROF366
PSIDFR
PAtAP1
GB1221
pROF441
gRNA(PSIDFR)
gRNA(PAtAP1)
GB2047
GB0109
RLuc
b
c
Luminescence FLuc/RLuc ratio (RLU)
Dark
Red
12.8 x
3.0 x
3.6 x
4.7 x
2.4 x
2.4 x
dCas9-PIF3AAfus
dCas9-PIF6(10-52)
dCas9-PIF6(1-100)
gRNA(PSIDFR) PhyB-TV
gRNA(PSIDFR) dCas9-TV
PSIDFR-FLuc + RLuc
gRNA(PAtAP1) PhyB-TV
gRNA(PAtAP1) dCas9-TV
PAtAP1-FLuc + RLuc

# Expanding the toolbox of optogenetic switches for red and blue light control of gene expression in plant cells

Rocio Ochoa-Fernandez[1,2], Mara Schuler-Bermann[1], Matias D. Zurbriggen[1,2,3,#]

[1]Institute of Synthetic Biology, University of Düsseldorf, Germany

[2]iGRAD Plant Graduate School, University of Düsseldorf, Germany.

[3]CEPLAS - Cluster of Excellence on Plant Sciences, Düsseldorf, Germany

[#]Corresponding author: MDZ matias.zurbriggen@uni-duesseldorf.de

## Supplementary Tables

**Supplementary Table S1.** Plasmids used in this work (grey shading). Plasmids below in the hierarchy were used as intermediate plasmids for cloning purposes.

| Plasmid name | Description | Insert | Backbone | Cloning procedure |
|---|---|---|---|---|
| GB0109 | $P_{CaMV35s}$-RLuc-$T_{nos}$[1] | | | |
| GB1159 | $P_{SlDFR}$-FLuc-$T_{nos}$[2] | | | |
| GB1221 | $P_{AtU6\text{-}26}$-gRNA($P_{SlDFR}$)-sgRNA[2] | | | |
| GB2047 | $P_{CaMV35S}$-dCas9-2xNLS-TV-$T_{nos}$[2] | | | |
| pKM351 | $P_{CaMV35S}$-NLS-VP16-EL222-$T_{nos}$ | NLS-VP16-EL222 was amplified from pVP-EL222[3] with oligos oKM611/oKM612 | pMZ827[4] digested with NdeI/EcoRI | Gibson assembly of backbone and PCR insert |
| pKT011 | $P_{CaMV35S}$-E-VP16-$T_{35S}$ | GB0030[1], pKT002, GB0036[1] | EC47742 | BsaI restriction-ligation reaction (GoldenGate) |
| ↳ pKT002 | E-VP16-NLS (Position B3-B5) | VP16-NLS was amplified from pMZ824[4] with oligos oKT003/oKT016. | pUPD2[6] | BsmBI restriction-ligation reaction (Golden Braid) |
| pKT0121 | $P_{CaMV35S}$-E-2xNLS-TV-$T_{35S}$ | GB0030[1], pROF483, GB2001[2], GB0036[1] | EC47742[5] | BsaI restriction-ligation reaction (GoldenGate) |
| ↳ pROF483 | E (Pos. B3-B4) | E was amplified from pMZ827[4] with oligos oROF580/oROF581 | pUPD2[6] | BsmBI restriction-ligation reaction (GB) |
| pMZ824 | $P_{CaMV35S}$-E-VP16-NLS-$T_{SV40}$[4] | | | |
| pMZ827 | $P_{CaMV35S}$-E-PIF6$_{(1\text{-}100)}$-NLS-$T_{SV40}$[4] | | | |
| pMZ828 | $P_{CaMV35S}$-PhyB$_{(1\text{-}650)}$-VP16-NLS-$T_{SV40}$[4] | | | |
| pMZ836 | $(etr)_8$-$P_{hCMVmin}$-FLuc-$T_{SV40}$[4] | | | |
| pROF021 | $(etr)_8$-$(C120)_5$-$P_{hCMVmin}$-FLuc-$T_{SV40}$ | FLuc was excised from pMZ836[4] with NotI/EcoRI | pROF020 digested with EcoRI/NotI | Ligation with T4 DNA ligase |
| ↳ pROF020 | $(etr)_8$-$(C120)_5$-$P_{hCMVmin}$-SEAP-$T_{SV40}$ | $(C120)_5$ was amplified from pGL4.32-C120-FLuc[3] with oligos oROF027/oROF028. | pKM081[7] digested with NheI | Ligation with T4 DNA ligase |
| pROF366 | $P_{AtAP1}$-FLuc-$T_{SV40}$ | $P_{AtAP1}$ was amplified from Arabidopsis genomic DNA with oligos oROF401/oROF403 | pROF021 digested with PstI/ EcoRI | Gibson assembly of backbone and PCR insert |

| | | | | | |
|---|---|---|---|---|---|
| pROF441 | | $P_{AtU6-26}$-gRNA($P_{AtAP1}$)-sgRNA | gRNA($P_{AtAP1}$) was constructed using oligos oROF537/oROF538 at 1 µM; 5 µl of each were mixed and incubated for 30 min at RT. Then 1 µl of the mixture was combined with pROF440 and pROF446. | pDGB 1alpha2[1] | BsaI restriction-ligation reaction (GB) |
| ↳ | pROF440 | $P_{AtU6-26}$ (Pos. A1-B2) | $P_{AtU6-26}$ was amplified from pEn-Chimera[8] with oligos oROF137/oROF545 | pUPD2[6] | BsmBI restriction-ligation reaction (GB) |
| ↳ | pROF446 | sgRNA | sgRNA was amplified from pEN-Chimera[8] with oligos oROF546/oROF140 | pUPD2[6] | BsmBI restriction-ligation reaction (GB) |
| pROF472 | | $P_{35Senhancer(-149\ to\ -51)}$-$(etr)_8$-$P_{hCMVmin}$-FLuc-$T_{35S}$ | pROF338, pROF468, pROF375, GB0096[1], GB0036[1] | pDGB 1alpha1[1] | BsaI restriction-ligation reaction (GB) |
| ↳ | pROF338 | $P_{35Senhancer(-149\ to\ -51)}$ (Pos. A1) | $P_{35Senhancer(-149\ to\ -51)}$ was amplified from GB0030[1] with oligos oROF377/oROF378 | pUPD2[6] | BsmBI restriction-ligation reaction (GB) |
| ↳ | pROF468 | $(etr)_8$ (Pos. A2) | $(etr)_8$ was amplified from pKM081[7] with oligos oROF594/oROF591 | pUPD2[6] | BsmBI restriction-ligation reaction (GB) |
| ↳ | pROF375 | $P_{hCMVmin}$ (Pos. A3-B2) | $P_{hCMVmin}$ was amplified from pMZ836[4] with oligos oROF083/oROF084 | pUPD2[6] | BsmBI restriction-ligation reaction (GB) |
| pROF473 | | $P_{35Senhancer(-953\ to\ -51)}$-$(etr)_8$-$P_{hCMVmin}$-FLuc-$T_{35S}$ | pROF339, pROF468, pROF375, GB0096[1], GB0036[1] | pDGB 1alpha1[1] | BsaI restriction-ligation reaction (GB) |
| ↳ | pROF339 | $P_{35Senhancer(-953\ to\ -51)}$ (Pos. A1) | $P_{35Senhancer(-953\ to\ -51)}$ was amplified from GB0030[1] with oligos oROF376/oROF378 | pUPD2[6] | BsmBI restriction-ligation reaction (GB) |
| ↳ | pROF468 | $(etr)_8$ (Pos. A2) | $(etr)_8$ was amplified from pKM081[7] with oligos oROF594/oROF591 | pUPD2[6] | BsmBI restriction-ligation reaction (GB) |
| ↳ | pROF375 | $P_{hCMVmin}$ (Pos. A3-B2) | $P_{hCMVmin}$ was amplified from pMZ836[4] with oligos oROF083/oROF084 | pUPD2[6] | BsmBI restriction-ligation reaction (GB) |
| pROF474 | | $P_{35Senhancer(-953\ to\ +1)}$-$(etr)_8$-$P_{hCMVmin}$-FLuc-$T_{35S}$ | pROF340, pROF469, GB0096[1], GB0036[1] | pDGB 1alpha1[1] | BsaI restriction-ligation reaction (GB) |
| ↳ | pROF340 | $P_{35Senhancer(-953\ to\ +1)}$ (Pos. A1-B1) | $P_{35Senhancer(-953\ to\ +1)}$ was amplified from GB0030[1] with oligos oROF376/oROF379 | pUPD2[6] | BsmBI restriction-ligation reaction (GB) |
| ↳ | pROF469 | $(etr)_8$ (Pos. B2) | $(etr)_8$ was amplified from pKM081[7] with oligos oROF595/oROF593 | pUPD2[6] | BsmBI restriction-ligation reaction (GB) |

| | | | | | |
|---|---|---|---|---|---|
| pROF475 | | $P_{CaMV35S}$-PhyB-linker-SRDX-NLS-$T_{nos}$ | PhyB-linker-SRDX-NLS was amplified from pMZ828[4] with oligos oROF574/oROF575 | pGEN016[9] digested with AgeI/EcoRI | AQUA assembly of backbone and PCR insert |
| pROF476 | | $P_{CaMV35S}$-NLS-linker-SRDX-$T_{nos}$ | PhyB-NLS-linker-SRDX was amplified from pMZ828[4] with oligos oROF574/oROF576 | pGEN016[9] digested with AgeI/EcoRI | AQUA assembly of backbone and PCR insert |
| pROF487 | | $P_{CaMV35S}$-dCas9-PIF6$_{(1-100)}$-NLS-$T_{35S}$ | GB0030[1], GB1079[2], pROF484, GB0036[1] | pDGB 3alpha1[1] | BsaI restriction-ligation reaction (GB) |
| ↳ | pROF484 | Linker-PIF6$_{(1-100)}$-NLS (Pos. B5) | Linker-PIF6$_{(1-100)}$-NLS was amplified rom pMZ827[4] with oligos oROF582/oROF583 | pUPD2[6] | BsmBI restriction-ligation reaction (GB) |
| pROF488 | | $P_{CaMV35S}$-dCas9-PIF6$_{(10-52)}$-NLS-$T_{35S}$ | GB0030[1], GB1079[2], pROF485, GB0036[1] | pDGB 3alpha1[1] | BsaI restriction-ligation reaction (GB) |
| ↳ | pROF485 | Linker-PIF6$_{(10-52)}$-NLS (Pos. B5) | Linker-PIF6$_{(10-52)}$-NLS was amplified from pMZ827[4] with oligos oROF584/oROF585 | pUPD2[6] | BsmBI restriction-ligation reaction (GB) |
| pROF489 | | $P_{CaMV35S}$-dCas9-PIF3$_{AAfus}$-$T_{35S}$ | GB0030[1], GB1079[2], pROF486, GB0036[1] | pDGB 3alpha1[1] | BsaI restriction-ligation reaction (GB) |
| ↳ | pROF486 | Linker- PIF3$_{AAfus}$-NLS (Pos. B5) | Linker- PIF3$_{AAfus}$-NLS was amplified from pDG366[10] with oligos oROF586/oROF587 | pUPD2[6] | BsmBI restriction-ligation reaction (GB) |
| pROF490 | | $P_{CaMV35S}$-E-PIF6$_{(1-100)}$-NLS-$T_{35S}$ | GB0030[1], pROF483, pROF484, GB0036[1] | pDGB 3alpha1[1] | BsaI restriction-ligation reaction (GB) |
| ↳ | pROF483 | E (Pos. B3-B4) | E was amplified from pMZ827[4] with oligos oROF580/oROF581 | pUPD2[6] | BsmBI restriction-ligation reaction (GB) |
| ↳ | pROF484 | Linker-PIF6$_{(1-100)}$-NLS (Pos. B5) | Linker-PIF6(1-100)-NLS was amplified rom pMZ827[4] with oligos oROF582/oROF583 | pUPD2[6] | BsmBI restriction-ligation reaction (GB) |
| pROF491 | | $P_{CaMV35S}$-E- PIF6$_{(10-52)}$-NLS-$T_{35S}$ | GB0030[1], pROF483, pROF485, GB0036[1] | pDGB 3alpha1[1] | BsaI restriction-ligation reaction (GB) |
| ↳ | pROF483 | E (Pos. B3-B4) | E was amplified from pMZ827[4] with oligos oROF580/oROF581 | pUPD2[6] | BsmBI restriction-ligation reaction (GB) |
| ↳ | pROF485 | Linker-PIF6$_{(10-52)}$-NLS (Pos. B5) | Linker-PIF6$_{(10-52)}$-NLS was amplified from pMZ827[4] with oligos oROF584/oROF585 | pUPD2[6] | BsmBI restriction-ligation reaction (GB) |
| pROF492 | | $P_{CaMV35S}$-E-PIF3$_{AAfus}$-$T_{35S}$ | GB0030[1], pROF483, pROF486, GB0036[1] | pDGB 3alpha1[1] | BsaI restriction-ligation reaction (GB) |
| ↳ | pROF483 | E (Pos. B3-B4) | E was amplified from pMZ827[4] with oligos oROF580/oROF581 | pUPD2[6] | BsmBI restriction-ligation reaction (GB) |
| ↳ | pROF486 | Linker- PIF3$_{AAfus}$-NLS (Pos. B5) | Linker- PIF3$_{AAfus}$-NLS was amplified from | pUPD2[6] | BsmBI restriction- |

| | | | | | |
|---|---|---|---|---|---|
| | | | pDG366[10] with oligos oROF586/oROF587 | | ligation reaction (GB) |
| pROF531 | | $P_{CaMV35S}$-PhyB-2xNLS-TV-$T_{35S}$ | GB0030[1], pKT097, GB2001[2], GB0036[1] | pDGB 1alpha2[1] | BsaI restriction-ligation reaction (GB) |
| ↳ | pKT097 | PhyB (Pos. B3-B4) | PhyB was amplified from pMZ828[4] with oligos oKT090/oKT091 | pUPD2[6] | BsmBI restriction-ligation reaction (GB) |
| pROF538 | | $P_{CaMV35S}$-PhyB-linker-VP16-NLS-$T_{35S}$ | GB0030[1], pMV003, GB0036[1] | pDGB 1alpha1[1] | BsaI restriction-ligation reaction (GB) |
| ↳ | pMVV003 | PhyB-VP16-NLS (Pos. B3-B5) | PhyB-VP16-NLS was amplified from from pMZ828[4] | pUPD[1] | BsmBI restriction-ligation reaction (GB) |
| pROF539 | | $(etr)_8$-$P_{hCMVmin}$-FLuc-$T_{nos}$ | pROF447, GB0096[1], GB0037[1] | pDGB 1alpha2[1] | BsaI restriction-ligation reaction (GB) |
| ↳ | pROF447 | $(etr)_8$-$P_{hCMVmin}$ (Pos. A1-B2) | $(etr)_8$-$P_{hCMVmin}$ was amplified from pKM081[7] with oligos oROF071/oROF042 | pUPD2[6] | BsmBI restriction-ligation reaction (GB) |
| pROF551 | | $P_{CaMV35S}$-NLS-dCas9-$T_{35S}$ | GB0030[1], pROF550, GB0036[1] | pDGB 1alpha1[1] | BsaI restriction-ligation reaction (GB) |
| ↳ | pROF550 | NLS-dCas9 (Pos. B3-B5) | NLS-dCas9 was amplified from GB1079[2] with oligos oROF610/oROF611 | pUPD2[6] | BsmBI restriction-ligation reaction (GB) |
| pROF554 | | $P_{CaMV35S}$-NLS-dCas9-NLS-SRDX-$T_{35S}$ | GB0030[1], pROF553, GB0036[1] | pDGB 1alpha1[1] | BsaI restriction-ligation reaction (GB) |
| ↳ | pROF553 | NLS-dcas9-NLS-SRDX (Pos. B3-B5) | NLS-dcas9-NLS-SRDX was amplified from GB1079[2] with oligos oROF610/oROF612 | pUPD2[6] | BsmBI restriction-ligation reaction (GB) |
| pROF556 | | $P_{CaMV35S}$-E-NLS-SRDX-$T_{35S}$ | GB0030[1], pROF555, GB0036[1] | pDGB 1alpha1[1] | BsaI restriction-ligation reaction (GB) |
| ↳ | pROF555 | E-NLS-SRDX (Pos. B3-B5) | E-NLS-SRDX was amplified from pMZ827[4] with oligos oROF580/oROF613 | pUPD2[6] | BsmBI restriction-ligation reaction (GB) |
| pRSET | | PT7-driven bacterial expression vector (ThermoFisher) | | | |

dCas9, CRISPR associated protein 9 nuclease deficient; E, macrolide-responsive repressor protein; EL222, transcription factor from *Erythrobacter litoralis*; $(etr)_8$, 8 repeats of the DNA cognate sequence of E; FLuc, Firefly luciferase; gRNA, part of the guide RNA containing the 20 bp target sequence; NLS, nuclear localization signal from the simian virus 40 large T antigen; $P_{35Senhancer}$, enhancer region of the *cauliflower mosaic virus* 35S promoter; $P_{AtU6\text{-}26}$, *A. thaliana* U6-26 RNA polymerase III promoter; $P_{AtAP1}$, *A. thaliana* APETALA1 promoter; $P_{AtUbq10}$, *A. thaliana* Ubiquitin-10 promoter; $P_{CaMV35S}$, *cauliflower mosaic virus* 35S terminator; $P_{hCMVmin}$, minimal human cytomegalovirus immediate early promoter; $PhyB_{(1–650)}$, N-terminus of *A. thaliana* phytochrome B including amino acids 1–650; $PIF3_{AAfus}$, fusion of two times the APB.A motif of *A. thaliana* phytochrome-interacting factor 3; $PIF6_{(1–100)}$, N-terminus of *A.*

*thaliana* phytochrome-interacting factor 6 including amino acids 1–100; $PIF6_{(10–52)}$, APB.A motif of *A. thaliana* phytochrome-interacting factor 6 including amino acids 10–52; $P_{nos}$, *Agrobacterium thumefaciens* nopaline synthase promoter; $P_{SlDFR,}$ *Solanum lycopersicum* dihydroflavonol 4-reductase promoter; $P_{SV40}$, simian virus 40 early promoter; RLuc, Renilla luciferase; SRDX, EAR repression domain from *A. thaliana*; SEAP, human secreted alkaline phosphatase; sgRNA, single guide RNA from combined bacterial crRNA and tracrRNA without the target sequence; $T_{SV40}$, simian virus 40 early terminator; TV, activation domain composed by 6x TAL and 2x VP64 and NLS sequence; VP16, *Herpes simplex* virus-derived transactivation domain.

**Supplementary Table S2.** Oligonucleotides used in this work (lowercase correspond to annealing part and uppercase corresponds to overhangs)

| Oligonucleotide name | Sequence 5'→3' |
|---|---|
| oKM611 | CGGTTGGCTAGGTAAGCTTGGTACCACCTGAACGACGCATATGTGCTAGC gccaccatgggccctaaaaag |
| oKM612 | ATCTAGATCCGGTGGATCCAAGCTTCTCGAGCCCGGGGAATTCttagattccgg cttcgacggc |
| oKT003 | GCGCCGTCTCGCTCGAatgccccgccccaagc |
| oKT016 | GCGCCGTCTCGCTCAAAgcctacaccttcctcttcttctttgg |
| oKT090 | GCGCCGTCTCGCTCGaatggtttccggagtcg |
| oKT091 | GCGCCGTCTCGCTCACGAACcacctaactcatcaatcccc |
| oROF027 | tacgggaggtattggacagg |
| oROF028 | TGATGCCGCTAGCtctagtgtctaagcttcatgg |
| oROF042 | GCGCCGTCTCGCTCGCATTaggctggatcggtcccggtg |
| oROF071 | GCGCCGTCTCGCTCGGGAGgtttaaacgattgaatataaccgac |
| oROF083 | GCGCCGTCTCGCTCGTCCCGCGGCCGCcctatataagcagagctcgtt |
| oROF084 | GCGCCGTCTCGCTCGCATTACCGGTaggctggatcggtcccggtg |
| oROF137 | GCGCCGTCTCGCTCGGGAGctttttttcttcttcttcgttcatac |
| oROF140 | GCGCCGTCTCGCTCAAGCGtaatgccaactttgtacaagaaag |
| oROF376 | GCGCCGTCTCGCTCGGGAGactagagccaagctgatctc |
| oROF377 | GCGCCGTCTCGCTCGGGAGagcatcgtggaaaaagaagac |
| oROF378 | GCGCCGTCTCGCTCAGTCAatagtgggattgtgcgtcatc |
| oROF379 | GCGCCGTCTCGCTCAATGGtcgactagaatagtaaattgtaatgt |
| oROF537 | ATTGTATATCTCGTACTAATGTC |
| oROF538 | AAACGACATTAGTACGAGATATA |
| oROF545 | GCGCCGTCTCGCTCAcaatcactacttcgactctag |
| oROF546 | GCGCCGTCTCGCTCGgttttagagctagaaatagcaagt |
| oROF574 | TTTGGAGAGAACACGGGGACTCTAGCGCTACCGGTatggtttccggagtcgg |
| oROF575 | CCGGTGGATCCAAGCTTCTCGAGCCCGGGGAATTCCTACACCTTCCTCTT CTTCTTTGGAGCAAAACCAAGTCTAAGTTCAAGATCAAGCATaccagcactacc agcactac |
| oROF576 | CCGGTGGATCCAAGCTTCTCGAGCCCGGGGCTAAGCAAAACCAAGTCTA AGTTCAAGATCAAGCATAGCTCCAGCTCCCACCTTCCTCTTCTTCTTTGGa ccagcactaccagcactac |
| oROF580 | GCGCCGTCTCGCTCGAATGccccgccccaagct |
| oROF581 | GCGCCGTCTCGCTCACGAACCgctgtacgcggacgc |
| oROF582 | GCGCCGTCTCGCTCGTTCGagtgctggtagtgctggtag |
| oROF583 | GCGCCGTCTCGCTCAAAGCctacaccttcctcttcttctt |

| | |
|---|---|
| oROF584 | GCGCCGTCTCGCTCGTTCGAGTGCTGGTAGTGCTGGTAGTGCTGGTtgcaggttaagcgatcaa |
| oROF585 | GCGCCGTCTCGCTCAAAGCCTACACCTTCCTCTTCTTCTTTGGtgcctcataca aatccatg |
| oROF586 | GCGCCGTCTCGCTCGTTCGtctgccggctctgccggctc |
| oROF587 | GCGCCGTCTCGCTCAAAGCtcagtgatgattcagccacg |
| oROF591 | GCGCCGTCTCGCTCAGGGAgctagcatccctaaatgtaac |
| oROF593 | GCGCCGTCTCGCTCACATTgctagcatccctaaatgtaac |
| oROF594 | GCGCCGTCTCGCTCGTGACgcaaaaagcttcgaagtttaaac |
| oROF595 | GCGCCGTCTCGCTCGCCATgcaaaaagcttcgaagtttaaac |
| oROF610 | GCGCCGTCTCGctcgaatgcccaagaagaagaggaag |
| oROF611 | GCGCCGTCTCGCTCAAAGCTCAatcagccctgctgtctc |
| oROF612 | GCGCCGTCTCGCTCAAAGCTCAAGCAAAACCAAGTCTAAGTTCAAGATCA AGATCAAGCACCTTCCTCTTCTTCTTGGGatcagccctgctgtctc |
| oROF613 | GCGCCGTCTCGCTCAAAGCTCAAGCAAAACCAAGTCTAAGTTCAAGATCA AGATCAAGCACCTTCCTCTTCTTCTTGGGgctgtacgcggacgca |

## Supplementary References

1. Sarrion-Perdigones, A. *et al.* GoldenBraid 2.0: A Comprehensive DNA Assembly Framework for Plant Synthetic Biology. *Plant Physiol.* **162**, 1618 (2013).
2. Selma, S. *et al.* Strong gene activation in plants with genome-wide specificity using a new orthogonal CRISPR/Cas9-based programmable transcriptional activator. *Plant Biotechnol. J.* **17**, 1703–1705 (2019).
3. Motta-Mena, L. B. *et al.* An optogenetic gene expression system with rapid activation and deactivation kinetics. *Nat. Chem. Biol.* **10**, 196–202 (2014).
4. Müller, K. *et al.* A red light-controlled synthetic gene expression switch for plant systems. *Mol. Biosyst.* **10**, 1679–1688 (2014).
5. Weber, E., Engler, C., Gruetzner, R., Werner, S. & Marillonnet, S. A Modular Cloning System for Standardized Assembly of Multigene Constructs. *PLoS ONE* **6**, e16765 (2011).
6. Vazquez-Vilar, M. *et al.* GB3.0: a platform for plant bio-design that connects functional DNA elements with associated biological data. *Nucleic Acids Res.* **45**, 2196–2209 (2017).
7. Müller, K. *et al.* Multi-chromatic control of mammalian gene expression and signaling. *Nucleic Acids Res.* **41**, e124 (2013).
8. Fauser, F., Schiml, S. & Puchta, H. Both CRISPR/Cas-based nucleases and nickases can be used efficiently for genome engineering in Arabidopsis thaliana. *Plant J.* **79**, 348–359 (2014).
9. Samodelov, S. L. *et al.* StrigoQuant: A genetically encoded biosensor for quantifying strigolactone activity and specificity. *Sci. Adv.* **2**, e1601266–e1601266 (2016).
10. Golonka, D. *et al.* Deconstructing and repurposing the light-regulated interplay between Arabidopsis phytochromes and interacting factors. *Commun. Biol.* **2**, 448 (2019).

# PULSE – Optogenetic control of gene expression in plants in the presence of ambient white light

Rocio Ochoa-Fernandez[1,2], Nikolaj B. Abel[3], Franz-Georg Wieland[4], Jenia Schlegel[2,5], Leonie A. Koch[1], J. Benjamin Miller[6], Raphael Engesser[4], Giovanni Giurani[1], Simon M. Brandl[3], Johanna Plum[1], Jens Timmer[4,7], Wilfried Weber[3,7], Thomas Ott[3,7], Rüdiger Simon[2,5,8], Matias D. Zurbriggen[1,2,8,#]

[1]Institute of Synthetic Biology, University of Düsseldorf, Germany

[2]iGRAD Plant Graduate School, University of Düsseldorf, Germany.

[3]Faculty of Biology, University of Freiburg, Germany

[4]Institute of Physics, University of Freiburg, Germany

[5]Institute of Developmental Genetics, University of Düsseldorf, Germany

[6]School of Biological Sciences, University of East Anglia, Norwich, UK.

[7]Signalling Research Centres BIOSS and CIBSS, University of Freiburg, Germany

[8]CEPLAS - Cluster of Excellence on Plant Sciences, Düsseldorf, Germany

[#]Corresponding author: MDZ matias.zurbriggen@uni-duesseldorf.de

lxx

**ABSTRACT**

Optogenetics, the genetic approach of controlling cellular processes with light, is revolutionizing signalling and metabolic studies in biology. It provides unmatched spatiotemporal, quantitative and reversible control, with minimized invasiveness, thereby overcoming limitations of chemically-inducible systems. However, optogenetics severely lags behind in plant research because ambient light required for growth leads to undesired system activation. We solved this major issue by engineering PULSE (Plant Usable Light-Switch Elements), the first optogenetic tool for reversibly controlling gene expression in plants under ambient light. PULSE combines a blue light-regulated repressor with a red light-inducible switch. Gene expression is only activated under red light and remains inactive under white light/darkness. Supported by a quantitative mathematical model we characterized PULSE performance in protoplasts achieving up to 400-fold induction rates, plant leaves and also in transgenic plants. We combined PULSE with CRISPR/Cas9-based technologies to control synthetic signalling and developmental pathways in cells and immune responses *in planta*. PULSE will enable broad experimental avenues for plant research and biotechnology.

## INTRODUCTION

The reversible and orthogonal control of cellular processes with high spatiotemporal resolution is key for quantitatively understanding the dynamics of biological signalling networks as well as for programming desired phenotypes. The optimal stimulus for such cellular control is light as it can be applied with unmatched spatiotemporal precision in a quantitative manner, with minimized toxicity and invasiveness. Accordingly, optogenetics, the control of cellular events by using genetically encoded, light-responsive switches is opening revolutionary avenues in mammalian systems. A non-limiting list of successfully manipulated and regulated cellular and physiological processes with optogenetic switches includes neuromodulation, gene expression, epigenetics, protein and organellar activity, and subcellular localization[1–7].

While similar approaches to address important biological questions are needed in plant research, the use of optogenetics to answer them is limited by the intrinsic need of plants for broad-spectrum light which would erroneously activate the engineered light-responsive switches. We have recently developed and successfully implemented the first two optogenetic systems for the control of gene expression in plant cells. The systems are regulated by red and green light and proved useful for the quantitative manipulation of hormone signalling pathways and recombinant protein expression control[8,9]. However, due to the spectral compatibility limitations described above or the need for co-factors difficult to administer to whole plants, these tools could only be applied in transiently transformed plant cells such as mesophyll protoplasts from *Nicotiana tabacum* or *Arabidopsis thaliana,* and the moss *Physcomitrella patens* which can be kept in the dark prior to the optogenetic experiment[8–10]. Despite their utility for transient signalling studies in cell culture, it is highly desirable to have an optogenetic tool functional in whole plants and being insensitive to broad-spectrum white light to harness the full potential of optogenetics in the plant kingdom.

Towards this goal, we set here to develop the first optogenetic system for the control of gene expression in plants that is silent under white light and can be active with monochromatic red light. The system, termed PULSE (Plant Usable Light-Switch Elements), comprises two engineered photoreceptors exerting a combined activity over the regulation of transcription initiation: one actively represses gene expression under blue light ($B_{Off}$, Blue Light-repression) engineered from the EL222 photoreceptor[11], and the second one activates gene expression with red light ($R_{On}$, Red Light-activation) based on a Phytochrome B (PhyB) - PIF6 optoswitch[8,10] (**Fig. 1**). We first engineered and characterized PULSE in protoplasts of Arabidopsis and later applied it in complex tissues, using *Nicotiana benthamiana* leaves as model system. PULSE provides quantitative and spatiotemporal reversible control over gene expression, achieving high induction rates (up to *ca.* 400-fold) while being Off under white light or in the dark. We developed a mathematical model to quantitatively characterize the dynamic behaviour of the system and guide designing experimental setups. We combined it with a plant transcription factor (TF) or a CRISPR/Cas9-derived gene activator and showed its functionality for the light-controlled activation of target promoters. Furthermore, we applied PULSE to engineer light-inducible immunity *in planta* and tested its functionality in whole Arabidopsis plants. These results demonstrate the wide applicability of PULSE, opening up novel perspectives for the targeted spatiotemporal and quantitative study and control of plant signalling, genetic and metabolic networks as well as its implementation for biotechnological approaches.

## RESULTS

### Design, implementation, and test of the Plant Usable Light Switch-Elements (PULSE) in plant cells

PULSE is an integrated optogenetic molecular device, consisting of two components, a module providing activation of gene expression under red light ($R_{On}$) and a second one ensuring effective transcriptional repression under blue light ($B_{Off}$) (**Fig. 1**). The rationale behind this new conceptual and experimental approach is that the combination of both switches will yield a system that is inactive in ambient growth conditions (light and darkness) and only active upon irradiation with red light. This enables full applicability in plants growing under standard light conditions.

We first constructed a blue light-regulated gene repression switch $B_{Off}$ based on the transcription factor EL222 from the bacterium *Erythrobacter litoralis*[11] which has a Light-Oxygen-Voltage (LOV) dependent motif and an Helix-Turn-Helix (HTH) domain. Upon blue light it binds as a dimer to the target DNA sequence C120[12]. $B_{Off}$ thus comprises (**Fig. 2a**): i) the constitutively expressed EL222 fused to a transcriptional repressor domain (REP), and ii) a reporter module driving the expression of a reporter gene (*e.g.* Firefly luciferase, FLuc) under the control of a synthetic tripartite promoter. The promoter comprises a quintuple-repeat target sequence for EL222, termed $(C120)_5$, flanked by the enhancer sequence of the CaMV35S promoter and the minimal domain of the constitutive promoter hCMV.

We evaluated three versions of the blue light-repressor module by fusing either of three different known transrepressor domains to the N-terminus of EL222, one from the human Krüppel Associated Box (KRAB)[13,14] protein, and two from Arabidopsis, namely the B3 repression domain (BRD)[15] and the EAR repression domain (SRDX)[15] (**Fig. 2a**). The functionality of the $B_{Off}$ optoswitches was assayed by transient co-transformation with the reporter construct into Arabidopsis protoplasts. Constitutively expressed Renilla luciferase, RLuc, was included for normalization. The cells were illuminated for 18 h at different light intensities of blue light (0, 0.25, 0.5, 1, 5 and 10 µmol $m^{-2}$ $s^{-1}$), and FLuc/RLuc activity was quantified (**Fig. 2b**). These blue light

intensities had no negative effect on protoplast performance. All three versions of the repressor modules were functional although with different efficiencies, yielding a range of repression levels (SRDX, 92%; BRD, 84%; and KRAB, 53%; at 10 µmol $m^{-2}$ $s^{-1}$ blue light). Based on the highest repression level and dynamic range achieved, we decided to use SRDX-EL222 as a trans-repressor module for all subsequent experiments.

To allow gene induction with PULSE, we then combined the novel blue light-repressible ($B_{Off}$) module with our previously developed PhyB – PIF6 red light-inducible split transcription factor switch ($R_{On}$)[8,10] (**Fig. 3a**). PULSE thus integrates: i) a constitutively expressed red light-activation module composed of PhyB-VP16 and E-PIF6, ii) a constitutively expressed blue light-repressor module SRDX-EL222, and iii) a synthetic target promoter, $P_{Opto}$, integrating the binding domains for both switches, namely $(C120)_5$ and $(etr)_8$, upstream of a hCMV minimal promoter sequence driving the expression of a gene of interest. In the presence of blue or white light (a combination of blue, green, red and far-red wavelengths as present in ambient light) both photoreceptors PhyB and EL222 bind to $P_{Opto}$. The net result of the recruitment of the transcriptional activator and repressor near to the minimal promoter sets the system to the Off state. This also applies to darkness and far red-light conditions, as the red light-switch is rendered inactive under these wavelengths. Under any other illumination condition lacking the blue light component, SRDX-EL222 is unable to bind $P_{Opto}$ and thus to repress transcription. The system is, however, exclusively in the On state upon monochromatic red light-illumination when the interaction between PhyB and PIF6 leads to the recruitment of the activation domain to the minimal promoter inducing gene expression (**Fig. 3a**).

The PULSE system controlling FLuc expression was first introduced and tested in isolated Arabidopsis protoplasts (**Fig. 3b**). The plasmids coding for the $R_{on}$ switch were co-transformed either with or without $B_{Off}$, and the protoplasts were incubated for 18 h

under either red, blue, white or far-red light (as described in **Methods**). In the absence of the repressor module (equivalent to $R_{On}$), efficient activation of PhyB was observed by red light but also under blue and white, as UV and blue light (300 - 460 nm) also activate PhyB[16,17]. Upon addition of the $B_{Off}$ repressor module (PULSE system) we observed induction under red light treatment only, showing a high dynamic range, with up to 396.5-fold-induction rates relative to darkness, and a very low basal level of expression in blue and white light (1.7- and 1.6-fold, respectively).

**Development of a quantitative model to describe and predict the PULSE activity**

In order to quantitatively understand the dynamics and functional characteristics of PULSE and to guide the experimental design of future applications concerning optimal light quality, intensity, and duration, we developed an ordinary differential equations (ODE)-based quantitative mathematical model. To parameterize the quantitative model, we used kinetic mRNA and protein production data. The model was based on the following set of ODEs describing the changes in the molecule concentrations of the:

blue-light sensitive, closed LOV complex

$$\frac{\mathrm{d}[\mathrm{LOV}_{\mathrm{closed}}](t)}{\mathrm{dt}} = \quad k_{\mathrm{off,LOV}}\,[\mathrm{LOV}_{\mathrm{open}}] - k_{\mathrm{on,LOV}} I_{\mathrm{blue}}(t)[\mathrm{LOV}_{\mathrm{closed}}]. \qquad (1)$$

open LOV complex

$$\frac{\mathrm{d}[\mathrm{LOV}_{\mathrm{open}}](t)}{\mathrm{dt}} = -k_{\mathrm{off,LOV}}\,[\mathrm{LOV}_{\mathrm{open}}] + k_{\mathrm{on,LOV}}\, I_{\mathrm{blue}}(t)[\mathrm{LOV}_{\mathrm{closed}}]. \qquad (2)$$

active PhyB complex, sensitive to red and far-red light with different rates

lxxvi

$$\frac{d[PhyB_{fr}](t)}{dt} = k_{on,PhyB,red}\, I_{red}(t)\, [PhyB_r] - k_{off,PhyB,red}\, I_{red}(t)\, [PhyB_{fr}] + k_{on,PhyB,farred}\, I_{farred}(t)\, [PhyB_r] - k_{off,PhyB,farred}\, I_{farred}(t)\, [PhyB_{fr}] - k_{off,PhyB,dark}\, [PhyB_{fr}]. \quad (3)$$

inactive PhyB complex, sensitive to red and far-red light with different rates

$$\frac{d[PhyB_r](t)}{dt} = -k_{on,PhyB,red}\, I_{red}(t)\, [PhyB_r] + k_{off,PhyB,red}\, I_{red}(t)\, [PhyB_{fr}] - k_{on,PhyB,farred}\, I_{farred}(t)\, [PhyB_r] + k_{off,PhyB,farred}\, I_{farred}(t)\, [PhyB_{fr}] + k_{off,PhyB,dark}\, [PhyB_{fr}]. \quad (4)$$

mRNA of FLuc including basal transcription and degradation

$$\frac{d[FLuc_{mRNA}](t)}{dt} = b_{transcription} - k_{deg,FLuc_{mRNA}}\, [FLuc_{mRNA}] + \frac{k_{transcript}\, [PhyB_r]}{1 + k_{inh,LOV}{}^2\, [LOV_{open}]^2}. \quad (5)$$

FLuc protein including basal degradation

$$\frac{d[FLuc](t)}{dt} = k_{transl,FLuc}\, [FLuc_{mRNA}] - k_{deg,FLuc}\, [FLuc]. \quad (6)$$

Calibration of the model was performed using a maximum likelihood approach[17] with time-series mRNA and protein FLuc measurements (**Fig. 3c,d, Supplementary Fig. S1a**) as well as light dose-response FLuc measurements (**Supplementary Fig. S1b,c**). The **Supplementary Information** provides a more detailed derivation of the model equations, error measurements, system parameters estimations and uncertainty analysis performed using the Data2Dynamics framework[18].

To parameterize the model, On-Off kinetic studies of the PULSE system were performed in protoplasts of *A. thaliana* by monitoring FLuc protein and mRNA levels (**Fig. 3c,d**). Protoplasts transformed for PULSE-controlled FLuc expression were kept

in darkness for 12 h. Illumination was started and after 3 h of red light-treatment, the samples were divided and incubated for the next 13 h: either i) in red light to quantify sustained activation, ii) transferred to darkness to assess the passive reversion of the system, or iii) transferred to blue light to determine active shut down of the system (On-Off) (**Fig. 3c**). An increase of FLuc was observed under red light treatment while transfer to the dark or blue light led to termination of gene expression (faster and stronger under blue light). In addition, the latter samples (On-Off) were split after 6 h of blue light treatment further into blue and red light-incubation conditions (On-Off-On). Re-activation of gene expression was observed, demonstrating the reversibility of the system. Samples illuminated for the whole period (15 h) with blue light showed only background levels of expression. To determine mRNA kinetics (**Fig. 3d**), after transformation followed by 16 h of dark incubation, the protoplasts were illuminated for 4 h with red light and then transferred to blue light for additional 3 h. Samples were collected at the indicated time points and analyzed by RT-qPCR.

In order to further characterize thresholds of time and intensity of red light illumination for protein production, endpoint measurements and dose-response experiments were performed (**Supplementary Fig. S1a,b**). As little as 15 min of 10 µmol $m^{-2}$ $s^{-1}$ red light treatment or very low intensities of red light (0.25 µmol $m^{-2}$ $s^{-1}$ for 18 h) was observed to be sufficient to strongly activate expression. Similarly, a blue light dose-response study, while keeping the red illumination constant, indicated that blue light-mediated repression overrides red light-mediated activation effects (**Supplementary Fig. S1c**).

**Application of the mathematical model to predict the behaviour of PULSE**

Next, we used the parameterized model to predict the experimental gene expression outcomes of the system as a function of different light intensities, wavelengths and illumination times.

lxxviii

The dynamic behaviour of PULSE was simulated at different red light-doses and illumination times and in the absence of blue light (**Fig. 3e**), or upon simultaneous irradiation with different red and blue light intensities for 12 h (**Fig. Supplementary Fig. S2**). The resulting heatmaps will aid in the experimental design by guiding the targeted selection of conditions to obtain a given expression level of interest (**Fig. 3e,f, Supplementary Fig. S2**). To illustrate this, PULSE was transformed into protoplasts and kept 12 h in the dark prior to incubation under six different combinations of red light intensities and illumination durations selected from the heatmap (**Fig. 3e**). **Fig 3f** shows the experimental validation of the model predictions, namely the FLuc/RLuc ratio for the indicated experimental conditions. The two experimental conditions varied are the red light intensity and the time of continuous red light illumination. There is a strong correspondence between predicted and experimental FLuc/RLuc determined values ($\chi^2$ = 405.93, $p$ = 0.18) (**Fig. 3f**), which indicates the applicability of the model to determine the experimental conditions (light intensity and time ranges) needed to achieve a tight control over the levels of gene expression with PULSE.

**PULSE-controlled expression of CRISPR/Cas9-derived gene activator and plant transcription factors to regulate orthologous and endogenous promoters in Arabidopsis protoplasts**

We next set out to customize PULSE to achieve quantitative and temporally resolved control over the expression of genes from any given promoter of interest, be it orthologous, synthetic or endogenous (downstream activation). For this we devised two approaches applying PULSE: i) to induce the synthesis of a CRISPR/Cas9-derived gene activator, or ii) to induce expression of an endogenous TF. These expressed transcriptional activators, in turn, activate expression from a target orthologous promoter (**Fig. 4a,b**) or a target Arabidopsis promoter (**Fig. 4c-f**). The Cas9-derived

gene activator is targeted to its cognate promoter by an *ad-hoc* designed guide RNA, whereas the endogenous TF binds its natural target promoter.

*i) Optogenetic-controlled expression of a Cas9-derived gene activator*

To achieve optogenetic and customizable control of potentially any target promoter, PULSE was set to control expression of a nuclease-deficient *Streptococcus pyogenes* Cas9 protein fused to a strong activation domain (termed dCas9TV)[19,20]. In a first proof of principle application, PULSE-induced dCas9-TV was used to drive expression from the orthologous promoter, the *Solanum lycopersicum* dihydroflavonol 4-reductase promoter ($P_{SlDFR}$) using FLuc as a quantitative readout in Arabidopsis protoplasts (**Fig. 4a**). To target the promoter, a gRNA against the -150 bp region relative to the transcription start site (TSS) of $P_{SlDFR}$ was used[20]. PULSE-controlled dCas9-TV led to activation of the promoter only upon red illumination, achieving 24.5- and 40.0-fold induction rate compared to blue light and dark treatments, respectively (**Fig. 4b**). Constitutive expression of dCas9-TV served as a positive control yielding the maximum activation capacity of $P_{SlDFR}$, 105.1-fold induction relative to the configuration without dCas9-TV **(Supplementary Fig. S3a).** In a second set up, optogenetically-induced dCas9-TV targeted the promoter of the Arabidopsis gene APETALA1 ($P_{AtAP1}$) which includes the 5'UTR and 2781 bp upstream of the TSS fused to the reporter FLuc ($P_{AtAP1}$-FLuc) in a plasmid. A gRNA was designed to target the -100 bp region relative to the TSS of $P_{AtAP1}$ (**Fig. 4c**). Red light induction of dCas9-TV yielded 17.9- and 14.1-fold FLuc induction rates from the $P_{AtAP1}$-FLuc construct compared to blue and dark illumination (**Fig. 4e**). Constitutive expression of dCas9-TV yielded a 28.6-fold induction relative to the configuration without dCas9-TV (**Supplementary Fig. S3b**).

*ii) Optogenetically induced expression of the Arabidopsis transcription factor LEAFY*

For the second approach, we configured PULSE to drive the expression of the Arabidopsis transcription factor LEAFY (LFY) that is known to bind $P_{AtAP1}$ and promote the expression of AP1[21]. LFY and AP1 are involved in Arabidopsis flowering and both are expressed in the floral primordia. LFY was fused to the transactivator VP16 and RLuc using a self-cleaving 2A sequence, which yields equimolar amounts of both proteins from a single transcript[22] ($P_{Opto}$-LFY-VP16-2A-RLuc). The luminescence determination of RLuc allows the indirect quantification of the amount of LFY protein synthesized (**Fig. 4d**). The plasmids coding for PULSE were co-transformed in Arabidopsis protoplasts either with or without the optogenetically inducible LFY, and a $P_{AtAP1}$-FLuc target plasmid**.** RLuc luminescence values indicate expression of LFY-VP16 upon red light treatment, while only basal levels were obtained upon blue light or dark treatment (17.5- and 26.6-fold induction, respectively). The red light-induced expression of LFY-VP16 led to activation of $P_{AtAP1}$ and, therefore, FLuc expression achieving 31.4- and 7.4-fold induction rates compared to blue and darkness conditions, respectively (**Fig. 4f**, controls in **Supplementary Fig. S3c**; FLuc determinations of the configuration without LFY-VP16-2A-RLuc were used to quantify the background promoter levels and subtracted from the samples with LFY).

***In planta* optogenetic control of gene expression with PULSE**

We next set to evaluate the functionality of PULSE in plants. For this, a new set of vectors was first designed and constructed for transformation via *Agrobacterium tumefaciens* with all necessary components in one binary plasmid. The vectors comprise a reporter gene under the control of PULSE ($P_{Opto}$), PULSE expressed under a constitutive promoter (either $P_{CaMV35S}$ or $P_{AtUbi10}$), and optionally, a constitutively

expressed reporter gene as a normalization element and a plant selection cassette nptII which confers kanamycin resistance (for a full description of all vectors used see **Supplementary Table S1**).

*N. benthamiana* leaves were transformed with a construct having a fluorescent protein gene as a reporter (Venus fused to histone H2B for nuclear localization, $P_{Opto}$-Venus-H2B) placed under the control of PULSE. The performance of the system was analyzed using fluorescence microscopy. Constitutively expressed Cerulean fused to a nuclear localization sequence (NLS) was included as a marker for transformation. Infiltrated plants were placed in darkness for 2.5 days prior to illumination with red, blue, white light, or dark treatment. Samples were collected at different time points for analysis using confocal microscopy (**Fig. 5a** and **Supplementary Fig. S4**)**.** Plots were generated after determining the Venus and Cerulean mean fluorescence intensities in nuclei (**Fig. 5b**). We observed an increase over time in the Venus/Cerulean ratio only in samples illuminated with red light (28.7-fold induction after 9 h), demonstrating expected activation characteristics of the system *in planta*. Additionally, PULSE control over a β-glucuronidase gene ($P_{opto}$-GUS) is shown in **Supplementary Fig. S5**.

### *In planta* optogenetic induction of immunity and conditional subcellular fluorescent targeting of receptors

In plants, signal integration of extracellular stimuli is predominantly mediated by membrane-resident receptor and transport complexes. To mechanistically understand their function, we require non-invasive inducible systems that allow transcriptional induction or complex formation with high temporal precision in order to reconstitute these functional entities in homologous as well as heterologous systems. To test this, we asked whether PULSE allows the generation of immune-competent leaf epidermal cells by introducing a heterologous pattern recognition receptor.

In *Arabidopsis*, the recognition of the bacterial microbe-associated molecular pattern (MAMP) elf18 by the plant innate immune EF-Tu Receptor (EFR) results in a fast and transient increase in cellular reactive oxygen species (ROS)[23]. By contrast, Solanaceae species such as *N. benthamiana* are devoid of EFR and therefore unable to perceive the elf18 peptide. However, genetic transformation of *N. bethamiana* and tomato (*Solanum lycopersicum*) with *At*EFR allows these plants to recognize elf18 and confers increased resistance against phytopathogens such as *Ralstonia solanacearum*[23,24].

*Optogenetic control of plant immunity*

To achieve optogenetically controlled induction of immunity we expressed an EFR-GFP fusion protein under the control of PULSE ($P_{Opto}$-EFR-GFP) in *N. benthamiana* leaf epidermal cells (**Fig. 6a**). Illumination of leaves for 16 h with red light resulted in a clear GFP signal at the cell periphery indicating that EFR-GFP was successfully localized to the plasma membrane (**Supplementary Fig. S6**). To test whether optogenetically controlled EFR provides susceptibility of these cells towards elf18, we applied 1 μM of the elf18 ligand. Indeed, a strong and transient production of ROS was observed approximately 10 min after elf18 application in leaves that have been red light-treated (red filled circles; **Fig. 6b**). Quantitative assays showed 10-fold lower ROS burst triggered in white light-grown plants (black filled circles; **Fig. 6b**), demonstrating light-repression by PULSE under ambient light conditions. No responses were found in untransformed tissue and leaves expressing EFR but incubated in the absence of elf18. These data show that PULSE can be used for inducing physiological responses *in planta* in a time-controlled manner.

*Conditional targeting of receptors using nanobodies*

In mammalian cells, receptor complexes have been reconstituted and modulated using genetically encoded nanobodies[25,26]. Given their small size and their high-affinity

binding characteristics, nanobodies can be used to selectively target effector proteins to receptor complexes, to subcellularly relocalize proteins in a stimulus-dependent manner or to visualize endogenous proteins using fluorophore-tagged nanobodies. To test the applicability of PULSE for such experiments, we constitutively expressed the immune receptor EFR in *N. benthamiana* leaf epidermal cells and co-transformed a genetically encoded GFP nanobody (GFP binding protein, GBP) that binds GFP in plant cells[27]. To monitor receptor targeting, we additionally fused GBP to a mCherry fluorophore (GBP-mCherry). As the inducibility of effector delivery to receptor complexes will provide the basis for modulating their activity, PULSE provides a temporal control over GBP-mCherry expression ($P_{Opto}$-GBP-mCherry) and, therefore, conditionally controls nanobody targeting (**Fig. 6c**). While EFR-deficient cells illuminated with white light did not yield any detectable fluorescence, red light-induction of GBP-mCherry resulted in a cytosolic localization of the soluble protein. By contrast, red light-induced cells constitutively expressing EFR-GFP and co-transformed with $P_{Opto}$-GBP-mCherry showed an almost exclusive targeting of the fluorescently-tagged nanobody to the plasma membrane, indicating efficient binding of the GFP-tag by GBP (**Fig. 6d**). This demonstrates the ability to conduct time-resolved conditional targeting experiments by using a PULSE/nanobody combination allowing precision targeting of receptors and consequently modulating receptor complex composition and/or activity in future experiments.

**PULSE functionality in stable Arabidopsis transgenic lines**

To test the functionality of PULSE in whole plants, transgenic Arabidopsis lines were generated using the plasmids coding for PULSE and $P_{Opto}$-FLuc as a reporter. Different versions were engineered with either of two constitutive promoters controlling the expression of the three light switchable elements of PULSE, either $P_{CaMV35S}$ (BM00654)

or $P_{AtUbi10}$ (BM00655). Seedlings of homozygous T3 plants were grown in media in a multi-well plate for 7 days, were incubated with luciferin and the luminescence was quantified while the plate was subjected to different light treatments as indicated in **Fig. 6e**. Results for three independent PULSE lines (two with the $P_{CaMV35S}$ and one with the $P_{AtUbi10}$ promoters) show different levels of expression with activation levels ranging from 10- to 372-fold, depending on the choice of promoters driving PULSE expression and the integration event of the transgene. For all lines, transfer from simulated white light to red light led to activation of expression, and subsequent reversion was achieved when the plants were moved back to white light (**Fig. 6e**), demonstrating reversibility of the system. This is the first example of an optogenetic tool controlling gene expression in whole plants, opening up unforeseen opportunities for plant research and biotechnology.

## DISCUSSION

In this work, we pioneer the optogenetic control of gene expression in plants and apply it to manipulate synthetic and endogenous signalling pathways.

In order to study and understand cellular processes, it is required to be able to achieve precise spatiotemporal and quantitative control over their regulation. Genetically encoded chemical-inducible systems have been widely employed for the targeted manipulation of gene expression and other signalling events in prokaryotic and diverse eukaryotic organisms, including plants[28–30]. However, they suffer from intrinsic drawbacks including limited temporal and spatial resolution due to the reduced availability of highly specific promoters, diffusion effects, and constrains to deactivate the system after the application of the inducer, in addition to potential pleiotropic activity and toxicity. Some of these experimental constraints can be solved by using light as an inducer. In this direction, recently, an optogenetic approach was developed to

overcome a plant intrinsic physiological conundrum. Namely, how to conserve water under hydric stress by minimizing transpiration, when this actually leads to a simultaneous reduction in the availability of the carbon source for photosynthesis – $CO_2$ – due to the fact that both water and $CO_2$ use the same gate for atmospheric exchange, the stomata. Genetic and molecular approaches used until now were not capable of improving water use efficiency without paying a cost at the level of carbon assimilation. Papanatsiou *et al.*[31] hypothesized that by enhancing the performance of an endogenous process, i.e. improving stomatal response inducing a synergistic, faster response to changes of light, plants would be able to cope with a varying environment. For this, they resorted to a synthetic, blue light-gated $K^+$ channel (BLINK1), engineered by integrating the LOV2-J$\alpha$ domain from *Avena sativa* phototropin 1 with the viral Kcv channel for the control of $K^+$ conductance in animal cells[32]. It was placed under the control of a tissue-specific promoter for guard cell expression in Arabidopsis plants. BLINK1 led to accelerated kinetics, with a reduction of mean stomatal opening and closure half-life times by 40-70% in comparison to wild type controls (specific full activation after 2 min in blue light and inactivation upon 8-10 min in the dark). Faster stomatal movements improved gas exchange efficiency under fluctuating light conditions, resulting in more efficient water use without a trade-off in carbon assimilation. This tool profits from the fact that it is applied to a process that is photosynthesis-dependent therefore occurring already naturally under ambient light.

The introduction of a broad set of optogenetic tools and approaches is currently revolutionizing fundamental and applied animal research. A plant´s requirement for light to grow, however, limits the implementation of optogenetic approaches, as ambient light leads to undesired activation of most currently available light-controlled systems. Consequently, most of the optogenetic tools are simply not applicable in plants.

lxxxvi

We set here to engineer an optogenetic device for the control of gene expression in plants that overcomes these challenges, namely, that is non-responsive to ambient illumination conditions and can be activated by illuminating with a specific, narrow wavelength spectrum. The novel conceptual approach implements the design of a dual-wavelength optogenetic switch combining a blue light-regulated repressor with a red light-inducible gene expression switch. In this way, PULSE shuts expression off under ambient light, and induces transcription under red light only. In darkness the system is otherwise off.

PULSE introduces the superior experimental assets of optogenetic systems into plants. The system showed a high dynamic range in Arabidopsis protoplasts with approximately a 400-fold (red light vs. darkness) induction, reversibility and no toxicity. PULSE is applicable for the targeted study of signalling and metabolic networks by, in principle, allowing the control of any endogenous or synthetic promoter of interest. This was exemplified with the light-driven expression of an endogenous TF, which in turn activates expression of its target promoter, or upon the use of a CRISPR/Cas9-derived transcriptional activator. *In planta*, implementation of PULSE demonstrated tight temporal control over subcellular conditional protein targeting, and the capability to induce immunity in *N. benthamiana* leaves. We show that the system is functional in Arabidopsis whole plants to control the expression of a transgene. It shows high dynamic ranges of expression when activated with red light and the expression is terminated upon returning the plants to white light showing that the system is reversible. The transgenic PULSE lines are viable and the transgenes stable (T3 generation). PULSE could in the future be combined with tissue-specific promoters for organ or developmentally specific expression and activity, as currently done for genetically encoded biosensors and other tools. When using different promoters, the

dynamic range of induction might be affected (**Fig 6e**), therefore possibly making usage-specific optimizations necessary.

It is worth noting that by using only the N-terminus of PhyB (amino acids 1-650) and the first 100 amino acids of PIF6, we intend to minimize potential interactions of the system with endogenous plants components (EL222 is of bacterial origin, therefore, we do not expect any considerable effect on plant signalling). However, we cannot rule out a possible cross-talk with the endogenous signalling (PhyB) pathway when introducing PULSE into plants, this is an unavoidable cost to pay in exchange of getting a new functionality as it is also the case when using chemically inducible switches or genetically encoded biosensors, *e.g.* auxin DII-Venus sensor[33]. All in all, this is the first example of an optogenetic tool controlling gene expression applied *in planta*, showing the potential of the switch for future applications.

This work reflects the ground-breaking opportunities for plant fundamental and biotechnological fields provided by optogenetics. Due to the high quantitative modulation, spatiotemporal resolution and the reversible control capabilities provided, we think that a generalized application of PULSE will facilitate the targeted manipulation and study of biological processes including plant development, metabolic engineering, hormone perception and signalling, and stress responses.

## METHODS

### Plasmid construction

A description of the plasmid construction can be found in **Supplementary Table S1.** DNA fragments were released by restriction from existing plasmids, amplified by PCR using primers synthesized by Sigma Aldrich or Eurofins genomic (listed in **Supplementary Table S2**), or synthesized by GeneArt, Invitrogen. The PCR reactions were performed using Q5 High-Fidelity DNA Polymerase (New England Biolabs). Gel extractions were performed using NucleoSpin® Gel and PCR Clean-up kit (Macherey-Nagel), or Zymoclean Gel DNA Recovery Kit (Zymo Research). Assemblies were performed using either Gibson[34], AQUA[35], GoldenBraid[36] or Golden Gate[37,38] cloning methods prior to transformation into chemically competent *Escherichia coli* strain 10-beta (NEB) or TOP10 (Invitrogen). The plasmid purifications were performed using Wizard® Plus SV Minipreps DNA Purification Systems (Promega), NucleoBond® Xtra Midi kit (Macherey-Nagel) or GeneJET Plasmid Miniprep Kit (Thermo Scientific). All preparations were tested by restriction enzyme digests and sequencing (GATC-biotech/SeqLab). All restriction enzymes were purchased from New England Biolabs or Thermo Scientific.

### Arabidopsis protoplast isolation and transformation

Protoplasts were isolated from two- to three-week-old *Arabidopsis thaliana* plantlet leaves, grown on 12 cm square plates containing SCA medium (0.32 % (w/v) Gamborg B5 basal salt powder with vitamins (bioWORLD), 4 mM $MgSO_4 \cdot 7H_2O$, 43.8 mM sucrose and 0.8% (w/v) phytoagar in $H_2O$, pH 5.8, autoclaved, 0.1 % (v/v) Gamborg B5 Vitamin Mix (bioWORLD), in a 23 °C, 16 h light - 8 h dark regime. A floatation method was employed for isolation and the plasmids were transferred by polyethylene glycol-mediated transformation as described before[10]. Shortly, plant leaf material was sliced with a scalpel and incubated in dark at 23 °C overnight in MMC solution (10 mM

MES, 40 mM $CaCl_2 \cdot H_2O$, mannitol 85 g $L^{-1}$, pH 5.8, sterile filtered) containing 0.5 % cellulase Onozuka R10 and macerozyme R10 (SERVA Electrophoresis GmbH). After release of the protoplasts with a pipette, the suspension was transferred to a MSC solution (10 mM MES, 0.4 M sucrose, 20 mM $MgCl_2 \cdot 6H_2O$, 85 g $L^{-1}$ mannitol, pH 5.8, sterile filtered) and overlaid with MMM solution (15 mM $MgCl_2$, 5 mM MES, 85 g $L^{-1}$ mannitol, pH 5.8, sterile filtered). The protoplasts were collected at the interphase and transferred to a W5 solution (2 mM MES, 154 mM NaCl, 125 mM $CaCl_2 \cdot 2H_2O$, 5 mM KCl, 5 mM glucose, pH 5.8, sterile filtered) prior to counting in a Rosenthal chamber. Mixtures of the different plasmids, as described in the figures, to a final amount of 30-35 µg DNA were used to transform 500,000 protoplasts by dropwise addition of a PEG solution (4 g $PEG_{4000}$, 2.5 mL of 0.8 M mannitol, 1 mL of 1 M $CaCl_2$ and 3 mL $H_2O$). After 8 min incubation, 120 µL of MMM and 1,240 µL of PCA (0.32 % (w/v) Gamborg B5 basal salt powder with vitamins (bioWorld)), 2 mM $MgSO_4 \cdot 7H_2O$, 3.4 mM $CaCl_2 \cdot 2H_2O$, 5 mM MES, 0.342 mM L-glutamine, 58.4 mM sucrose, 80 g $L^{-1}$ glucose, 8.4 µM Ca-panthotenate, 2 % (v/v) biotin from a biotin solution 0.02 % (w/v) 0.1 % (v/v) in $H_2O$, pH 5.8, sterile filtered, 0.1 % (v/v) Gamborg B5 Vitamin Mix, 64.52 µg $µL^{-1}$ ampicillin) were added to get a final volume of 1.6 mL of protoplast suspension.

After transformation, protoplasts were then divided in different 24-well plates in 960 µL aliquots (300,000 protoplasts-necessary to measure six technical replicates for both FLuc and RLuc) or in 640 µL aliquots (200,000 protoplasts-necessary to measure 4 technical replicates for both FLuc and RLuc). Afterwards, the plates were either illuminated with LED arrays with the appropriate wavelength and intensity (as indicated in the figures) for 18 - 20 h at 19 - 23 °C unless indicated otherwise.

**Illumination conditions**

Custom made LED light boxes were used as described before[10,39]. The panels contain LEDs from Roithner: blue (461 nm), red (655 nm), far-red (740 nm) and white LEDs

(4000K). For blue, red or far-red light treatment, the intensity was adjusted to 10 µmol $m^{-2}$ $s^{-1}$ unless indicated otherwise. White LEDs were supplemented with blue and far-red LEDs in order to have an equivalent ratio of blue, red and far-red light similar to the sunlight spectra (simulated white light)**.** The intensity of the white light LED was adjusted to 10 µmol $m^{-2}$ $s^{-1}$ for the following wavelength ranges: blue 420 - 490 nm, red 620 - 680 nm, and far-red 700 - 750 nm[40] (see spectra shown in **Supplementary Fig. S7)**. For the *Nicotiana benthamiana* GUS experiment the plants were kept, prior light treatment, in the plant incubator with fluorescent tubes (cool daylight, OSRAM). Cell- and plant- handling and sampling were done, when needed, under green LED (510 nm) light which does not affect the PULSE system. Spectra and intensities were obtained with a spectroradiometer (AvaSpec-ULS2048 with fiber-optic FC-UVIR200-2, AVANTES).

**Luciferase protoplasts assay**

Firefly (FLuc) and Renilla luciferase (RLuc) activities were quantified in intact protoplasts as detailed elsewhere[10]. Six technical replicates of 80 µL protoplast suspensions (approximately 25,000 protoplasts) were pipetted into two separate 96-well white flat-bottom plates (Costar) for simultaneous parallel quantification of both luciferases. Addition of 20 µL of either FLuc substrate (0.47 mM D-luciferin (Biosynth AG), 20 mM tricine, 2.67 mM $MgSO_4 \cdot 7H_2O$, 0.1 mM $EDTA \cdot 2H_2O$, 33.3 mM dithiothreitol, 0.52 mM adenosine 5′-triphosphate, 0.27 mM acetyl–coenzyme A, 5 mM NaOH, 264 µM $MgCO_3 \cdot 5H_2O$, in $H_2O$, pH 8), or RLuc substrate (0.472 mM coelenterazine stock solution in methanol, diluted directly before use, 1:15 in phosphate buffered saline, PBS) was performed prior luminescence determination in a plate reader (determination of 20 min kinetics, integration time 0.1 s). RLuc luminescence was measured with a BertholdTriStar2 S LB 942 multimode plate reader and FLuc luminescence was determined with a Berthold Centro XS3 LB 960 microplate

luminometer. When applicable, FLuc/RLuc was determined and the average of the replicates and SEM was plotted (*n* = 4 - 6).

**RNA isolation and quantitative RT-qPCR**

Protoplasts were isolated and transformed as described before. The protoplasts were kept in the dark, at room temperature for 16 h prior illumination treatment. At the indicated time point and illumination condition, samples containing ca. $10^6$ protoplasts were collected by centrifugation (10 min, 100 *g*) and were frozen in liquid $N_2$ for posterior RNA extraction. The RNA was extracted with a PeqGold Plant RNA kit following the user specifications. The samples were treated with DNase I (Thermo Scientific). The cDNA was synthesized from 500 ng of the RNA samples, using the Revert Aid Reverse Transcriptase (Thermo Scientific) and diluted 1:100 prior to qPCR. Expression levels on the samples were measured in duplicates using SYBR® Green Master Mix (Bio-Rad) with specific primer pairs in a Real-time PCR cycler CFX96 (Bio-Rad) as described before[41]. A DNA mass standard for each gene was prepared in serial dilutions of $10^2$ to $10^7$ copies and measured in parallel with the samples. The genes Tip41-like family protein, Tip41L (*At4g34270*), and elongation factor, EF (*At5g19510*), were used as internal reference genes. Starting quantity values of the samples were calculated using the mass standard curve and normalized with the reference genes. Primer pairs used to amplify the DNA mass standard were oROF422/oROF423 for FLuc, oROF518/oROF519 for Tip41L, and EF STD 5'/3'[41] for EF. Specific primer pairs used for the qPCR were oROF424/oROF425 for the FLuc cDNA, oROF514/oROF515 for Tip41L cDNA, and EFc RT 5'/3'[41] for EF cDNA (**Supplementary Table S2**).

***Agrobacterium tumefaciens* transformation**

Electro-competent *Agrobacterium tumefaciens* strains C58 (pM90), GV3101 (pM90), containing pSOUP helper plasmid, or AGL1 was transformed with the plasmid of interest. Clones growing in YEP media (10 g $L^{-1}$ yeast extract, 10 g $L^{-1}$ bacto peptone, 5 g $L^{-1}$ NaCl, pH 7.0) supplemented with appropriate antibiotics were selected and

each transcriptional unit was confirmed by colony PCR using Q5 DNA polymerase (New England Biolabs).

**Transient transformation of *Nicotiana benthamiana* plants**

*A. tumefaciens* cultures were adjusted to $OD_{600nm}$ = 0.1 - 0.2 in infiltration medium (10 mM $MgCl_2$,10 mM MES, 200 µM acetosyringone, in $H_2O$, pH 5.6). The cultures were mixed in a volume ratio 1:1 with an *A. tumefaciens* culture coding for the RNA silencing suppressor p19. The cultures were incubated for 3 h at room temperature in the dark prior infiltration through the adaxial part of leaves from 4- to 5-week old *N. benthamiana* grown in the greenhouse as described before[42]. The plants were incubated for 2-3 days in the indicated illumination conditions prior to light treatment and analysis by microscopy or enzymatic GUS reporter assay.

**GUS reporter assay in *Nicotiana benthamiana* leaves**

After the illumination of the plants as depicted in the **Supplementary Fig. S5**, two disks of 0.8 cm diameter from different leaves for each illumination treatment were cut and incubated on GUS substrate (100 mM $Na_2HPO_4$, 100 mM $NaH_2PO_4$, adjusted to pH 7.0, 2 mM $K_3Fe(CN)_6$, 2 mM $K_4Fe(CN)_6$, 2 mM X-Gluc, 0.20 % Triton X-100, in $H_2O$) for 3 h at 37°C in dark[43]. The stained disks were washed several times with 70% ethanol to remove the chlorophylls and the pictures were taken with a Nikon D3200 camera.

**Confocal imaging of *Nicotiana benthamiana* leaf material**

For the experiments of optogenetically controlled Venus, transformed plants were incubated for 2.5 days in the dark and afterwards illuminated for 2 h, 6 h or 9 h with the appropriate wavelength as indicated in **Fig. 5a,b** and imaged with a LSM 780 Zeiss laser scanning confocal microscope. The constitutive Cerulean was excited with a Diode 405-30 at 405 nm. The optogenetically controlled Venus expression was excited with an Argon laser at 514 nm. The emission was detected at 440-500 nm for Cerulean

and 516-560 nm for Venus. The fluorescence intensities of nuclei were quantified using ImageJ. For each nucleus, an area was selected by using the elliptical selection tool and the mean grey values of the Cerulean and Venus channels were measured, respectively. The ratio of Venus and Cerulean was calculated and expressed in percentage, and plotted for 12 - 34 nuclei.

For the experiments of conditional targeting and immunity control, *N. benthamiana* were grown for 2 d in 16 h simulated white light – 8 h dark cycle (see **Supplementary Fig. S7**), hereafter half of the plants were grown for 16 h in red light only to induce expression (red light-induced), the other half were grown in simulated white light for 16 h (white light control). The white light control plants were further grown for 16 h after the experiments in red light to induce expression as control for successful transformation. Samples were taken for confocal observation. Confocal laser scanning microscopy was performed with a Leica SP8 confocal microscope using a 20×/0.75 HC PL APO CS IMM CORR lens with a scanning speed of 200 Hz. EFR-GFP and GBP-mCherry were excited with a white light laser at 488 nm and 561 nm, respectively. The emission was detected at 500 - 550 nm for GFP and 575 - 630 nm for mCherry.

**Reactive oxygen species (ROS) burst assay**

Samples were collected from *N. benthamiana* leaves transformed with the indicated constructs or only infiltration buffer (two plants were used for each illumination treatment). ROS production was determined using a BMG CLARIOstar plate reader and following the protocol by Trujillo *et al.* [44] for Arabidopsis leaves with the following modifications: samples were prepared with a 4 mm biopsy puncher and placed in 150 µL sterile tap water for 3 h in dark to get rid of any ROS production originating from the sample harvest before elf18 or control treatment. Approximately 20 min before addition of 1 µM elf18, water was removed from leaf samples and replaced with reaction solution[44], incubated for *ca.* 3 min before background measurement of ROS production

was performed for *ca*. 15 min followed by addition of reaction solution with elf18 or without (mock control).

**Stable transformation of *Arabidopsis thaliana***

Four to five week old *A. thaliana* ecotype Columbia plants grown in a plant chamber (16 h light – 8 h dark, 22°C) were transformed via *Agrobacterium tumefaciens* by floral dip as described earlier[45] with minor modifications. Agrobacterium cells transformed with the corresponding plasmids were grown to $OD_{600nm}$ values between 0.6 and 0.9, centrifuged and gently resuspended in 2.4 g/L Murashige & Skoog medium including vitamins (Duchefa Biochemie), 5% (w/v) sucrose, 0.05% (v/v) Silwet L-77 (bioWORLD) and 222 nM 6-Benzylaminopurine (Duchefa Biochemie).

Transformants were selected by seeding in SCA plates (0.32 % (w/v) Gamborg B5 basal salt powder with vitamins (bioWORLD), 4 mM $MgSO_4 \cdot 7H_2O$, 43.8 mM sucrose, 0.8 % (w/v) phytoagar, 0.1 % (v/v) Gamborg B5 Vit Mix (bioWORLD), pH 5.8) containing 30 µg $mL^{-1}$ kanamycin (Duchefa Biochemie) and 150 µg $mL^{-1}$ ticarcillin disodium/potassium clavulanate (Duchefa Biochemie). The positive T1 plants were checked for expression of the reporter/normalization gene when possible, and the T2 seeds were collected and selected in kanamycin containing media. The lines exhibiting a segregation ratio 3:1 (resistant to sensitive) were propagated to a T3 generation and homozygous lines were selected and used for further experiments.

**Luciferase assay in *Arabidopsis thaliana* plants**

Seeds (*n* = 26 - 28 for the PULSE lines, *n* = 6 - 8 for the controls) from every *A. thaliana* line were seeded in individual wells of white 96-well white flat-bottom plates (Costar), containing 200 µL of 2.4 g $L^{-1}$ Murashige & Skoog medium including vitamins (M0222, Duchefa Biochemie ) and 0.8 % (w/v) phytoagar (bioWORLD). They were kept for 3 - 4 days at 4°C in the dark, and illuminated for 1 h with simulated white light (see spectra

in **Supplementary Fig. S7**) on the fourth day. Then the plate was placed in simulated white light with photoperiod (16 h light – 8 h dark) for 4 days. Addition of 20 µL of FLuc substrate 1.667 mM D-luciferin (from a 20 mM stock in DMSO, Biosynth AG) and 0.01 % Triton in $H_2O$ was performed on the fourth day prior to starting the measurements. The plate was sealed with an optically clear film (Sartedt) thinly perforated. Luminescence was measured, 1 - 2 days after addition of the substrate, in a Berthold Centro XS3 LB 960 microplate reader every hour during several days (1 min delay, 0.5 integration time) while being illuminated as indicated. Seedlings that did not germinate were excluded. The background readout levels of Arabidopsis wildtype seedlings were averaged, and the value was subtracted from the rest of the lines for each time point.

**Statistical analysis**

Data shown in the figures are representative experiments, the sample number per experiment is indicated in each corresponding figure. Plotting and statistical tests were performed with GraphPad software.

**Acknowledgments**

This study was supported by the German Research Foundation (DFG) under Germany's Excellence Strategy/Initiative (CEPLAS – EXC-1028 Project ID 194465578 to RS and MDZ, EXC-2048/1 – Project ID 390686111 to RS and MDZ, CIBSS – EXC-2189 – Project ID 390939984 to TO, JT and WW, and BIOSS – EXC-294 to TO and WW), the iGRAD Plant (IRTG 1525 to ROF, JS, RS, MDZ), and the Collaborative Research Center SFB924 (INST 95/1126-2; project B4 to TO). JBM is supported by a fellowship from the Eastern Academic Research Consortium. We thank Diego Orzaez for kindly providing the GoldenBraid plasmids, Tzvetina Brumbarova for aid on RT-qPCR experiments, Reinhild Wurm and Michaela Gerads for technical assistance, and Jürgen Schmidt (Technical Workshop, University of Freiburg) for designing and

constructing the light boxes used in this work. We are indebted to Jorge Casal, Dmitri Nusinow, Sofia Romero and Uriel Urquiza for careful reading and suggestions to improve the manuscript.

**Author Contributions**

ROF, NBA, LAK, BM, and SB designed and cloned the constructs. SB performed preliminary tests and ROF conducted all Arabidopsis protoplasts experiments. FGW and RE developed the mathematical model. ROF, NBA, JS, and LAK contributed to the establishment of PULSE *in planta*. NBA conducted the conditional targeting and immunity induction *in planta*. ROF and GG generated the transgenic Arabidopsis PULSE lines and performed the experiments. ROF, NBA, TO, RS, and MDZ designed the experiments. JT, WW, TO, RS, MDZ supervised the research. TO, RS, and MDZ analyzed the data and discussed results. MDZ planned and directed the project. ROF and MDZ designed the system and wrote the initial manuscript with input from all authors. All authors contributed to editing and read the final version of the manuscript.

**Competing interests**

The authors declare no competing interests.

**References**

1. Deisseroth, K. & Hegemann, P. The form and function of channelrhodopsin. *Science* **357**, eaan5544 (2017).
2. Alberio, L. *et al.* A light-gated potassium channel for sustained neuronal inhibition. *Nat. Methods* **15**, 969–976 (2018).
3. Ye, H., Baba, M. D.-E., Peng, R.-W. & Fussenegger, M. A Synthetic Optogenetic Transcription Device Enhances Blood-Glucose Homeostasis in Mice. *Science* **332**, 1565 (2011).
4. Strickland, D. *et al.* TULIPs: tunable, light-controlled interacting protein tags for cell biology. *Nat. Methods* **9**, 379–84 (2012).
5. Shin, Y. *et al.* Spatiotemporal Control of Intracellular Phase Transitions Using Light-Activated optoDroplets. *Cell* **168**, 159-171.e14 (2017).
6. van Bergeijk, P., Adrian, M., Hoogenraad, C. C. & Kapitein, L. C. Optogenetic control of organelle transport and positioning. *Nature* **518**, 111–4 (2015).
7. Kolar, K., Knobloch, C., Stork, H., Žnidarič, M. & Weber, W. OptoBase: A Web Platform for Molecular Optogenetics. *ACS Synth. Biol.* **7**, 1825–1828 (2018).
8. Müller, K. *et al.* A red light-controlled synthetic gene expression switch for plant systems. *Mol Biosyst* **10**, 1679–88 (2014).
9. Chatelle, C. *et al.* A Green-Light-Responsive System for the Control of Transgene Expression in Mammalian and Plant Cells. *ACS Synth. Biol.* **7**, 1349–1358 (2018).
10. Ochoa-Fernandez, R. *et al.* Optogenetics: Methods and Protocols. in (ed. Kianianmomeni, A.) 125–139 (Springer New York, 2016). doi:10.1007/978-1-4939-3512-3_9.
11. Nash, A. I. *et al.* Structural basis of photosensitivity in a bacterial light-oxygen-voltage/helix-turn-helix (LOV-HTH) DNA-binding protein. *Comput. Biol.* **108**, 9449–945 (2011).

12. Motta-Mena, L. B. *et al.* An optogenetic gene expression system with rapid activation and deactivation kinetics. *Nat. Chem. Biol.* **10**, 196–202 (2014).
13. Moosmann, P., Georgiev, O., Thiesen, H., Hagmann, M. & Schaffner, W. Silencing of RNA polymerases II and III-dependent transcription by the KRAB protein domain of KOX1, a Krüppel-type zinc finger factor. *Biol. Chem.* **378**, 669–677 (1997).
14. Baaske, J. *et al.* Dual-controlled optogenetic system for the rapid down-regulation of protein levels in mammalian cells. *Sci. Rep.* **8**, 15024 (2018).
15. Ikeda, M. & Ohme-Takagi, M. A novel group of transcriptional repressors in Arabidopsis. *Plant Cell Physiol.* **50**, 970–975 (2009).
16. Kelly, J. M. & Lagarias, J. C. Photochemistry of 124-kilodalton Avena phytochrome under constant illumination in vitro. *Biochemistry* **24**, 6003–6010 (1985).
17. Müller, K. *et al.* Multi-chromatic control of mammalian gene expression and signaling. *Nucleic Acids Res.* **41**, e124 (2013).
18. Raue, A. *et al.* Data2Dynamics: a modeling environment tailored to parameter estimation in dynamical systems. *Bioinformatics* **31**, 3558–3560 (2015).
19. Li, Z. *et al.* A potent Cas9-derived gene activator for plant and mammalian cells. *Nat. Plants* **3**, 930–936 (2017).
20. Selma, S. *et al.* Strong gene activation with genome-wide specificity using a new orthogonal CRISPR/Cas9-based Programmable Transcriptional Activator. *bioRxiv* 486068 (2018) doi:10.1101/486068.
21. Simon, R., Igeño, M. I. & Coupland, G. Activation of floral meristem identity genes in Arabidopsis. *Nature* **384**, 59–62 (1996).
22. de Felipe, P. *et al. E unum pluribus*: multiple proteins from a self-processing polyprotein. *Trends Biotechnol.* **24**, 68–75 (2006).
23. Zipfel, C. *et al.* Perception of the Bacterial PAMP EF-Tu by the Receptor EFR Restricts Agrobacterium-Mediated Transformation. *Cell* **125**, 749–760 (2006).

24. Lacombe, S. *et al.* Interfamily transfer of a plant pattern-recognition receptor confers broad-spectrum bacterial resistance. *Nat. Biotechnol.* **28**, 365 (2010).
25. Kirchhofer, A. *et al.* Modulation of protein properties in living cells using nanobodies. *Nat. Struct. Mol. Biol.* **17**, 133 (2009).
26. Gulati, S. *et al.* Targeting G protein-coupled receptor signaling at the G protein level with a selective nanobody inhibitor. *Nat. Commun.* **9**, 1996 (2018).
27. Schornack, S. *et al.* Protein mislocalization in plant cells using a GFP-binding chromobody. *Plant J.* **60**, 744–754 (2009).
28. Moore, I., Samalova, M., Kurup, S., For, T. & Analysis, M. Transactivated and chemically inducible gene expression in plants. *Plant J.* **45**, 651–683 (2006).
29. Zuo, J. & Chua, N. H. Chemical-inducible systems for regulated expression of plant genes. *Curr. Opin. Biotechnol.* **11**, 146–151 (2000).
30. Andres, J., Blomeier, T. & Zurbriggen, M. D. Synthetic Switches and Regulatory Circuits in Plants. *Plant Physiol.* **179**, 862–884 (2019).
31. Papanatsiou, M. *et al.* Optogenetic manipulation of stomatal kinetics improves carbon assimilation, water use, and growth. *Science* **363**, 1456–1459 (2019).
32. Cosentino, C. *et al.* Engineering of a light-gated potassium channel. *Science* **348**, 707–710 (2015).
33. Brunoud, G. *et al.* A novel sensor to map auxin response and distribution at high spatio-temporal resolution. *Nature* **482**, 103–106 (2012).
34. Gibson, D. G. *et al.* Enzymatic assembly of DNA molecules up to several hundred kilobases. *Nat. Methods* **6**, 343 (2009).
35. Beyer, H. M. *et al.* AQUA Cloning: A Versatile and Simple Enzyme-Free Cloning Approach. *PLoS ONE* **10**, e0137652 (2015).
36. Sarrion-Perdigones, A. *et al.* GoldenBraid 2.0: A Comprehensive DNA Assembly Framework for Plant Synthetic Biology. *Plant Physiol.* **162**, 1618 (2013).

c

37. Binder, A. *et al.* A Modular Plasmid Assembly Kit for Multigene Expression, Gene Silencing and Silencing Rescue in Plants. *PLoS ONE* **9**, e88218 (2014).

38. Weber, E., Engler, C., Gruetzner, R., Werner, S. & Marillonnet, S. A Modular Cloning System for Standardized Assembly of Multigene Constructs. *PLoS ONE* **6**, e16765 (2011).

39. Müller, K., Zurbriggen, M. D. & Weber, W. Control of gene expression using a red- and far-red light–responsive bi-stable toggle switch. *Nat. Protoc.* **9**, 622 (2014).

40. Sellaro, R. *et al.* Cryptochrome as a Sensor of the Blue/Green Ratio of Natural Radiation in Arabidopsis. *Plant Physiol.* **154**, 401 (2010).

41. Bauer, P. Regulation of iron acquisition responses in plant roots by a transcription factor: Regulation of Iron Acquisition Responses. *Biochem. Mol. Biol. Educ.* **44**, 438–449 (2016).

42. Vazquez-Vilar, M. *et al.* GB3.0: a platform for plant bio-design that connects functional DNA elements with associated biological data. *Nucleic Acids Res.* **45**, 2196–2209 (2017).

43. Naranjo-Arcos, M. A. *et al.* Dissection of iron signaling and iron accumulation by overexpression of subgroup Ib bHLH039 protein. *Sci. Rep.* **7**, 10911 (2017).

44. Trujillo, M. Analysis of the Immunity-Related Oxidative Bursts by a Luminol-Based Assay. in *Environmental Responses in Plants: Methods and Protocols* (ed. Duque, P.) 323–329 (Springer New York, 2016). doi:10.1007/978-1-4939-3356-3_26.

45. Clough, S. J. & Bent, A. F. Floral dip: A simplified method for *Agrobacterium*-mediated transformation of *Arabidopsis thaliana*. *Plant J.* **16**, 735–743 (1998).

**Figure Legends**

**Fig. 1.** Design of PULSE, a functional optogenetic system for the control of gene expression in plants grown under light/dark cycles. Plants require light to grow and this poses an experimental challenge to the implementation of optogenetic switches in plants as they will be activated under ambient conditions. To avoid this issue, we designed PULSE (Plant Usable Light Switch-Element), an optogenetic tool that combines a blue light-regulated repressor ($B_{Off}$) with a red light-inducible gene-expression switch ($R_{On}$). In this way gene expression is active only upon illumination with monochromatic red light, while remaining inactive in darkness and under blue, far-red, and white light, hence being applicable to plants grown under day/night cycles. (+), presence; (-), absence.

**Fig. 2**: Design and characterization of the blue light-regulated gene repression switch ($B_{Off}$) in Arabidopsis protoplasts**. (a)** Constructs and mode of function. The components engineered and characterized in plant cells are: i) the blue light-responsive *E. litoralis* photoreceptor EL222 fused to either of three different repressor (REP-EL222) domains: KRAB, BRD, SRDX and placed under the control of the constitutive promoter $P_{CaMV35S}$, ii) a synthetic promoter composed of the enhancer region of $P_{CaMV35S}$, five repeats of C120 - $(C120)_5$ - and a minimal promoter $P_{hCMV}$, driving the expression of the reporter gene FLuc, and iii) $P_{CaMV35S}$ driving the constitutive expression of the normalization element RLuc. The transcription factor EL222 has a Light-Oxygen-Voltage (LOV) dependent domain and a Helix-Turn-Helix (HTH) domain. The photoreceptor is folded in the dark due to a flavin-protein adduct and incapable of binding to the $(C120)_5$ element. As a result, expression of FLuc is constitutively active. Upon blue light illumination REP-EL222 unfolds allowing the formation of dimers

cii

binding to the $(C120)_5$ element via the HTH. As a result, the initiation of FLuc transcription is repressed**. (b)** Characterization of the system. Arabidopsis protoplasts were transformed with the reporter module (pROF402) and the blue light-responsive element (photoreceptor, EL222) fused to either repressor: KRAB (pROF018), BRD (pROF050), and SRDX (pROF051) or without the optoswitch (Ø, stuffer plasmid). Constitutively expressed RLuc (GB0109) was included for normalization. After transformation, protoplasts were kept in darkness or illuminated with different intensities of blue light (0.25, 0.5, 1, 5, 10 µmol $m^{-2}$ $s^{-1}$), and FLuc and RLuc were determined after 18 h. Shown data are the mean FLuc/RLuc ratios. Error bars indicate standard error of the mean (SEM), *n* = 6. RLU = Relative Luminescence Units. NLS = Nuclear Localization Sequence.

**Fig. 3**: Molecular design, functional and model-based characterization of PULSE. **(a)** Mode of function of PULSE and constructs. The constructs are: i) the blue light-responsive element EL222 fused to the SRDX repressor domain, placed under the control of the constitutive promoter $P_{CaMV35S}$ ($B_{Off}$), ii) the red light-activated, far-red light-inactivated (reversible) split switch comprising the first 650 amino acids of the PhyB photoreceptor ($PhyB_{1-650}$) fused to the VP16 transactivation domain, and the macrolide repressor DNA-binding protein E 8mphR(A) fused to the first 100 amino acids of PIF6 $(PIF_{1-100})^8$ ($R_{On}$). The two modules of the switch are constitutively expressed from the promoter $P_{CaMV35S}$, iii) a synthetic promoter $P_{Opto}$ comprising eight repeats of the target sequence of the protein E, etr - $(etr)_8$ -, five repeats of C120 - $(C120)_5$ -, and the minimal promoter $P_{hCMVmin}$, driving the expression of the reporter gene FLuc, iv) the normalization element RLuc expressed constitutively from $P_{CaMV35S}$. Under white/ambient light or blue light, SRDX-EL222 dimerizes and binds the $(C120)_5$ element through the HTH domain. Under these conditions PhyB is also active ($PhyB_{fr}$),

due to the blue and red light components of white light[16,17], and therefore able to interact with PIF6, which is bound to $(etr)_8$ through the E protein. In consequence there is recruitment of both the transactivator VP16 and the transcriptional repressor SRDX to the minimal promoter, resulting in no expression of FLuc as the repressor has a dominant effect on gene expression (left). In darkness or in far-red light EL222 and PhyB are in the inactive form ($PhyB_r$), therefore, both are unable to bind to $P_{Opto}$, resulting in no FLuc transcription (middle). There is induction of FLuc expression only under monochromatic red light, in which EL222 is inactive and PhyB is in its active conformation binding PIF6 (right). **(b)** Functional characterization of PULSE in Arabidopsis protoplasts. Protoplasts were transformed with the $R_{On}$ module (pMZ827, pMZ828), the reporter $P_{Opto}$-FLuc (pROF021) and either with the $B_{Off}$ module (pROF051, PULSE system complete) or without $B_{Off}$ (stuffer plasmid, equivalent to the $R_{On}$ system alone). The normalization element (GB0109) is additionally included. Protoplasts were kept in the dark or illuminated with white LEDs adjusted to simulate ambient light (see **Supplementary Fig. S7** and **Methods**), or 10 µmol $m^{-2}$ $s^{-1}$ of $red_{\lambda max\ 655\ nm}$, $blue_{\lambda max\ 461\ nm}$, or $far\text{-}red_{\lambda max\ 740\ nm}$ light. Data shows mean FLuc/RLuc ratios determined 18 h after illumination, SEM (*n* = 6). **(c,d)** Quantitative characterization of On-Off FLuc expression kinetics. Protoplasts of Arabidopsis were transformed with PULSE and first kept in the dark, 12 h for protein (c) and 16 h for mRNA (d) determination assays. Samples were afterwards illuminated with either 10 µmol $m^{-2}$ $s^{-1}$ of red or blue light, or kept in darkness for the indicated time periods. Arrows indicate the time point where the samples were split into different illumination conditions for response and reversibility analyses, *e.g.* red to dark, red to blue (On-Off), red to blue to red (On-Off-On). Samples were collected every 3 h for 15 h for FLuc and RLuc determinations in a plate reader; and at 15 min, 30 min, 1 h, 2 h, 4 h, 4 h 15 min, 4 h 30 min, 6 h, 7 h for RT-qPCR determinations of mRNA production. The curves are the

fits to the ODE-based model. The shaded areas represent the error bands as calculated in 95% confidence intervals with a constant Gaussian error model using the profile likelihood method. Depicted are the FLuc/RLuc ratios for protein expression kinetics, (*n* = 6) (c), and the starting quantity (SQ) of FLuc transcript normalized with the internal controls EF and Tip41L, of two technical replicates (d). **(e)** Model aided prediction of PULSE-controlled protein expression levels as a function of red light intensities and illumination times. The calibrated model yields estimated FLuc/RLuc expression ranges (heatmap). **(f)** Experimental validation of the model predictions of the operating range of PULSE. Selected model simulated expression levels at different red light intensities and illumination times as indicated in (e) were experimentally tested and the resulting FLuc/RLuc ratios (2xSEM, *n* = 6) were compared to the predicted values (error bars calculated as in (c,d)). RLU = Relative Luminescence Units. NLS = Nuclear Localization Sequence.

**Fig. 4**: PULSE-controlled expression of a Cas9-derived gene activator (dCas9-TV) and an Arabidopsis transcription factor for the targeted activation of target promoters in Arabidopsis protoplasts. **(a,b)** Optogenetically controlled dCas9-TV expression to activate a target orthologous promoter. In the presence of PULSE, dCas9-TV is expressed from $P_{Opto}$-dCas9-TV only under red light. dCas9-TV targets the orthologous $P_{SlDFR}$ promoter via a gRNA (a). Activation of $P_{SlDFR}$-FLuc is quantified through the reporter FLuc, and RLuc is used for normalization (b)**.** Data shown are means of FLuc/RLuc ratio, SEM (*n* = 4) (b). **(c-f)** Optogenetic control of an Arabidopsis plant promoter from a plasmid construct ($P_{AtAP1}$-FLuc). In a first approach, PULSE is co-transformed with $P_{Opto}$-dCas9-TV, a gRNA directed specifically to the AtAP1 promoter sequence and the $P_{AtAP1}$-FLuc construct (c). Activation of $P_{AtAP1}$-FLuc is quantified through the reporter FLuc, and RLuc is used for normalization (e). Data shown are

means of FLuc/RLuc ratio, SEM ($n$ = 4) (e). In a second approach, PULSE controlled the expression of the transcription factor LFY-VP16, from the $P_{Opto}$-LFY-VP16-2A-RLuc construct. RLuc is co-expressed (via a 2A self-cleaving peptide) and used as a proxy of LFY-VP16 expression. LFY binds the $P_{AtAP1}$ promoter hence activating FLuc expression from the $P_{AtAP1}$-FLuc construct (d). FLuc and RLuc determinations in protoplasts co-expressing PULSE, $P_{Opto}$-LFY-VP16-2A-RLuc (stripped bars) and $P_{AtAP1}$-FLuc (solid bars) under different light conditions, SEM ($n$ = 6) (f). Data shown are means of RLuc, and means of FLuc after subtraction of background values (configuration without $P_{Opto}$-LFY-VP16-2A-RLuc). **(b,e,f)** The protoplasts were incubated in darkness, red or blue light, and luminescence determinations performed after 18 h. RLU = Relative Luminescence Units.

**Fig. 5**: Implementation and characterization of PULSE in *Nicotiana benthamiana* leaves. Plants infiltrated with PULSE, $P_{Opto}$-Venus and a constitutively expressed Cerulean cassette (pROF346) were kept in dark for 2.5 days prior to light treatment for 2 h, 6 h, 9 h (10 µmol $m^{-2}$ $s^{-1}$ of red light, 10 µmol $m^{-2}$ $s^{-1}$ of blue light, simulated white light, or darkness (as described in **Supplementary Fig. S7 and Methods**). **(a)** Samples were taken at indicated time points for fluorescence confocal microscopy observation. **(b)** Data shown are the ratio of nuclear Venus and Cerulean fluorescence intensities, $12 \leq n \leq 34$. The horizontal line in the box represents the median and the statistical significance is determined by a one way-ANOVA and Dunnett's multiple comparison test (**$p < 0.01$, ***$p < 0.001$, ****$p \leq 0.0001$, *ns* not significant).

**Fig. 6**: *In planta* optogenetic heterologous induction of immunity and conditional subcellular targeting of receptors, and functionality in stable Arabidopsis transgenic lines. **(a,b)** PULSE-controlled conditional gain of immunity *in planta*. *N. benthamiana*

leaves were infiltrated with PULSE and $P_{Opto}$-EFR-GFP. Two plants were used for each illumination condition. Four disks from one leaf of each plant were collected and treated with 1 µM elf18 or mock previous to ROS quantification. Data shown are luminescence mean values, SEM (*n* = 8). **(c,d)** Conditional targeting of receptors by optogenetically controlled expression of a nanobody (GBP-mCherry). The figure shows representative results of *N. benthamiana* leaves infiltrated with PULSE, $P_{Opto}$-GBP-mCherry, and $P_{CaMV35S}$-EFR-GFP and with different illumination treatments prior to observation in the fluorescence confocal microscope. As a control plants were infiltrated with PULSE and $P_{Opto}$-GBP-mCherry. **(b,d)** Plants were kept in standard growth conditions (16 h simulated white light – 8 h dark) for 2 d prior to induction with 10 µmol $m^{-2}$ $s^{-1}$ red light for additional 16 h (white light illumination was used as control). **(e)** PULSE functionality in whole plants. Stable Arabidopsis transgenic lines transformed with PULSE controlling $P_{opto}$-FLuc, were seeded in a white 96-well plate with plant growth media. Transgenic plants constitutively expressing FLuc and wild type plants were used as positive and negative controls, respectively. After 8 d, luminescence determinations in a plate reader started with data points taken every hour for over 4 days while the plate was under illumination as indicated (simulated white light and red light as described in **Supplementary Fig. S7** and **Methods**). Three different independent homozygous PULSE lines were tested with the components under the control of the CaMV35S – PULSE ($P_{CaMV35S}$) + $P_{Opto}$-FLuc #4 and #6 – and AtUbi10 – PULSE ($P_{AtUbi10}$) + $P_{Opto}$-FLuc #2 – constitutive promoters. *n* = 25 – 26 for PULSE lines and *n* = 6 – 7 for the controls. The determinations of six wild type seedlings at each time point were averaged and subtracted from the measurements of the lines. Plotted data are averages and SEM. RLU = Relative Luminescence Units.

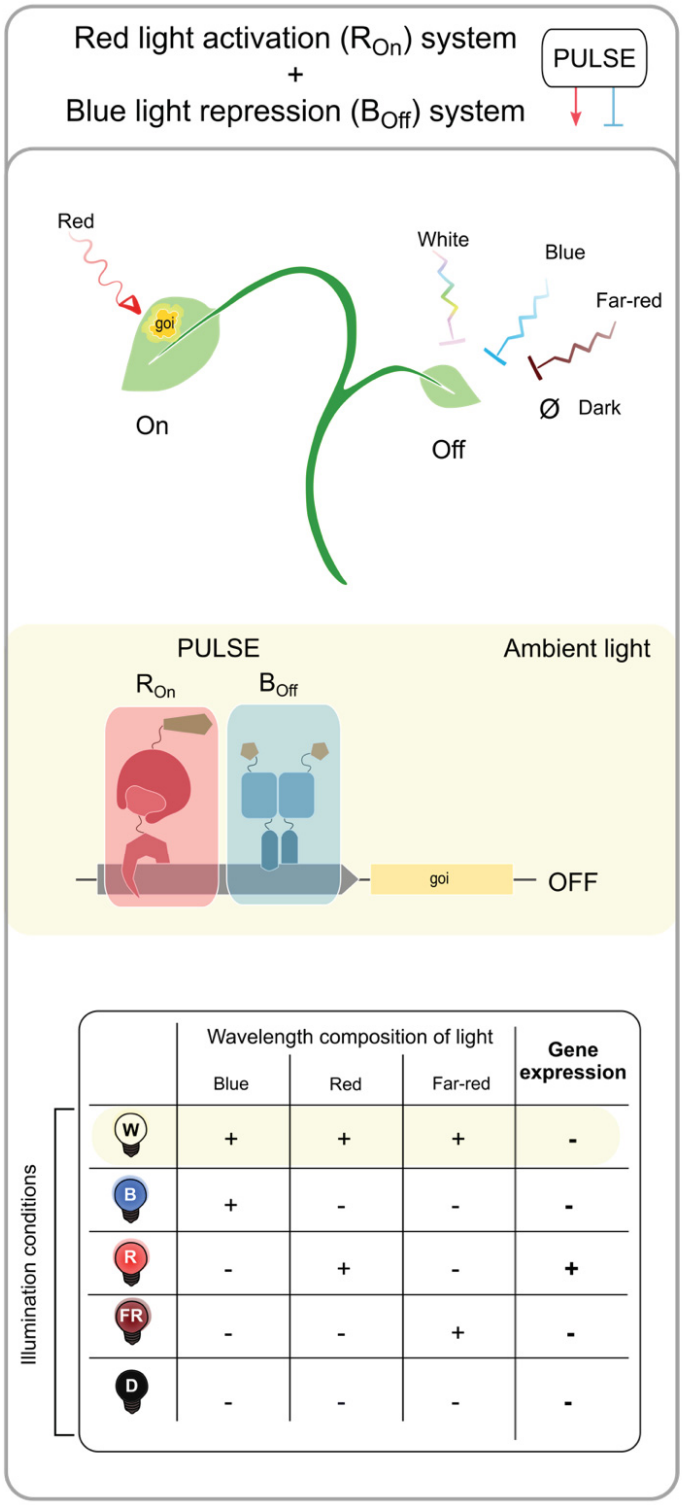


| | Wavelength composition of light | | | Gene expression |
|---|---|---|---|---|
| | Blue | Red | Far-red | |
| W | + | + | + | - |
| B | + | - | - | - |
| R | - | + | - | + |
| FR | - | - | + | - |
| D | - | - | - | - |

a

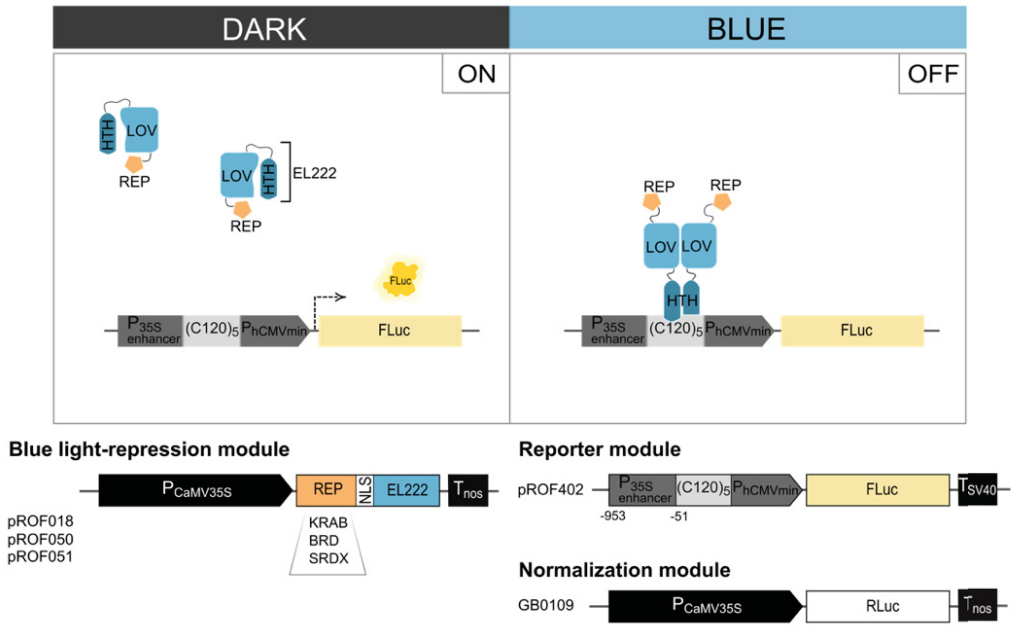
DARK
BLUE
ON
OFF
HTH
LOV
REP
EL222
FLuc
P35S enhancer
(C120)5
PhCMVmin
Blue light-repression module
PCaMV35S
REP
NLS
EL222
Tnos
pROF018
pROF050
pROF051
KRAB
BRD
SRDX
Reporter module
pROF402
TSV40
-953
-51
Normalization module
GB0109
RLuc

b

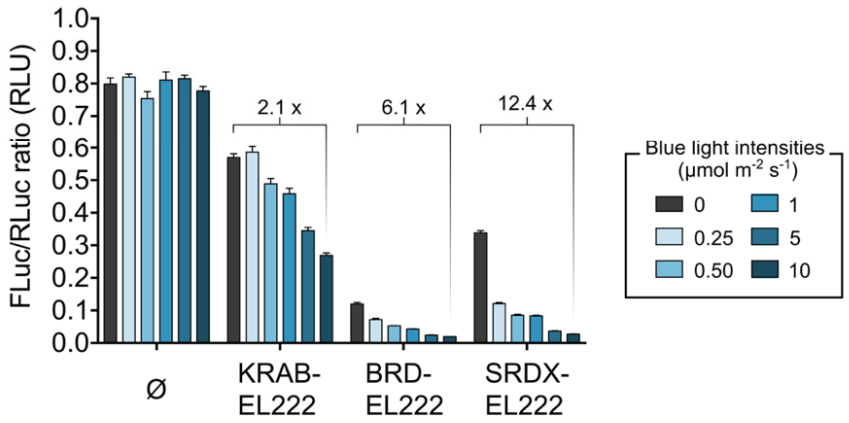
FLuc/RLuc ratio (RLU)
1.0
0.9
0.8
0.7
0.6
0.5
0.4
0.3
0.2
0.1
0.0
2.1 x
6.1 x
12.4 x
Ø
KRAB-EL222
BRD-EL222
SRDX-EL222
Blue light intensities (µmol m-2 s-1)
0
0.25
0.50
1
5
10

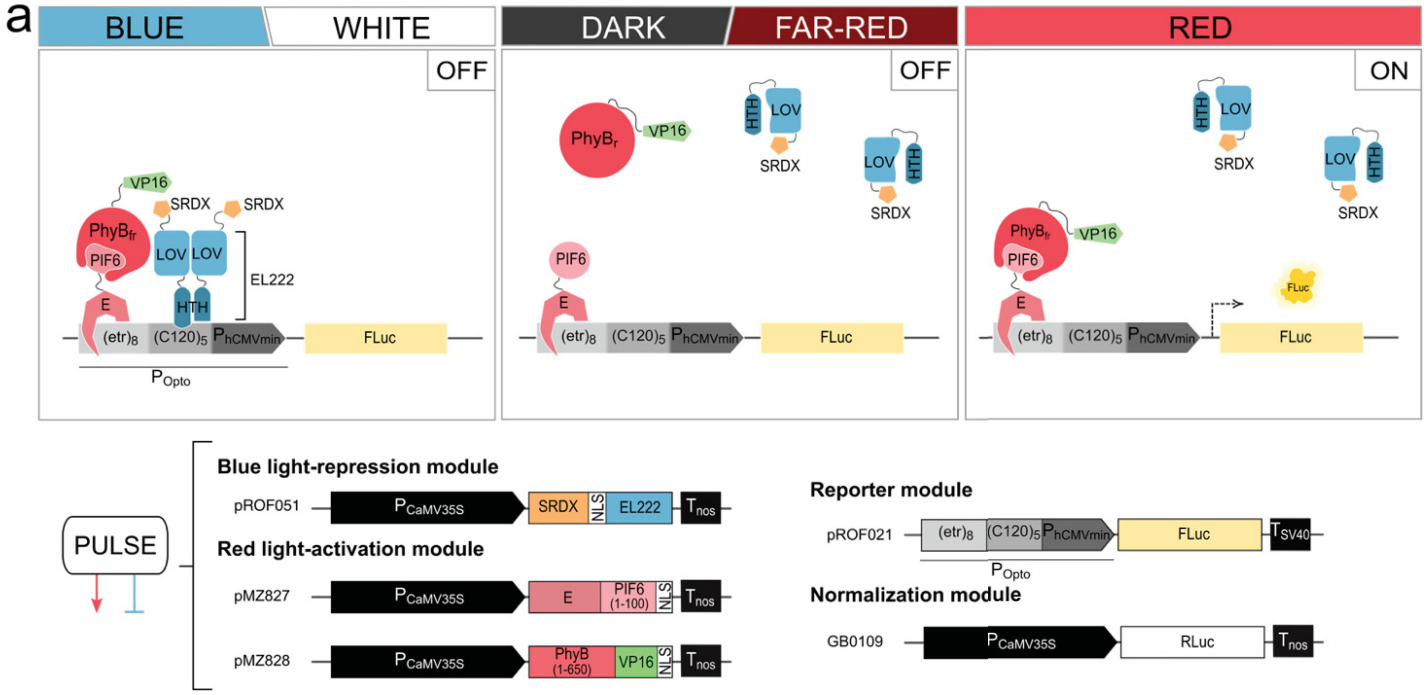





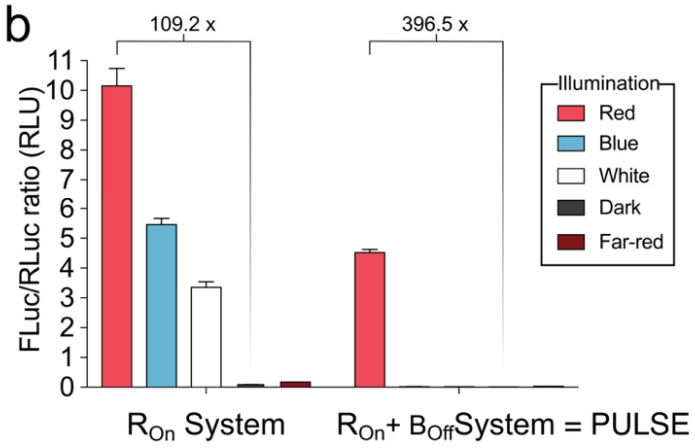


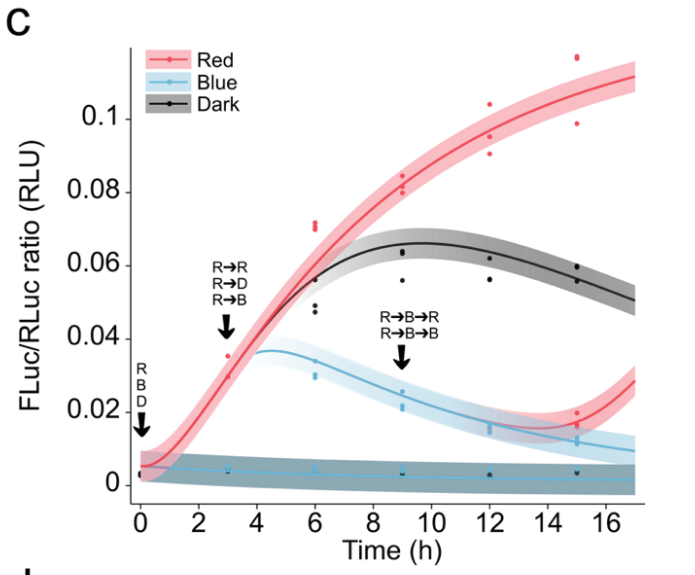


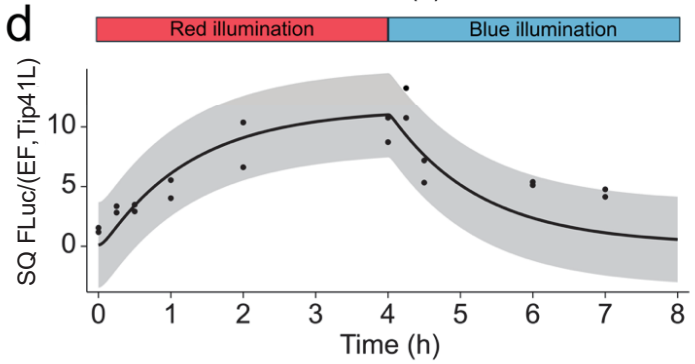


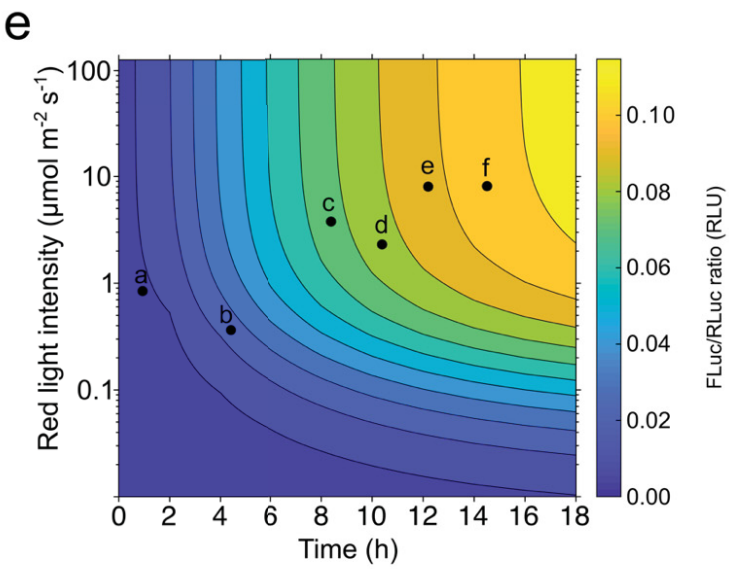


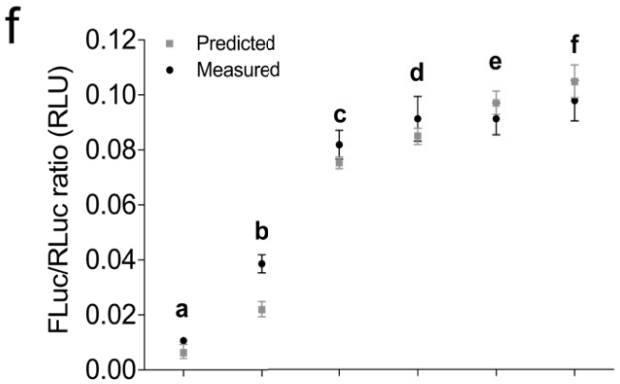


| | a | b | c | d | e | f |
|---|---|---|---|---|---|---|
| Intensity (µmol m$^{-2}$ s$^{-1}$) | 0.86 | 0.30 | 3.78 | 2.27 | 8.14 | 8.14 |
| Time(h) | 0.98 | 4.37 | 8.20 | 10.20 | 12.07 | 14.33 |

cx

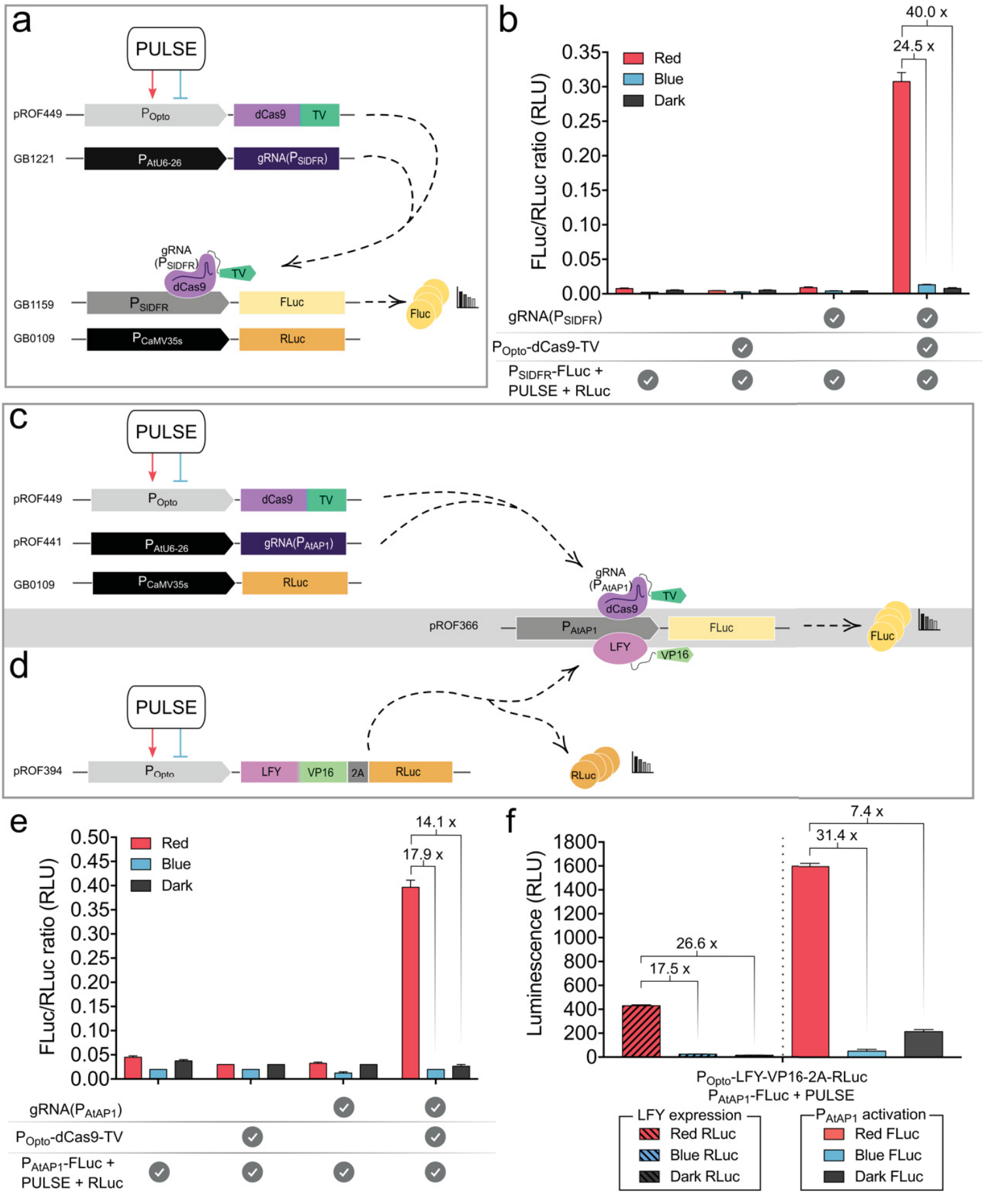
a
PULSE
pROF449
P Opto
dCas9
TV
GB1221
P AtU6-26
gRNA(P SIDFR)
gRNA (P SIDFR)
dCas9
TV
GB1159
P SIDFR
FLuc
Fluc
GB0109
P CaMV35s
RLuc
b
40.0 x
24.5 x
FLuc/RLuc ratio (RLU)
0.35
0.30
0.25
0.20
0.15
0.10
0.05
0.00
Red
Blue
Dark
gRNA(P SIDFR)
P Opto-dCas9-TV
P SIDFR-FLuc +
PULSE + RLuc
c
PULSE
pROF449
P Opto
dCas9
TV
pROF441
P AtU6-26
gRNA(P AtAP1)
GB0109
P CaMV35s
RLuc
gRNA
(P AtAP1)
TV
dCas9
pROF366
P AtAP1
FLuc
FLuc
LFY
VP16
d
PULSE
pROF394
P Opto
LFY
VP16
2A
RLuc
RLuc
e
14.1 x
17.9 x
FLuc/RLuc ratio (RLU)
0.50
0.45
0.40
0.35
0.30
0.25
0.20
0.15
0.10
0.05
0.00
Red
Blue
Dark
gRNA(P AtAP1)
P Opto-dCas9-TV
P AtAP1-FLuc +
PULSE + RLuc
f
7.4 x
31.4 x
26.6 x
17.5 x
Luminescence (RLU)
1800
1600
1400
1200
1000
800
600
400
200
0
P Opto-LFY-VP16-2A-RLuc
P AtAP1-FLuc + PULSE
LFY expression
Red RLuc
Blue RLuc
Dark RLuc
P AtAP1 activation
Red FLuc
Blue FLuc
Dark FLuc

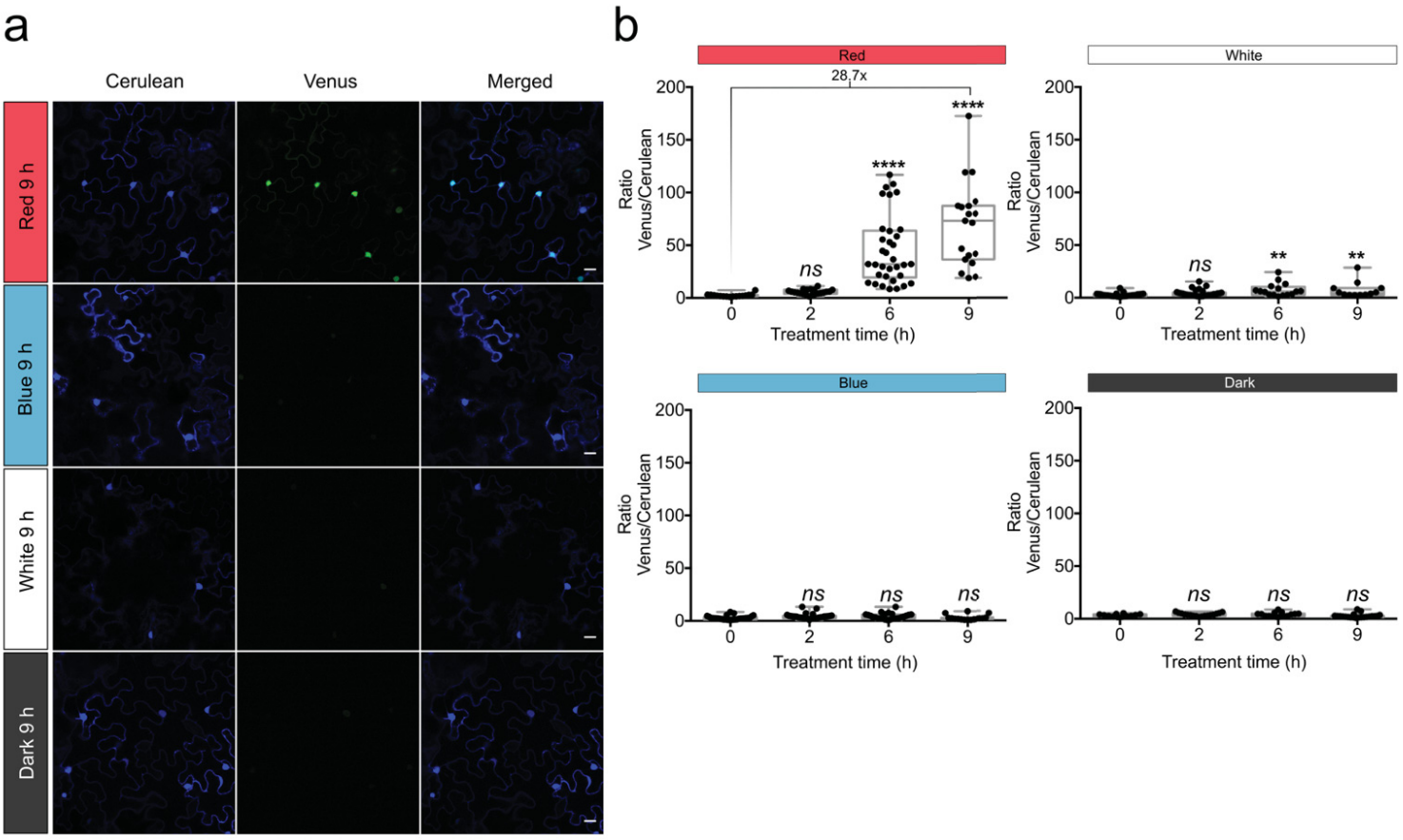
a
Cerulean
Venus
Merged
Red 9 h
Blue 9 h
White 9 h
Dark 9 h
b
Red
White
Blue
Dark
28,7x
****
****
ns
**
**
ns
ns
ns
ns
ns
ns
Ratio Venus/Cerulean
Treatment time (h)
0
2
6
9
0
50
100
150
200

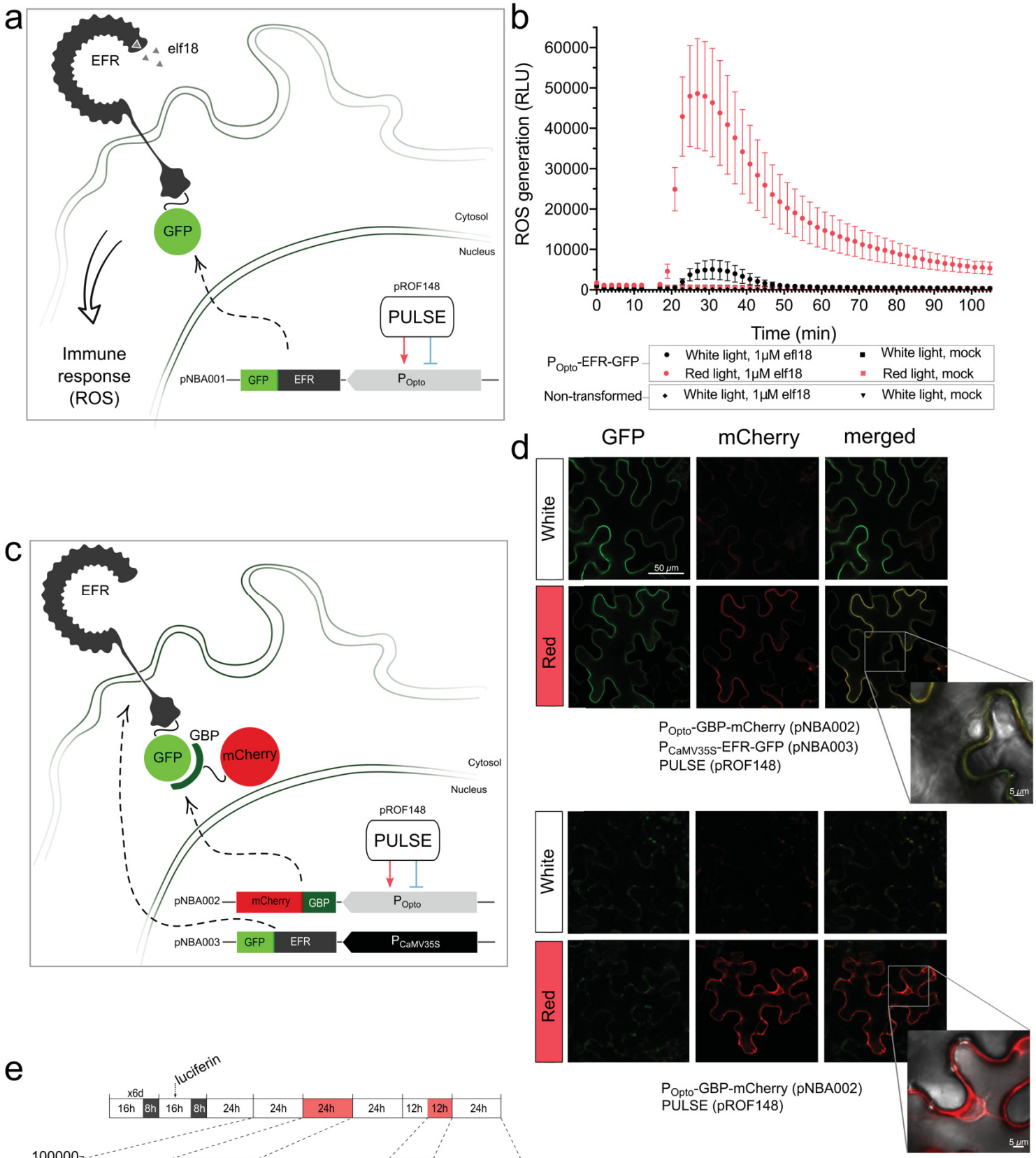
a
EFR
elf18
GFP
Cytosol
Nucleus
pROF148
PULSE
Immune response (ROS)
pNBA001
GFP
EFR
P Opto
b
ROS generation (RLU)
60000
50000
40000
30000
20000
10000
0
0 10 20 30 40 50 60 70 80 90 100
Time (min)
P Opto -EFR-GFP
White light, 1µM efl18
White light, mock
Red light, 1µM elf18
Red light, mock
Non-transformed
White light, 1µM elf18
White light, mock
c
EFR
GBP
GFP
mCherry
Cytosol
Nucleus
pROF148
PULSE
pNBA002
mCherry
GBP
P Opto
pNBA003
GFP
EFR
P CaMV35S
d
GFP
mCherry
merged
White
Red
50 µm
P Opto -GBP-mCherry (pNBA002)
P CaMV35S -EFR-GFP (pNBA003)
PULSE (pROF148)
5 µm
White
Red
P Opto -GBP-mCherry (pNBA002)
PULSE (pROF148)
5 µm
e
luciferin
x6d
16h 8h 16h 8h 24h 24h 24h 24h 12h 12h 24h
Fold induction (x)
Luminescence (RLU)
100000
10000
1000
100
10
1
0 5 10 15 20 25 30 35 40 45 50 55 60 65 70 75 80 85 90 95 100 105 110 115 120
Time (h)
P CaMV35S -FLuc #1, n = 7, x = 1
PULSE(P CaMV35S ) + P Opto -FLuc #4, n = 26, x = 10
PULSE(P CaMV35S ) + P Opto -FLuc #6, n = 26, x = 21
PULSE(P AtUbi10 ) + P Opto -FLuc #2, n = 25, x = 372
Dark
White
Red

# PULSE – Optogenetic control of gene expression in plants in the presence of ambient white light

Rocio Ochoa-Fernandez[1,2], Nikolaj B. Abel[3], Franz-Georg Wieland[4], Jenia Schlegel[2,5], Leonie A. Koch[1], J. Benjamin Miller[6], Raphael Engesser[4], Giovanni Giurani[1], Simon M. Brandl[3], Johanna Plum[1], Jens Timmer[4], Wilfried Weber[3,7], Thomas Ott[3,7], Rüdiger Simon[2,5,8], Matias D. Zurbriggen[1,2,8,#]

[1]Institute of Synthetic Biology, University of Düsseldorf, Germany

[2]iGRAD Plant Graduate School, University of Düsseldorf, Germany.

[3]Faculty of Biology, University of Freiburg, Germany

[4]Institute of Physics, University of Freiburg, Germany

[5]Institute of Developmental Genetics, University of Düsseldorf, Germany

[6]School of Biological Sciences, University of East Anglia, Norwich, UK.

[7]Signalling Research Centres BIOSS and CIBSS, University of Freiburg, Germany

[8]CEPLAS - Cluster of Excellence on Plant Sciences, Düsseldorf, Germany

[#]Corresponding author: MDZ matias.zurbriggen@uni-duesseldorf.de

**Supplementary Information.** Development and calibration of the mathematical model

## 1. Describing PULSE with a mathematical model

We developed a mathematical model to describe the complex dynamical changes of the optogenetic PULSE system systematically. The modelling is performed by creating a model of the system using kinetic rate equations. These equations describe the dynamics underlying the entire system with ten dynamic parameters.

Experimental limitations make it impossible to measure all concentrations at play. Only the FLuc protein levels as well as FLuc-mRNA levels can be measured. Thus, by only inferring parameters from single experiments, the processes underlying the optogenetic activation and repression cannot be described reliably. For this reason, we used a comprehensive approach, in which all experiments are used as joint basis to infer parameters from the model. Using this approach makes it possible to infer all parameters and their uncertainties. This methodology has been widely used and is the standard in the field[1–4].

In order to use this approach, the experimental data under different conditions have to be made comparable, thus a scaling parameter is included for each experimental dataset. These scaling parameters were estimated together with dynamical parameters and the initial concentration of FLuc.

Including the error estimation, this leads to 24 parameters, which were inferred simultaneously from all experimental data, making it possible to describe the optoswitch with reliably determined parameters.

In the following, the modelling process is described in detail. In Section 2, the mathematical model with its equations will be derived, while in Section 3, the methodology of the parametrization and uncertainty analysis of the model is introduced. Furthermore, Section 4 characterizes the link to the experimental data and

Sections 5 and 6 show the results of the parameter estimation and the predictions of the model.

## 2. Derivation of the mathematical model

We derive a mathematical model for PULSE in the following chapter based on ordinary differential equations.

The EL222 photoreceptor consists of the LOV-Jα-HTH domains (LOV) and has a light-dependent transitioning behaviour between its two conformations. It transitions to its folded state $LOV_{closed}$ with a constant rate $k_{off,LOV}$ and unfolds into its active open state $LOV_{open}$ under blue light (460 nm) with the rate $k_{on,LOV}\, I_{blue}(t)$, dependent on the light intensity

$$LOV_{closed} \underset{k_{on,LOV} I_{blue}(t)}{\overset{k_{off,LOV}}{\rightleftarrows}} LOV_{open}.$$

The interaction factor PhyB-VP16 is similarly light-dependent. The light-sensitive Phytochrome B (PhyB) has two conformational states, an active state sensitive to far-red light $PhyB_{fr}$ in which it can bind to PIF6 as well as an inactive state sensitive to red light $PhyB_r$. A constant revision from the active to the inactive state is modelled

$$PhyB_{fr} \xrightarrow{k_{off,PhyB,dark}} PhyB_r,$$

therefore, in the dark all of the complex will be in its inactive state.

Under both far-red light (740 nm) in the infrared spectrum as well as red light (660 nm) the two conformations exhibit probabilistic conformational changes into each other

$$PhyB_{fr} \underset{k_{off,PhyB,red}\, I_{red}(t)}{\overset{k_{on,PhyB,red}\, I_{red}(t)}{\rightleftarrows}} PhyB_r,$$

$$\mathrm{PhyB_{fr}} \underset{k_{off,PhyB,farred}\, I_{farred}(t)}{\overset{k_{on,PhyB,farred}\, I_{farred}(t)}{\rightleftharpoons}} \mathrm{PhyB_r},$$

dependent on the light intensities $I_{farred}(t)$ and $I_{red}(t)$

The reporter Firefly luciferase (FLuc) mRNA is transcribed with a basal production $b_{transcription}$ and degraded with a constant degradation rate $k_{deg,FLuc_{mRNA}}$. Furthermore, the activation of the mRNA transcription by the active state of the PhyB-VP16 complex $PhyB_r$ is modelled by the Michaelis-Menten reaction with the rate $k_{transcript,extended}$ and the Michaelis-Menten constant $K_m$. However, the activated EL222 ($LOV_{open}$) inhibits this activation with the inhibition strength $k_{inh,LOV}$. Thus, the total dynamic transcription including the two non-competitive inhibitions becomes

$$\frac{d[FLuc_{mRNA}](t)}{dt} = \frac{k_{transcript,extended}\,[PhyB_{fr}]}{(K_m + [PhyB_{fr}])\,(1 + k_{inh,LOV}{}^2\,[LOV_{open}]^2)}$$

To account for cooperative binding effects an exponent of two is used for the inhibition. The extended model including this reactions shows two linearly dependent parameters $k_{transcript,extended}$, and $K_m$. Both parameters are non-identifiable and compatible with infinity (**Supplementary Fig. S8**). Their ratio, however, is constant and thus can be used to create an identifiable parameter

$$\frac{k_{transcript,extended}}{K_m} = k_{transcript} = const.$$

Using this ratio and setting $K_m$ to infinity

$$\lim_{K_m\to\infty} \frac{k_{transcript,extended}\,[PhyB_{fr}]}{(K_m + [PhyB_{fr}])\,(\blacksquare)} = \lim_{K_m\to\infty} \frac{k_{transcript}\,[PhyB_{fr}]}{(1 + \frac{[PhyB_{fr}]}{K_m})\,(\blacksquare)} = \frac{k_{transcript}\,[PhyB_{fr}]}{(\blacksquare)},$$

where ■ describes the inhibition term due to the LOV system, leads to a simplification of the transcription. This simplification can be explained by the fact, that the Michaelis-Menten reaction is in its linear limit, i.e. the saturation does not influence the behaviour

of the system for the measured conditions. The full equation describing the transcription thus becomes

$$\frac{\mathrm{d}[\mathrm{FLuc_{mRNA}}](t)}{\mathrm{dt}} = \frac{k_{\mathrm{transcript}}\,[\mathrm{PhyB_{fr}}]}{1 + k_{\mathrm{inh,LOV}}{}^{2}\,[\mathrm{LOV_{open}}]^{2}}.$$

The target protein FLuc is translated from the $\mathrm{FLuc_{mRNA}}$ with the rate $k_{\mathrm{transl,FLuc}}$. It degrades linearly with the rate $k_{\mathrm{deg,FLuc}}$.

This leads us to the full set of coupled differential equations describing the model:

$$\frac{\mathrm{d}[\mathrm{LOV_{closed}}](t)}{\mathrm{dt}} = k_{\mathrm{off,LOV}}\,[\mathrm{LOV_{open}}] - k_{\mathrm{on,LOV}} I_{\mathrm{blue}}(t)[\mathrm{LOV_{closed}}] \tag{1}$$

$$\frac{\mathrm{d}[\mathrm{LOV_{open}}](t)}{\mathrm{dt}} = -k_{\mathrm{off,LOV}}\,[\mathrm{LOV_{open}}] + k_{\mathrm{on,LOV}}\, I_{\mathrm{blue}}(t)[\mathrm{LOV_{closed}}] \tag{2}$$

$$\begin{aligned}\frac{\mathrm{d}[\mathrm{PhyB_{fr}}](t)}{\mathrm{dt}} = {} & k_{\mathrm{on,PhyB,red}}\, I_{\mathrm{red}}(t)\,[\mathrm{PhyB_r}] - k_{\mathrm{off,PhyB,red}}\, I_{\mathrm{red}}(t)\,[\mathrm{PhyB_{fr}}] \\ & + k_{\mathrm{on,PhyB,farred}}\, I_{\mathrm{farred}}(t)\,[\mathrm{PhyB_r}] - k_{\mathrm{off,PhyB,farred}}\, I_{\mathrm{farred}}(t)\,[\mathrm{PhyB_{fr}}] \\ & - k_{\mathrm{off,PhyB,dark}}\,[\mathrm{PhyB_{fr}}]\end{aligned} \tag{3}$$

$$\begin{aligned}\frac{\mathrm{d}[\mathrm{PhyB_r}](t)}{\mathrm{dt}} = {} & -k_{\mathrm{on,PhyB,red}}\, I_{\mathrm{red}}(t)\,[\mathrm{PhyB_r}] + k_{\mathrm{off,PhyB,red}}\, I_{\mathrm{red}}(t)\,[\mathrm{PhyB_{fr}}] \\ & - k_{\mathrm{on,PhyB,farred}}\, I_{\mathrm{farred}}(t)\,[\mathrm{PhyB_r}] + k_{\mathrm{off,PhyB,farred}}\, I_{\mathrm{farred}}(t)\,[\mathrm{PhyB_{fr}}] \\ & + k_{\mathrm{off,PhyB,dark}}\,[\mathrm{PhyB_{fr}}]\end{aligned} \tag{4}$$

$$\begin{aligned}\frac{\mathrm{d}[\mathrm{FLuc_{mRNA}}](t)}{\mathrm{dt}} = {} & b_{\mathrm{transcription}} - k_{\mathrm{deg,FLuc_{mRNA}}}\,[\mathrm{FLuc_{mRNA}}] \\ & + \frac{k_{\mathrm{transcript}}\,[\mathrm{PhyB_r}]}{1 + k_{\mathrm{inh,LOV}}{}^{2}\,[\mathrm{LOV_{open}}]^{2}}\end{aligned} \tag{5}$$

$$\frac{\mathrm{d}[\mathrm{FLuc}](t)}{\mathrm{dt}} = k_{\mathrm{transl,FLuc}}\,[\mathrm{FLuc_{mRNA}}] - k_{\mathrm{deg,FLuc}}\,[\mathrm{FLuc}] \tag{6}$$

3. Parametrization of the model and identifiability analysis with maximum likelihood approach

We used a maximum likelihood approach to determine the unknown parameters of the model by fitting it to the experimental data. The identifiability analysis was performed using the profile likelihood method. Both methods were previously described in the supporting information of Beyer *et al.*[5] and the following introduction is based on this description.

The ordinary differential equations (1)-(6) describing the model can be generalized to

$$\frac{\mathrm{d}}{\mathrm{dt}}\vec{x}(t) = \vec{f}\left(\vec{x}, \vec{p}, \vec{u}(t)\right) \tag{7}$$

where $\vec{x}$ is the state vector of the system describing the dynamics of the concentrations and $\vec{p}$ contains the dynamic parameters. $\vec{u}(t)$ is a function containing the external inputs. The initial conditions of the concentrations, i.e. the concentrations at the time $t = 0$ are given by $\vec{x}(0) = \vec{x}_0$. Since the concentrations themselves can not be measured, an observation function

$$y(t) = g(\vec{x}(t), \vec{s}) + \vec{\varepsilon}(t) \tag{8}$$

is necessary for each experiment to link the measured data to the model states $\vec{x}(t)$. The observation parameters $\vec{s}$ contain the scaling parameters of the measurements. We used a constant Gaussian error model with variance $\sigma^2$ to model the measurement error, i.e.

$$\varepsilon(t) \sim N(0, \sigma^2). \tag{9}$$

Using this error model, the probability of the measured data from $\vec{y}^D$ from a single experiment with $N_D$ data points given the complete set of parameters $\vec{\theta} = (\vec{p}, \vec{x}_0, \vec{s}, \sigma)$ becomes

$$L(\vec{y}^D, \vec{\theta}) = \prod_{j=1}^{N_D} \exp\left(\frac{\left(y_j^D - g(\vec{x}(t_j), \vec{s})\right)^2}{2\sigma^2}\right). \tag{10}$$

Here $\vec{x}(t_j)$ denotes the concentrations at the time of the measurement $y_j^D$. Combining $N_{exp}$ experiments leads to the likelihood function

$$L(\vec{y}^D, \vec{\theta}) = \prod_{k=1}^{N_{exp}} \mathrm{L}(\vec{y}^{D_k}, \vec{\theta}_k). \tag{11}$$

The parameters, for which the data is most probable, i.e. the parameter set with the maximum likelihood can be found with the maximum likelihood estimator

$$\hat{\theta} = \underset{\vec{\theta}}{\operatorname{argmax}}\left(L(\vec{y}^D, \vec{\theta})\right). \tag{12}$$

For numerical reasons, it is more efficient to minimize the equivalent

$$\begin{aligned} -2\log L = \sum_{j=1}^{N_D} \exp\left(\frac{\left(y_j^D - g(\vec{x}(t_j), \vec{s})\right)^2}{2\sigma^2}\right) + 2\, N_D \log\left(\sqrt{2\pi\, \sigma^2}\right) \quad = \\ = \chi^2(\vec{\theta}) + 2\, N_D \log\left(\sqrt{2\pi\, \sigma^2}\right) =: \chi^2_{mod}(\vec{\theta})\,. \end{aligned} \tag{13}$$

This term contains the sum of the weighted residuals $\chi^2(\vec{\theta})$ as well as an error model correction term.

The uncertainty and identifiability analysis of the parameters is performed using the profile likelihood method[6]. The profile likelihood of parameter $\theta_i$is determined by

$$\chi^2_{PL}(\theta_i) = \min_{\theta_{i\neq j}}\left(\chi^2_{mod}\left(\vec{\theta}\right)\right). \quad (14)$$

The 95 % confidence intervals of parameter $\theta_i$ can then be calculated by

$$CI(\theta_i) = \left\{\theta \mid \chi^2_{PL}(\theta) - \chi^2_{PL}\left(\vec{\theta}\right) < \chi^2(95\%, \mathrm{df} = 1)\right\}. \quad (15)$$

$\chi^2(95\%, \mathrm{df} = 1)$ describes the 95$^{th}$ quantile of the $\chi^2$- distribution with one degree of freedom.

4. Implementation of the single experiments, simplifications of the model, and stoichiometric considerations

Each experiment used for the calibration of the model needs a specific observation function. The observed FLuc or FLuc mRNA concentrations were first normalized over a constitutive control. The normalized concentrations are then linked to the internal states of FLuc and FLuc mRNA with a scaling factor. Thus, only relative concentrations are considered.

In general, not all protoplasts are transformed and thus FLuc transcripts only derive from transfected protoplasts. In contrast, the constitutive control's transcripts derive from all protoplasts. Thus, the normalized concentrations contain an unknown factor scaling the normalized concentrations of FLuc and FLuc mRNA with the fraction of transfected cells. In our modelling process, this scaling is entailed in the scaling parameter of each experiment and does not alter the model's description of the system and its predictions.

   a. Experiment 1: Characterization of the combined blue-red system after 18 hours

In the first experiment (shown in **Fig. 3b**) we measured the FLuc concentrations after 18 hours of expression under different light conditions with six replicates per measurement. We normalized the FLuc concentrations using the also measured RLuc as normalization factor. The experiment was repeated four times, thus necessitating a scaling factor for each repetition. The observation function of the normalized FLuc of repetition *i* thus becomes

$$\frac{\text{FLuc\_observed}}{\text{RLuc\_observed}} = \text{scale}_{\text{FLuc,Exp1,Rep\_}i}\,[\text{FLuc}]. \tag{16}$$

The constant Gaussian error parameter for the experiment is the same for all four repetitions.

b. Experiment 2: Characterization of kinetics of the combined blue-red system

In the second experiment (shown in **Fig. 3c**) we measured a time series of the FLuc concentrations with six different lighting regimes. We normalized the FLuc concentrations using the also measured RLuc as normalization factor as in Experiment 1. Thus, the observation function of Experiment 2 becomes

$$\frac{\text{FLuc}_{\text{observed}}}{\text{RLuc}_{\text{observed}}} = \text{scale}_{\text{FLuc,Exp2}}\,[\text{FLuc}]. \tag{17}$$

Scaling factors are necessary to couple different measurements with relative scale in the same model. However, since the absolute scale of the relative FLuc concentration is unknown, the scaling factor of one FLuc measurement has to be set to one to avoid over-parametrization. Since all other FLuc measurements of Experiments 1 have a scaling factor, we set

$$\text{scale}_{\text{FLuc,Exp2}} = 1. \tag{18}$$

c. Experiment 3: Characterization of mRNA kinetics

In the third experiment (shown in **Fig. 3d**) we measured a time series of the FLuc mRNA concentration with the same lighting regimes as in experiment 2. We

normalized the FLuc mRNA concentrations using the geometric mean (geomean) of the measured mRNA levels of EF and Tip41L housekeeping genes. We repeated the experiment twice with two technical replicates for each transcript per measurement. Both experiments were used for the parameterization. The observation function of repetition *i* is

$$\frac{\mathrm{FLuc}_{\mathrm{mRNA,observed}}}{\mathrm{geomean(EF,Tip41L)}_{\mathrm{mRNA,observed}}} = \mathrm{scale}_{\mathrm{FLuc}_{\mathrm{mRNA}},\mathrm{Exp3},\mathrm{Rep\_}i}\,[\mathrm{FLuc}_{\mathrm{mRNA}}]. \quad (19)$$

As discussed in Experiment 2, one of the two scaling factors can be set to one, because the absolute concentration of the normalized $\mathrm{FLuc}_{\mathrm{mRNA}}$ is unknown.

$$\mathrm{scale}_{\mathrm{FLuc}_{\mathrm{mRNA}},\mathrm{Exp3},\mathrm{Rep\_1}} = 1. \quad (20)$$

d. Experiment 4: Characterization of the red-on system for different illumination times

In the fourth experiment (shown in **Supplementary Fig. S1a**) we measured the response of the system to different times of stimulation with red light from 0 to 12 hours. The FLuc concentration was measured and normalized with RLuc similarly to experiments 1 and 2. The observation function of repetition *i* of the two repetitions is

$$\frac{\mathrm{FLuc\_observed}}{\mathrm{RLuc\_observed}} = \mathrm{scale}_{\mathrm{FLuc},\mathrm{Exp4},\mathrm{Rep\_}i}\,[\mathrm{FLuc}]. \quad (21)$$

e. Experiment 5: Characterization of “dose-response” to different light intensities

In the fifth experiment (shown in **Supplementary Fig. S1b,c**) we measured the response of the system to different blue and red light intensities. The observation function and normalization are similar to Experiments 1, 2 and 4:

$$\frac{\text{FLuc\_observed}}{\text{RLuc\_observed}} = \text{scale}_{\text{FLuc,Exp5,Color}}\ [\text{FLuc}]. \quad (22)$$

with the colour either being red or blue.

f. Initial conditions

The initial conditions of the LOV and PhyB complexes were set to

$$\text{LOV}_{\text{closed}}(0) = 1 \quad (23)$$

$$\text{LOV}_{\text{open}}(0) = 0 \quad (24)$$

$$\text{PhyB}_{\text{r}}(0) = 1 \quad (25)$$

$$\text{PhyB}_{\text{fr}}(0) = 0, \quad (26)$$

i.e. their inactive states, because before each experiment the system was left in the dark.

For the initial concentration of $\text{FLuc}_{\text{mRNA}}$ we assumed a steady state between the basal transcription of the mRNA and its degradation

$$\text{FLuc}_{\text{mRNA}}(0) = \frac{b_{\text{transcription}}}{k_{\text{deg,FLuc}_{\text{mRNA}}}}. \quad (27)$$

We estimated the initial concentration of FLuc together with the other model parameters as a model parameter:

$$\text{FLuc}(0) = \text{init}_{\text{FLuc}}. \quad (28)$$

g. Simplifications

Müller *et al.* 2013[7] previously showed, that under far-red light the PhyB system is completely in the $PhyB_r$ state. We incorporated this information in the model by setting

$$k_{\text{off,PhyB,farred}} = 100\ h^{-1}. \tag{29}$$

The ratios of the two complexes of Phytochrome B under red light (660 nm) and far-red light (740 nm) were calculated using the data of Kelly and Lagarias 1985[8] according to Legris *et al.* 2016[9] . They describe the ratio of $PhyB_{fr}$ to the total PhyB population in these light conditions including the effects of the constant dark reversion $k_{\text{off,PhyB,dark}}$. These ratios are

$$r_{PhyB_{fr},red} = \frac{[PhyB_{fr}]}{[PhyB_r]+[PhyB_{fr}]} = 0.728 \qquad \text{at 10 µmol m}^{-2}\text{ s}^{-1}\text{ of red light,} \tag{30}$$

$$r_{PhyB_{fr},farred} = \frac{[PhyB_{fr}]}{[PhyB_r]+[PhyB_{fr}]} = 0.002 \qquad \text{at 10 µmol m}^{-2}\text{ s}^{-1}\text{ of far-red light.} \tag{31}$$

Since the ratios were measured under constant red light intensity $I_{\text{red}}$ and temperature, we assumed a quasi-steady state of the PhyB system. Thus, using the relation

$$\frac{[PhyB_{fr}]}{[PhyB_r]} = \frac{r_{PhyB_{fr},red}}{1-r_{PhyB_{fr},red}} = K_{PhyB_{fr},red} \tag{32}$$

Eqs. (3) and (4) lead to

$$K_{PhyB_{fr},red} = \frac{-k_{\text{on,PhyB,red}}\, I_{\text{red}} + k_{\text{off,PhyB,red}}\, I_{\text{red}}\, K_{PhyB_{fr},red} + k_{\text{off,PhyB,dark}}\, K_{PhyB_{fr},red}}{k_{\text{on,PhyB,red}} \frac{I_{\text{red}}}{K_{PhyB_{fr},red}} - k_{\text{off,PhyB,red}}\, I_{\text{red}} - k_{\text{off,PhyB,dark}}}. \tag{33}$$

By algebraic calculation we obtain

$$k_{\text{on,PhyB,red}} = \left(k_{\text{off,PhyB,red}} + \frac{k_{\text{off,PhyB,dark}}}{I_{\text{red}}}\right) \mathrm{K}_{\mathrm{PhyB_{fr}},\text{red}} \,. \tag{34}$$

Since the intensity $I_{\text{red}}$ =10 µmol $m^{-2}$ $s^{-1}$ is known, this equation simplifies the model by one parameter, the On-rate of the PhyB complex in red light. An identical calculation was performed for the far-red rate $k_{\text{on,PhyB,farred}}$.

h. Stoichiometric considerations between the blue-off and red-on factors

The stoichiometry between the blue-off and the red-on factors does not influence the system's behaviour. This can be concluded both from the computational model as well as from the experiments. In the computational model, a change in concentration of one of two systems corresponds to a change in the scaling parameters described in the previous sections. The system equations and reactions would remain unchanged and only the scaling parameter would encode the changed stoichiometric balance. This analysis is consistent with the experiments under varying experimental conditions that show that all relevant effects can be derived from the relative concentrations. Furthermore, it indicates that the stoichiometry between the two factors plays no role since their effects are uncorrelated. The Blue-off complex inhibition of the transcription is independent of the red-on systems state, i.e. relative or absolute concentration.

5. Results of parameter estimation

The complete model including the observation functions of the experiments was fitted to 406 data points using the maximum likelihood approach. 25 parameters were

estimated, of which one was an initial value, ten were dynamic parameters, nine were scaling parameters and five were error parameters.

The numerical integration, fitting process and identifiability analysis with the profile likelihood method were performed in MATLAB using the freely available Data2Dynamics software[10]. It uses the CVODES[11] solver to numerically integrate the ordinary differential equations. The parameter estimation was performed using the trust region algorithm LSQNONLIN[12]. We optimized the parameter space in logarithmic space, thus naturally enabling a scan of the parameters over many orders of magnitude.

A thorough search for the global optimum requires multiple optimization runs with randomly sampled initial parameter sets. We thus performed 200 runs, of which 20 converged to the lowest minimum, suggesting that it is the global optimum (**Supplementary Fig. S9a**). Other local optima were found, but because they are significantly worse than the best optimum they are not included in the further analysis.

The identifiability analysis using the profile likelihood method showed two practically non-identifiable parameters (**Supplementary Fig. S10**). The two parameters describe the LOV systems inhibitory behaviour, i.e. $k_{on,LOV}$ describes the rate, at which LOV is created and $k_{inh,LOV}$ describes the inhibition strength of the LOV complex on the mRNA transcription. The practical non-identifiabilities in these two parameters stem from the fact, that the absolute concentration of LOV is unknown, thus the LOV concentration and its inhibition strength are symmetrically linked. A reduction of the model should thus fix one of the dynamic parameters. The inhibition strength is the natural choice since it has the unit of an inverse concentration.

After fixing the inhibition strength $k_{inh,LOV}$

$$k_{\text{inh,LOV}} = 25.04 \quad (35)$$

to the value of the global optimum, the previously described analysis pipeline was performed again on the reduced model with now 24 dynamic parameters.

From 200 runs, 97 converged to the lowest minimum, strongly indicating, that it is the global optimum (**Supplementary Fig. S9b**). One other local minimum was found, however, it was significantly worse than the lowest minimum. The profile likelihood analysis (**Supplementary Fig. S11**) shows, that all parameters are identifiable. The 95 % point-wise confidence intervals of the parameters are shown in **Supplementary Table S3**.

6. Characterization of the system by simulations and validation

We performed simulations to characterize the behaviour of the system under different light conditions. For this purpose we used the model, calibrated to the optimal parameter set with all data discussed in Section 4, *i.e.* the time-series mRNA and protein FLuc measurements (**Fig. 3c,d, Supplementary Fig. S1a**) as well as light dose-response FLuc measurements (**Supplementary Fig. S1b,c**). **Fig. 3e** shows a simulation of the normalized FLuc concentration from 0 to 18 hours given different red light intensities as stimuli of the system. **Supplementary Fig. S2** shows a simulation of the normalized FLuc concentration given different light conditions after 12 hours.

The above-mentioned characterization was validated by measuring the expression level of FLuc for different experimental conditions, i.e. red-light intensities and illumination periods. These validation measurements were then compared to the model predictions, as can be seen in **Fig. 3f** The prediction uncertainty was determined by evaluating the prediction profile likelihood for each prediction, i.e. each experimental condition of the validation measurements[13].

## Supplementary Figures

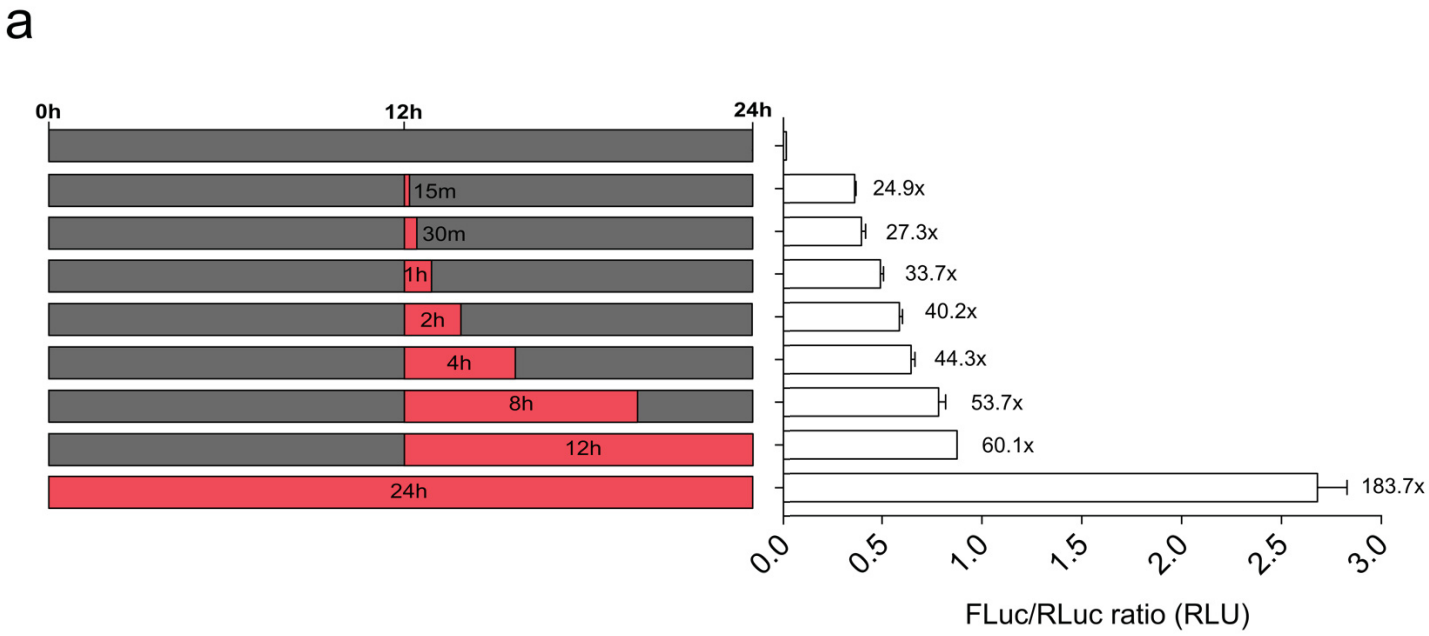


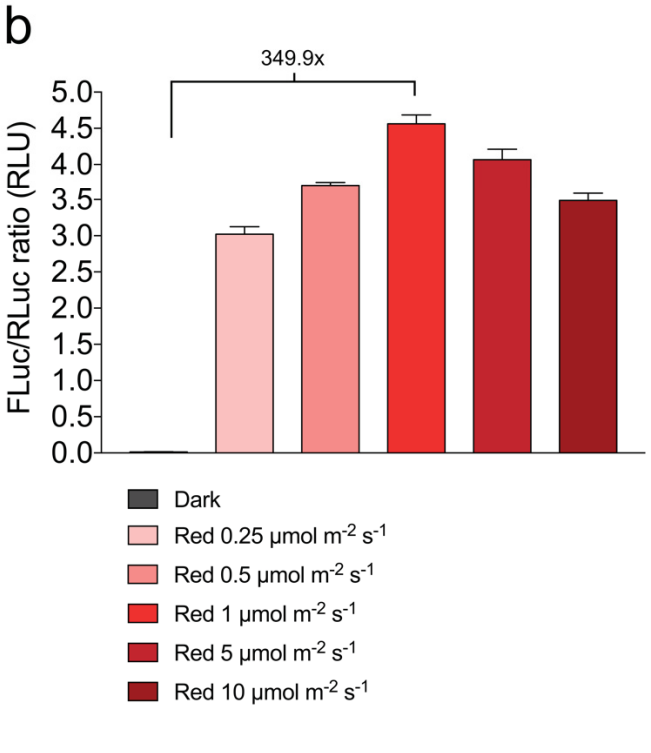


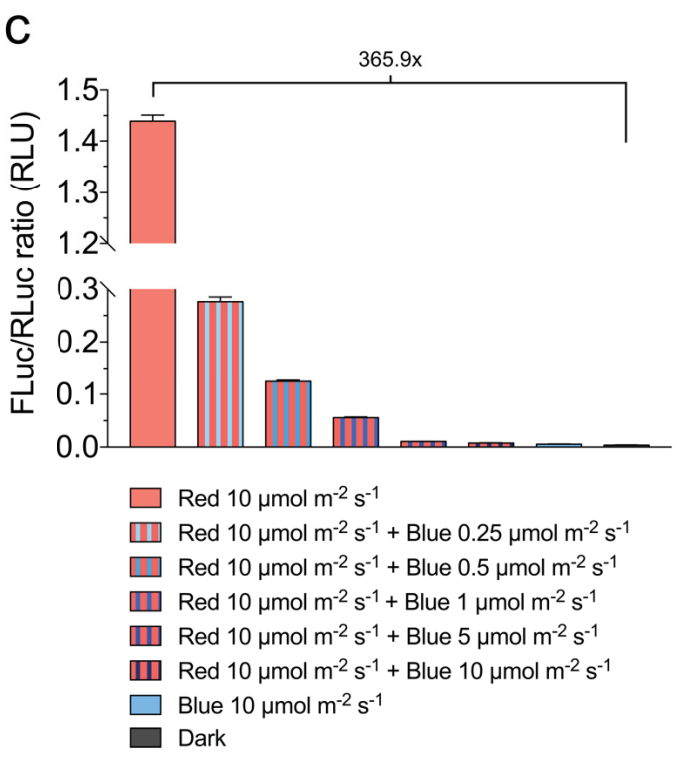

**Supplementary Figure S1.** Characterization of PULSE in Arabidopsis protoplasts to calibrate the mathematical model. **(a)** end point kinetics with red light treatment (10 µmol $m^{-2}$ $s^{-1}$) of different durations, as indicated. Dose-response after 18 h of light treatment with **(b)** different intensities of red light, **(c)** red light and different intensities of blue light**.** Data shown is the mean ratio of FLuc and RLuc, SEM (*n* = 6). Indicated induction folds are relative to dark.

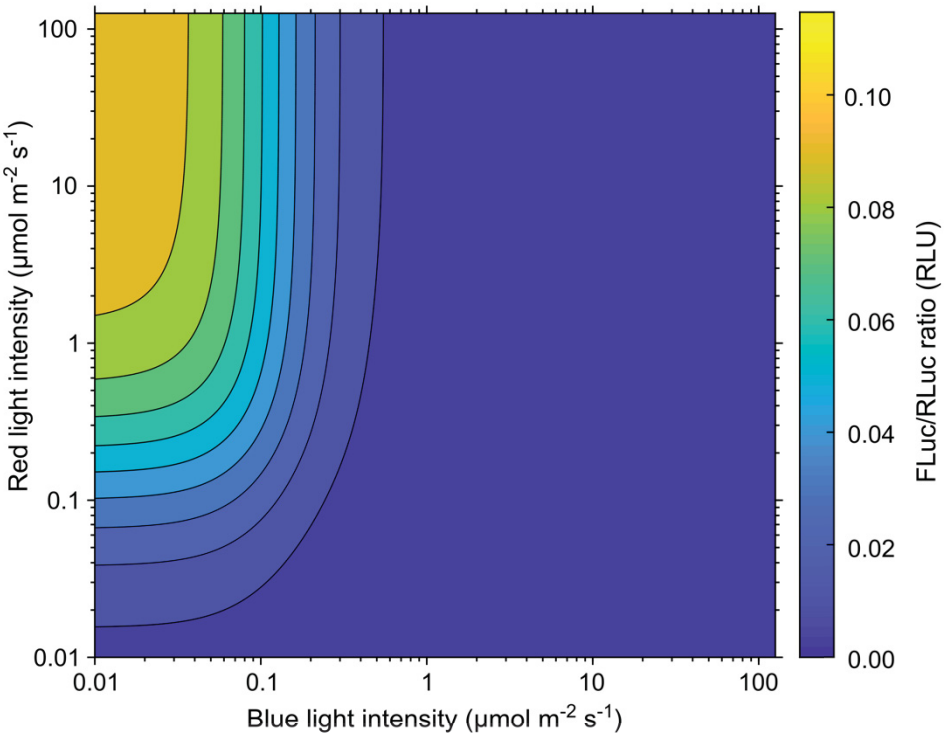


**Supplementary Figure S2.** Heatmap representation of the model predictions of PULSE-controlled protein expression levels as a function of light intensities. The calibrated model yields estimated FLuc/RLuc expression ranges under simultaneous illumination with a range of red and blue light intensities for 12 h.

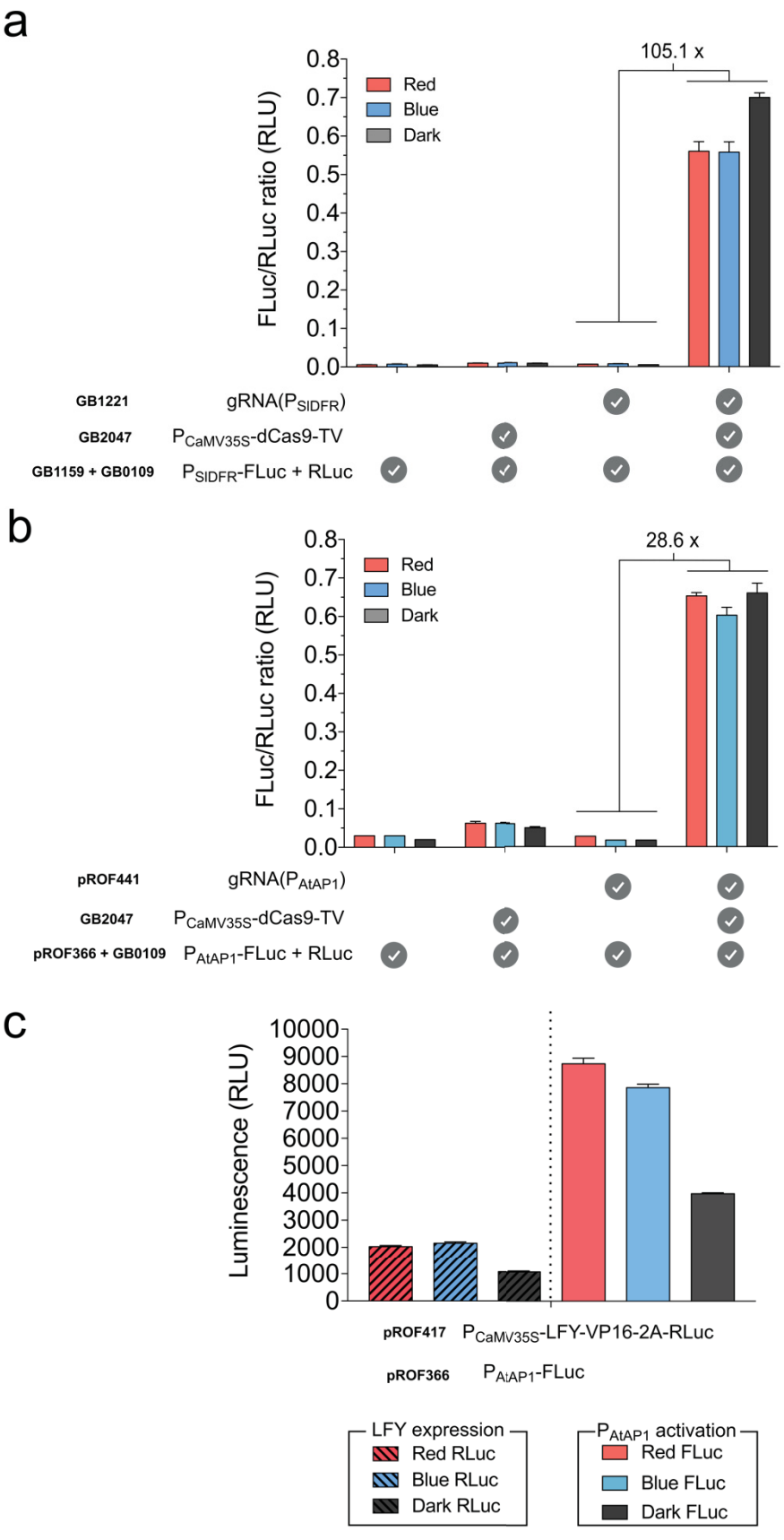
a
105.1 x
FLuc/RLuc ratio (RLU)
0.8
0.7
0.6
0.5
0.4
0.3
0.2
0.1
0.0
Red
Blue
Dark
GB1221 gRNA(PSlDFR)
GB2047 PCaMV35S-dCas9-TV
GB1159 + GB0109 PSlDFR-FLuc + RLuc
b
28.6 x
FLuc/RLuc ratio (RLU)
0.8
0.7
0.6
0.5
0.4
0.3
0.2
0.1
0.0
Red
Blue
Dark
pROF441 gRNA(PAtAP1)
GB2047 PCaMV35S-dCas9-TV
pROF366 + GB0109 PAtAP1-FLuc + RLuc
c
Luminescence (RLU)
10000
9000
8000
7000
6000
5000
4000
3000
2000
1000
0
pROF417 PCaMV35S-LFY-VP16-2A-RLuc
pROF366 PAtAP1-FLuc
LFY expression
Red RLuc
Blue RLuc
Dark RLuc
PAtAP1 activation
Red FLuc
Blue FLuc
Dark FLuc

**Supplementary Figure S3.** Constitutively expressed controls, dCas9-TV and LFY-VP16, in protoplasts of *Arabidopsis thaliana*. **(a)** FLuc and RLuc determinations in protoplasts co-expressing $P_{CaMV35S}$-dCas9-TV and a gRNA directed specifically to the SlDFR promoter sequence, and the $P_{SlDFR}$-FLuc construct. **(b)** FLuc and RLuc determinations in protoplasts co-expressing $P_{CaMV35S}$-dCas9-TV and a gRNA directed specifically to the AtAP1 promoter sequence, and the $P_{AtAP1}$-FLuc construct. **(a,b)** Data shown are the mean ratio of FLuc and RLuc, SEM (*n* = 4). **(c)** FLuc and RLuc determinations in protoplasts co-expressing $P_{CaMV35S}$-LFY-VP16-2A-RLuc (stripped bars) and $P_{AtAP1}$-FLuc (solid bars) under different light conditions. Data shown are means of RLuc, and means of FLuc data after subtraction of background values (configuration without $P_{CaMV35S}$-LFY-VP16-2A-RLuc), and SEM (*n* = 6). **(a-c)** The protoplasts were incubated in darkness, red or blue light, and luminescence determinations performed after 18 - 19 h.

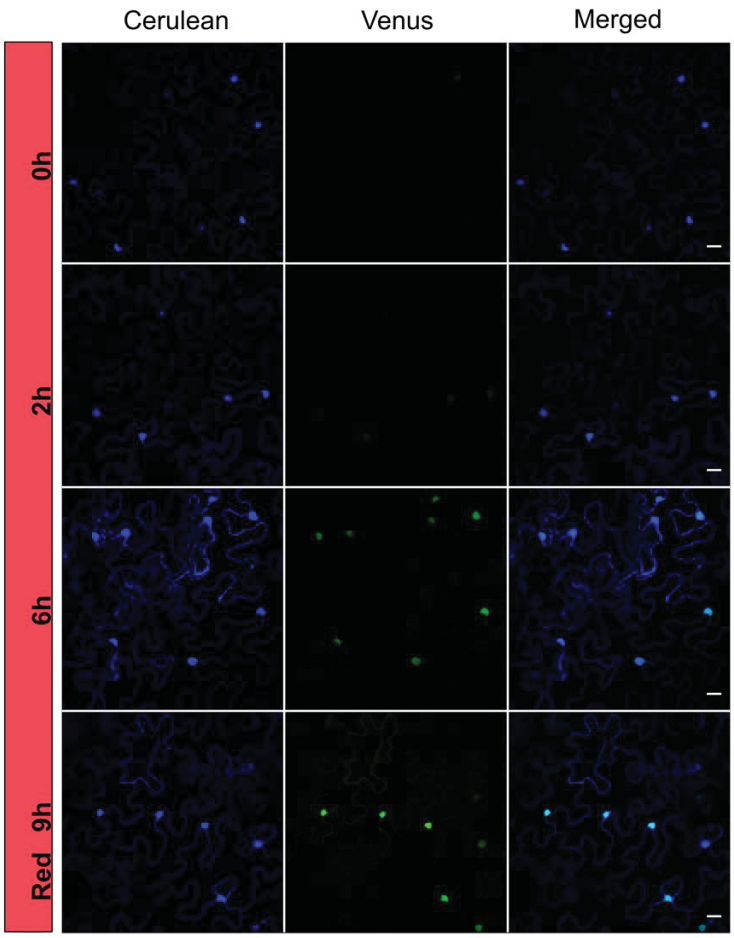
Cerulean
Venus
Merged
Red
0h
2h
6h
9h

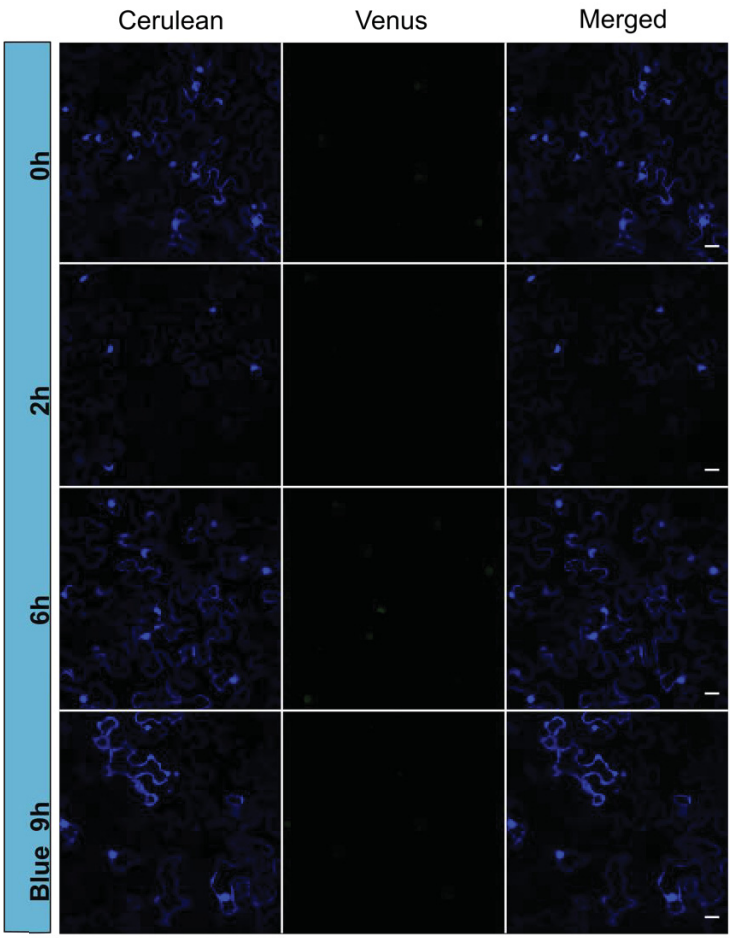
Cerulean
Venus
Merged
Blue
0h
2h
6h
9h

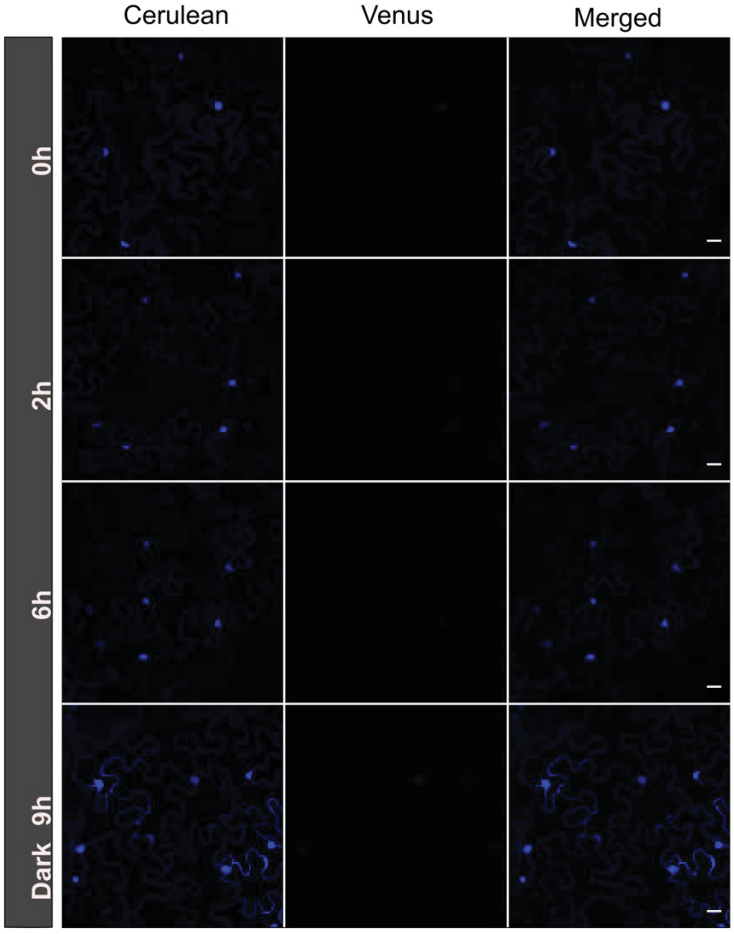
Cerulean
Venus
Merged
Dark
0h
2h
6h
9h

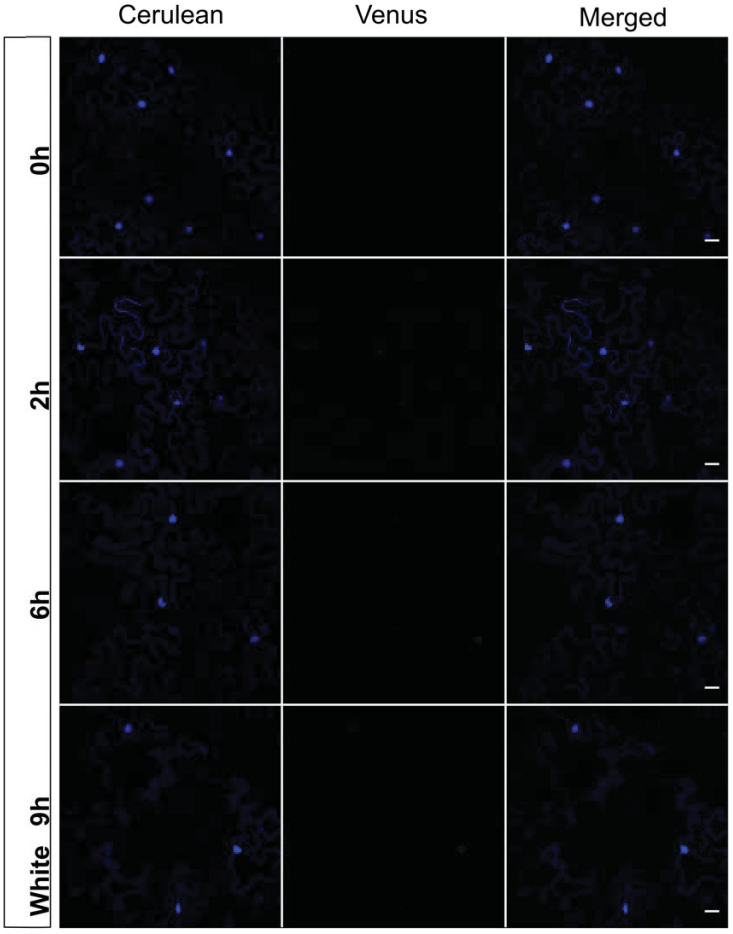
Cerulean
Venus
Merged
White
0h
2h
6h
9h

**Supplementary Figure S4**. Optogenetically controlled Venus and constitutive Cerulean expression in *Nicotiana benthamiana* leaves. Full set of images. Plants infiltrated with Agrobacterium transformed with the PULSE and $P_{Opto}$-Venus and a constitutively expressed Cerulean cassette constructs (pROF346) and incubated for 2.5 d in dark were subjected for 2 h, 6 h, or 9 h to the indicated light treatments (10 μmol $m^{-2}$ $s^{-1}$ of red or blue light, simulated white light, or darkness). Samples were collected at the indicated time points for microscopy visualisation of nuclear Venus and Cerulean fluorescence.

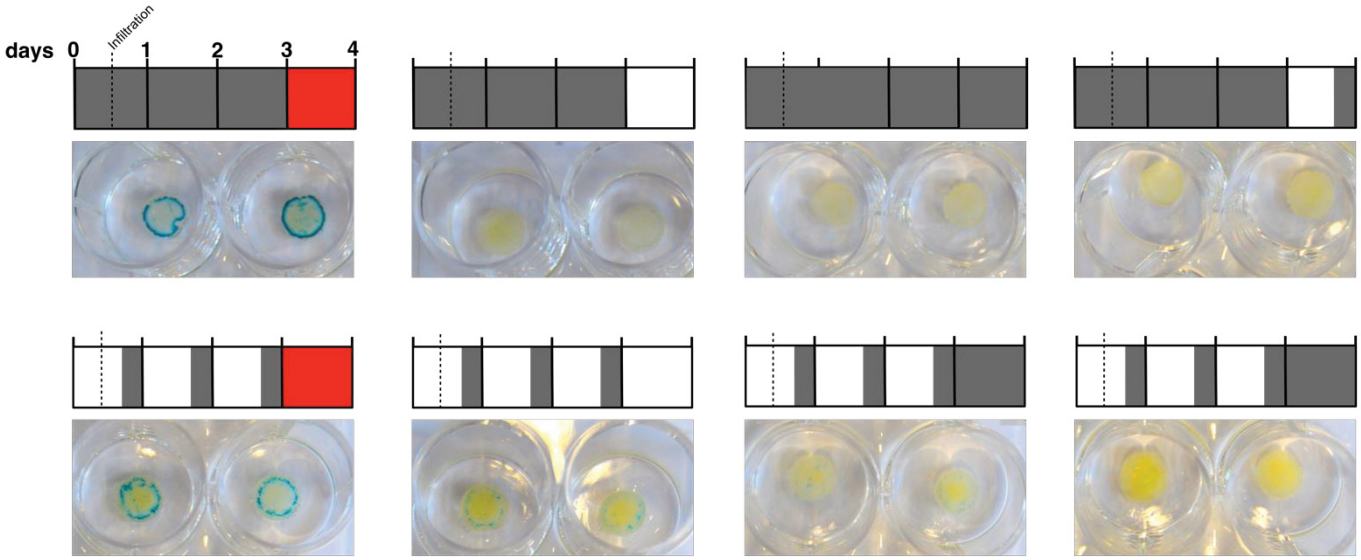


**Supplementary Figure S5.** Optogenetically controlled GUS expression in *N. benthamiana* leaves. Plants infiltrated with Agrobacterium transformed with the PULSE and $P_{Opto}$-GUS construct (BM00369) were kept in darkness or in a plant incubator for 2.5 days (16 h light - 8 h darkness) prior to illumination with LED panels for 1 day with red light (655 nm, 10 μmol $m^{-2}$ $s^{-1}$), simulated white light (as described in **Supplementary Fig. S7** and **Methods**) or darkness. Two disks from different leaves with the same treatment were incubated with GUS staining solution.

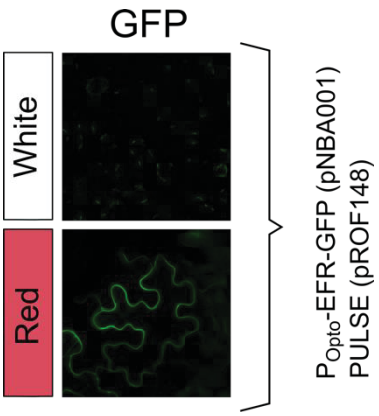


**Supplementary Figure S6**. Expression of optogenetically controlled EFR-GFP under different light condition. Plants infiltrated with agrobacterium transformed with the $P_{Opto}$-EFR-GFP and PULSE constructs were incubated for 2 d prior to induction with 10 µmol $m^{-2}$ $s^{-1}$ red light for additional 16 h (white light illumination was used as control). The leaves were analyzed microscopically for correct expression prior sampling and ROS quantification.

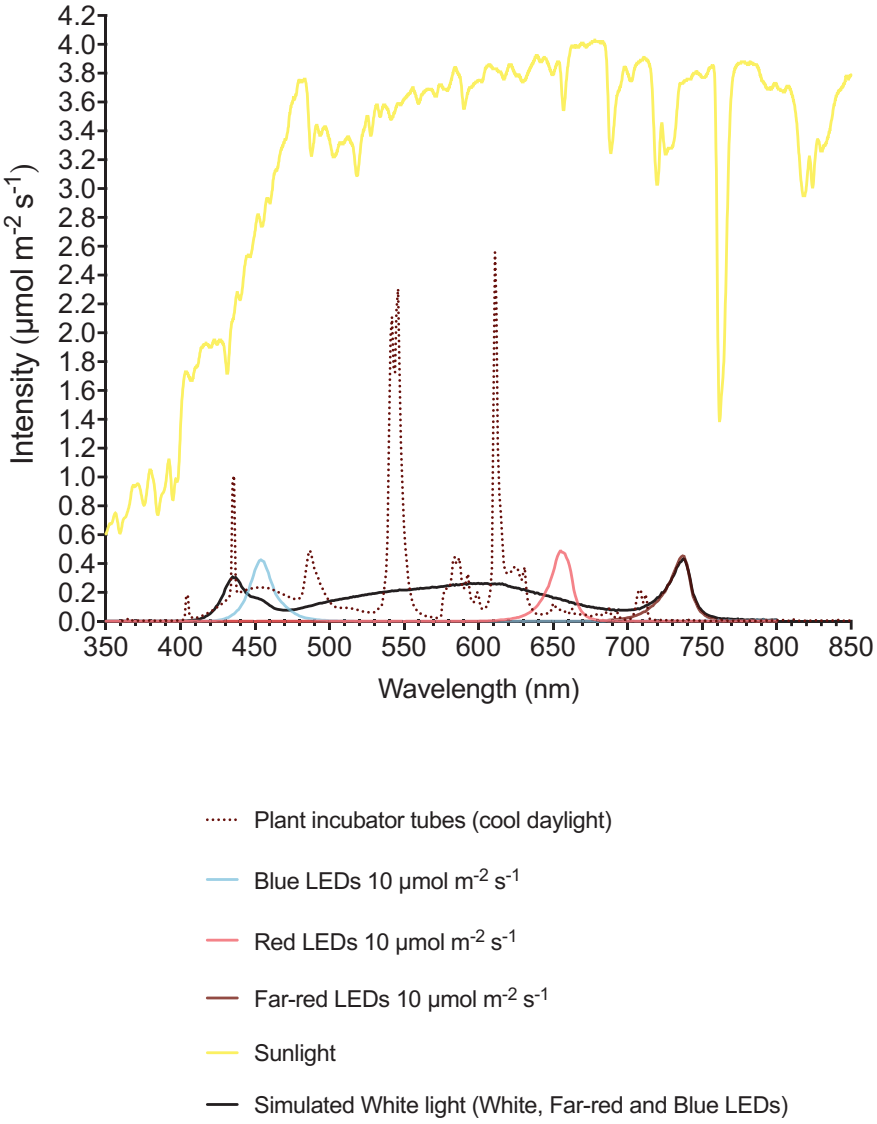


**Supplementary Figure S7.** Spectra of the LEDs used for the illumination treatments. Illumination treatments were performed with LED panels adjusted to intensities of 10 µmol $m^{-2}$ $s^{-1}$ for the red ($\lambda_{max}$ 655 nm), blue ($\lambda_{max}$ 461 nm), or far-red ($\lambda_{max}$ 740 nm). For the simulated white illumination treatments (continuous dark line), white, blue and far-red LEDs were used and the intensity was adjusted in order to have 10 µmol $m^{-2}$ $s^{-1}$ of blue light 420-490 nm, red light 620-680 nm, and far-red light 700-750 nm (light ranges according to Sellaro *et al.* 2010)[14]. Discontinuous dark line corresponds to fluorescent tubes (cool daylight OSRAM). The sunlight spectrum (yellow line) is adapted from Casal[15].

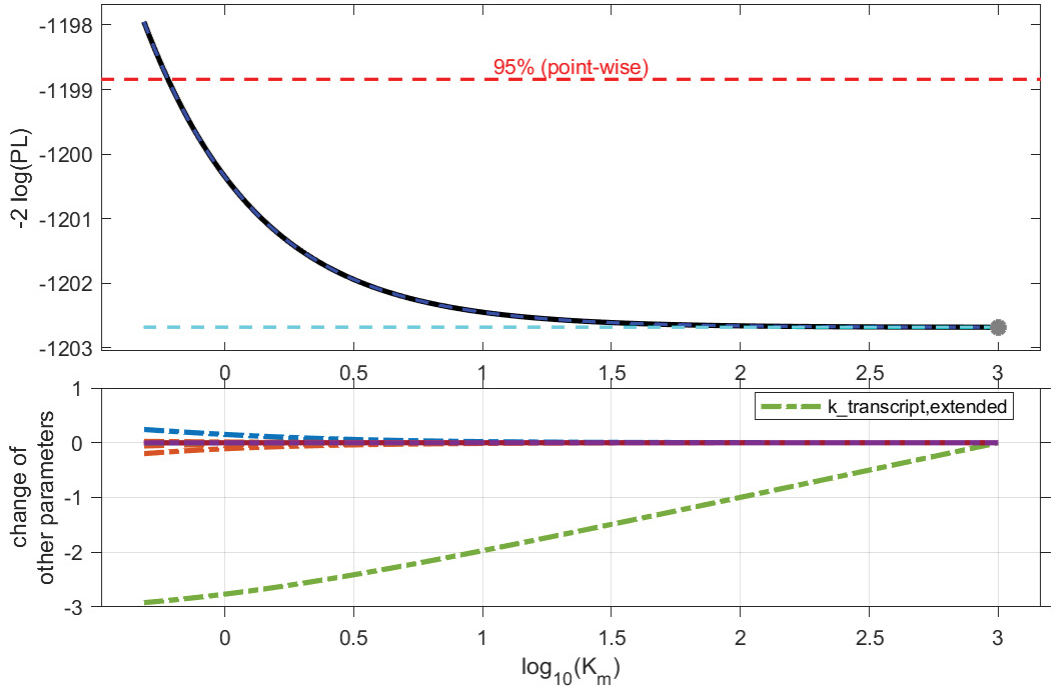


**Supplementary Figure S8**. Parameter profile likelihood of the non-identifiable parameter of the FLuc mRNA transcription when including saturation dynamics and changes in other parameters over the range of profile. The black lines show the profile likelihood, while the optimal parameter value is shown as a grey dot. The dashed red line indicates the 95 % confidence level. Its intersection points with the profile likelihood yield the point-wise 95 % confidence intervals of the parameter. The dashed blue lines indicates the -2log(PL) value of the optimal parameter set. The parameter $K_m$ is practically non-identifiable towards infinity, indicating that the Michaelis-Menten kinetics are in its linear limit, i.e. the saturation is not relevant to describe the data. The lower graph shows the changes in the other parameters in orders of magnitude over the range of the profile. It can clearly be seen, that $K_m$ and $k_{\text{transcript,extended}}$ are linearly linked and their ratio constant over the entire parameter space.

a

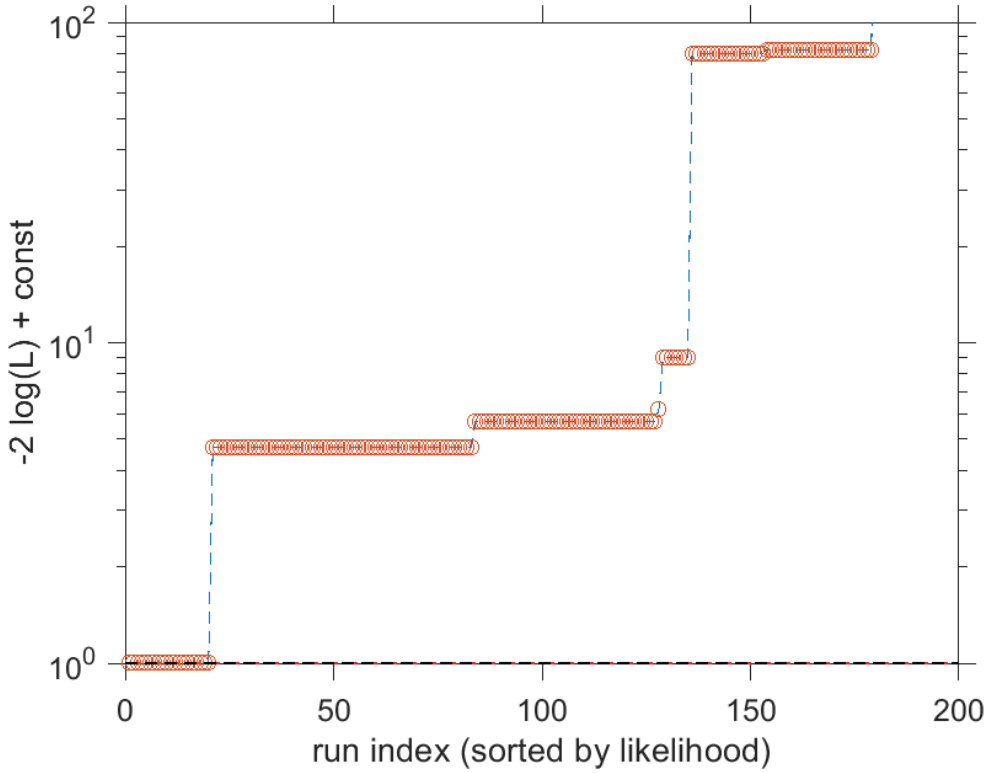
$10^2$
$10^1$
$10^0$
-2 log(L) + const
0
50
100
150
200
run index (sorted by likelihood)

b

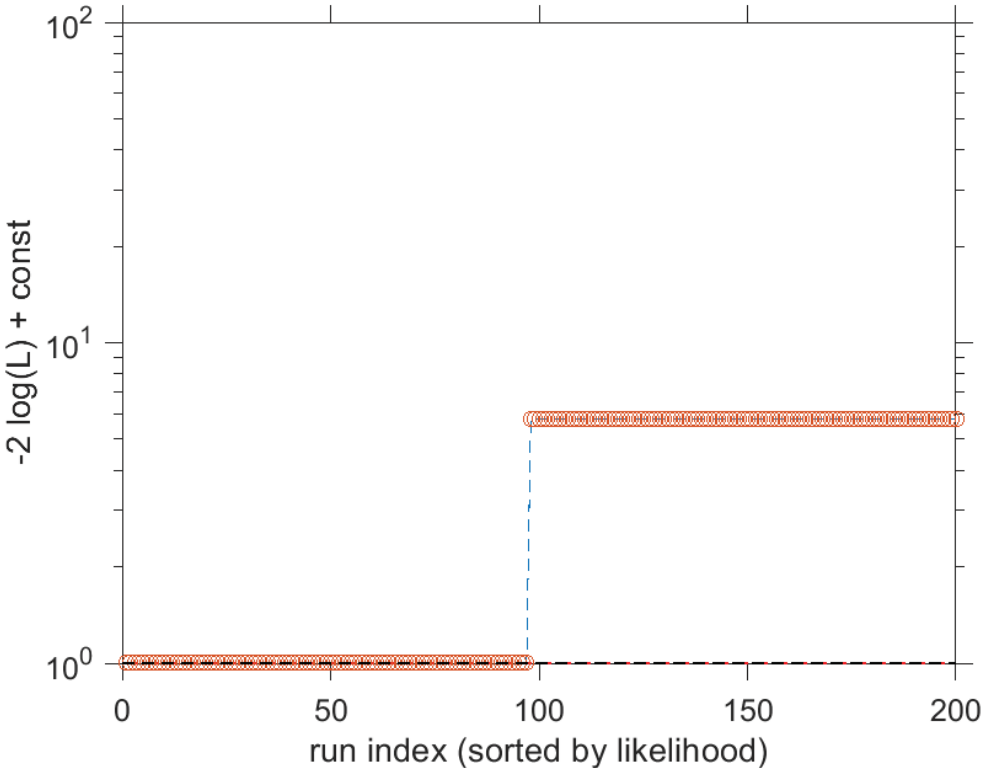
$10^2$
$10^1$
$10^0$
-2 log(L) + const
0
50
100
150
200
run index (sorted by likelihood)

**Supplementary Figure S9**. Multiple optimization runs with random initial parameter guesses. **(a)** 200 optimization runs with random initial parameters sorted by the – 2 log(L) value for the full model. The lowest minima were found in 20 of the runs. All other local minima are significantly higher than the lowest minima. **(b)** 200 optimization runs with random initial parameters sorted by the – 2 log(L) value for the reduced model. The lowest minima were found in 97 of the runs. The other local minimum is significantly higher than the lowest minimum.

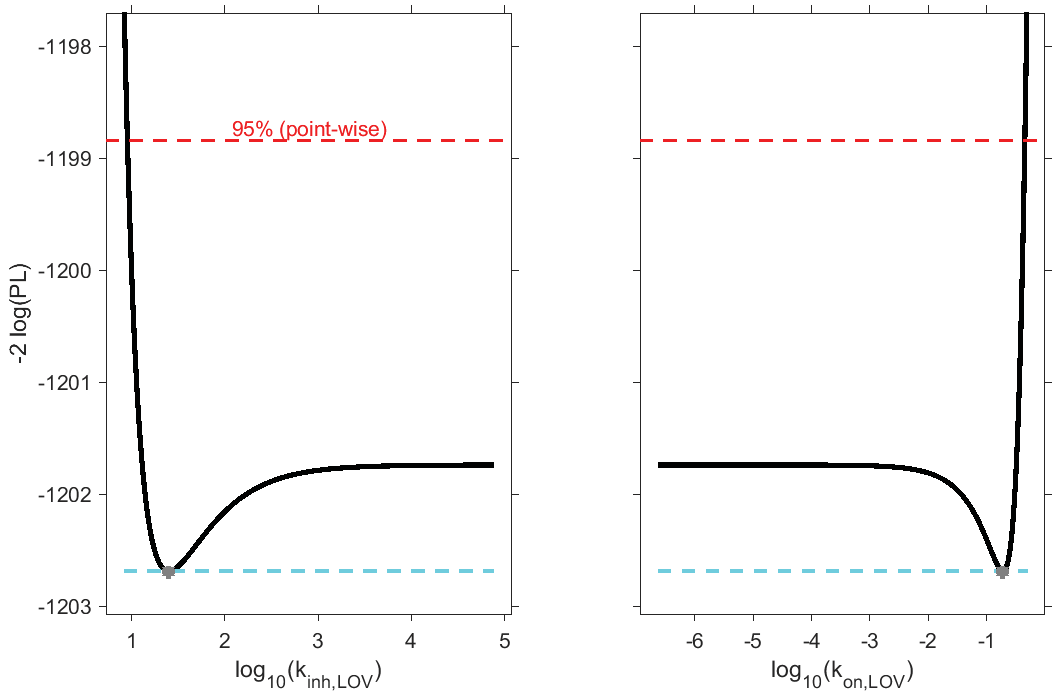


**Supplementary Figure S10.** Parameter profile likelihood of the two non-identifiable parameters of the full model. The black lines show the profile likelihood, while the optimal parameter value is shown as a grey dot. The dotted red line indicates the 95 % confidence level. Its intersection points with the profile likelihood yield the point-wise 95 % confidence intervals of the parameter. The dotted blue lines indicate the – 2 log(PL) value of the optimal parameter set.

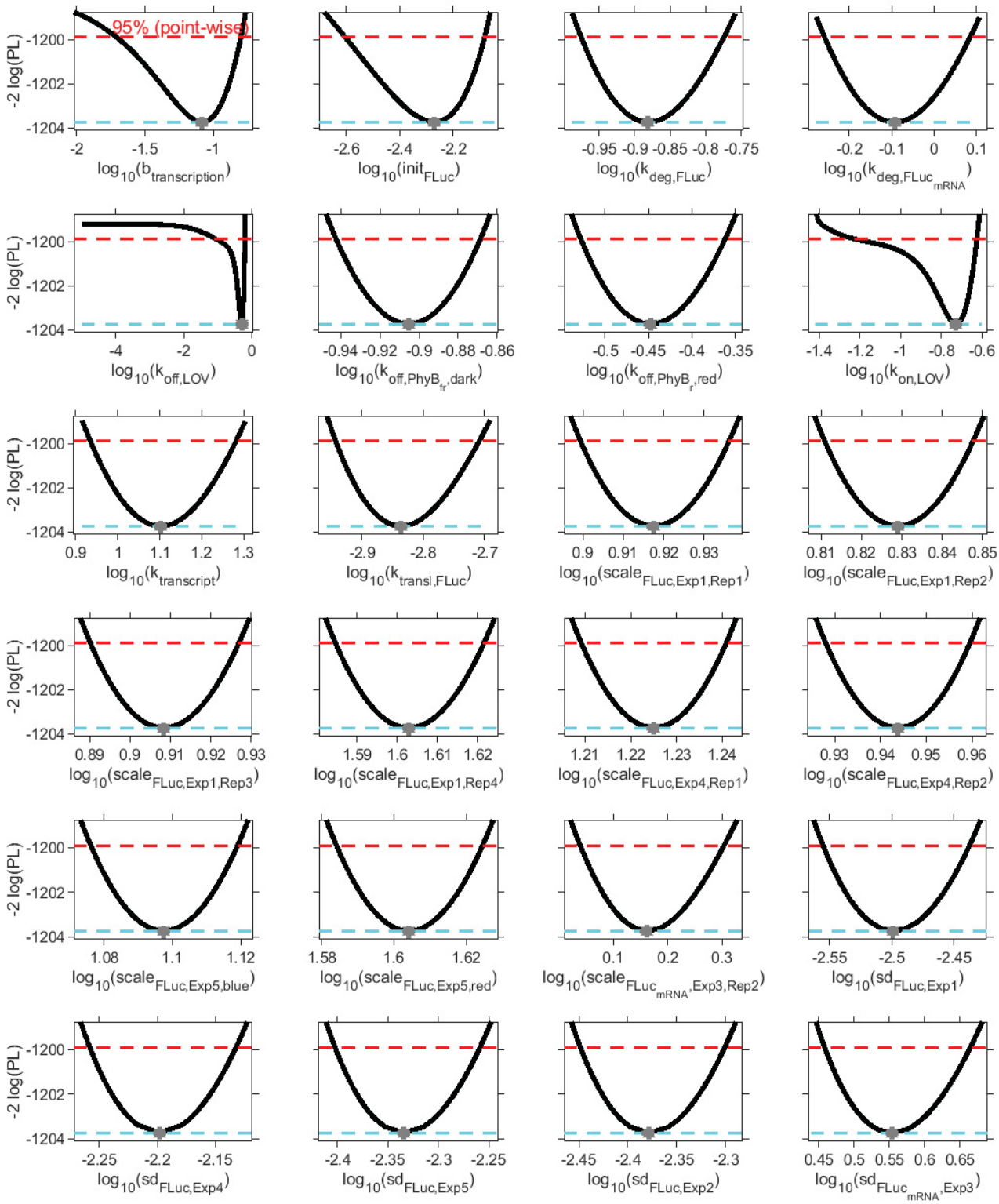


**Supplementary Figure S11.** Parameter profile likelihood of the estimated parameters of the reduced model. The black lines show the profile likelihood, while the optimal parameter value is shown as a grey dot. The dotted red lines indicate the 95 % confidence level. Its intersection points with the profile likelihood yield the point-wise 95 % confidence intervals of the parameter. The dotted blue lines indicate the – 2 log(PL) value of the optimal parameter set. All parameters are identifiable, i.e. they have finite 95 % confidence intervals.

## Supplementary Tables

**Supplementary Table S1.** Plasmids used in this work (grey shading). Plasmids below in the hierarchy were used as intermediate plasmids for cloning purposes.

| Plasmid name | Description | Insert | Backbone | Cloning procedure |
|---|---|---|---|---|
| BM00369 | $T_{nos}$-nptII-$P_{nos}$_$T_{nos}$-NLS-PIF6-E-$P_{CaMV35S}$_$T_{nos}$ -dsRed-$P_{AtUbi10}$_$T_{nos}$-NLS-VP16-PhyB-$P_{CaMV35S}$_$T_{nos}$-EL222-NLS-SRDX-$P_{CaMV35S}$_$T_{35s}$-GUS-$P_{hCMVmin}$-$(C120)_5$-$(etr)_8$ | EC15029, BM00092, EC15034[16], BM00093, BM00368, BM00367, EC41822[16] | EC50505[17] | BpiI restriction-ligation reaction (Golden Gate) |
| ↳ EC15029 | $P_{nos}$-nptII-$T_{nos}$ | EC15057, EC15068 (same sequence as nptII cassette from LucTrap-1[18]), EC41421[16] | EC47802[17] | BsaI restriction-ligation reaction (Golden Gate) |
| ↳ BM00092 | $P_{CaMV35S}$-E-PIF6-NLS-$T_{nos}$ | EC15058[16], EC10991, EC41421[16] | EC47811[17] | BsaI restriction-ligation reaction (Golden Gate) |
| ↳ EC10991 | E-PIF6-NLS | E-PIF6-NLS was synthetized (same sequence as pMZ827[19]) and provided in a Golden Gate L0 plasmid. | EC41308[17] | BpiI restriction-ligation reaction (Golden Gate) |
| ↳ EC15034 | $P_{AtUbi10}$-dsRed-$T_{nos}$[16] | | | |
| ↳ BM00093 | $P_{CaMV35S}$-PhyB-VP16-NLS-$T_{nos}$ | EC15058[16], EC10992, EC41421[16] | EC47831[17] | BsaI restriction-ligation reaction (Golden Gate) |
| ↳ EC10992 | PhyB-VP16-NLS | PhyB-VP16-NLS was synthetized (same sequence as pMZ828[19]) and provided in a Golden Gate L0 plasmid. | EC41308[17] | BpiI restriction-ligation reaction (Golden Gate) |
| ↳ BM00368 | $P_{CaMV35S}$-SRDX-NLS-EL222-$T_{nos}$ | EC15058[16], BM00103, EC41421[16] | EC47841[17] | BsaI restriction-ligation reaction (Golden Gate) |
| ↳ BM00103 | SRDX-NLS-EL222 | SRDX-NLS-EL222 was amplified from pROF051 with oligos oBM0080 and oBM0081. | EC41308[17] | BpiI restriction-ligation reaction (Golden Gate) |
| ↳ BM00367 | $(etr)_8$-$(C120)_5$-$P_{hCMVmin}$-GUS-$T_{35s}$ | BM00102, EC75111[16], EC41414[16] | EC47852[17] | BsaI restriction-ligation reaction (Golden Gate) |

| | | | | | |
|---|---|---|---|---|---|
| ↳ | BM00102 | $(etr)_8$-$(C120)_5$-$P_{hCMVmin}$ | $(etr)_8$-$(C120)_5$-$P_{hCMVmin}$ was amplified from pROF021 with oligos oBM0083 and oBM0079. | EC41295[17] | BpiI restriction-ligation reaction (Golden Gate) |
| BM00654 | | $T_{nos}$-nptII-$P_{nos}$_$T_{nos}$-NLS-PIF6-E-$P_{CaMV35S(short)}$_$T_{nos}$-AsiSI-RLuc-NruI-$P_{AtUbi10}$_$T_{nos}$-NLS-VP16-PhyB-$P_{CaMV35S(short)}$_$T_{nos}$-EL222-NLS-SRDX- $P_{CaMV35S(short)}$_$T_{35S}$-SbfI-FLuc-SpeI-$P_{hCMVmin}$-$(C120)_5$-$(etr)_8$ | EC15029, BM00092, BM00644, BM00093, BM00368, BM00643, EC41822[16] | EC50505[17] | BpiI restriction-ligation reaction (Golden Gate) |
| ↳ | EC15029 | $P_{nos}$-nptII-$T_{nos}$ | EC15057, EC15068 (same sequence as nptII cassette from LucTrap-1[18]), EC41421[16] | EC47802[17] | BsaI restriction-ligation reaction (Golden Gate) |
| ↳ | BM00092 | $P_{CaMV35S(short)}$-E-PIF6-NLS-$T_{nos}$ | EC15058[16], EC10991, EC41421[16] | EC47811[17] | BsaI restriction-ligation reaction (Golden Gate) |
| ↳ | EC10991 | E-PIF6-NLS | E-PIF6-NLS was synthetized (same sequence as pMZ827[19]) and provided in a Golden Gate L0 plasmid. | EC41308[17] | BpiI restriction-ligation reaction (Golden Gate) |
| ↳ | BM00644 | $P_{AtUbi10}$-NruI-RLuc-AsiSI-$T_{nos}$ | EC15062[16], BM00646, EC41421[16] | EC47822[17] | BsaI restriction-ligation reaction (Golden Gate) |
| ↳ | BM00646 | NruI-RLuc-AsiSI | NruI-RLuc-AsiSI was amplified from EC15806[16] with oligos oBM0207 oBM0208. | EC41308[17] | BpiI restriction-ligation reaction (Golden Gate) |
| ↳ | BM00093 | $P_{CaMV35S(short)}$-PhyB-VP16-NLS-$T_{nos}$ | EC15058[16], EC10992, EC41421[16] | EC47831[17] | BsaI restriction-ligation reaction (Golden Gate) |
| ↳ | EC10992 | PhyB-VP16-NLS | PhyB-VP16-NLS was synthetized (same sequence as pMZ828[19]) and provided in a Golden Gate L0 plasmid. | EC41308[17] | BpiI restriction-ligation reaction (Golden Gate) |
| ↳ | BM00368 | $P_{CaMV35S(short)}$-SRDX-NLS-EL222-$T_{nos}$ | EC15058[16], BM00103, EC41421[16] | EC47841[17] | BsaI restriction-ligation reaction (Golden Gate) |
| ↳ | BM00103 | SRDX-NLS-EL222 | SRDX-NLS-EL222 was amplified from pROF051 with oligos oBM0080 and oBM0081. | EC41308[17] | BpiI restriction-ligation reaction (Golden Gate) |
| ↳ | BM00643 | $(etr)_8$-$(C120)_5$-$P_{hCMVmin}$-SpeI-FLuc-SbfI-$T_{35s}$ | BM00102, BM00645, EC41414[16] | EC47852[17] | BsaI restriction-ligation reaction (Golden Gate) |
| ↳ | BM00102 | $(etr)_8$-$(C120)_5$-$P_{hCMVmin}$ | $(etr)_8$-$(C120)_5$-$P_{hCMVmin}$ was amplified from pROF021 with oligos oBM0083 and oBM0079. | EC41295[17] | BpiI restriction-ligation reaction (Golden Gate) |

| | | | | | |
|---|---|---|---|---|---|
| ↳ | BM00645 | SpeI-FLuc-SbfI | SpeI-FLuc-SbfI was amplified from EC15217[16] with oligos oBM0205 oBM0206. | EC41308[17] | BpiI restriction-ligation reaction (Golden Gate) |
| BM00655 | | $T_{nos}$-nptII-$P_{nos}$_$T_{nos}$-NLS-PIF6-E-$P_{AtUbi10(short)}$_$T_{nos}$-AsiSI-RLuc-NruI-$P_{AtUbi10}$_$T_{nos}$-NLS-VP16-PhyB-$P_{AtUbi10}$_$T_{nos}$-EL222-NLS-SRDX-$P_{AtUbi10(short)}$_$T_{35S}$-SbfI-FLuc-SpeI-$P_{hCMVmin}$-$(C120)_5$-$(etr)_8$ | EC15029, BM00648, BM00644, BM00649, BM00650, BM00643, EC41822[16] | EC50505[17] | BpiI restriction-ligation reaction (Golden Gate) |
| ↳ | EC15029 | $P_{nos}$-nptII-$T_{nos}$ | EC15057, EC15068 (same sequence as nptII cassette from LucTrap-1[18]), EC41421[16] | EC47802[17] | BsaI restriction-ligation reaction (Golden Gate) |
| ↳ | BM00648 | $P_{AtUbi10(short)}$-E-PIF6-NLS-$T_{nos}$ | BM00647, EC10991, EC41421[16] | EC47811[17] | BsaI restriction-ligation reaction (Golden Gate) |
| ↳ | BM00647 | $P_{AtUbi10(short)}$ | $P_{AtUbi10(short)}$ was amplified from EC15062[16] using oligos oBM0209 and oBM0210. | EC41295[17] | BpiI restriction-ligation reaction (Golden Gate) |
| ↳ | EC10991 | E-PIF6-NLS | E-PIF6-NLS was synthetized (same sequence as pMZ827[19]) and provided in a Golden Gate L0 plasmid. | EC41308[17] | BpiI restriction-ligation reaction (Golden Gate) |
| ↳ | BM00644 | $P_{AtUbi10}$-NruI-RLuc-AsiSI-$T_{nos}$ | EC15062[16], BM00646, EC41421[16] | EC47822[17] | BsaI restriction-ligation reaction (Golden Gate) |
| ↳ | BM00646 | NruI-RLuc-AsiSI | NruI-RLuc-AsiSI was amplified from EC15806[16] with oligos oBM0207 oBM0208. | EC41308[17] | BpiI restriction-ligation reaction (Golden Gate) |
| ↳ | BM00649 | $P_{AtUbi10(short)}$-PhyB-VP16-NLS-$T_{nos}$ | BM00647, EC10992, EC41421[16] | EC47831[17] | BsaI restriction-ligation reaction (Golden Gate) |
| ↳ | BM00647 | $P_{AtUbi10(short)}$ | $P_{AtUbi10(short)}$ was amplified from EC15062[16] using oligos oBM0209 and oBM0210. | EC41295[17] | BpiI restriction-ligation reaction (Golden Gate) |
| ↳ | EC10992 | PhyB-VP16-NLS | PhyB-VP16-NLS was synthetized (same sequence as pMZ828[19]) and provided in a Golden Gate L0 plasmid. | EC41308[17] | BpiI restriction-ligation reaction (Golden Gate) |
| ↳ | BM00650 | $P_{AtUbi10(short)}$-SRDX-NLS-EL222-$T_{nos}$ | BM00647, BM00103, EC41421[16] | EC47841[17] | BsaI restriction-ligation reaction (Golden Gate) |

| | | | | | |
|---|---|---|---|---|---|
| ↳ | BM00647 | $P_{AtUbi10(short)}$ | $P_{AtUbi10(short)}$ was amplified from EC15062[16] using oligos oBM0209 and oBM0210. | EC41295[17] | BpiI restriction-ligation reaction (Golden Gate) |
| ↳ | BM00103 | SRDX-NLS-EL222 | SRDX-NLS-EL222 was amplified from pROF051 with oligos oBM0080 and oBM0081. | EC41308[17] | BpiI restriction-ligation reaction (Golden Gate) |
| ↳ | BM00643 | $(etr)_8$-$(C120)_5$-$P_{hCMVmin}$-SpeI-FLuc-SbfI-$T_{35s}$ | BM00102, BM00645, EC41414[16] | EC47852[17] | BsaI restriction-ligation reaction (Golden Gate) |
| ↳ | BM00102 | $(etr)_8$-$(C120)_5$-$P_{hCMVmin}$ | $(etr)_8$-$(C120)_5$-$P_{hCMVmin}$ was amplified from pROF021 with oligos oBM0083 and oBM0079. | EC41295[17] | BpiI restriction-ligation reaction (Golden Gate) |
| ↳ | BM00645 | SpeI-FLuc-SbfI | SpeI-FLuc-SbfI was amplified from EC15217[16] with oligos oBM0205 oBM0206. | EC41308[17] | BpiI restriction-ligation reaction (Golden Gate) |
| GB0109 | | $P_{CaMV35s}$-RLuc-$T_{nos}$[20] | | | |
| GB1159 | | $P_{SlDFR}$-FLuc-$T_{nos}$[21] | | | |
| GB1221 | | $P_{AtU6\text{-}26}$-gRNA($P_{SlDFR}$)-sgRNA[21] | | | |
| GB2047 | | $P_{CaMV35S}$-dCas9-TV-$T_{nos}$[21] | | | |
| pMZ827 | | $P_{CaMV35S}$-E-PIF6(1-100)-NLS-$T_{nos}$[19] | | | |
| pMZ828 | | $P_{CaMV35S}$-PhyB(1-650)-VP16-NLS-$T_{nos}$[19] | | | |
| pNBA001 | | $(etr)_8$-$(C120)_5$-$P_{hCMVmin}$-EFR-GFP-$T_{35S}$ | pNBA004, pNBA005, GFP[22], $T_{35S}$[22] | Xpre2-S[22] | BsaI restriction-ligation reaction (Golden Gate) |
| ↳ | pNBA004 | $(etr)_8$-$(C120)_5$-$P_{hCMVmin}$ | $(etr)_8$-$(C120)_5$-$P_{hCMVmin}$ was amplified from pROF021 with oligos oNBA160/oNBA176. | CloneJET (ThermoFisher) | Blunt end cloning of PCR product with T4 DNA ligase |
| ↳ | pNBA005 | EFR | EFR was amplified from pNBA003 with oligos oNBA289/oNBA290. | CloneJET (ThermoFisher) | Blunt end cloning of PCR product with T4 DNA ligase |
| pNBA002 | | $(etr)_8$-$(C120)_5$-$P_{hCMVmin}$-GBP-mCherry-$T_{35S}$ | pNBA004,pNBA006,$T_{35S}$[22] | Xpre2-S[22] | BsaI restriction-ligation reaction (Golden Gate) |
| ↳ | pNBA004 | $(etr)_8$-$(C120)_5$-$P_{hCMVmin}$ | $(etr)_8$-$(C120)_5$-$P_{hCMVmin}$ was amplified from pROF021 with oligos oNBA160/oNBA176. | CloneJET (ThermoFisher) | Blunt end cloning of PCR product with T4 DNA ligase |
| ↳ | pNBA006 | GBP-mCherry | GBP was synthesized (plant codon optimized sequence[23]) with BsaI. | pUC57[22] | BpiI restriction-ligation reaction (Golden Gate) |

| | | | | | |
|---|---|---|---|---|---|
| | | | overhangs and assembled to mCherry[22] by BsaI restriction-ligation reaction. The product was amplified with oligos oNBA145/oNBA146. | | |
| pNBA003 | | $P_{CaMV35S}$-EFR-GFP-$T_{OCS}$[24] | | | |
| pROF018 | | $P_{CaMV35S}$-NLS-KRAB-EL222-$T_{nos}$ | NLS-KRAB-EL222 was amplified from pKM565[25] with oligos oROF023/oROF024. | pMZ827[19] digested with NdeI/EcoRI | Gibson assembly of backbone and PCR insert |
| pROF021 | | $(etr)_8$-$(C120)_5$-$P_{hCMVmin}$-FLuc-$T_{SV40}$ | FLuc was excised from pMZ836[19] with NotI/EcoRI. | pROF020 digested with EcoRI/NotI | Ligation with T4 DNA ligase |
| ↳ | pROF020 | $(etr)_8$-$(C120)_5$-$P_{hCMVmin}$-SEAP-$T_{SV40}$ | $(C120)_5$ was amplified from pGL4.32-C120-FLuc[26] with oligos oROF027/oROF028. | pKM081[27] digested with NheI | Ligation with T4 DNA ligase |
| pROF050 | | $P_{CaMV35S}$-BRD-NLS-EL222-$T_{nos}$ | NLS-linker-EL222 was amplified from pVP-EL222[26] with oligos oROF068/oROF024. BRD was added in a second PCR step with oligos oROF069/oROF024. | pMZ827[19] digested with NdeI/EcoRI. | Gibson assembly of backbone and second PCR insert |
| pROF051 | | $P_{CaMV35S}$-SRDX-NLS-EL222-$T_{nos}$ | NLS-linker-EL222 was amplified from pVP-EL222[26] with oligos oROF068/oROF024. SRDX was added in a second PCR step with oligos oROF070/oROF024. | pMZ827[19] digested with NdeI/EcoRI. | Gibson assembly of backbone and second PCR insert |
| pROF141 | | $P_{AtUbi10}$-SRDX-NLS-EL222-$T_{nos}$_SF_$P_{AtUbi10}$-E-PIF6-NLS-$T_{nos}$_$P_{AtUbi10}$-PhyB-VP16-NLS-$T_{nos}$ | pROF121, pROF120 | pDGB 1alpha2[20] | BsaI restriction-ligation reaction (GB) |
| ↳ | pROF121 | $P_{AtUbi10}$-SRDX-NLS-EL222-$T_{nos}$_SF | pROF117, GB0107[20] | pDGB 1omega1[20] | BsmBI restriction-ligation reaction (GB) |
| ↳ | pROF117 | $P_{AtUbi10}$-SRDX-NLS-EL222-$T_{nos}$ | GB0223[20], pROF081, GB0037[20] | pDGB 1alpha1[20] | BsaI restriction-ligation reaction (GB) |

| | | | | | |
|---|---|---|---|---|---|
| ↳ | pROF081 | SRDX-NLS-linker-EL222 (Pos. B3-B5) | The SRDX-NLS-linker-EL222 was amplified from pROF051 in two fragments in order to domesticate an internal restriction site. Patch A with oligos oROF095/oROF091, and Patch B with oligos oROF092/oROF093. | pUPD[20] | BsmBI restriction-ligation reaction (GB) of Patch A, PatchB and pUPD |
| ↳ | pROF120 | $P_{AtUbi10}$-E-PIF6-NLS-$T_{nos}$_$P_{AtUbi10}$-PhyB-VP16-NLS-$T_{nos}$ | pROF104, pROF105 | pDGB 1omega2[20] | BsmBI restriction-ligation reaction (GB) |
| ↳ | pROF104 | $P_{AtUbi10}$-E-PIF6-NLS-$T_{nos}$ | GB0223[20],pROF098, GB0037[20] | pDGB 1alpha1[20] | BsaI restriction-ligation reaction (GB) |
| ↳ | pROF098 | E-PIF6-NLS (Pos. B3-B5) | E-PIF6-NLS was amplified from pMZ827[19] with oligos oROF100/oROF101. | pUPD[20] | BsmBI restriction-ligation reaction (GB) |
| ↳ | pROF105 | $P_{AtUbi10}$-PhyB-VP16-NLS-$T_{nos}$ | GB0223[20], pMVV003, GB0037[20] | pDGB 1alpha2[20] | BsaI restriction-ligation reaction (GB) |
| ↳ | pMVV003 | PhyB-VP16-NLS (Pos. B3-B5) | PhyB-VP16-NLS was amplified from from pMZ828[19] | pUPD[20] | BsmBI restriction-ligation reaction (GB) |
| pROF148 | | $T_{nos}$-nptII-$P_{nos}$_$P_{AtUbi10}$-SRDX-NLS-EL222-$T_{nos}$_$P_{AtUbi10}$-E-PIF6-NLS-$T_{nos}$_$P_{AtUbi10}$-PhyB-VP16-NLS-$T_{nos}$ | pROF136, pROF120 | pDGB 1alpha2[20] | BsaI restriction-ligation reaction (GB) |
| ↳ | pROF136 | $T_{nos}$-nptII-$P_{nos}$_$P_{AtUbi10}$-SRDX-NLS-EL222-$T_{nos}$ | pROF124, pROF103 | pDGB 1omega1[20] | BsmBI restriction-ligation reaction (GB) |
| ↳ | pROF124 | $P_{nos}$-nptII-$T_{nos}$ | GB0034 (gbcloning.org) | pDGB 1alpha1R[20] | BsaI restriction-ligation reaction (GB) |
| ↳ | pROF103 | $P_{AtUbi10}$-SRDX-NLS-EL222-$T_{nos}$ | GB0223[20], pROF081, GB0037[20] | pDGB 1alpha2[20] | BsaI restriction-ligation reaction (GB) |
| ↳ | pROF081 | SRDX-NLS-linker-EL222 (Pos. B3-B5) | The SRDX-NLS-linker-EL222 was amplified from pROF051 in two fragments in order to domesticate an internal restriction site. Patch A with oligos oROF095/oROF091, and Patch B with oligos oROF092/oROF093 | pUPD[20] | BsmBI restriction-ligation reaction (GB) of Patch A, Patch B and pUPD |
| ↳ | pROF120 | $P_{AtUbi10}$-E-PIF6-NLS-$T_{nos}$_$P_{AtUbi10}$-PhyB-VP16-NLS-$T_{nos}$ | pROF104, pROF105 | pDGB 1omega2[20] | BsmBI restriction-ligation reaction (GB) |

| | | | | | |
|---|---|---|---|---|---|
| ↳ | pROF104 | $P_{AtUbi10}$-E-PIF6-NLS-$T_{nos}$ | GB0223[20], pROF098, GB0037[20] | pDGB 1alpha1[20] | BsaI restriction-ligation reaction (GB) |
| ↳ | pROF098 | E-PIF6-NLS (Pos. B3-B5) | E-PIF6-NLS was amplified from pMZ827[19] with oligos oROF100/oROF101 | pUPD[20] | BsmBI restriction-ligation reaction |
| ↳ | pROF105 | $P_{AtUbi10}$-PhyB-VP16-NLS-$T_{nos}$ | GB0223[20],pMVV003, GB0037[20] | pDGB 1alpha2[20] | BsaI restriction-ligation reaction (GB) |
| ↳ | pMVV003 | PhyB-VP16-NLS (Pos. B3-B5) | PhyB-VP16-NLS was amplified from from pMZ828[19] | pUPD[20] | BsmBI restriction-ligation reaction (GB) |
| pROF346 | | $T_{nos}$-nptII-$P_{nos}$_$T_{nos}$-NLS-PIF6-E-$P_{AtUbi10}$_$T_{nos}$-AsiSI-NLS-Cerulean-NruI-$P_{AtUbi10(short)}$_$T_{nos}$-NLS-VP16-PhyB- $P_{AtUbi10}$_$T_{nos}$-EL222-NLS-SRDX- $P_{AtUbi10}$_$T_{35S}$-SbfI-H2B-Venus-SpeI-$P_{hCMVmin}$-$(C120)_5$-$(etr)_8$ | Venus-H2B was amplified from pAB146 with oligos oROF436/oROF442. | pROF345 digested with SpeI/SbfI | Gibson assembly of backbone and PCR insert |
| ↳ | pAB146 | attR2-Venus-H2B-$T_{3A}$[28] | | | |
| ↳ | pROF345 | $T_{nos}$-nptII-$P_{nos}$_$T_{nos}$-NLS-PIF6-E-$P_{AtUbi10}$_$T_{nos}$-AsiSI-NLS-Cerulean-NruI-$P_{AtUbi10(short)}$_$T_{nos}$-NLS-VP16-PhyB- $P_{AtUbi10}$_$T_{nos}$-EL222-NLS-SRDX- $P_{AtUbi10}$_$T_{35S}$-SbfI-FLuc-SpeI-$P_{hCMVmin}$-$(C120)_5$-$(etr)_8$ | Cerulean-NLS was amplified from pAPB131 with oligos oROF415/ oROF417. | BM0655 digested with NruI/AsiSI | Gibson assembly of backbone and PCR insert |
| ↳ | pAPB131 | attR2-Cerulean-$T_{3A}$[28] | | | |
| pROF349 | | $T_{nos}$-nptII-$P_{nos}$_$T_{nos}$-NLS-PIF6-E-$P_{CaMV35S(short)}$_$T_{nos}$-AsiSI-RLuc-NruI-$P_{AtUbi10}$_$T_{nos}$-NLS-VP16-PhyB-$P_{CaMV35S(short)}$_$T_{nos}$-EL222-NLS-SRDX- $P_{CaMV35S(short)}$_$T_{35S}$-SbfI-H2B-Venus-SpeI-$P_{hCMVmin}$-$(C120)_5$-$(etr)_8$ | Venus-H2B was amplified from pAB146[28] with oligos oROF436/oROF442. | pROF348 digested with SpeI/SbfI | Gibson assembly of backbone and PCR insert |
| ↳ | pROF348 | $T_{nos}$-nptII-$P_{nos}$_$T_{nos}$-NLS-PIF6-E-$P_{CaMV35S(short)}$_$T_{nos}$-AsiSI-RLuc-NruI-$P_{AtUbi10}$_$T_{nos}$-NLS-VP16-PhyB-$P_{CaMV35S(short)}$_$T_{nos}$-EL222-NLS- | Cerulean-NLS was amplified from pAPB131[28] with oligos oROF415/oROF417. | BM00654 digested with NruI/AsiSI | |

| | | | | | |
|---|---|---|---|---|---|
| | | SRDX- $P_{CaMV35S(short)}$_$T_{35S}$-SbfI-FLuc-SpeI-$P_{hCMVmin}$-$(C120)_5$-$(etr)_8$ | | | |
| pROF366 | | $P_{AtAP1}$-FLuc-$T_{SV40}$ | $P_{AtAP1}$ was amplified from Arabidopsis genomic DNA with oligos oROF401/403. | pROF021 digested with PstI/EcoRI | Gibson assembly of backbone and PCR insert |
| pROF394 | | $(etr)_8$-$(C120)_5$-$P_{hCMVmin}$-LFY-VP16-NLS-2A-RLuc-$T_{SV40}$ | LFY-VP16-NLS was amplified from pROF367 with oligos oROF427/oROF429.<br>2A-RLuc was amplified from pROF202 with oligos oROF420/392. | pROF021 digested with EcoRI/SpeI | Gibson cloning of backbone and the PCR |
| ↳ | pROF367 | $P_{CaMV35S}$-LFY-VP16-NLS-$T_{nos}$ | LFY-VP16-NLS was amplified from pJA082 with oligos oROF404/oROF405. | pGEN016[29] digested with AgeI/EcoRI | Gibson assembly of backbone and PCR insert |
| ↳ | pJA082 | $P_{SV40}$-LFY-VP16-NLS-HAtag-$T_{SV40}$ | LFY (AT5G61850) was amplified from Arabidopsis cDNA with oligos oJA181/oJA163. VP16 was amplified from pKM018[7] with oligos oJA060/oSLS466. | pMZ333[25] digested with NotI/XbaI | AQUA cloning |
| ↳ | pROF202 | 2A-RLuc (Pos. B5) | 2A-linker-RLuc was generated with sequential PCRs. First PCR was amplified from pSW209[30] with oligos oROF205/207, and this product was used as template with oligos oROF206/207. | pUPD2[31] | BsmBI restriction-ligation reaction (GB) |
| pROF402 | | $P_{35Senhancer(-953\ to\ -51)}$-$(C120)_5$-$P_{hCMVmin}$-FLuc-$T_{35S}$ | pROF339, pROF054, pROF375, GB0096[20], GB0036[20] | pDGB 1alpha2[20] | BsaI restriction-ligation reaction (GB) |
| ↳ | pROF339 | $P_{35Senhancer(-953\ to\ -51)}$ (Pos. A1) | $P_{35Senhancer(-953\ to\ -51)}$ was amplified from GB0030[20] with oligos oROF377/oROF378. | pUPD2[31] | BsmBI restriction-ligation reaction (GB) |

cl

| | | | | | |
|---|---|---|---|---|---|
| ↳ | pROF054 | $(C120)_5$ (Pos. A2) | $(C120)_5$ was amplified from pGL4.32-C120-FLuc[26] with oligos oROF073/oROF074. | pUPD2[31] | BsmBI restriction-ligation reaction (GB) |
| ↳ | pROF375 | $P_{hCMVmin}$ (Pos. A3-B2) | $P_{hCMVmin}$ was amplified from pMZ836[19] with oligos oROF083/oROF084. | pUPD2[31] | BsmBI restriction-ligation reaction (GB) |
| pROF405 | | Tnos-KanR-$P_{nos}$_$T_{nos}$-PIF6-E-$P_{AtUbi10}$_Tnos-AsiSI-venus-H2B-NruI-$P_{AtUbi10(short)}$_Tnos-VP16-PhyB-$P_{AtUbi10}$_$T_{nos}$-EL222-SRDX_$P_{AtUbi10}$-T35s-SbfI-FT-VP16-NLS-HAtag-SpeI-$P_{CMVmini}$-$(C120)_5$-$(etr)_8$ | SbfI-FT-VP16-NLS-HAtag-SpeI was amplified from pJA037 with oligos oROF458/oROF459. | pROF313 digested with SpeI/SbfI. | Gibson assembly of backbone and PCR insert |
| ↳ | pJA037 | $P_{SV40}$-FT-VP16-NLS-HAtag-$T_{SV40}$ | FT (AT1G65480) was amplified from Arabidopsis cDNA with oligos oJA015/oJA072.<br>VP16 was amplified from pKM018[7] with oligos oJA060/oSLS466. | pMZ333[25] digested with NotI/XbaI | AQUA assembly of backbone and PCR insert |
| ↳ | pROF313 | Tnos-KanR-$P_{nos}$_$T_{nos}$-PIF6-E-$P_{AtUbi10}$_Tnos-AsiSI-venus-H2B-NruI-$P_{AtUbi10(short)}$_Tnos-VP16-PhyB-$P_{AtUbi10}$_$T_{nos}$-EL222-SRDX_$P_{AtUbi10}$-T35s-SbfI-FLuc-SpeI-$P_{CMVmini}$-$(C120)_5$-$(etr)_8$ | Venus-H2B was amplified from pAB146[28] with oligos oROF415/oROF416. | BM00655 digested with NruI/AsiSI | Gibson assembly of backbone and PCR insert |
| pROF415 | | Tnos-KanR-$P_{nos}$_$T_{nos}$-PIF6-E-$P_{AtUbi10}$_Tnos-AsiSI-venus-H2B-NruI-$P_{AtUbi10(short)}$_Tnos-VP16-PhyB-$P_{AtUbi10}$_$T_{nos}$-EL222-SRDX_$P_{AtUbi10}$-T35s-SbfI-FT-SpeI-$P_{CMVmini}$-$(C120)_5$-$(etr)_8$ | SbfI-FT-SpeI was amplified from pJA037 with oligos oROF458/oROF473. | pROF313 digested with SpeI/SbfI | Gibson assembly of backbone and PCR insert |
| ↳ | pJA037 | $P_{SV40}$-FT-VP16-NLS-HAtag-$T_{SV40}$ | FT (AT1G65480) was amplified from Arabidopsis cDNA with oligos oJA015/oJA072.<br>VP16 was amplified from pKM018[7] with oligos oJA060/oSLS466. | pMZ333[25] digested with NotI/XbaI | AQUA assembly of backbone and PCR insert |

| | | | | | |
|---|---|---|---|---|---|
| ↳ | pROF313 | Tnos-KanR-$P_{nos}$_$T_{nos}$-PIF6-E-$P_{AtUbi10}$_Tnos-AsiSI-venus-H2B-NruI-$P_{AtUbi10(short)}$_Tnos-VP16-PhyB-$P_{AtUbi10}$_$T_{nos}$-EL222-SRDX_$P_{AtUbi10}$-T35s-SbfI-FLuc-SpeI-$P_{CMVmini}$-$(C120)_5$-$(etr)_8$ | Venus-H2B was amplified from pAB146[28] with oligos oROF415/ oROF416. | BM00655 digested with NruI/AsiSI | Gibson assembly of backbone and PCR insert |
| pROF417 | | $P_{CaMV35S}$-LFY-VP16-NLS-2A-linker-RLuc-$T_{nos}$ | LFY-VP16-NLS was amplified from pROF367 with oligos oROF404/oROF429. 2A-RLuc was amplified from pROF202 with oligos oROF420/oROF474. | pGEN016[29] digested with AgeI/EcoRI | Gibson assembly of backbone and PCR insert |
| pROF441 | | $P_{AtU6-26}$-gRNA($P_{AtAP1}$)-sgRNA | gRNA($P_{AtAP1}$) was constructed using oligos oROF537/oROF538 at 1 µM; 5 µl of each were mixed and incubated for 30 min at RT. Then 1 µl of the mixture was combined with pROF440 and pROF446. | pDGB 1alpha2[20] | BsaI restriction-ligation reaction (GB) |
| ↳ | pROF440 | $P_{AtU6-26}$ (Pos. A1-B2) | $P_{AtU6-26}$ was amplified from pEn-Chimera[32] with oligos oROF137/oROF545. | pUPD2[31] | BsmBI restriction-ligation reaction (GB) |
| ↳ | pROF446 | sgRNA | sgRNA was amplified from pEN-Chimera[32] with oligos oROF546/oROF140. | pUPD2[31] | BsmBI restriction-ligation reaction (GB) |
| pROF449 | | $(etr)_8$-$(C120)_5$-$P_{hCMVmin}$-dCas9-TV-$T_{35S}$ | pROF053, pROF054, pROF375, GB1079[21], GB2001[21], GB0036[20] | pDGB 1alpha1[20] | BsaI restriction-ligation reaction (GB) |
| ↳ | pROF053 | $(etr)_8$ (Pos. A1) | $(etr)_8$ was amplified from pKM081[27] with oROF071/oROF072. | pUPD2[31] | BsmBI restriction-ligation reaction (GB) |
| ↳ | pROF054 | $(C120)_5$ (Pos. A2) | $(C120)_5$ was amplified from pGL4.32-C120-FLuc[26] with oligos oROF073/oROF074. | pUPD2[31] | BsmBI restriction-ligation reaction (GB) |
| ↳ | pROF375 | $P_{hCMVmin}$ (Pos. A3-B2) | $P_{hCMVmin}$ was amplified from pMZ836[19] with oligos oROF083/oROF084. | pUPD2[31] | BsmBI restriction-ligation reaction (GB) |
| pROF450 | | SF_$T_{nos}$-nptII-$P_{nos}$_$P_{AtUbi10}$-SRDX-NLS-EL222-$T_{nos}$_$P_{AtUbi10}$-E-PIF6-NLS-$T_{nos}$_$P_{AtUbi10}$-PhyB-VP16-NLS-$T_{nos}$ | GB0106[20], pROF148 | pDGB 3omega1[20] | BsmBI restriction-ligation reaction (GB) |

| | | | | |
|---|---|---|---|---|
| pRSET | PT7-driven bacterial expression vector (ThermoFisher) | | | |

2A, F2A self-cleaving peptide derived from the foot-and-mouth disease virus; BRD, B3 repression domain from *A. thaliana*; $(C120)_5$, 5 repeats of the DNA cognate sequence of EL222; dCas9, CRISPR associated protein 9 nuclease deficient; E, macrolide-responsive repressor protein; EFR, LRR receptor-like serine/threonine-protein kinase from *A. thaliana*; EL222, transcription factor from *Erythrobacter litoralis*; $(etr)_8$, 8 repeats of the DNA cognate sequence of E; FLuc, Firefly luciferase; GBP, GFP binding protein; GFP, green fluorescent protein; gRNA, part of the guide RNA containing the 20 bp target sequence; GUS, β-glucuronidase from *E. coli*; H2B, *A. thaliana* histone B2; HA-tag, human influenza hemagglutinin-derived epitope tag; KRAB, transcriptional repressor domain from human Krüppel Associated Box; LFY, LEAFY transcription factor from *A. thaliana*; NLS, nuclear localization signal from the simian virus 40 large T antigen; nptII, neomycin phosphotransferase; $P_{35Senhancer}$(-953 to -51), enhancer region of the *cauliflower mosaic virus* 35S promoter; $P_{AtU6\text{-}26}$, *A. thaliana* U6-26 RNA polymerase III promoter; $P_{AtAP1}$, *A. thaliana* APETALA1 promoter; $P_{AtUbi10}$, *A. thaliana* Ubiquitin-10 promoter; $P_{CaMV35S}$, *cauliflower mosaic virus* 35S promoter; $P_{hCMVmin}$, minimal human cytomegalovirus immediate early promoter; PhyB(1–650), N-terminus of *A. thaliana* phytochrome B with amino acids 1–650; PIF6(1–100), N-terminus of *A. thaliana* phytochrome-interacting factor 6 with amino acids 1–100; $P_{nos}$, *Agrobacterium tumefaciens* nopaline synthase promoter; $P_{SlDFR,}$ *Solanum lycopersicum* dihydroflavonol 4-reductase promoter; $P_{SV40}$, simian virus 40 early promoter; RLuc, Renilla luciferase; SF, stuffer DNA fragment; SRDX, EAR repression domain from *A. thaliana*; SEAP, human secreted alkaline phosphatase; sgRNA, single guide RNA from combined bacterial crRNA and tracrRNA without the target sequence; $T_{35S}$, *cauliflower mosaic virus* 35S terminator; $T_{3A}$, ribulose-1,5-bisphosphate carboxylase 3A subunit terminator; $T_{nos}$, *A. tumefaciens* nopaline synthase terminator; $T_{OCS}$, *A. tumefaciens* octopine synthase terminator; $T_{SV40}$, simian virus 40 early terminator; TV, activation domain composed by 6x TAL and 2x VP64 and NLS sequence; VP16, *Herpes simplex* virus-derived transactivation domain.

**Supplementary Table S2.** Oligonucleotides used in this work (lowercase correspond to annealing part and uppercase corresponds to overhangs)

| Oligonucleotide name | Sequence 5'→3' |
|---|---|
| oBM0083 | CTGTGGTCTCAGGAGcttcgaagtttaaacgattg |
| oBM0079 | CCCGAAGACTCCATTaggctggatcggtcccg |
| oBM0080 | TGTGAAGACCAAATGatgcttgatcttgaacttagac |
| oBM0081 | CCCGAAGACTCAAGCttagattccggcttcgac |
| oBM0205 | TGTGAAGACCAAATGactagtatggaagatg |
| oBM0206 | CCCGAAGACTCAAGCcctgcaggttacacggcg |
| oBM0207 | TGTGAAGACCAAATGtcgcgaatggcttcg |
| oBM0208 | CCCGAAGACTCAAGCgcgatcgcctattgttca |
| oBM0209 | TGTGAAGACCAggaggacgagtcagtaataaac |
| oBM0210 | CCCGAAGACTCcattctgttaatcagaaaaac |
| oJA015 | TCTTTTATTTCAGGTCCCGGATCGAATTGCCCACCatgtctataaatataagagaccctcttatag |
| oJA060 | TCTTCTTCTCACCATACCAACTGGTCTCTCACCggtgaattcgatagtgctggtagtgctggtag |
| oJA072 | ACTACCAGCACTACCAGCACTATCGAATTCACCGGTaagtcttcttcctccgca |
| oJA163 | CACTACCAGCACTACCAGCACTATCGAATTCACTAGTgaaacgcaagtcgtcgc |
| oJA181 | TTTTATTTCAGGTCCCGGATCGAATTGCGGGCGCGGCCGCCACCatggatcctgaaggtttcacg |
| oNBA145 | AAGAAGACTATACGGGTCTCAAAGGgaatggcggatgtgaacctggtgg |
| oNBA146 | AAGAAGACTACAGAGGTCTCAGATTcttgtacagctcgtccatg |
| oNBA160 | CGGGTCTCTGCGGcttcgaagtttaaacgattgaat |
| oNBA176 | GGTCTCACAGAGAaggctggatcggtcccggtgtc |

cliv

| | |
|---|---|
| oNBA289 | TAGGTCTCACACCatgaagctgtccttttcacttg |
| oNBA290 | TAGGTCTCACCTTcatagtatgcatgtccgta |
| oROF023 | TACCGGTTGGCTAGGTAAGCTTGGTACCACCTGAACGACGCATATGatctaagctagccccacca |
| oROF024 | GTTATCTAGATCCGGTGGATCCAAGCTTCTCGAGCCCGGGGAATTCgggaggtgtgggaggtttt |
| oROF027 | tacgggaggtattggacagg |
| oROF028 | TGATGCCGCTAGCtctagtgtctaagcttcatgg |
| oROF068 | CCAAAGAAGAAGAGGAAGGTGGGAGCTGGAGCTggggcagacgacaca |
| oROF069 | AGGTAAGCTTGGTACCACCTGAACGACGCATATGGGTAATTCTAAGACTCTTAGACTTTTTGGTGTTAATATGGAATGTccaaagaagaaga ggaaggt |
| oROF071 | GCGCCGTCTCGCTCGGGAGgtttaaacgattgaatataaccgac |
| oROF072 | GCGCCGTCTCGCTCGGTCAgctagcatccctaaatgtaac |
| oROF073 | GCGCCGTCTCGCTCGTGACgctagcctcgagtaggtagc |
| oROF074 | GCGCCGTCTCGCTCGGGGAaagcttcatggactaaaggct |
| oROF083 | GCGCCGTCTCGCTCGTCCCGCGGCCGCcctatataagcagagctcgtt |
| oROF084 | GCGCCGTCTCGCTCGCATTACCGGTaggctggatcggtcccggtg |
| oROF091 | GCGCCGTCTCGCAagacgcggatcggacacg |
| oROF092 | GCGCCGTCTCGCTTgccgacaatccgctgat |
| oROF093 | GCGCCGTCTCGCTCGAAGCttagattccggcttcgacgg |
| oROF095 | GCGCCGTCTCGCTCGAatgcttgatcttgaacttagactt |
| oROF100 | GCGCCGTCTCGCTCGAatgacaacaatgccccgccccaa |
| oROF101 | GCGCCGTCTCGCTCGAAgcctacaccttcctcttcttctt |
| oROF137 | GCGCCGTCTCGCTCGGGAGctttttttcttcttcttcgttcatac |

| | |
|---|---|
| oROF140 | GCGCCGTCTCGCTCAAGCGtaatgccaactttgtacaagaaag |
| oROF205 | GAATCAAATCCTGGACCCGCGCGCGGTGCAGGCGCTGGAGCCGGTGCCGGGGCAGGCGCTGGCGCTatgacttcgaaagtttatgatcca |
| oROF206 | GCGCCGTCTCGCTCGTTCGGACCCGTGAAACAGCTGCTCAACTTCGATCTCCTCAAACTGGCCGGCGACGTGgaatcaaatcctggacccg |
| oROF207 | GCGCCGTCTCGCTCAAAGCTTAgaattcttgttcatttttgagaac |
| oROF377 | GCGCCGTCTCGCTCGGGAGagcatcgtggaaaaagaagac |
| oROF378 | GCGCCGTCTCGCTCAGTCAatagtgggattgtgcgtcatc |
| oROF392 | ACGCGTATTTAAATTAATTAAGCGATCGCACTAGTTTAttgttcatttttgagaactcgct |
| oROF401 | CCACCTGACGTCGTCGACGATCGACCTGCAGtgtttaacatccaagatttgttttac |
| oROF403 | CTGACTCTAGAGGATCCCCGGGCGAGCTCGAATTCcatttttgatccttttttaagaaact |
| oROF404 | TTTGGAGAGAACACGGGGACTCTAGCGCTACCGGTgcggccgccaccat |
| oROF405 | CCGGTGGATCCAAGCTTCTCGAGCCCGGGGAATTCCTAcaccttccgctttttcttggg |
| oROF406 | CCGGTGGATCCAAGCTTCTCGAGCCCGGGGAATTCCTACACCTTCCGCTTTTTCTTGGGgaaacgcaagtcgtcgcc |
| oROF415 | TCTGATTAACAGATGCAGATCTTAATGTCGCGAatggtgagcaagggc |
| oROF416 | TGTTTGAACGATCTGCTTGACAAGCGCGATCGCctagttaattaaagaactcgtaaact |
| oROF417 | TGTTTGAACGATCTGCTTGACAAGCGCGATCGCTCACACCTTCCGCTTTTTCTTGGGgttaattaacttgtacagctcg |
| oROF420 | cccgtgaaacagctg |
| oROF422 | agaactgcctgcgtgagatt |
| oROF423 | ttttccgtcatcgtctttcc |
| oROF424 | gaggcgaactgtgtgtgaga |
| oROF425 | gtgttcgtcttcgtcccagt |
| oROF427 | ACCGATCCAGCCTCCGCGGCCCCGGTACCGAATTCgcggccgccaccat |
| oROF429 | TTGAGCAGCTGTTTCACGGGcaccttccgctttttcttggg |

| | |
|---|---|
| oROF436 | GAAGACACCGGGACCGATCCAGCCTAATGACTAGTatggtgagcaagggcg |
| oROF442 | TCGATCGACTCTAGCTAGAGAAGCCCTGCAGGctagttaattaaagaactcgtaaacttcg |
| oROF458 | GAAGACACCGGGACCGATCCAGCCTAATGACTAGTatgtctataaatataagagaccctct |
| oROF459 | TCGATCGACTCTAGCTAGAGAAGCCCTGCAGGctaagcgtaatctggaacatc |
| oROF473 | TCGATCGACTCTAGCTAGAGAAGCCCTGCAGGTTAaagtcttcttcctccgcag |
| oROF474 | GAAGACACCGGGACCGATCCAGCCTAATGACTAGTatgtctttctccgtga |
| oROF514 | gtgaaaactgttggagagaagcaa |
| oROF515 | tcaactggatacccttcgca |
| oROF518 | ggtggtcgataaagatgttctga |
| oROF519 | aagcctctgactgatggagc |
| oROF537 | ATTGTATATCTCGTACTAATGTC |
| oROF538 | AAACGACATTAGTACGAGATATA |
| oROF545 | GCGCCGTCTCGCTCAcaatcactacttcgactctag |
| oROF546 | GCGCCGTCTCGCTCGgttttagagctagaaatagcaagt |
| oSLS466 | CTTGGGCTGCAGGTCGACTCTAGACTAAGCGTAATCTGGAACATCGTATGGGTacaccttccgctttttcttgggcc |

**Supplementary Table S3.** Estimated model parameters and confidence intervals on linear scale. Estimated parameters $\hat{\theta}$ were obtained by maximum likelihood estimation and their point-wise 95 % confidence intervals with lower bound $(\widehat{\theta - \sigma^-})$ and upper bound $(\hat{\theta}+\sigma^+)$ were obtained with the profile likelihood method. Fixed variables have no confidence intervals.

| Parameter | $\widehat{\boldsymbol{\theta}}\ (\widehat{\boldsymbol{\theta}} - \boldsymbol{\sigma}^-, \widehat{\boldsymbol{\theta}} + \boldsymbol{\sigma}^+)$ |
|---|---|
| $init_{FLuc}$ | 5.35 (2.49, 8.26) •$10^{-03}$ |
| $b_{transcription}$ | 0.83 (0.20, 15.8) •$10^{-01}$ |
| $k_{transcript}$ | 1.26 (0.86, 1.91) •$10^{+01}$ |
| $k_{transl,FLuc}$ | 1.46 (1.14, 1.95) •$10^{-03}$ |
| $k_{deg,FLuc}$ | 1.32 (1.06, 1.68) •$10^{-01}$ |
| $k_{deg,FLucmRNA}$ | 0.81 (0.55, 1.22) •$10^{+00}$ |
| $k_{off,LOV}$ | 5.10 (0.92, 6.30) •$10^{-01}$ |
| $k_{on,LOV}$ | 1.88 (0.60. 2.37) •$10^{-01}$ |
| $k_{off,PhyBfr,dark}$ | 1.24 (1.14, 1.35) •$10^{-01}$ |
| $k_{off,PhyBr,red}$ | 3.57 (2.97, 4.35) •$10^{-01}$ |
| $scale_{FLuc,Exp1,Rep1}$ | 8.27 (7.93, 8.63) •$10^{+00}$ |
| $scale_{FLuc,Exp1,Rep2}$ | 6.75 (6.47, 7.04) •$10^{+00}$ |
| $scale_{FLuc,Exp1,Rep3}$ | 8.10 (7.77, 8.45) •$10^{+00}$ |
| $scale_{FLuc,Exp1,Rep4}$ | 4.01 (3.84, 4.18) •$10^{+01}$ |
| $scale_{FLuc,Exp4,Rep1}$ | 1.68 (1.62, 1.74) •$10^{+01}$ |
| $scale_{FLuc,Exp4,Rep2}$ | 8.79 (8.47, 9.11) •$10^{+00}$ |
| $scale_{FLuc,Exp5,blue}$ | 1.25 (1.19, 1.32) •$10^{+01}$ |
| $scale_{FLuc,Exp5,red}$ | 4.02 (3.84, 4.21) •$10^{+01}$ |
| $scale_{FLucmRNA,Exp3,Rep2}$ | 1.45 (1.09, 2.01) •$10^{+00}$ |
| $sd_{FLuc,Exp1}$ | 3.17 (2.78, 3.65) •$10^{-03}$ |
| $sd_{FLuc,Exp4}$ | 6.34 (5.52, 7.38) •$10^{-03}$ |
| $sd_{FLuc,Exp5}$ | 4.63 (3.96, 5.51) •$10^{-03}$ |
| $sd_{FLuc,Exp2}$ | 4.19 (3.56, 5.00) •$10^{-03}$ |
| $sd_{FLucmRNA,Exp3}$ | 3.58 (2.87, 4.62) •$10^{+00}$ |
| $k_{inh,LOV}$ | 2.50•$10^{+01}$ |
| $k_{off,PhyBr,farred}$ | 1.00•$10^{+03}$ |
| $r_{PhyBfr,red}$ | 7.28•$10^{-01}$ |
| $r_{PhyBfr,farred}$ | 2.00•$10^{-03}$ |

**Supplementary References**


1. De Caluwé, J. *et al.* A Compact Model for the Complex Plant Circadian Clock. *Front. Plant Sci.* **7**, 74–74 (2016).
2. Locke, J. C. W., Millar, A. J. & Turner, M. S. Modelling genetic networks with noisy and varied experimental data: the circadian clock in Arabidopsis thaliana. *J. Theor. Biol.* **234**, 383–393 (2005).
3. Pokhilko, A. *et al.* The clock gene circuit in Arabidopsis includes a repressilator with additional feedback loops. *Mol. Syst. Biol.* **8**, 574 (2012).
4. Raue, A. *et al.* Lessons Learned from Quantitative Dynamical Modeling in Systems Biology. *PLoS ONE* **8**, e74335 (2013).
5. Beyer, H. M. *et al.* Synthetic Biology Makes Polymer Materials Count. *Adv. Mater.* **30**, 1800472 (2018).
6. Raue, A. *et al.* Structural and practical identifiability analysis of partially observed dynamical models by exploiting the profile likelihood. *Bioinformatics* **25**, 1923–1929 (2009).
7. Müller, K. *et al.* A red/far-red light-responsive bi-stable toggle switch to control gene expression in mammalian cells. *Nucleic Acids Res.* **41**, e77–e77 (2013).
8. Kelly, J. M. & Lagarias, J. C. Photochemistry of 124-kilodalton Avena phytochrome under constant illumination in vitro. *Biochemistry* **24**, 6003–6010 (1985).
9. Legris, M. *et al.* Phytochrome B integrates light and temperature signals in Arabidopsis. *Science* **354**, 897 (2016).
10. Raue, A. *et al.* Data2Dynamics: a modeling environment tailored to parameter estimation in dynamical systems. *Bioinformatics* **31**, 3558–3560 (2015).
11. Hindmarsh, A. C. *et al.* SUNDIALS: Suite of nonlinear and differential/algebraic equation solvers. *ACM Trans. Math. Softw.* **31**, 363–396 (2005).
12. Coleman, T. & Li, Y. An Interior Trust Region Approach for Nonlinear Minimization Subject to Bounds. *SIAM J. Optim.* **6**, 418–445 (1996).
13. Kreutz, C., Raue, A. & Timmer, J. Likelihood based observability analysis and confidence intervals for predictions of dynamic models. *BMC Syst. Biol.* **6**, 120 (2012).
14. Sellaro, R. *et al.* Cryptochrome as a Sensor of the Blue/Green Ratio of Natural Radiation in Arabidopsis. *Plant Physiol.* **154**, 401 (2010).
15. Casal, J. J. Photoreceptor Signaling Networks in Plant Responses to Shade. *Annu. Rev. Plant Biol.* **64**, 403–427 (2013).

16. Feike, D. *et al.* Characterizing standard genetic parts and establishing common principles for engineering legume and cereal roots. *Plant Biotechnol. J.* **0**, (2019).
17. Weber, E., Engler, C., Gruetzner, R., Werner, S. & Marillonnet, S. A Modular Cloning System for Standardized Assembly of Multigene Constructs. *PLoS ONE* **6**, e16765 (2011).
18. Calderon-Villalobos, L. I. A. *et al.* LucTrap Vectors Are Tools to Generate Luciferase Fusions for the Quantification of Transcript and Protein Abundance in Vivo. *Plant Physiol.* **141**, 3 (2006).
19. Müller, K. *et al.* A red light-controlled synthetic gene expression switch for plant systems. *Mol. Biosyst.* **10**, 1679–1688 (2014).
20. Sarrion-Perdigones, A. *et al.* GoldenBraid 2.0: A Comprehensive DNA Assembly Framework for Plant Synthetic Biology. *Plant Physiol.* **162**, 1618 (2013).
21. Selma, S. *et al.* Strong gene activation in plants with genome-wide specificity using a new orthogonal CRISPR/Cas9-based programmable transcriptional activator. *Plant Biotechnol. J.* **17**, 1703–1705 (2019).
22. Binder, A. *et al.* A Modular Plasmid Assembly Kit for Multigene Expression, Gene Silencing and Silencing Rescue in Plants. *PLoS ONE* **9**, e88218 (2014).
23. Schornack, S. *et al.* Protein mislocalization in plant cells using a GFP-binding chromobody. *Plant J.* **60**, 744–754 (2009).
24. Schwessinger, B. *et al.* Phosphorylation-Dependent Differential Regulation of Plant Growth, Cell Death, and Innate Immunity by the Regulatory Receptor-Like Kinase BAK1. *PLoS Genet.* **7**, e1002046 (2011).
25. Baaske, J. *et al.* Dual-controlled optogenetic system for the rapid down-regulation of protein levels in mammalian cells. *Sci. Rep.* **8**, 15024 (2018).
26. Motta-Mena, L. B. *et al.* An optogenetic gene expression system with rapid activation and deactivation kinetics. *Nat. Chem. Biol.* **10**, 196–202 (2014).
27. Müller, K. *et al.* Multi-chromatic control of mammalian gene expression and signaling. *Nucleic Acids Res.* **41**, e124 (2013).
28. Bleckmann, A. Untersuchungen zur Stammzellregulation im Sprossapikalmeristem von Arabidopsis thaliana. (PhD Thesis, Heinrich-Heine-Universität Düsseldorf, 2010).
29. Samodelov, S. L. *et al.* StrigoQuant: A genetically encoded biosensor for quantifying strigolactone activity and specificity. *Sci. Adv.* **2**, e1601266–e1601266 (2016).

30. Wend, S. *et al.* A quantitative ratiometric sensor for time-resolved analysis of auxin dynamics. *Sci. Rep.* **3**, 2052 (2013).
31. Vazquez-Vilar, M. *et al.* GB3.0: a platform for plant bio-design that connects functional DNA elements with associated biological data. *Nucleic Acids Res.* **45**, 2196–2209 (2017).
32. Fauser, F., Schiml, S. & Puchta, H. Both CRISPR/Cas-based nucleases and nickases can be used efficiently for genome engineering in Arabidopsis thaliana. *Plant J.* **79**, 348–359 (2014).

## B. Other publications

Gratz, R., Brumbarova, T., Ivanov, R., Trofimov, K., Tünnermann, L., Ochoa-Fernandez, R., Blomeier, T., Meiser, J., Weidtkamp-Peters, S., Zurbriggen, M., *et al*. (2019). Phospho-mutant activity assays provide evidence for alternative phospho-regulation pathways of the transcription factor FIT. New Phytol. *225*, 250-257.